ANL-00/15

Argonne National Laboratory
9700 South Cass Avenue
Argonne, IL 60439

1999

Chemical Technology Division

Annual Technical Report

David Lewis — Division Director
J. F. Miller — Electrochemical and Basic Science Department
R. E. Einziger — Waste Materials Research Department
E. C. Gay — Nuclear Technology Department
D. W. Green — Analytical Chemistry Laboratory

June 2000

DISCLAIMER

TABLE OF CONTENTS

TABLE OF CONTENTS (contd)

TABLE OF CONTENTS (contd)

1999

Chemical Technology Division

Annual Technical Report

Abstract

The Chemical Technology (CMT) Division is a diverse chemical engineering organization with principal emphases in development of advanced energy sources and environmental management. The Division conducts research and development in three general areas: (1) development of advanced power sources for stationary and transportation applications and for consumer electronics, (2) management of high- and low-level nuclear wastes and hazardous wastes, and (3) electrometallurgical treatment of spent nuclear fuel. The Division also performs basic research in catalytic chemistry involving molecular energy resources, mechanisms of ion transport in lithium battery electrolytes, and the chemistry of technology-relevant materials. In addition, the Division operates the Analytical Chemistry Laboratory, which conducts research in analytical chemistry and provides analytical services for programs at Argonne National Laboratory (ANL) and other organizations. Technical highlights of the Division's activities during 1999 are presented.

Summary

Electrochemical Technology

The CMT Division conducts research, development, engineering, and performance/life evaluation studies of advanced power sources for vehicle propulsion, utility load-leveling, and other applications. The Division is also responsible for the technical management of industrial contracts for the Department of Energy (DOE) related to the development of fuel cells for transportation applications.

During the past year, the in-house battery R&D has focused on the lithium-ion and lithium-polymer battery systems. In late 1998, a new CMT program was initiated to support the DOE Partnership for a New Generation Vehicle (PNGV), which has the objective of developing an 80 mpg (34 km/L) passenger vehicle with negligible environmental emissions. As part of this effort, CMT is leading a multi-laboratory program to assist industrial developers of high-power lithium ion-batteries to overcome the calendar life, safety, and cost barriers for this technology. During the past year, CMT developed the chemistry for the first generation of high-power lithium-ion cell and arranged for an industrial firm to fabricate 300 such cells for testing by the participating national laboratories. Work is now underway on development of the next generation of these cells, as well as innovative approaches for reducing cell packaging costs by a factor of five or six.

A research program is being carried out in CMT to develop new and improved electrode materials for lithium-ion batteries. The past year's effort focused on the development of manganese oxide-based cathode materials as a replacement for the present $LiCoO_2$ cathodes. (There are concerns about the use of $LiCoO_2$ because of its high cost and safety hazards.) These studies yielded the first evidence that some of the capacity fade previously observed when high-voltage (4-V) $Li/Li_x[Mn_2]O_4$ cells are deeply discharged may be attributed to structural fatigue at the electrode surface, and that this effect might be mitigated by creating a more stable surface in modified $Li_{1+x}[Mn_{2-x}]O_4$ electrodes.

Under a cooperative R&D agreement, the Division is working with 3M Corp. and Hydro-Québec to develop lithium-polymer batteries for transportation applications. These batteries show promise for meeting the demanding performance requirements of electric vehicles and operate at slightly elevated temperatures (typically 80°C). This effort involves engineering studies, development of electrode materials, and electrochemical modeling and characterization of electrodes, cells, and multicell modules. During the past year, the transport properties of possible electrolytes for lithium-polymer batteries were modeled on the basis of concentrated solution theory. It was also demonstrated that the transport and thermodynamic properties for a binary lithium salt in a polymer electrolyte can be determined with only two sets of experiments: AC impedance studies and potential measurements with test cells.

The Electrochemical Analysis and Diagnostic Laboratory is a CMT facility that conducts evaluations of battery performance and lifetime under simulated application conditions.

Evaluations during 1999 have involved the testing of (1) nickel/metal hydride cells and modules from GM-Ovonics and SAFT (France) for the U.S. Advanced Battery Consortium and (2) a variety of different batteries from foreign manufacturers for the DOE. These evaluations are expected to continue through 2000.

Fuel cells convert chemical energy directly into electricity by electrochemical reaction, thereby eliminating the need for heat engines and rotating machinery. Since fuel cells have very low environmental emissions and high efficiency, interest in their development for stationary and transportation applications continues to grow. To aid in the development of polymer electrolyte fuel cells for transportation applications, CMT researchers are developing a partial oxidation reformer that converts hydrocarbon fuels into a hydrogen-rich gaseous fuel. In earlier work, we developed new catalysts, for use in our partial oxidation reformer, that are fuel flexible. The catalyst has been demonstrated to work effectively with a wide variety of fuels, including methanol, ethanol, gasoline, and diesel fuel. Efforts in the past year concentrated on improving the ceramic support material and synthesis method for these catalysts.

The Division is also involved in developing a process that will decrease the H_2S content of the reformate that would be produced from sulfur-containing fuels, such as retail gasoline. Sulfur must be removed to prevent poisoning of anode materials and, potentially, certain fuel processing catalysts. The process under investigation is based on chemical reaction with a ZnO sorbent. Another potential contaminant in the reformed fuel is carbon monoxide, which must be reduced below 100 ppm to avoid significant degradation in cell performance caused by poisoning of the platinum-based anode catalyst. Researchers in CMT are studying several approaches for converting the CO to CO_2, via a water-gas shift reaction, and removing traces of CO by selective sorption/desorption. Significant advances were made in both areas.

A major accomplishment during the past year was the design and building of an engineering-scale fuel processor that would be suitable for a fuel-cell-powered vehicle. This reformer has a fuel processing capacity sufficient to supply a 5- to 10-kW fuel cell stack and has been successfully tested with iso-octane and methanol fuels.

A computer simulation model was developed for polymer electrolyte fuel cell systems operating in light-duty vehicles. Efforts this past year focused on applying the model to calculate the effects of operating pressure on the design and operation of these fuel cells. Results are summarized.

Efforts continue on developing molten carbonate and solid oxide fuel cells for utility applications. One problem area with the molten carbonate fuel cell is corrosion of the bipolar plates, which are currently made from Type 316L stainless steel. The corrosion behavior of various metal alloys was determined to identify the best candidate alloy for continued development. Promising results were obtained with stainless steels containing manganese as the alloying element (Nitronic series). In the area of solid oxide fuel cells, CMT is searching for ways to improve the ionic conductivity and catalytic activity of the strontium-doped lanthanum cathode used in the current cells, which are operated at about 1000°C. In half-cell tests, use of either Ga or Al as dopants for Mn(III) in the strontium-doped lanthanum was found to substantially improve cathodic overpotential. Further characterization of these materials is

needed. Researchers in CMT are also exploring new cathode materials that would allow operation of solid oxide fuel cells at temperatures at or below 800°C. Such lower operating temperatures would reduce cost and improve performance. Several perovskite-based materials have shown promising performance as cathodes in half-cell tests.

The Division continues to provide support to the DOE Office of Transportation Technologies and the DOE Office of Buildings Technology in the form of technical management of R&D contracts with industrial developers of fuel cells and related components. Major ongoing projects managed by CMT include DOE contracts with Plug Power, Honeywell (formerly Allied Signal Corp.), Energy Partners L.C., 3M Corp., McDermott Technology, Inc., and the Institute of Gas Technology, as well as several other fuel-cell component suppliers.

Waste Materials Research

The primary CMT research in waste management involves the determination of the corrosion behavior of various nuclear waste forms in adverse atmospheres in support of disposal in approved repositories. This includes chemical and physical characterization, testing, and analyses of the results in terms of mechanisms of release.

Qualification testing is being conducted on all the major waste forms intended for interment: DOE spent nuclear fuel, spent fuel from commercial light water reactors (LWRs), the ceramic waste form being developed for plutonium disposition, glasses developed for the Defense Waste Processing Facility and the West Valley Demonstration Project, and the ceramic waste form resulting from the electrometallurical treatment of spent sodium-bonded fuel from Experimental Breeder Reactor-II (EBR-II). Besides the work on spent fuel and high-level waste, projects are also underway on characterization and testing of low-level waste and the behavior of actinide species in various subsurface environments.

The DOE has over 200 types of spent fuel from a variety of testing programs and research reactors. These fuels have been divided into groups to facilitate degradation testing. Fuels from four of the major groups have been selected for testing at CMT: N-Reactor fuel, mixed oxide fuel, UAl_x fuel, and graphite fuel. Of these groups, the mixed oxide and N-Reactor fuels have been characterized and are being tested. The aluminum fuels are expected to be received shortly for characterization and testing. The results of the degradation tests will be compared with the release of elements from LWR spent fuel to determine a relative source term.

The license application is being prepared for the candidate Yucca Mountain repository, which will be used primarily for disposing spent fuel from commercial reactors. Both long-term drip tests and vapor hydration tests are underway in support of that effort. In drip tests for up to 14 years, the uranium release from unirradiated UO_2 samples has been determined to be rapid during the first one to two years of testing and to remain relatively low after that. The composition of the alteration phase formation as a function of location on the pellet surface is also under investigation. Drip tests with nominal-burnup irradiated UO_2 fuels have been underway for nearly 5 years. It was found that several radionuclides in the fuel matrix (U, Np, and Pu) accumulate in the alteration phases on the fuel surface, whereas the technetium is highly soluble. Work has started on vapor tests with clad samples to determine if the alteration phases

have the ability to split the cladding. Drip tests on clad segments have also been initiated to determine the tortuosity of water flow through the fuel rods. High-burnup fuel has been characterized and is being tested to determine if the altered structure of the fuel caused by prolonged irradiation will affect its dissolution properties.

The DOE is considering several alternatives for the disposal of excess plutonium resulting from the dismantlement of nuclear weapons. One alternative is immobilization, where the plutonium is fixed in a stable waste form. A titanate-based ceramic has been selected as the preferred waste form. Researchers in CMT investigated the effect of carbon in the waste stream on the densification of this waste form. It was determined that residual carbon levels had to be held below 3 wt%. Several types of corrosion tests (MCC-1, product consistency, vapor hydration) with a Ba-Zr, zirconolite-rich ceramic indicated that, upon dissolution, this material releases elements incongruently, and that the corrosion rate depends on the test duration and type. The test results will be used in development of a qualitative corrosion model.

Waste glass testing under unsaturated conditions was conducted to support models being developed for the release rate of radionuclides as solutes and colloids when waste glass is eventually contacted by dripping water or humid air in the repository. Studies indicated that the water volume in a standard hydration test does not lead to an upper bound on the thickness of the alteration layer. This occurs at a slightly lower water content. An upper bound on the alternative layer thickness occurs under conditions not relevant to a repository. In other work, MCC-1 tests were conducted on two glasses (LD6-5412 and PNL 7668) to expand the compositional range of glasses with measured forward reaction rates. These rates along with others in the data base were used to determine input parameters for a glass dissolution model. The results from previous corrosion tests have been used for modeling colloid formation during glass dissolution.

A glass-bonded sodalite waste form is being proposed to immobilize salt wastes generated during the electrometallurgical treatment of EBR-II fuel. Preliminary testing is in progress to evaluate the response of this waste form in standard tests, determine the mechanisms of corrosion, obtain data to support mechanistic models of its corrosion behavior, and develop a method for monitoring the consistency of the waste form over the range of processing variables. Tests conducted to date suggest that the glass-bonded sodalite dissolves at a rate similar to high-level waste glasses in highly dilute solutions, but has a much lower solubility than waste glasses. Ceramic waste form materials with added U, Pu, and fission products were characterized by electron microscopy. The $(U,Pu)O_2$ clusters were found to cluster in the glass phase at the phase boundaries. Tests are underway to determine if the presence of the actinides modifies the ceramic waste form behavior, and whether the PuO_2 is released in a colloidal form.

Fundamental studies on actinide behavior have concentrated on the interaction of subsurface microbes with the actinides, actinide stability, and actinide oxidation states in both the waste forms and alteration products that form on the surface. Two studies were completed on the radiotoxicity of actinides toward soil bacteria. The emphases was on studying the fate of neptunium because its migration and release from waste sites could constitute a long-term health risk. Neptunium speciation studies in microbiological systems were also extended to investigate the fate of neptunium in sulfate-reducing bacteria under anaerobic conditions. The Advanced

Photon Source at Argonne was used to determine the oxidation state of aqueous, absorbed, and solid actinides important to environmental and nuclear waste issues.

The DOE has contracted British Nuclear Fuels, Ltd. (BNFL), to vitrify tank wastes at the Hanford, Washington, site. Researchers in CMT are evaluating the durability of low-activity waste glasses being developed by BNFL in support of the performance assessment of the proposed low-level disposal system at Hanford. Also, CMT researchers have formulated test methods for low-activity product acceptance that will be used by DOE in acceptance testing of the waste products. They are working with the American Society for Testing and Materials to develop standards for waste-form testing and extension of the dry storage of spent fuel. Fundamental studies are being conducted to determine the effects of radiation on crystalline waste forms.

The Division's R&D has three major thrusts in separation science and technology: (1) substitution of low- for high-enriched uranium in the production of ^{99}Mo, (2) treatment of radioactive, mixed, and hazardous waste, and (3) novel applications of separation science to industrial processes.

As part of the first effort, we are working to convert all current processes, worldwide, from high- to low-enriched uranium. The program is international, with ongoing and new initiatives with partners in Indonesia, Canada, the United States, Korea, Australia, and Argentina. Our particular research deals with fabricating and dissolving the new targets and converting current processes to allow the use of low-enriched uranium. A new target was designed and tested that is significantly cheaper to fabricate than older designs and has improved cooling capabilities. After irradiation in Indonesia, the targets were processed and purified in satisfactory manner, producing an acceptable product. In cooperation with Argentina, we are in the process of modifying their current process to accept the new target. In other work, an alkaline-side cesium-extraction process for solvent extraction was pursued in cooperation with Oak Ridge National Laboratory, the Savannah River Technical Center, and the Savannah River Site. New flowsheets were developed that reduced the number of contactor stages for ^{137}Cs removal from 30 to 18. A significant effort is also underway to develop a magnetically assisted chemical separation process for treatment of several waste-treatment feed streams and a novel decontamination solvent for decontamination of stainless-steel reactor components. Significant success has been achieved in both areas. Research on aqueous biphase separations and rheological controls is also being pursued.

Electrometallurgical Treatment Technology

The CMT Division is developing an electrometallurgical process for treatment of spent nuclear fuels. It is capable of handling most types of spent fuel and is especially intended for fuels at risk of chemical reaction with the groundwater in the repository. The central feature of the electrometallurgical treatment is electrorefining of the spent fuel in a molten salt electrolyte at 500°C. An effort has been underway for several years to develop an advanced electrorefiner having high throughput (>40 kg uranium per hour) for treating large quantities of spent fuel. Effort this past year focused on determining the operating procedure and conditions that would provide sustained operation of the high-throughput electrorefiner that will be used to treat EBR-II

fuel in the Fuel Conditioning Facility at ANL-West. In tests at ANL-West, the operating procedure developed in tests at ANL-East achieved a throughput rate of 167 g uranium per hour, which is sufficient to meet the goal set for the demonstration phase of this effort. Further development work is needed to meet the goal of 450 kg/month set for the treatment phase.

After electrorefining, the fuel cladding and fission products will be placed in two stable waste forms (one a ceramic, the other metal), which are suitable for disposal in a geologic repository. There are no other high-level wastes, and only negligible amounts of low-level waste are generated. The ceramic waste form contains the transuranic elements and the most easily oxidized fission products that accumulate in the electrorefiner salt. The reference ceramic waste form is a sodalite-glass composite. Hot isostatic pressing was initially developed as the consolidation method for this material, but there are several logistical problems with implementing this method in a remote-operation hot cell. A pressureless consolidation method has been developed as an alternative. This method appears amenable to remote processing and employs simple powder preparation and handling techniques. The largest sample produced thus far by pressureless consolidation is 26 kg with a diameter of 26 cm and height of 4 cm. A full-scale waste form is expected to have a mass of ~250 kg. Work is now in progress on conceptual design of full-scale processing equipment and facilities.

Several conclusions were reached from both experimental and theoretical studies on producing a ceramic waste form: the cation size of sodium and the prominent fission products from the spent fuel will play a significant role when the waste salt is incorporated into a zeolite structure, the uranium chloride in the waste salt will not react with the zeolite, and the uranium and plutonium chlorides in the waste salt will form very fine oxide particles.

In the metal waste form, those components of the high-level waste that are chemically unaffected by the electrometallurgical process—cladding hulls, zirconium alloying additions, and noble metal fission products—are combined with small amounts of particulate materials from electrolyte filters and melted to form a highly durable waste form. Work in the past year was done in support of the demonstration project with spent EBR-II fuel. The baseline metal waste form for this fuel is stainless steel-15 wt% zirconium (SS-15Zr). Synthesis and analysis of various SS-Zr compositions indicated that the SS-15Zr waste form can readily accommodate the noble metal fission products and actinides from the EBR-II fuel. However, fission-product rich phases may be present in alloys containing $\leq$5 wt% zirconium. The present emphasis is on qualification of the metal waste form for geologic disposition. A wide variety of earlier experiments point to the corrosion mechanism of the metal waste form being oxidation and passivation through the formation of a thin adherent surface layer. Future work will be focused on quantifying this corrosion behavior for use in developing a predictive model required for repository qualification.

The electrometallurgical treatment of spent oxide fuels requires that the oxides first be reduced to metals that can be processed in an electrorefiner. A lithium reduction process has been selected to convert the spent oxide fuels into metals. During the past year, work continued to develop both the reduction and the salt-recovery portions of this process. Laboratory-scale experiments demonstrated that the lithium reduction process can handle a wide range of fuel morphologies: from relatively large, intact UO_2 fragments inside cladding hulls to fragments of

UO_2 dislodged from the cladding, including very small particles. Both laboratory- and engineering-scale experiments showed that a porous stainless steel crucible would hold the fine particle sizes (<45 μm) during reduction. Preliminary experiments also indicated that SnO_2 could be employed to replace the costly platinum now used as the anode material in the electrowinning cell employed for salt recovery. In addition, laboratory-scale experiments indicated that a Li-Al alloy could be used for reducing the concentrations of uranium, plutonium, and rare earth chlorides to very low values in the waste salt from electrometallurgical treatment of spent fuel.

Basic Chemistry Research

Basic chemistry research is being pursued on fundamental issues that relate to physical organometallic chemistry (more specifically, homogeneous catalysis and ion transport mechanisms in electrochemical devices), heterogeneous catalysis, processing and characterization of high-critical-temperature superconducting materials, and the decontamination of radionuclide-contaminated materials.

The activities in physical organometallic chemistry continue to emphasize (1) *in situ* spectroscopic investigations of the chemistry associated with the conversion of some key industrial homogeneous catalytic processes to more energy-efficient and more environmentally benign supercritical ones, (2) synthesis and high-pressure studies of new catalysts to develop an aqueous-phase version of the Shell process for the hydroformylation of olefins, and (3) the investigation of ion transport mechanisms relevant to the lithium-polymer electrolyte battery by means of advanced spectroscopic methods.

Experimental studies have shown that supercritical CO_2 solutions containing high concentrations of relatively pure monomeric formaldehyde are easily made by heating solid paraformaldehyde in CO_2 near its critical density. Earlier research had shown that use of the supercritical fluid avoids the troublesome homologation of byproduct alcohols, and this new process is being testing for other potential benefits.

The development of homogeneous catalysts for use in aqueous phase processes that normally use organic solvents is both challenging and highly desirable from both a cost and environmental perspective. Researchers in CMT have been studying the hydroformylation of olefins using water-soluble, phosphine-modified cobalt catalysts. Early tests with a water-soluble sulfonated arylphosphine revealed that ligand displacement by CO is a problem with use of this type of ligand. Experiments with more basic aliphatic ligands are planned.

The goal of the advanced battery project is to investigate the mechanism(s) of ion transport in lithium-polymer electrolyte battery materials by using a new *in situ* magnetic resonance imaging technique developed earlier. Recently, CMT researchers demonstrated a new method of collecting images that provides a substantial improvement in the data acquisition time. This new data collection method is able to follow fast kinetic processes that occur on or near the working electrode by rapidly collecting repetitive images. Significantly, this method achieves the same distance resolution, 2 μm, as the original rotating frame imaging method, yet on a millisecond time scale.

In heterogeneous catalysis research, fundamental analysis methods have been integrated with reactor studies to improve the general understanding of catalysis. In the area of desulfurization, careful control of pore diameters of the catalyst supports to match feed characteristics has allowed us to develop catalysts that are more selective for sulfur removal. In our etherification work, the increased acidity created by sulfonating γ-Al_2O_3 has been shown to produce a more active catalyst. In the selective oxidation of benzene to phenol, our understanding of the redox potentials of the supported catalysts is leading the way toward catalysts that have sufficient oxidizing power to catalyze benzene without over-oxidation to CO_2.

The research on high-critical-temperature superconducting materials continues to focus on the development of the silver-sheathed $(Bi,Pb)_2Sr_2Ca_2Cu_3O_x$ (Ag/Bi-2223) composite conductor in multifilament form. The aim of this work is to explore novel processing methods that lead to improved performance in terms of current-carrying capacity under conductor operating conditions that prevail in electric power devices. During the past year, a new method has been demonstrated for producing Bi-2223 in a silver sheath with an extended grain colony microstructure of the type required to obtain high critical current densities in long-length wire. This method is based on the decomposition of a fully-sheathed, fine-grained Bi-2223 precursor and the subsequent reformation of the Bi-2223 phase under heat treatment conditions that produce the desired contiguous large-grain microstructure.

Highlights of research exploring the mechanisms by which radionuclides incorporate into metal/metal oxide surfaces have included (1) the observation that U(VI) does not readily exchange into and occupy lattice sites in the types of passive films that tend to form on nickel (and nickel alloy) surfaces and (2) the stabilization and X-ray spectroscopic characterization of Fe(VI) produced under strongly alkaline conditions. The general findings of this work over the past three years have provided seminal insights that connect the relative difficulty of removing heavy metal cations from passivated surfaces with the nature of their complexation and the degree of substitution of the heavy metal cation into the passive film.

Analytical Chemistry Laboratory

The Analytical Chemistry Laboratory (ACL) is administratively within CMT, its principal client, but collaborates as a full-cost-recovery service center with many technical divisions and programs at ANL. In addition, the ACL conducts research in analytical chemistry and provides analytical services for governmental, educational, and industrial organizations.

During the past year, ACL was involved in a diverse array of analytical activities. These included analyses in support of the Argonne projects to develop an electrometallurgical treatment for spent nuclear fuels; preparation and characterization of simulated waste samples in support of the Waste Isolation Pilot Plant; participation in a comprehensive program to provide DOE with information on data quality from laboratories analyzing environmental and waste samples; preparation of osmium-189 targets for photon excitation studies; analysis of environmental samples submitted for the determination of hazardous or radiological components; analysis of lithium aluminate prepared for use in tritium production targets, as well as development of improved methods for this analysis; analysis of chemical warfare agents for the U.S. Army; development of a method for detecting halide impurities in refractory materials; and

identification of volatile and semivolatile byproducts produced by new lubricants developed to reduce the friction between rail tracks and locomotive wheels.

I

Electrochemical Technology

A. Advanced Battery Research and Development

Rechargeable lithium-ion batteries are becoming increasingly popular as power sources for consumer electronics, such as cellular phones, camcorders, and laptop computers. Because of the commercial success of these batteries in this market, they are being seriously considered for other applications that require high energy and power density, combined with long life.

The advanced battery program in the CMT Division is involved in the research and development of lithium-ion and lithium-polymer batteries, as well as lithium battery materials. The program focuses on the development of advanced rechargeable lithium battery systems that are acceptable for electric vehicles (EVs) and hybrid electric vehicles (HEVs). Complementary R&D is being conducted on lithium-based cells and batteries for industrial partners with interests in a variety of other applications.

1. High-Power Lithium-Ion Batteries for HEVs

Through the Partnership for a New Generation of Vehicles (PNGV) program, the federal government and the U.S. auto industry are working together to develop a passenger car with a fuel economy of 80 mpg. In the area of energy storage, the PNGV is focusing its R&D efforts on high-power lithium-ion batteries. These batteries would meet the energy storage requirements for leveling the load on a prime power source and for capturing regenerative braking energy. The CMT Division is playing a key role in these R&D efforts.

The PNGV sponsors industrial R&D projects on this technology with several industrial developers. These firms demonstrated that lithium-ion batteries are capable of meeting the performance and cycle life requirements for this application, but barriers to commercialization remain in the areas of calendar life, abuse tolerance, and cost. To reduce the R&D risk associated with overcoming these barriers, DOE's Office of Advanced Automotive Technologies established a technical support program at DOE's national laboratories, called the Advanced Technology Development Program. Argonne is the lead laboratory, and the other participants are

Brookhaven National Laboratory (BNL), Idaho National Engineering and Environmental Laboratory (INEEL), Lawrence Berkeley National Laboratory (LBNL), and Sandia National Laboratories (SNL).

The program has two major objectives: (1) to develop, demonstrate, and validate diagnostic tools that can identify the factors that limit calendar life and abuse tolerance, with a view to assisting in the development of practical solutions and (2) to develop innovative solutions for reducing cell costs. The program consists of the following five projects:

- Development and evaluation of baseline (Gen 1) cells
- Diagnostic evaluation of Gen 1 cells
- Development of second-generation (Gen 2) cells
- Development of advanced materials for third-generation (Gen 3) cells
- Development of low-cost cell packaging

The first two projects focus on the development of a high-power baseline cell chemistry (employing commercially available materials), fabrication and accelerated calendar-life testing of Gen 1 cells (cylindrical-wound design), and diagnostic evaluations of these cells to identify the factors limiting their calendar life and abuse tolerance. The next two projects involve sequential iterations on the baseline cell technology (Gen 2 and Gen 3 cells) that incorporate feedback from the diagnostic evaluations, with the aim of providing improved cell chemistries and further validation of the diagnostic tools. Additionally, lower cost materials and lower cost processing are secondary goals for the Gen 2 and Gen 3 cell technologies. The last project targets the development of unique approaches for reducing the costs associated with packaging full-size, high-power lithium-ion cells for HEVs.

a. Development and Evaluation of Baseline (Gen 1) Cells

To study the technical barriers of abuse tolerance and calendar life, it is necessary to have detailed knowledge about the cell chemistry, as well as cell performance, life, and safety characteristics. Because it is not possible to share cell technology from one industrial developer with the other developers, one objective of this project is to rapidly develop a baseline high-power lithium-ion cell chemistry, based on commercially available materials, that all the developers can use.

Argonne screened many commercially available $LiNi_{0.8}Co_{0.2}O_2$ positive electrode, graphite negative electrode, electrode additive, and binder materials as potential candidates for use in Gen 1 high-power cells. Electrode and additive materials were characterized for their particle shape, size distribution, and chemical homogeneity. Promising materials were processed into electrodes and evaluated in 32-cm^2 laboratory cells that employed conventional electrolytes [mixtures of ethylene carbonate with either diethyl carbonate or dimethyl carbonate (EC:DEC or EC:DMC) with 1 M $LiPF_6$ salt]. Reversible and irreversible capacity density, rate capability, and

reactivity with the electrolytes (through differential scanning calorimetry [DSC]) were established for each material. Combinations of the best materials were engineered into optimal high-power electrodes. The chemistry selected for use in Gen 1 cells is summarized in Table I-1. The unit cell performance characteristics (e.g., area specific impedance [ASI]) obtained from these cells were used to establish engineering specifications for the high-power cylindrical-wound cells. The specifications were calculated by using an ANL-developed spreadsheet cell design model. Figure I-1 shows ASI values during 18-s high-current discharge and 2-s high-current charge pulses as a function of depth of discharge. Argonne's battery design model was used to establish the target discharge and charge ASI values (35 and 25 $\Omega \cdot cm^2$, respectively) needed to meet the PNGV power-assist HEV battery requirements. Argonne contracted with an industrial firm to fabricate 300 high-power cells, using the Gen 1 cell chemistry, and the 300 cells were distributed to participating DOE laboratories.

A second objective of this project is to establish the performance, life, and thermal abuse characteristics of these Gen 1 cells. Argonne is working with INEEL and SNL to conduct the accelerated calendar-life tests, while SNL is conducting the thermal abuse tests. The life test matrix for the Gen 1 cells distributes 135 cells over three states of charge (80%, 60%,

Table I-1. Baseline Cell Chemistry

Positive Electrode	Electrolyte	Negative Electrode	Separator
84 wt% $LiNi_{0.8}Co_{0.2}O_2$ 8 wt% PVDF binder 4 wt% SFG-6 graphite 4 wt% carbon black	1 M $LiPF_6$ in EC/DEC (1:1)	75 wt% MCMB-6 graphite 16 wt% SFG-6 graphite 9 wt% PVDF binder	37-μm-thick polyethylene, Celgard
PVDF: polyvinylidene fluoride EC: ethylene carbonate DEC: diethyl carbonate			

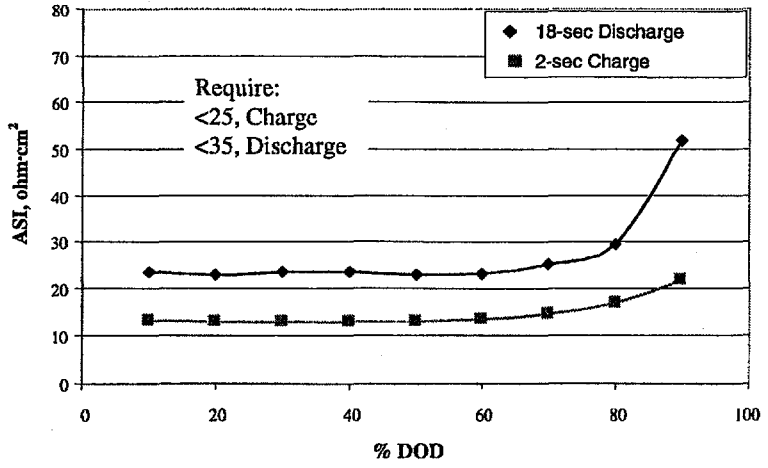

Fig. I-1. Area-Specific Impedance (ASI) versus Depth of Discharge (DOD) for a Gen 1 cell. Results show the Gen 1 cell chemistry readily achieves the ASI values required for a power-assist HEV battery.

and 40% SOC), four temperatures (40°C, 50°C, 60°C, and 70°C), and four life-cycle profiles (0%, 3%, 6%, and 9% ΔSOC pulse profiles). New, mid-life, end-of-life, and thermally abused cells will be provided to the diagnostic laboratories.

b. Diagnostic Evaluation of Gen 1 Cells

The primary objective of the diagnostic work is to determine the structural and chemical changes that lead to performance degradation, including catastrophic failure, as well as the factors that control the abuse tolerance of cells. Because of the varied nature of the cell component materials and the degradation products, many diagnostic techniques are being evaluated. One objective is to identify the most effective and efficient diagnostic techniques, and a second objective is to elucidate the key properties of the starting materials that determine battery performance and life. The results will be used as a guide to develop improved (Gen 2 and 3) cell chemistries.

The diagnostics team draws upon the expertise and special equipment at four national laboratories (ANL, BNL, LBNL and SNL). Table I-2 summarizes the diagnostic techniques that are being studied for their applicability. These diagnostic methods are being applied to new and tested lithium-ion cells, as well as to cell materials, as-prepared cell components, and components from fresh and tested cells, to identify degradation and failure mechanisms. A combination of thermal analysis techniques and the diagnostic methods is being used to identify the mechanism(s) of thermal runaway in cells. Real-time sharing of diagnostic data among the laboratories facilitates feedback to the Gen 2 cell and Gen 3 materials R&D efforts and enhances the effectiveness, efficiency, and coordination of the diagnostic team. Over the next two years, these techniques and procedures will be refined and applied to Gen 2 and 3 cells and cell components, with the end result being an optimal set of diagnostic techniques and procedures.

c. Development of Second-Generation (Gen 2) Cells

Although the Gen 1 cell chemistry is capable of providing adequate high-power performance at room temperature for meeting the PNGV requirements for a fast-response engine, it is known to suffer from poor low-temperature performance and insufficient abuse tolerance and calendar life. The objective of this project is to develop a second-generation cell chemistry that exhibits improved low-temperature performance, calendar life, abuse tolerance, and/or cost effectiveness over the Gen 1 cell chemistry. On this project, ANL is working in collaboration with the Illinois Institute of Technology (IIT) and the Army Research Laboratory (ARL).

Argonne is procuring and evaluating advanced materials and components that are being developed by chemical supply companies, both domestic and foreign, for use in the next generation of lithium-ion consumer batteries. The following types of advanced materials are being evaluated for use in Gen 2 cells: new graphites (some of which are surface treated), doped lithium nickel cobalt oxides, soft nonfluorinated binders, electronic additives, and coated current collectors. Candidate electrode, additive, and binder materials are chemically and physically

Table I-2. Matrix of Diagnostic Techniques

Source of Degradation	Technique
Electrolyte decomposition and reactions	GC/MS, TGA, HPLC, DSC, ion chromotography, CE, ARC, microcalorimetry, voltammetry
Current collector corrosion	SEM
Electrode structural/chemical changes	SEM, Raman spectroscopy, XRD, XAS, ATRIR, AEA, ISVS, microelectrode techniques, EIS
Electrode delamination	Sonography, SEM, EIS, post-test inspection
Cathode dissolution	XRD, ICP, AAS, SEM with EDAX
Separator breakdown	Separator swapping, mechanical tests, BET, flow porometry
Binder breakdown	SEM, AFM, FTIR, BET
Solid-electrolyte-interface (SEI) layer formation and dissolution	CSAFM, Raman spectroscopy, EIS, SE, ATRIR, HRTEM, ARC, microcalorimetry, DSC

Key

AAS – atomic absorption spectroscopy
AEA – acoustic emission analysis
AFM – atomic force microscopy
ARC – accelerating rate calorimeter
ATRIR – attenuated total reflectance infrared spectroscopy
BET – Brunauer-Emmett-Teller measurements
CE – capillary electrophoresis
CSAFM – current-sensing atomic force microscopy
DSC – differential scanning calorimetry
EDAX – energy dispersive analysis by X-ray
EIS – electrochemical impedance spectroscopy
FTIR – Fourier transform infrared spectroscopy
GC/MS – gas chromotography/mass spectroscopy
HPLC – high pressure liquid chromotography
HRTEM – high resolution transmission electron microscopy
ICP – inductively coupled plasma
ISVS – *in-situ* vibrational spectroscopy
SE – spectroscopic ellipsometry
SEM – scanning electron microscopy
TGA – thermo-gravimetric analysis
XAS – X-ray absorption spectroscopy
XRD – X-ray diffraction

characterized, processed into electrodes, characterized electrochemically (by means of PNGV high-power test procedures), and evaluated for their reduced chemical reactivity with the Gen 1 electrolyte (using DSC). In the electrolyte area, ANL is working with ARL to develop a multisolvent (ethylene carbonate, ethyl methyl carbonate, and propylene carbonate) electrolyte system, with $LiPF_6$ salt in concentrations >1 M. A 1.2 M $LiPF_6$ in EC/EMC (1:4 ratio) electrolyte system was developed that exhibits significantly improved performance at temperatures below 0°C, as compared to the 1.0 M $LiPF_6$ in EC/DEC Gen 1 electrolyte (Fig. I-2). This electrolyte system is currently the leading candidate for use in the Gen 2 cells. In the next year, the final Gen 2 cell chemistry will be selected and scaled up to the cylindrical-wound cells, at which time it will be evaluated thoroughly in a manner similar to that used to evaluate the Gen 1 cell chemistry.

d. Development of Advanced Materials for Third-Generation (Gen 3) Cells

The objective of this project is to develop new materials that are tailored to overcome the sources of the calendar life and abuse tolerance limitations of lithium-ion cells, while simultaneously addressing the need for low cost in both the starting materials and their

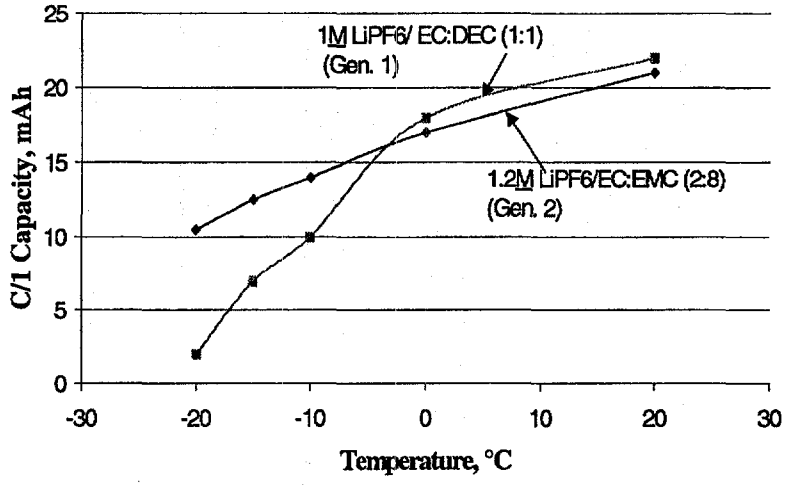

Fig. I-2. Cell Capacity versus Temperature for Cells Employing the Same Electrodes but Different Electrolytes. The 1.2 M $LiPF_6$ in EC/EMC (2:8) electrolyte system developed by ANL and ARL possesses significantly higher ionic conductivity at temperatures below 0°C and thus a higher delivered cell capacity.

processing. Additionally, advanced materials developed by other sources will continue to be evaluated as potential Gen 3 cell materials. Feedback from the diagnostic work is being used to guide this materials development project.

Initially, ANL is focusing its efforts on developing an improved positive electrode material. An approach based on selective, low-level multidoping of lithium nickel oxide offers opportunities to enhance both the rate capability and the chemical and structural stability of the positive electrode while also reducing its chemical reactivity with the electrolyte. Argonne is studying four synthesis approaches to identify the best preparation method for producing a multidoped $LiNi_{1-x}Co_yAl_zMg_eO_2$ material that possesses the desired product phase purity, morphology and particle size control, and, most importantly, the proper ordered structure. The four processes are co-precipitation-ion exchange, sol-gel, steam denitration, and solution combustion reaction. Preliminary results show that the electronic conductivity can be increased by more than two orders of magnitude by substituting 5% magnesium for cobalt. The Gen 3 cell chemistry is scheduled to be scaled up to cylindrical-wound cells in early 2001 and evaluated in a manner similar to that used to evaluate the Gen 1 and Gen 2 cells.

e. Development of Low-Cost Cell Packaging

To meet the PNGV production cost target of $300/battery (at a production rate of 100,000 units/year) for an HEV with a fast response engine, analyses indicate that the cost of a 10-Ah cell should be about $5.50. Such a cell currently costs about $30. Assuming design refinements and volume production, the industrial developers are projecting that they can reduce

costs to about $9/cell. The objective of this project is to develop innovative methods for reducing cell costs to meet the PNGV target. Near-term and longer term approaches are being pursued.

The near-term approach consists of developing a new, one-piece current-collector/feedthrough system in which the feedthroughs are connected to the cell cover by means of compression seals. The cover is designed to seal to the cell can via a simple crimping operation. This system is designed for low resistance and effective heat transfer (to facilitate thermal management). Argonne developed designs for 10-Ah cylindrical and flat-wound cells. The designs employ current-collection shoes that collect current from each wrap of the positive and negative current-collector foils and deliver the current to the terminal feedthroughs. The flat-wound design appears to have advantages over the cylindrical design because of reduced assembly costs and better heat transfer.

The longer term approach consists of developing a low-cost, flexible cell container based on plastic lamination technology. The concept is to fabricate a pouch-type container, consisting of a metal-alloy foil, that forms the support base for applying polymeric coatings. The different layers of the laminate provide barriers to different chemical species and/or contribute to the seal. The development of laminated pouch cell containers is being carried out in collaboration with industrial partners. An expert in plastic packaging technology is providing consulting services on the best materials to use for the air, moisture, electrolyte, and hydrogen fluoride barrier layers; recommending layer thicknesses; and helping to identify qualified laminate fabricators and permeation/strength testing service providers. Nondisclosure agreements were implemented with three fabricators, and discussions were initiated with them to fabricate several baseline laminates.

2. *Lithium-Polymer Electrolyte Battery System for Electric Vehicles*

The lithium-polymer battery (LPB) is a lightweight, high-energy system that can operate at moderate temperatures (typically 60-80°C). With a polymer electrolyte, this all-solid-state battery can be manufactured by using high-speed film-laminate technology. The battery's low weight translates into high specific energy. The Li/Li^+ redox reaction (negative electrode, -3.0 V) gives the battery its high power. The positive electrode is a reversible chemical host for intercalating lithium cations. Thus, during discharge, the lithium cations insert into the host material with simultaneous electrochemical reduction of the host's closest-neighbor redox sites. The host structure is highly reversible to both redox and insertion reactions; this allows the lithium cations to exit upon recharge.

The LPB for electric-vehicle applications is being developed under a Cooperative Research and Development Agreement (CRADA) with 3M and Hydro-Québec. Under the CRADA, ANL presently provides technical support in three main areas: electrochemical characterization and modeling, prototype testing and evaluation, and electrode materials development.

Electrochemical modeling of lithium-polymer cells is being conducted to elucidate the phenomena occurring in the cells during operation. This work involves simultaneously solving

differential mass, charge, energy, and momentum balances on every species in each phase and component of the fundamental electrochemical cell. Verifying such calculations experimentally is challenging because of the composite structure of the cathode and the thin cell geometry. Both factors make it difficult to separate phenomena occurring at the cathode from those occurring in the electrolyte.

An important part of our electrochemical modeling and characterization work is quantifying the transport properties of possible electrolytes for LPB technology. We have chosen to model the polymer electrolyte on the basis of concentrated solution theory. We have demonstrated that all the transport and thermodynamic parameters for a binary salt dissolved in a polymer electrolyte can be obtained with only two sets of experiments: AC impedance studies on symmetric cells and potential measurements on concentration cells. This approach has been suggested previously in the literature but not generally adopted by the technical community.

One such study was conducted with a binary lithium salt, $LiN(CF_3SO_2)_2$, dissolved in a dry polyether copolymer. Symmetric (Li/polymer/Li) cells were built to determine the electrolyte conductivity and salt diffusion coefficient over a range of temperatures (40-100°C) using an AC impedance technique. Duplicate cells and cells made with a double layer of polymer electrolyte laminate were also assembled and examined. These cells were used as an internal check on the standard set of cells and to help identify the complex arcs of the AC impedance results. The change in the salt diffusion coefficient and conductivity as a function of salt concentration in the electrolyte is shown in Fig. I-3. Also shown is the second-order polynomial fit of data used in the model. The AC impedance studies were combined with concentration cell ($Li/polymer_1/polymer_2/Li$) measurements to quantify the cation transference number and the activity coefficient of the salt in the electrolyte.

After the AC impedance studies were conducted, sample symmetric (Li/polymer/Li) cells were chosen for use in DC polarization studies. The symmetric cell potential was monitored

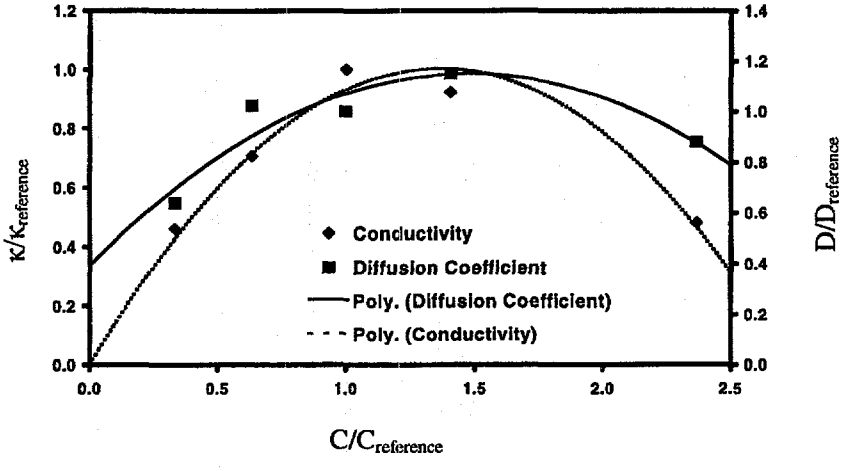

Fig. I-3. Dependence of Conductivity (κ) and Salt Diffusion Coefficient (D) on Electrolyte Salt Concentration (C) in a Polymer Electrolyte. Curves represent second-order polynomial (poly.) fit of data.

as increasing current steps were applied to a cell in alternating directions. The currents applied to the cells ranged from relatively low levels to a value greater than the mass-transfer-limiting current at steady state. A comparison of the electrochemical model simulations and DC polarization studies on one of the Li/polymer/Li cells is given in Fig. I-4. In general, the agreement between theory and experiment is quite good. The most significant difference occurred near the limiting current, at about 2200 s. The difference may be due to the effects of the high salt concentration gradient on the measured transport properties or to surface effects related to the plating rate of the lithium.

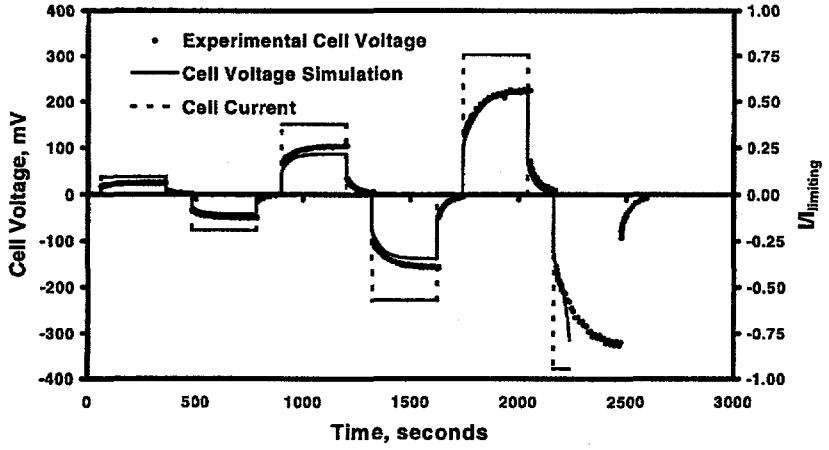

Fig. I-4. Comparison of Simulated and Measured Voltage Responses to Current Steps on a Li/Polymer/Li Cell

3. Materials Research

The exponential growth in the electronics industry is driving demand for cheaper, lighter, and more powerful rechargeable lithium batteries. The objective of this work is to find and develop new or improved electrode materials for these batteries. A specific goal is to find an alternative electrode to the present cathode material of choice, $LiCoO_2$, a material that is not only expensive but also unstable at high states of charge when lithium is extracted from the structure. Research at ANL has focused on developing manganese oxide cathode materials, specifically, those with a spinel-related structure.

One promising spinel is $Li[Mn_2]O_4$.[1-3] However, a disadvantage of $Li[Mn_2]O_4$ is that the electrode loses capacity on cycling, which limits the life of the cell.[3-5] The capacity loss is

[1] T. Ohzuku, M. Kitagawa, and T. Hirai, *J. Electrochem. Soc.* **137**, 769 (1990).

[2] J. M. Tarascon, E. Wang, F. K. Shokoohi, W. R. McKinnon, and S. Colson, *J. Electrochem. Soc.* **138**, 2859 (1991).

[3] R. J. Gummow, A. de Kock, and M. M. Thackeray, *Solid State Ionics* **69**, 59 (1994).

[4] G. G. Amatucci, C. N. Schmutz, A. Blyr, C. Sigala, A. S. Gozdz, D. Larcher, and J. M. Tarascon, *J. Power Sources* **69**, 11 (1997).

[5] A. Blyr, C. Sigala, G. G. Amatucci, D. Guyomard, Y. Chabres, and J. M. Tarascon, *J. Electrochem. Soc.* **145**, 194 (1998).

particularly noticeable at 50°C, which is a typical temperature that can be reached in devices such as laptop computers. It is well known that the cycle life of lithium-ion cells depends critically on the structural integrity of the host electrode structures during charge and discharge.[6] Several reasons have been proposed[3-5] for the capacity loss of 4-V $Li/Li_x[Mn_2]O_4$ cells:

1. Solubility of the spinel electrode in the electrolyte.

2. An instability of the delithiated spinel structure (for example, by oxygen loss) in organic electrolyte solvents at the top of charge.

3. The onset of an anisotropic distortion (Jahn-Teller effect) at the end of discharge (particularly at high current rates).

Most of the evidence reported thus far points to solubility at the top of charge as the major reason for the capacity fade in $Li/Li_x[Mn_2]O_4$ cells. No direct evidence had been obtained to support the hypothesis of structural fatigue, described in point 3 above, as a contributing factor to capacity loss. However, it has been proposed that, under dynamic, nonequilibrium conditions above 3 V, some crystallites can be more lithiated than others, with the result that the electrode structure at the surface of the crystallites transforms from cubic $Li[Mn_2]O_4$ to tetragonal $Li_2[Mn_2]O_4$.[3,6]

Therefore, to investigate the possibility that structural effects may also contribute to the capacity fade of $Li/Li_x[Mn_2]O_4$ cells, we initiated (in collaboration with Michigan Technological University) systematic studies of $Li_x[Mn_2]O_4$ electrodes using high-resolution electron diffraction and imaging. (Conventional powder X-ray and neutron diffraction techniques are not sufficiently sensitive for detecting such structural effects at the particle surface.) These studies yielded the first evidence that some of the capacity fade observed when high-voltage (4-V) $Li/Li_x[Mn_2]O_4$ cells are deeply discharged may be attributed to structural fatigue at the electrode surface.[7] These findings have implications for the development of stabilized $Li_{1+x}Mn_{2-x}O_4$ spinel electrodes ($0<x<0.1$).

Figures I-5a and I-5b show typical voltage profiles of $Li/Li_x[Mn_2]O_4$ cells in which the upper and lower voltage limits were 4.2-3.0 V, and 3.3-2.2 V, respectively. For clarity, only the first three cycles are shown. The data are consistent with earlier electrochemical studies of these materials[1-3] and clearly demonstrate that greater cycling stability is achieved in the upper voltage range.

The electron diffraction patterns of the $Li_x[Mn_2]O_4$ electrodes cycled in the lower voltage range, 3.3-2.2 V (i.e., over the range $1<x<2$), showed a two-phase electrode consisting of

[6] M. M. Thackeray, *J. Electrochem. Soc.* **142**, 2558 (1995).

[7] M. M. Thackeray, Y. Shao-Horn, A. J. Kahaian, K. D. Kepler, E. Skinner, J. T. Vaughey, and S. A. Hackney, *Electrochem. Solid State Lett.* 1(1), 7 (1998).

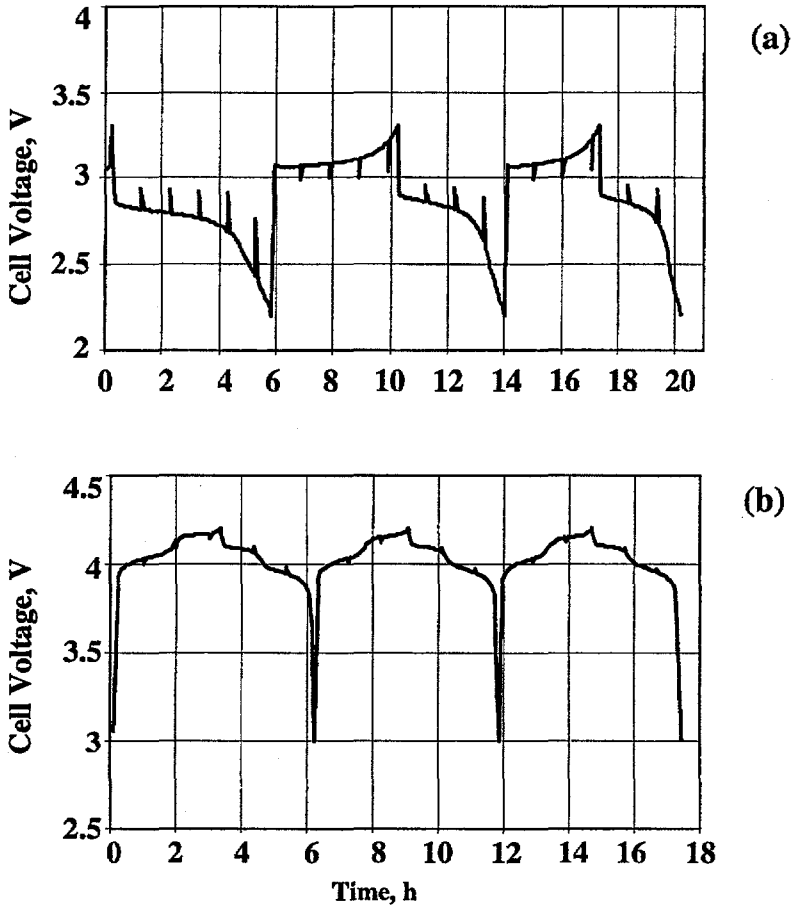

Fig I-5. Voltage Profiles for (a) the First Three Cycles of a $Li/Li_x[Mn_2]O_4$ Cell Charged and Discharged between 3.3 and 2.2 V and (b) a Similar Cell Charged and Discharged between 4.2 and 3.0 V. The spikes in the profiles indicate current interrupts.

cubic $Li[Mn_2]O_4$ and tetragonal $Li_2[Mn_2]O_4$, consistent with earlier X-ray diffraction studies.[8,9] Of particular significance, however, were the electron diffraction data of electrodes cycled in the high-voltage regions. Clear evidence of the tetragonal phase was found in cells discharged to 3.5, 3.3, and 3.0 V. Since these voltages are above the voltage expected for the onset of the Jahn-Teller distortion (2.96 V), this finding supports the hypothesis[3,6] that this damaging crystallographic effect can occur above 3 V under dynamic, nonequilibrium conditions; in fact, it can occur by as much as 500 mV above the thermodynamic value. A semiquantitative analysis of the electrodes by transmission electron microscopy showed, as expected, that the amount of the tetragonal phase increased on lowering the end voltage from 3.5 to 3.0 V. Fifty-five single-crystal electron diffraction patterns were obtained from $Li_x[Mn_2]O_4$ electrodes that had been

[8] M. M. Thackeray, W. I. F. David, P. G. Bruce, and J. B. Goodenough, *Mater. Res. Bull.* **18**, 461 (1983).

[9] A. Mosbah, A. Verbaere, and M. Tournoux, *Mater. Res. Bull.* **18**, 1375 (1983).

cycled between 4.2 and 3.3 V. Nine of these patterns (15%) could be indexed to the tetragonal $Li_2[Mn_2]O_4$ phase; high-resolution images showed that the tetragonal phase resided on the crystallite surface.

A high-resolution transmission electron micrograph of a spinel electrode crystallite extracted from a cell that had been discharged to 3.3 V is shown in Fig. I-6. The dark fringes in the image are associated with phase boundaries that separate the tetragonal phase at the surface of the crystallite from the cubic phase within the bulk. The structural differences within the crystallites were determined by convergent beam electron diffraction. Figure I-7a shows the <100> electron diffraction pattern of a typical parent $Li[Mn_2]O_4$ crystal from an uncycled cell. This pattern is consistent with the cubic symmetry of $Li[Mn_2]O_4$. The same cubic pattern was obtained from crystallites in all the cycled electrodes of this investigation. Electron diffraction patterns of cycled spinel crystallites also provided unequivocal evidence of the tetragonal $Li_2[Mn_2]O_4$ phase at the crystallite surface; see, for example, Fig. I-7b, which shows the pattern from a crystallite cycled in the range 4.2-3.3 V. (This pattern was obtained from the crystallite shown in Fig. I-6.) The absence of diffraction spots from the set of {220} planes and the non-equivalence of the (040) and (004) planes are consistent with the tetragonal rock-salt phase $Li_2[Mn_2]O_4$. The lattice parameters (a= ~8.0 Å, c= ~9.3 Å) obtained from these patterns are in good agreement with values previously determined by more accurate analyses of X-ray and neutron diffraction data of bulk powders of $Li_2[Mn_2]O_4$.[8-10]

For two reasons, the presence of $Li_2[Mn_2]O_4$ on the particle surface in discharged $Li_x[Mn_2]O_4$ electrodes may contribute to the capacity fade that has been observed during cycling of $Li/Li_x[Mn_2]O_4$ cells. First, $Li_2[Mn_2]O_4$ is a Mn^{3+}-rich spinel; it is likely, therefore, to dissolve in the electrolyte by a disproportionation reaction. Second, it is conceivable that the tetragonal phase may dissociate from the cubic phase of the bulk electrode, resulting in a loss of particle and electronic contact.

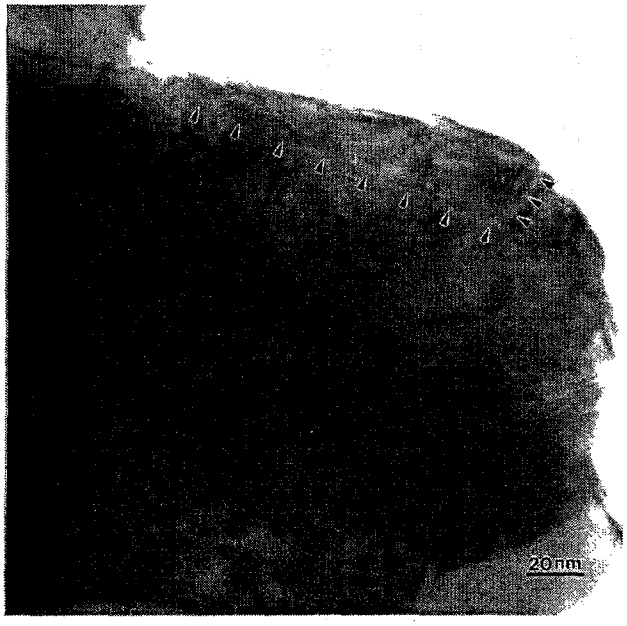

Fig. I-6.

Transmission Electron Micrograph of $Li_x[Mn_2]O_4$ Electrode Discharged from 4.2 to 3.3 V. The black lines (arrows) indicate the boundary between a tetragonal $Li_2[Mn_2]O_4$ crystal and a cubic $Li[Mn_2]O_4$ crystal.

[10]W. I. F. David, M. M. Thackeray, L. A. de Picciotto, and J. B. Goodenough, *J. Solid State Chem.* **67**, 316 (1987).

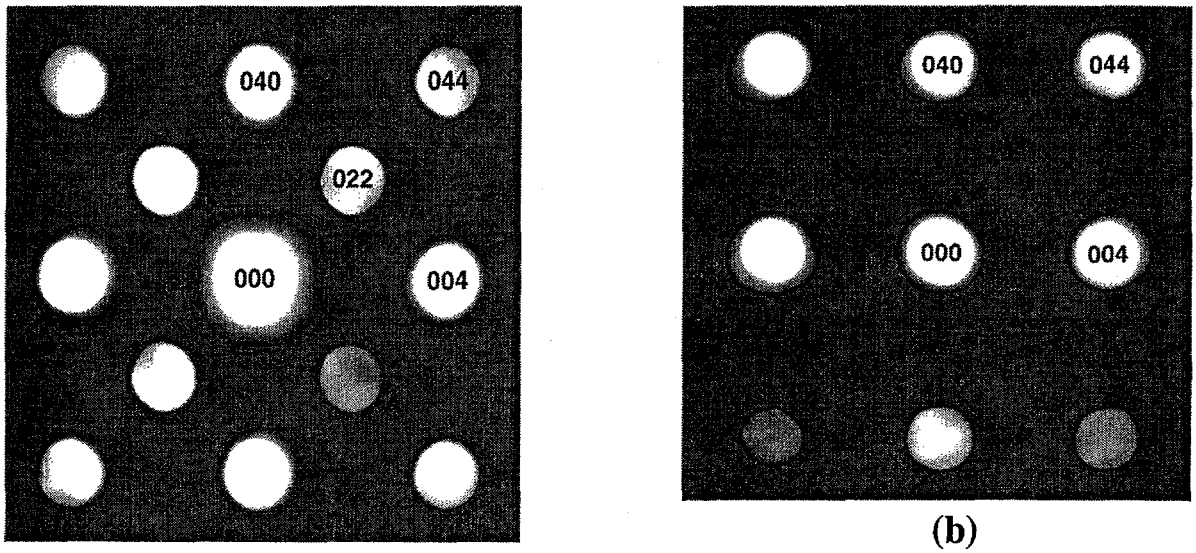

Fig. I-7. Convergent Beam Electron Diffraction Patterns ([100] zone axis) of (a) Cubic $Li[Mn_2]O_4$ (parent) Crystal and (b) Tetragonal $Li_2[Mn_2]O_4$ Crystal on the Surface of an Electrochemically Cycled Spinel Electrode (discharged from 4.2 to 3.3 V). Note that Fig. I-7 was obtained from the same crystallite as shown in Fig. I-6.

Gummow and co-workers have modified the composition of the spinel electrode by replacing a small fraction of the manganese by lithium in the structure to yield $Li[Mn_{2-x}Li_x]O_4$ (alternatively, $Li_{1+x}Mn_{2-x}O_4$), thereby significantly improving the cycling behavior of these cells.[3] The advantage of these modified electrodes, such as $Li_{1.05}Mn_{1.95}O_4$ (x=0.05), is that residual lithium remains in the structure to stabilize the electrode at the top of charge when the oxidation state of the manganese ions reaches 4.0 (i.e., at the composition $Li_{0.2}Mn_{1.95}O_4$). Moreover, at the end of discharge, for example, at 3.3 V, when the electrode approaches the stoichiometric spinel composition $Li_{1.05}Mn_{1.95}O_4$, the average oxidation state of the manganese ions (>3.56) is higher than it is in $Li[Mn_2]O_4$ (3.50). Gummow and co-workers, therefore, proposed[3] that this condition would prevent the immediate onset of the Jahn-Teller distortion, which occurs when the average manganese oxidation state reaches 3.5 and results in electrodes with higher performance.

We are now using transmission electron microscopy (TEM) techniques to investigate lithium-stabilized $Li_{1+x}Mn_{2-x}O_4$ electrodes. Preliminary data for $Li_{1.05}Mn_{1.95}O_4$ (x = 0.05) indicate that the electron diffraction patterns of the electrodes when discharged to 2.89 V are complex. Although it has not yet been possible to fully interpret these patterns, they seem to indicate strain and structural disorder in cubic spinel crystals. These patterns show no significant indication of a tetragonal phase on the surface of the particles, even when the end voltage of the cells is lowered to 2.89 V. These findings, therefore, provide strong support for the argument that electrodes with residual lithium (i.e., $Li_{1+x}Mn_{2-x}O_4$) have a cubic "buffer zone" that prevents the onset of the Jahn-Teller effect at the particle surface when the cells reach 3 V[3,6] and, therefore, that capacity fade due to structural fatigue in $Li_x[Mn_2]O_4$ electrodes toward the end of discharge can be mitigated by creating a more stable surface in modified $Li_{1+x}Mn_{2-x}O_4$ electrodes.

In future work, we will continue to identify new or improved electrode materials for lithium batteries and, at the same time, to study those factors that limit the performance of the batteries. Further effort is required to optimize the performance of $LiMn_2O_4$ electrodes by stabilizing the spinel, both with respect to lithium insertion and extraction and with respect to chemical stability with the organic-based electrolyte.

B. Electrochemical Analysis and Diagnostics Laboratory

The Electrochemical Analysis and Diagnostics Laboratory (EADL) was established at ANL to study advanced battery systems for applications such as EVs, HEVs, and electric load management for utilities. This facility has been cited as a valuable resource by battery users, developers, and program managers who must evaluate and choose battery technologies and research directions. Since it was established more than two decades ago, the EADL has tested more than 4000 cells, ranging from individual 4-Wh cells to 50-kWh batteries, representing 12 technologies and 18 battery developers.

The facilities include test laboratories equipped for conducting experimental evaluations of both batteries and fuel cells under simulated application conditions. Evaluations are performed for DOE, the U.S. Advanced Battery Consortium (USABC), and others to provide insight into factors that limit the performance and life of advanced battery systems. The results of these evaluations help identify the most promising R&D approaches for overcoming these limitations and provide the research sponsors with a measure of the progress being made in battery R&D programs, a comparison of battery technologies, and basic data for modeling.

During the past year, performance and life evaluations were continued under a CRADA with the USABC, a government-industry partnership formed to accelerate commercialization of advanced batteries for electric vehicles. These activities included evaluation of nickel-metal hydride (Ni/MH) modules from USABC battery contracts with SAFT (France) and evaluation of full-size EV battery packs. Currently, the EADL is evaluating the latest deliverable developed by SAFT as part a cost-reduction program sponsored by the USABC. The results of these tests and analyses will be released by the USABC at a later date.

During 1999, the EADL collaborated with SNL and INEEL in the electrochemical characterization and life testing of the first generation of spiral-wound lithium-ion cells produced as part of DOE's Advanced Technology Development Program (see Sec. I.A.1). These cells were subjected to accelerated calendar and cycle-life testing at four temperatures (40, 50, 60, and 70°C) and three states of charge (40, 60, and 80%). These results will be published at a later date.

An assessment of foreign EV battery technologies for DOE continued during 1999. During the year, the EADL evaluated six Ni/MH modules from Matsushita Battery Industrial Co. & Panasonic EV Energy Co. (MBI/PEVE). This evaluation included electrochemical characterization and life-cycling studies at ambient and elevated temperatures. The EADL also received an HEV battery pack from MBI/PEVE. The performance characterization studies of the HEV pack have started and will include electrochemical characterization and cycle-life studies.

In the next year, evaluations will continue for the USABC's SAFT cost-reduction program. We will also assist Argotech/Hydro-Québec in their lithium-polymer battery development program with the USABC. The assessment of foreign EV battery technologies for DOE will also continue.

C. Fuel Cell Research and Development

1. *Introduction*

Fuel cells convert chemical energy directly into electricity by electrochemical reactions, eliminating the need for heat engines. They hold the promise of clean electric power not only for cars and other vehicles but also for houses, commercial buildings, and industrial processes. Argonne has been a leader in fuel cell research for more than twenty years, drawing on a range of disciplines to create and improve materials and designs for fuel cells.

Because fuel cells are very energy efficient and produce almost no emissions, interest in this technology is growing. The polymer electrolyte fuel cell (PEFC), in particular, is attracting significant private investment for transportation and residential use. However, the PEFC technology presents some challenges to widespread adoption. Foremost among them today is providing a suitable fuel. Because no infrastructure exists to supply hydrogen, the ideal fuel for fuel cells, it has been necessary to develop fuel processors that can convert conventional fuels such as gasoline, alcohols, or natural gas into a hydrogen-rich (reformate) gas. The design of a fuel processor for an automotive fuel cell system is constrained by limitations of size and weight, and by the requirement for rapid-start and load-following capabilities. At the low operating temperature of the PEFCs (nominally, ~80°C), the reformate has to be free of chemical species that can poison the electrocatalyst. These include carbon monoxide and sulfur-bearing species.

Meeting all these requirements for the automotive fuel cell system is a challenge, and more than half of our effort is devoted to the development of fuel processing technology. This work encompasses development and demonstration of the individual components (reforming, shift reaction, sulfur removal, carbon monoxide removal, etc.). The demonstration of the fuel processor system is carried out through a combination of component and systems modeling, as well as demonstration of the components that are in series and integrated into a package. We also continue to lead the field in PEFC systems analysis and modeling. In the development of the more traditional molten carbonate and solid oxide fuel cells for stationary applications, we are working closely with industrial developers on specific issues related to technology improvement.

2. *Fuel Processing*

At the present time, gasoline is the commodity fuel for passenger cars, and natural gas predominates in stationary applications. To operate a fuel cell system on either of these two fuels requires converting a hydrocarbon to a hydrogen-rich stream that must be virtually free of CO. In industry, natural gas is processed by steam reforming and shifting. Although highly developed, the steam reforming process is bulky and has unacceptably slow response to changing fuel-processing rates. Argonne was the first to propose partial oxidation reforming as a better alternative. We continue to develop this process and also to seek better reformer catalysts.

a. Reforming Catalyst Development

The objective of this work is to improve the catalytic activity of the Argonne reforming catalyst. This catalyst consists of two phases: an active metal and an active ceramic support. In 1999, we investigated the effect of the ceramic support, the reactant flow rate, and the synthesis method.

To study the effect of the ceramic support material, we synthesized and tested several ceramic support materials (proprietary compositions). The type and amount of metal and the synthesis method were the same for all tests. Figure I-8 shows the amount of H_2 and unconverted hydrocarbons in the product after reforming iso-octane (C_8H_{18}) at 800°C with these synthesized catalysts. The gas hourly space velocity (GHSV) was 2602 h^{-1}. All the catalysts showed reasonably good activity for C_8H_{18} reforming. The catalyst with a ceramic support belonging to System 1 showed the best reforming activity: the product contained the highest H_2 concentration and was free of unconverted hydrocarbons.

Figure I-9 shows the effect of GHSV on an Argonne catalyst sample. This catalyst yielded more than 50% H_2, even at space velocities as high as 70,000 h^{-1}. The ability to produce a hydrogen-rich gas at high space velocities offers the possibility of reducing the size of Argonne's catalytic autothermal reforming reactor.

In addition to investigating the ceramic support, we have developed a new synthesis method that results in a more active catalyst. In this method, the catalyst was shaped by extrusion of ceramic powders made by combustion synthesis. The active metal was added to the extrusion paste in the form of a salt solution. After extrusion, the extrudate was dried and sintered at 900°C. Compared to catalysts made by conventional techniques (pressing of physically mixed ceramic and metal powders), catalysts made with the new synthesis method performed better, as shown in Fig. I-10. At temperatures up to 800°C, the new catalyst, which has a larger surface area, yielded a product with a higher H_2 concentration.

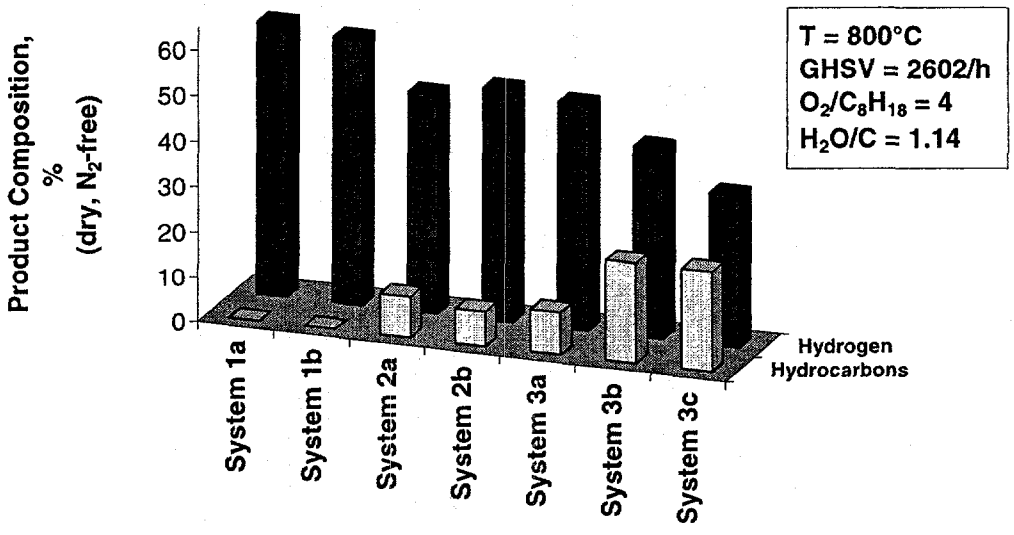

Fig. I-8. Results from the Reforming of Iso-Octane (C_8H_{18}) at 800°C Showing the Effect of the Ceramic System Used for Active Support. Metal loading and synthesis method were the same for all.

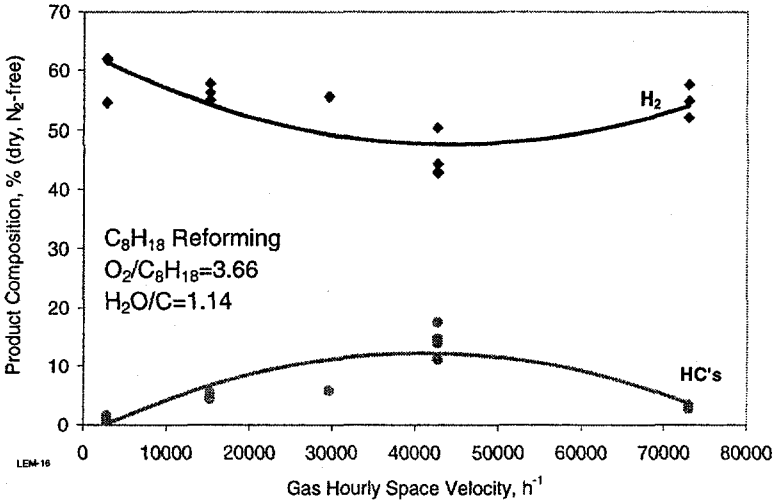

Fig. I-9. Product Composition vs. Gas Hourly Space Velocity (GHSV) for a Catalyst Based on System 1

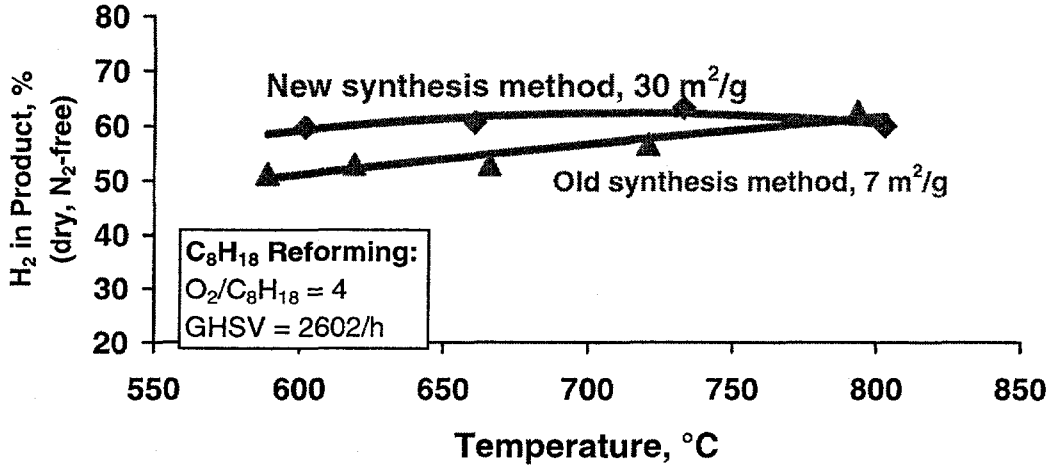

Fig. I-10. Effect of Synthesis Method on Activity of Argonne Reforming Catalysts. The two materials have the same chemical composition.

b. Sulfur Removal from Reformate

We are developing an efficient sulfur removal process to decrease the hydrogen sulfide (H_2S) content of the reformate produced from sulfur-containing fuels, such as commercial-grade gasolines, to a concentration of 1 ppm or less. Sulfur must be removed to prevent poisoning of the platinum in the anode of the fuel cell and, potentially, of certain fuel processing catalysts. During fuel reforming, sulfur in the fuel is converted to H_2S, with the concentration of H_2S in the reformate (parts per million by volume, ppmv) being approximately one-tenth the concentration of sulfur in the fuel (parts per million by weight, ppm). Thus, the H_2S concentration will be 30-35 ppmv in reformate produced from U.S. gasolines (average sulfur content 347 ppm). Even if the sulfur content of the U.S. gasolines is reduced to

30-80 ppm, as proposed for 2004, H_2S in the reformate will still be too high (3-8 ppmv), and will need to be reduced to <1 ppmv.

Our sulfur-removal process is based on chemical reaction with a suitable "sorbent," generally a metal oxide. The H_2S reacts with the sorbent to form a stable metal sulfide. On the basis of a thermodynamic analysis of various metal oxides under conditions that exist during fuel processing, we have selected zinc oxide (ZnO) as our initial candidate sorbent. However, the size and weight of a unit using commercial-grade ZnO would be prohibitively high for the automotive fuel processing system.

We have begun measuring the kinetic and physical parameters that determine the size and lifetime of ZnO beds. The objective is to develop a mathematical model that would allow us to design an engineered form of ZnO better suited for fuel processing. This improved version will be used to design and predict the performance of a ZnO bed for a variable-load, automotive-scale (50-kWe) fuel processor.

Experiments are in progress to measure the rate of H_2S removal by ZnO under transient conditions (e.g., varying space velocity, inlet H_2S concentration, and temperature) that are representative of the operating conditions for the fuel processing system. The data from these experiments will be used to validate the mathematical model of ZnO performance. Experimental results to date show that the operating lifetime of the ZnO bed is significantly decreased as the space velocity is increased from 4,800-50,000 h^{-1} for a given H_2S concentration, or the H_2S concentration is increased from 30 to 1,000 ppm (by volume) for a given space velocity. To minimize the ZnO bed size, the kinetic rate, which increases with temperature, must be balanced with the H_2S equilibrium concentration, which decreases with temperature. To achieve <1 ppm H_2S, the bed operating temperature should be 350-400°C.

Our future work will focus on two tasks: (1) developing an engineered form of ZnO that is effective at high space velocities and (2) evaluating the merits of a ZnO bed designed to last the lifetime of the fuel processor versus a bed designed to be replaced periodically. In addition, work is continuing on identifying alternatives to metal oxide sorbent that could improve the rate of H_2S removal or significantly reduce the size and weight of the process unit.

c. Catalyst Development for the Water-Gas Shift Reaction

The reforming of hydrocarbon fuels produces carbon monoxide, which must be reduced to trace levels to avoid poisoning of the electrocatalyst in the PEFCs. Most of the CO is removed by reaction with water to produce carbon dioxide and hydrogen, by the reversible water-gas shift reaction:

$$CO + H_2O \rightleftharpoons CO_2 + H_2 \qquad (1)$$

In industrial practice, this water-gas shift reaction is carried out in two stages at two temperatures. The high-temperature stage uses an iron-based catalyst, and the low-temperature stage uses a copper-zinc oxide catalyst. This low-temperature catalyst is synthesized as a mixture of copper oxide and zinc oxide supported on alumina. The catalyst must be

"activated" by reducing the copper oxide to copper metal. Once the catalyst has been reduced, it must be maintained in an inert or reducing environment at all times. Any exposure to oxygen, even at room temperature, leads to rapid, highly exothermic reoxidation of the copper, resulting in sintering that deactivates the catalyst. Our research is aimed at finding a thermally rugged and highly active catalyst for the water-gas shift reaction.

We have investigated several classes of catalysts for this purpose. The most active class of catalysts is believed to operate by a bifunctional mechanism: one component of the catalyst adsorbs and dissociates the water, and the other component adsorbs and oxidizes the carbon monoxide. Within this class, the most active catalyst uses platinum to adsorb carbon monoxide and a mixed oxide support to adsorb and dissociate water. We have found that this catalyst has water-gas shift activity comparable to the commercial copper-zinc oxide. However, unlike copper-zinc oxide, its activity is stable with temperature cycling and exposure to air.

In the past year, we have improved the activity of the platinum/mixed oxide catalyst, while lowering its platinum content. In Fig. I-11, this improvement is reflected in the higher slope for the later tests. These catalysts were prepared and tested as fine powders. To make a more rugged catalyst suitable for transportation applications, we have tested various approaches to supporting the catalyst on a high-surface-area substrate, such as γ-alumina. With the alumina support, the activity was maintained, while the overall catalyst loading was cut by half and the platinum content was reduced from 0.57 to 0.34 wt% of the total material.

Since this platinum/mixed oxide catalyst does not deactivate at higher temperatures, it opens up the possibility of performing the water-gas shift in a single stage rather than the two stages used at present. On the basis of kinetic parameters for the alumina-supported platinum/mixed oxide catalyst, we estimate that a water-gas shift reactor using this catalyst would be less than three-fourths (71%) the size of one using the copper zinc oxide catalyst.

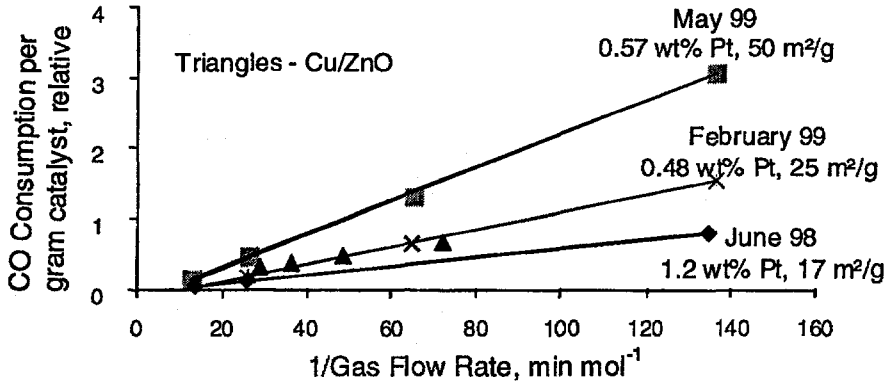

Fig. I-11. Activity of the Platinum/Mixed Oxide Water-Gas Shift Catalyst Developed at ANL. Increased activity was achieved by altering synthesis conditions. The copper-zinc oxide is United Catalysts, Inc., G-66B.

d. Carbon Monoxide Cleanup

Even though the water-gas shift reaction removes most of the CO from the reformate, PEFC-based transportation systems require that CO concentrations be further reduced to less than 100 ppmv. We have been investigating a regenerable sorption process based on the reversible complex-forming and dissociation reactions of CO and Cu(I).[11] This approach has advantages in terms of ease of control, cold start-up capability, and dynamic responsiveness.

In previous work,[12] we showed that a formulation of H-ZSM-5 zeolite and copper chloride is a stable sorbent for CO capture. The copper chloride was deposited on the zeolite by vapor ion exchange. In dynamic column tests, the CO sorption capacity was 1.5 mg CO/g sorbent for 1% CO in the feed. A preliminary design analysis based on these data showed that, for this process to be small and light enough for transportation use, the sorption capacity must be 5 to 10 times greater. Therefore, during the past year, we concentrated on exploring other potential substrates and Cu(I) ion-exchange techniques. At temperatures of 90-250°C, sorption capacity was roughly doubled with an LZY-84 molecular sieve and copper acetate ion exchange. For example, the capacity with this material was about 6 mg CO/g sorbent, versus 3 mg CO/g sorbent for the zeolite at 3% CO and 100°C. Using copper acetate solution instead of copper chloride vapor for ion exchange has several advantages: lower preparation temperature (60°C versus 450°C), sample stability, and chlorine-free synthesis. Despite these improvements, however, the attainable CO sorption capacity is still too low for a practical system.

We are presently evaluating a new proprietary commercial catalyst for preferential oxidation of the CO at 70°-100°C to reduce its concentration to the desired level of 100 ppmv or less.

e. Fuel Cell Process Train

We are investigating the integration of the individual process units required to convert a hydrocarbon fuel to hydrogen (and benign byproducts) to serve as a feed for a fuel cell stack. To this end, we have built and are testing a linear train of scaled-down process units. The system includes a reformer microreactor, a sulfur-removal bed, high- and low-temperature water-gas shift (HTS and LTS) units, and CO-removal units. The individual units within the process train can be readily changed to test new materials or processes.

In the baseline configuration, the sulfur-removal bed was loaded with commercial zinc oxide; the HTS bed was loaded with commercial iron-chromium oxide, and the LTS bed was loaded with the Argonne platinum/mixed-oxide catalyst. Manganese oxide/carbonate was used as the preferential oxidation (PrOx) catalyst for CO removal.

---

[11] J. J. Laidler et al., *Chemical Technology Division Annual Technical Report, 1997*, Argonne National Laboratory Report ANL-98/13, pp. 28-30 (1998).

[12] J. P. Ackerman et al., *Chemical Technology Division Annual Technical Report, 1998*, Argonne National Laboratory Report ANL-99/10, pp. 28-30 (1999).

The operating conditions for each of the reactors after the reformer were determined in initial testing with a simulated gasoline reformate containing 45% H_2, 30% N_2, 13% CO_2, 10% CO, and 2% CH_4. Flow rates were constant and comparable to those for the reformer microreactor to which the train is connected. Steam was introduced above the H_2S bed, and air was introduced at the first PrOx reactor. Operating on this simulated reformate, the microreactor train reduced CO levels from 13% to 4% (dry, nitrogen-free basis) in the HTS bed to between 1 and 2% (dry, nitrogen-free basis) in the LTS bed and to <500 ppmv in the PrOx bed, but not below the target of 100 ppmv.

To test the entire process, including the reformer, the process train was operated with iso-octane fuel as a surrogate for gasoline. Iso-octane, water, air, and nitrogen were fed to the reformer microreactor with the reformer bed maintained at 735°C. The variation in CO concentration with time is shown in Fig. I-12. The CO concentration in the effluent stream remained below 100 ppmv during most of the test. There was, however, a steady rise in CO content from about 10 ppmv to nearly 100 ppmv, with spikes approaching 200 ppmv. The spikes increased in intensity as the test proceeded. Further tests with synthetic reformate should allow us to determine whether the spikes observed are due to variations in the reformer effluent composition or in the operation of the components of the train.

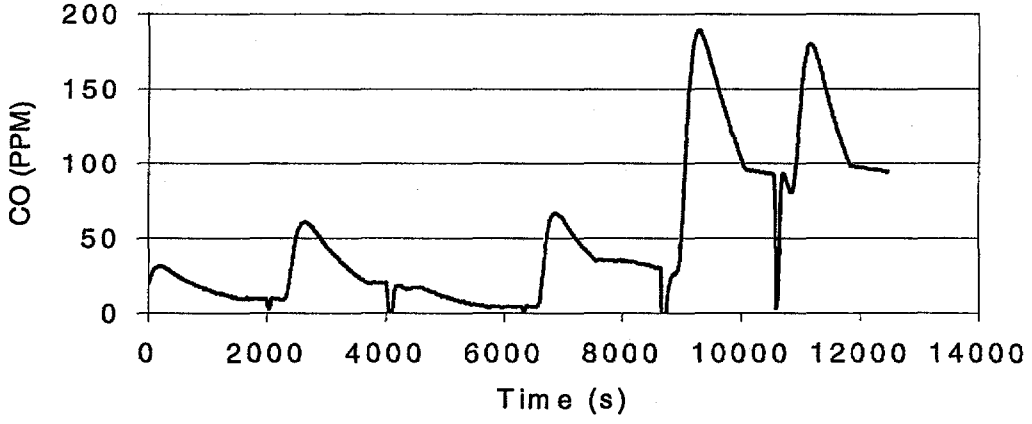

Fig. I-12. Carbon Monoxide Concentration in Process Train Effluent with Iso-Octane Feed

f. Integrated Fuel Processor

We have an ongoing program to demonstrate a fuel-flexible fuel processor suitable for use on-board a fuel-cell-powered vehicle. This year we took the next step forward by designing and building an engineering-scale integrated reformer, APOR3. The reformer is 180 mm in diameter and 310 mm long, with a fuel processing capacity sufficient to supply a 5- to 10-kW fuel cell stack. It consists of three major zones: the autothermal zone, the sulfur-removal zone, and the water-gas shift (WGS) zone. The air is preheated within the reformer before being mixed with vaporized fuel and steam; the mixture then enters the autothermal zone, which is filled with the Argonne autothermal catalyst. The gas emerging from the autothermal zone is cooled to below 450°C for the sulfur-removal zone, where a commercial zinc oxide

sorbent is used. The gas then passes through the WGS zone, which is packed with the platinum/mixed-oxide catalyst described earlier (Sec. I.C.1c).

The APOR3 fuel processor has been tested successfully with iso-octane and methanol fuels. Figure I-13 shows the product gas compositions obtained from the reforming of iso-octane. The fuel feed was started at 18.6 mL/min, increased to 39.1 mL/min at time 12:25, and then reduced back to the initial feed rate at time 14:30. The molar ratio of oxygen to fuel was maintained at 3.2. At the lower fuel feed rate, the product gas contained 39-41% H_2 (the theoretical maximum was 45%) and 4% CO. At the higher fuel feed rate, the H_2 concentration decreased to 37-39%, while the CO concentration increased. These changes occurred because the desired temperature profile could not be maintained in the WGS catalyst bed. The conversion of the iso-octane, however, was maintained at 99% over the entire duration of the test. The H_2 produced at the iso-octane feed rate of 39.1 mL/min was equivalent to 5 kW(e) power production. In testing with methanol, we obtained 46-47% H_2 (the theoretical maximum was 54%), again without the complete water-gas shift conversion of CO (which varied from 13 to 16%) because of the low temperature of the WGS bed. The methanol conversion was ~100%.

We are using the engineering data obtained from these tests as the basis for designing the next-generation reformer, APOR4. The goal for the new design is to increase the thermal integration among the zones to improve fuel conversion, H_2 output, and shift conversion of CO.

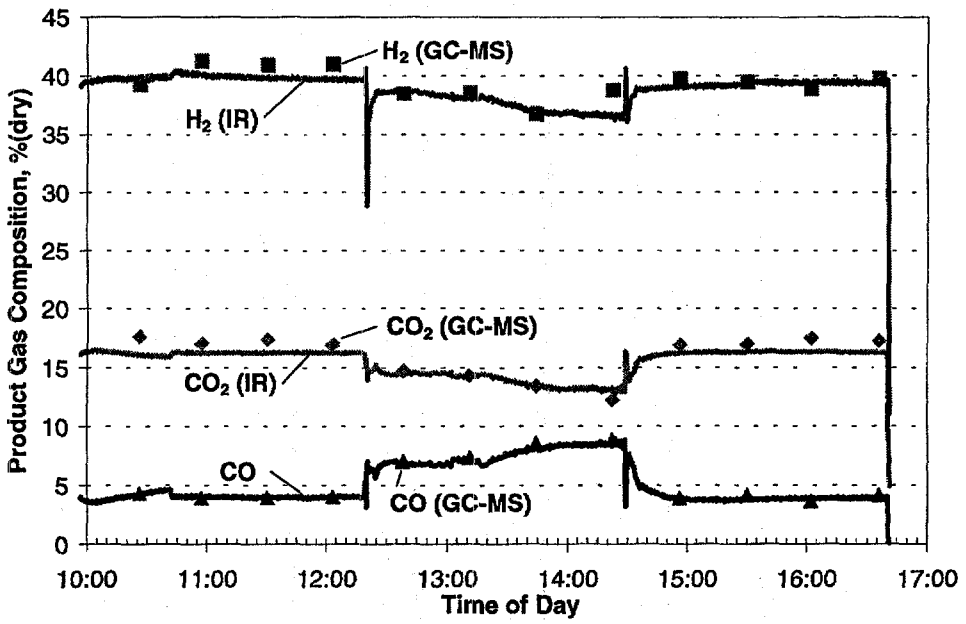

Fig. I-13. Product Gas Compositions Obtained from the Partial Oxidation Reforming of Iso-Octane in the Engineering-Scale Integrated Fuel Processor (APOR3). The discrete points are data from a gas chromatograph/mass spectrometer (GC-MS); the continuous traces show data from online infrared (IR) instruments.

3. Systems Analysis

The objective of the work is to develop models of automotive fuel cell systems that can be used to identify key design parameters and operating efficiencies; to model design, part-load, and dynamic performance; and to provide results and support to fuel cell developers, the relevant PNGV technical teams, and other researchers in the field. Modeling workshops were conducted to disseminate the results of this work, in particular, the software package called GCtool. This software has been documented with the National Energy Software Center. Unix and PC versions of this software are available for licensing.

This year we added three new component models to GCtool: (1) a two-dimensional, multinodal model of the PEFC, which can be used to investigate the effects of operating conditions (e.g., pressure, temperature, fuel utilization) in an internally consistent manner; (2) a transient model of an integrated fuel processor, similar to Argonne's APOR; and (3) a kinetic, finite-difference model of cylindrical chemical reactors. We used these models to study the effects of operating pressure on the design and operation of fuel cells and fuel processors, as described below.

a. Model Development

We have developed a detailed, multinodal model of a polymer electrolyte fuel cell. This model takes into account the Nernst potential and the ohmic, activation, and concentration overpotentials. It then calculates the actual cell voltage as a function of current density, anode and cathode pressures and temperatures, fuel and oxidant gas compositions, and hydrogen and oxidant utilizations. The predicted values were matched with experimental polarization curves by selecting appropriate values of the exchange current densities, membrane conductivity, and mass transfer coefficients. The model can now be used to simulate cell performance for any operating conditions.

In addition, we have set up two fuel processor models, a low-fidelity one and a detailed kinetic one, for reactor geometries similar to those used in our APOR series of fuel processors. The low-fidelity model can simulate steady-state or transient operation in a multiannular geometry and arbitrary flow configurations and bed arrangements. The model incorporates up to 10 axial nodes, with one radial node per annular channel. The model can be executed with chemical equilibrium, or with kinetic control of approach to equilibrium. It accounts for heat transfer between channels and the reactor walls, pressure drops, and heat losses. The detailed kinetic model is a two-dimensional finite-difference model in spherical coordinates (r,z) that can account for nonisothermal gas flows and catalyst beds. Processes simulated include fuel vaporization and dissociation, water vaporization and condensation, partial oxidation and steam reforming of the fuel, the water-gas shift reaction, combustion, and sulfidation. These two models are being used to support the engineering development of the APOR.

b. Analysis of Ambient-Pressure Systems

Although pressurized systems are currently being developed for automotive PEFCs, ambient-pressure systems may have some advantages. We analyzed the operating conditions that would yield optimum performance in an ambient-pressure system and compared such a system to a pressurized one.

In an ambient-pressure system, assuming equilibrium formation of methane and carbon, the fuel processor efficiency is highest at a partial-oxidation temperature (T_{POX}) of about 825°C. At higher temperatures, the efficiency suffers because of the need for higher air-to-fuel ratios to achieve the high T_{POX}. At lower temperatures, efficiency suffers because of the excess formation of methane.

Modeling results show that for a high-performance atmospheric-pressure system, the fuel processor should have a reforming temperature of 825°C, a fuel equivalence ratio[13] of 3.4, and a water-to-fuel mass ratio of 2.2 (possibly higher in practice for complete conversion of the fuel), yielding a hydrogen concentration of 44.4% in the reformate (dry basis). For a net system efficiency of 45% at the rated power level, the fuel cell stack needs to be operated with a cell voltage of 0.8 V, as well as hydrogen and oxygen utilizations of 90% and 50%, respectively. All three values are higher than those in current practice.

We also conducted several analyses concerning the condenser design and placement in relation to stack humidification, combustor exhaust cooling, and ambient temperature. One design option for atmospheric-pressure stacks is internal humidification, i.e., near-adiabatic operation with waste heat removed by vaporization of water. In such a system, the condenser must reject over 50% of the lower heating value of the fuel and recover all of the process water used in fuel reforming. For the nonadiabatic conditions summarized above, the heat loads on the radiator and the condenser are about equal. For the condenser, about 65% of this load is for removing water from the cathode exhaust. Under adiabatic conditions, the heat load shifts from the radiator to the condenser. Modeling results for the system described above showed that for the conventional system, the radiator and condenser loads would be 28.4 and 25.9 kW, respectively; for the adiabatic stack, the radiator would be eliminated, but the condenser would be 2.3 times larger, with a heat duty of 55.0 kW.

In recovering water from the exhaust of the catalytic combustor, which burns the residual hydrogen in the spent anode gas, 15-35% of the condenser cooling load is for sensible cooling of the combustor exhaust. Our analyses showed that moving the condenser upstream of the combustor could decreased the load by 15-20%. The burner exhaust could then be discharged directly to the atmosphere without cooling.

Finally, we considered the effect of ambient air temperature. Because the condenser operates with rather small log-mean temperature differences between the process gas and the ambient air, higher ambient temperatures would require a larger condenser for the same duty. Thus, we found that a condenser designed for an ambient temperature of 47°C would need

[13] For a given feed rate of air, the ratio between the fuel feed rate to the reformer and the fuel feed rate for complete oxidation of the fuel.

to be 60% larger than one sized for an ambient temperature of 27°C. Conversely, if a system is designed for 27°C, the maximum steady-state power rating would need to be decreased by 25% if the ambient temperature rises to 47°C.

We have conducted extensive analyses comparing the design and operation of pressurized and ambient-pressure systems. Some of the major results of these analyses are summarized in Table I-3. Features of the pressurized system are taken as the reference to which the ambient-pressure system is compared.

c. Startup Times for Fuel Processors

A critical challenge in the design of fuel processors is achieving practical startup times. Much of the current work on this issue focuses on developing high-activity catalysts. To investigate the effect of catalyst activity on startup time, we analyzed a relatively simplistic startup scenario for a gasoline reformer in which the water-to-fuel ratio was constant, but the air-to-fuel ratio was varied to obtain the highest heat generation tolerated by the partial-oxidation reactor. The different catalyst beds (POX, HTS, LTS, and PrOx) were represented by nominal gas hourly space velocities (GHSVs). For a base case with GHSVs comparable to today's practice in the chemical process industry, startup times would be more than 1200 s for each of the four stages. For GHSVs 20 times higher than current commercial practice, the startup time would be 285 s (the POX stage). We also considered the effect of increasing the fuel burn rate above the design rate for full power. Even with a GHSV 10 times greater than commercial practice and a fuel burn rate two times the feed rate at rated power, the startup time is still about 100 s (for PrOx). It is evident from these analyses that more active catalysts or highly improved reactor designs—or both—are required.

Table I-3. System Design and Performance at Operating Pressures of 1 atm and 3 atm

	3-atm System[a]	1-atm System
Compressor/expander	Critical component	Not needed
Methane and carbon formation	Higher potential, need higher T_{POX}	Lower potential, need lower T_{POX}
Fuel processor	Relative sizes of subsystems: POX = 0.33 HTS = 0.5 LTS = 0.5 PrOx = 0.2	• Larger weight and volume • longer startup times
PEFC stack	• Needs active cooling • In-cell condensation adds to cooling load • Cathode channels prone to flooding	• 25% larger cell active area • Potential for membrane to dry out • Stack cooling load reduced by water evaporation
Heat rejection and water balance	One-third of process water recovered in inertial separator, two-thirds in condenser	• Condenser 2.8 times larger • Smaller radiator
Response to high ambient temperatures	Power reduction determined by radiator size: ~35% reduction at 47°C	Power reduction determined by stack temperature rise: 25% reduction at 47°C

[a] Baseline for comparisons.

In future work, we will examine in detail the fuel cell and the balance-of-plant performance characteristics required to meet the PNGV targets of 80 miles per gallon of gasoline equivalent in fuel cell/battery hybrid propulsion systems.

4. Materials Development

a. Molten Carbonate Fuel Cells

Molten carbonate fuel cells (MCFC) offer the potential for high-efficiency energy conversion and reduced pollution. Corrosion of the bipolar plates and current collectors is, however, a life-limiting factor for these fuel cells. Another issue is the internal cell resistance: about 25% of this resistance can be attributed to the oxide layer that forms on the stainless steel used for the bipolar plate and current collector. In earlier work, we determined that the main factor influencing the corrosion behavior and the electrical resistivity of bipolar plate materials on the cathode side is the chromium content of the base metal.[14]

State-of-the-art, large-scale MCFCs use nickel-clad Type 316L stainless steel (SS) for the bipolar plates. This steel has low resistivity, but it is expensive and corrodes easily. Type 310 SS is inexpensive and corrosion resistant but forms a high-resistivity oxide scale. The objective of our work this year was to identify or develop a bipolar plate material that combines the best of both steels: the low oxide scale resistivity of Type 316L SS and the low corrosion rate of Type 310 SS. We approached this problem from two directions: alloy composition and surface modification.

We first investigated whether steels containing more manganese or cobalt than Type 310 or Type 316 SS have better properties. We chose four commercially available stainless steels with low chromium content: Nitronic 30, Nitronic 50, and Nitronic 60, which contain more manganese, and Haynes 556, which contains more cobalt. All combine very good corrosion behavior in many media with the requisite strength at the high operating temperatures (650°C) of MCFCs.

Our results show that the manganese in the Nitronic steels modifies the structure of the oxide scale and appears to improve the overall corrosion resistance.[15,16] Measurements of electrical resistivity show that the modified oxide scale has a low resistivity. Furthermore, all Nitronic alloys form dense scales without cracking or spallation. Nitronic 30 is about equal in performance to Nitronic 60, while Nitronic 50 is slightly less corrosion resistant. The cobalt-containing Haynes 556 (18 wt% Co) exhibited a somewhat higher corrosion rate than the

---

[14]T. D. Kaun, A. C. Schoeler, I. Bloom, M. Lanagan, and M. Krumpelt, "Resistivity of Bipolar Plate Materials at the Cathode Interface in Molten Carbonate Fuel Cells," Abstracts, 194th Meeting of Electrochem. Soc., Boston, MA, November 1-6, 1998, Vol. 98-2, Abstract No. 307 (1998).

[15]A. C. Schoeler, T. D. Kaun, and M. Krumpelt, "Influence of the Alloying Elements Mn and Co on the Electrical Resistance and Corrosion Behavior of Bipolar Plate Materials in MCFC," Abstracts, 196th Meeting of Electrochem. Soc., Honolulu, HI, October 17-22, 1999, Vol. 99-2, Abstract No. 1667 (1999).

[16]A. C. Schoeler, T. D. Kaun, and M. Krumpelt, "Influence of the Alloying Elements Mn and Co on the Electrical Resistance and Corrosion Behavior of Bipolar Plate Materials in MCFC," Proc. of 196th Meeting of Electrochem. Soc., Honolulu, HI, October 17-22, 1999, p. 158-168 (1999).

Nitronic alloys. This alloy formed an inner oxide scale rich in chromium, an outer oxide scale of $LiFeO_2$, and a thin surface layer of $LiCoO_2$. Very little cobalt was incorporated in the chromium-rich or $LiFeO_2$ scale. Although $LiCoO_2$ scale is reported to have a low resistivity,[17] the overall electrical resistance of Haynes 556 is not as low as expected and is higher than that of Type 316L SS.

In our second approach, we investigated two surface modifications intended to control corrosion of stainless steel: thermal spraying and a newly developed bond coating process. First, Type 316L SS was thermal-sprayed with cobalt. This coating was expected to form a $LiCoO_2$ outer oxide scale, which is also expected to have lower electrical resistivity than the usual $LiFeO_2$ scale.[17] Second, we coated Type 316L SS with Nitronic 50 and Nitronic 60 alloys by a newly developed commercial coating method (stainless steel bond coating process).

We then tested both steels under MCFC conditions. Our test results show that thermal spraying with cobalt improves the corrosion resistance and prevents spallation and microcracking in the oxide scale of Type 316L SS. An outer $LiCoO_2$ oxide scale did form and had low resistivity. The structural integrity and low resistivity of the scale led to overall resistivity values that were lower and more uniform than those of as-received Type 316L SS. Thus, thermal spraying with cobalt seems to be a cost-effective method to improve bipolar plates on the cathode side of MCFCs. The bond coating process achieved a dense, crack-free, 10- to 12-μm-thick coating of the promising Nitronic alloys on the Type 316L SS plate. Initial tests indicate low electrical resistivities, especially for the Type 316L SS samples coated with Nitronic 60.

In summary, our results show that stainless steels containing manganese as the alloying element are suitable materials to replace Type 316L SS as the bipolar plate material for MCFCs. Nitronic 60 is available in the required thickness and width for bipolar plates. A disadvantage of this material may be its relatively high cost due to the low volumes of production at present. In contrast, cobalt-containing Haynes 556 is not an attractive candidate material for this application. Further, thermal spraying with cobalt seems to be a potentially cost-effective method to improve bipolar plates, and the Nitronic coating process also looks promising. No further work on molten carbonate fuel cells is planned for the next year.

b. Solid Oxide Fuel Cells

During this year, the CMT work on solid oxide fuel cells (SOFCs) was focused on two areas: (1) improving cathode performance for high-temperature SOFCs (800-1000°C) and (2) developing cathode materials for low-temperature SOFCs (500-800°C).

1. High-Temperature Cathodes

The standard air electrode material for SOFCs is strontium-doped lanthanum manganite (LSM). It has good electronic conductivity and catalytic activity for oxygen reduction, but because its ionic conductivity is very low, the catalytic activity is limited

[17] I. Bloom, M. T. Lanagan, M. Krumpelt, and J. L. Smith, *J. Electrochem. Soc.* **146** (4), 1336 (1999).

to the triple-phase boundaries of electrode, electrolyte, and gas phase. This restriction results in a high cathodic overpotential and low cell efficiency. We are investigating ways to improve the ionic conductivity of this cathode material by appropriate doping. Our approach is to replace some of the trivalent manganese in LSM with other trivalent elements that prefer tetrahedral rather than octahedral coordination. This change should seed the structure with vacancies that become mobile at the operating temperatures. The presence of such vacancies would make it easier to transport oxygen ions to the cathode/electrolyte interface.

We tested both Ga(III) and Al(III) as dopants for Mn(III) in LSM cathodes. Figure I-14 shows the effect of the dopant level on the overpotential of the modified LSM cathode in half-cell tests at 1000°C. Without the dopants, the overpotential is 80 mV. As the dopant level increases, the overpotential decreases, reaches a minimum, and then increases. The optimal doping levels, 5% for Ga(III) and 4% for Al(III), decrease the cathodic overpotential by 60-75%. These results indicate that both dopants increase the ionic conductivity of the sample.

To further characterize the gallium-doped LSM cathode materials, we are measuring such complementary material properties as electrical conductivity and oxygen diffusivity. In addition, full-cell testing of these doped cathode materials is underway. Four-point conductivity tests have shown that gallium doping in the range of 0 to about 10% has little effect on the total electrical conductivity of the material. Preliminary data obtained from secondary ion mass spectroscopy at 800°C show little relationship between the oxygen diffusivity and gallium doping. However, the temperature used may not have been high enough to dislodge the vacancies created around the gallium cations. Further characterization at higher temperatures is needed.

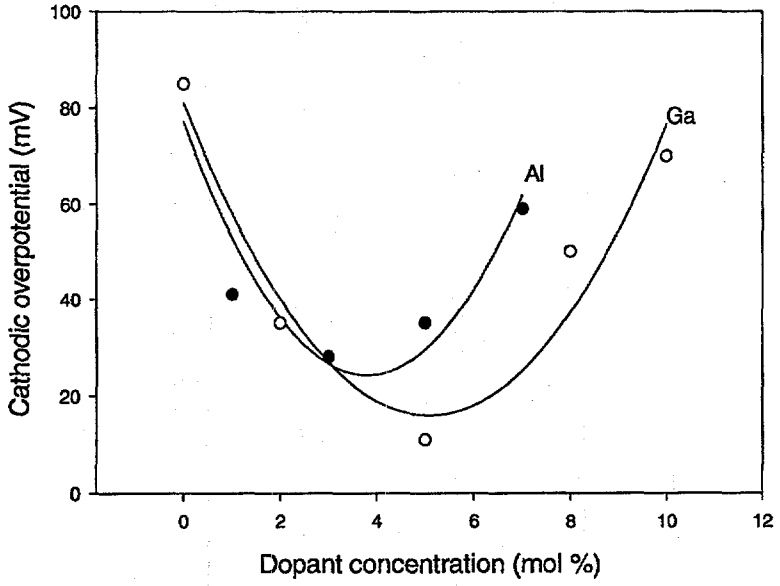

Fig. I-14. Effect of Aluminum and Gallium Doping on the Cathodic Overpotential of an LSM Cathode at 1000°C and 250 mA/cm^2

2. Low-Temperature Cathodes

In parallel with our work to improve the properties of LSM, we are exploring new cathode materials for low-temperature SOFCs. The development of cathode materials that are capable of working at temperatures in the range of 600–800°C is an important step for the next generation of SOFCs and oxygen separation membranes. Lower operating temperatures would reduce the cost of the balance-of-plant and improve the potential for commercializing SOFCs.

We screened several classes of perovskite-based materials to determine their suitability as air electrodes. Materials tested included various combinations of doped lanthanum ferrates (LSF), nickelates (LN), and cobaltates (LSC) with both A- and B-site doping. The materials were prepared on two electrolytes, yttria-stabilized zirconia (YSZ) and gadolinia-doped ceria (CGO), and evaluated using impedance analysis in half-cell tests. Figures I-15 and I-16 show the areal resistance as a function of temperature for all of the compositions prepared on CGO and YSZ, respectively. For CGO (Fig. I-15), lanthanum strontium cobalt ferrate (three preparations of LSCF) achieved the lowest areal resistance. Lanthanum strontium cobaltate (LSC) also looked promising at 700°C, but because of its large apparent activation energy, the resistance of the cathode is unacceptably high at lower temperatures. Samarium strontium cobaltate (SmSC) looks more promising in this respect, compared to LSCF, as the temperature is reduced below 700°C. For YSZ (Fig. I-16), two preparations of lanthanum strontium ferrate (LSF, LSF2) showed excellent performance.

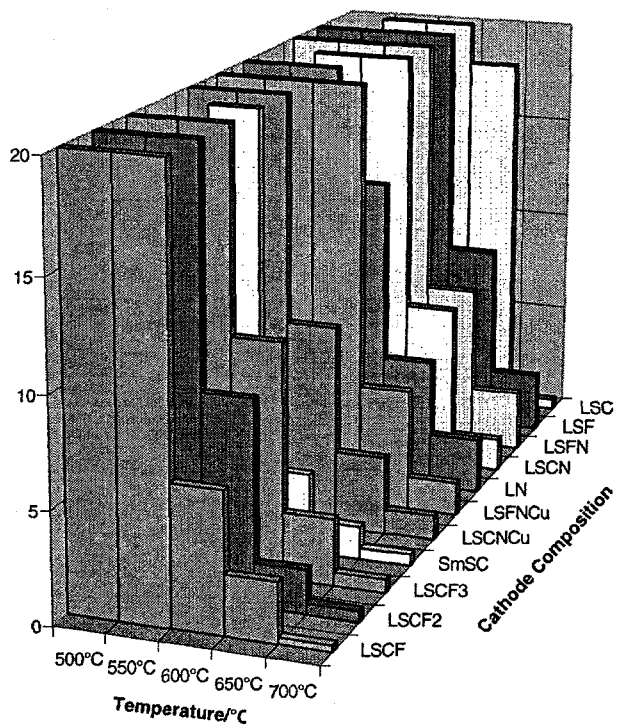

Fig. I-15. Areal Resistances (y-axis in units of Ω-cm^2) for Cathodes on Gadolinia-Doped Ceria as a Function of Temperature

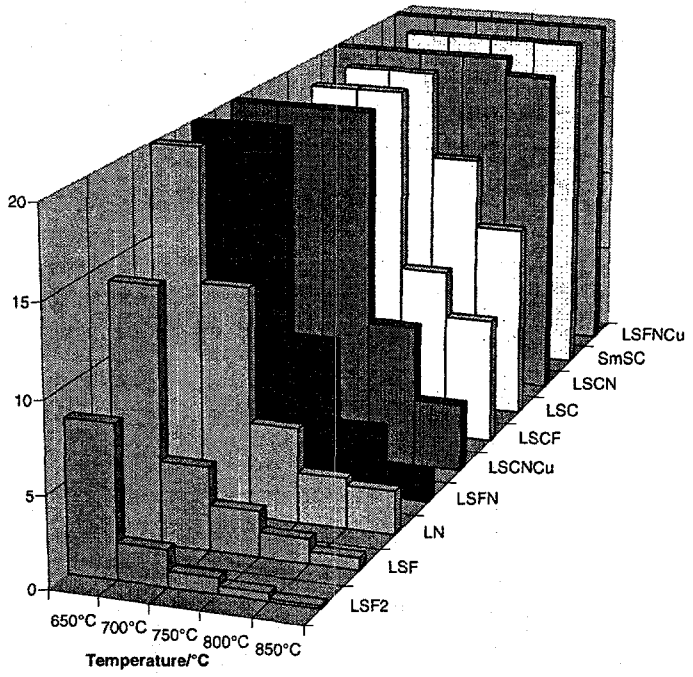

Fig. I-16. Areal Resistances (y-axis in units of Ω-cm^2) for Cathodes on Yttria-Stabilized Zirconia as a Function of Temperature

Additionally, we tested the chemical compatibility between the cathode materials and the electrolytes at the processing temperature, 1200°C, and the operating temperature, 800°C. At both temperatures, no reactions were observed between CGO and any of the cathode materials. However, for YSZ, a severe reaction was seen for the cobaltates, most ferrates, and nickelates, except for LSF at 1200°C. At 800°C, the cobaltates still showed severe reactions, but LN and LSF showed no reactivity. The apparent absence of reactivity between all cathode materials tested and CGO greatly expands the range of potentially suitable cathode materials for this electrolyte, and both LSF and LN are under study as potential cathode materials for use with YSZ.

5. Technical Management

The CMT Division, through the ANL Electrochemical Technology Program, provides support to the DOE Office of Transportation Technologies and to the DOE Office of Buildings Technology in the form of technical management of R&D contracts with industrial developers of fuel cells and related components. In this capacity, we prepare work statements, evaluate proposals, and conduct progress reviews. Major ongoing projects managed by CMT include DOE contracts with Plug Power, Inc.; Honeywell (previously AlliedSignal); Energy Partners L.C.; 3M Company; McDermott Technology, Inc.; the Institute of Gas Technology; and other suppliers of fuel cell components.

Plug Power completed the second year of a $14-million contract to develop an integrated 50-kW fuel cell system incorporating a fuel-flexible reformer. A major

accomplishment this year was the integration of a 10-kW fuel cell stack from Plug Power with a partial oxidation reformer developed by Epyx Corp. (a major subcontractor to Plug Power). The system produced electricity from the following fuels: ethanol, methanol, methane, Fischer-Tropsch synthetic gasoline, M-85 (85% methanol, 15% gasoline), low-sulfur gasoline, and California Phase II gasoline. During the operation of the integrated system, steady-state emissions were measured.

Honeywell and Energy Partners completed the second year of their respective contracts to develop reformate-tolerant PEFCs. Honeywell demonstrated two promising alternatives to conventional PrOx technology for reducing the CO content in reformate fuels to acceptable levels. Delivery of a 50-kW stack system to ANL is scheduled for July 2000. Energy Partners successfully demonstrated a low-cost (<$10/kW) injection molding process for bipolar plates that meet the DOE performance targets. The company is scheduled to deliver a 50-kW stack system to ANL in March 2000.

During the second year of its contract for development of membrane electrode assemblies (MEAs), 3M completed multiple deposition coating runs, producing more than 500 m of proprietary catalyst support material while exceeding targets for process control. The company also completed conversion of the catalyst support material to a nanostructured form (deposited on the 500 m of web material) and demonstrated feasibility of continuous formation of a three-layer catalyst-coated membrane (CCM) material. Samples of the CCM material are being evaluated by a fuel cell developer.

Honeywell, Arthur D. Little, Vairex Corp., and Meruit, Inc., continued developing advanced compressor/expander/motor machines to supply air at elevated pressure to the fuel cell system. These machines have a specified efficiency, size, weight, and net parasitic drain on the overall system. Argonne organized a nongovernmental panel to review the different concepts and to advise DOE and Argonne on selecting the most promising ones for continued research.

This year we successfully completed initial testing of a 30-kW Ballard fuel cell stack in the ANL Fuel Cell Test Facility. The facility fulfills DOE's need for an independent source for validating the performance of fuel cells fabricated by industrial developers under DOE sponsorship. The facility consists of a test cell with specially installed safety systems, an outdoor bulk hydrogen storage facility, and a gas management system to control the pressure, temperature, humidity level, and flow rate of both the fuel and oxidant gas supplies to the fuel cell. We also began modifying the facility to accommodate the testing of the Honeywell and Energy Partners systems that are scheduled for delivery to ANL in 2000.

II

Waste Materials Research

The Division has a wide variety of research efforts concerned with the management and disposal of waste materials, including high- and low-level nuclear wastes, spent nuclear fuel, surplus plutonium, and actinide species in subsurface groundwater.

A substantial effort is devoted to corrosion tests with simulated nuclear waste glasses and ceramics and with spent nuclear fuel under conditions expected for a geologic repository. Test durations run from a few days to more than a decade. Test methods include the Materials Characterization Center (MCC)-1, Product Consistency Test (PCT), Vapor Hydration Test (VHT), and drip tests. Samples of the waste solid and leachate are periodically taken for analysis to monitor reaction progress. Results are used to gain a better understanding of waste corrosion behavior and to support model development. Much of the present waste research on high-level waste and spent fuel supports the DOE effort to prepare a site recommendation for the proposed geologic repository at Yucca Mountain, Nevada.

Another component of the CMT waste materials research involves separation science and technology. There are two major thrusts: (1) substitution of low-enriched uranium (LEU) for high-enriched uranium (HEU) in the production of ^{99}Mo for medical applications and (2) treatment of radioactive, mixed, and hazardous waste. We are working to convert all current processes, worldwide, from HEU to LEU. The program is international, with ongoing and new initiatives with partners in Indonesia, Canada, the United States, Korea, Australia, and Argentina. Other research includes developing a solvent extraction process for removal of ^{137}Cs from alkaline supernatant from radioactive waste stored at the Savannah River Site, a magnetically assisted chemical separation process for several waste-treatment and environmental-cleanup applications, and a novel decontamination solvent for metals typical of nuclear reactor piping.

A. Testing of Spent Nuclear Fuel

1. *Spent Nuclear Fuel at DOE Sites*

The DOE currently owns over 200 types of spent nuclear fuels that it intends to store permanently in the Mined Geological Disposal System at Yucca Mountain. Before the fuels are accepted for storage, however, DOE must demonstrate that the mobilization rate of radionuclides from corroding fuel is sufficiently low in the repository environment that release criteria at the site boundary are not compromised. Because it is not practical to test the corrosion characteristics of every type of fuel, DOE has authorized testing of three fuel types: mixed oxide (MOX), metallic uranium, and aluminum-based uranium dispersion fuels. During the past year, corrosion tests were conducted on MOX and metallic uranium fuels, and plans were developed for corrosion testing of aluminum-based uranium dispersion fuels. It is expected that corrosion tests will be performed on all three fuel types in the next year.

a. Sample Characterization

Prior to planned corrosion tests, characterization activities were conducted on spent MOX and uranium fuels. These included physical characterization of the MOX fuel, as well as determination of phase and elemental distribution by macrophotography, scanning electron microscopy, and electron microprobe analysis. The results include determination of (1) the distribution and specific location of intermetallic particulates known as five-metal or epsilon phase (important because it may preferentially release Mo and Tc to a leachant solution in corrosion tests) and (2) radial profiles of specific elements.

The following conclusions were reached from characterization of irradiated uranium metal fuel: cracks and dispersed uranium hydrides and uranium carbides appeared throughout the fuel segments; no significant crack networks were found to exist with the possible exception of the interface region between fuel and cladding; and the presence of hydrides was not associated with crack locations.

Other characterization activities included development of an appropriate input code for ORIGEN-RA (a modified version of the ORIGEN code developed at Oak Ridge National Laboratory and used to perform detailed nuclide transmutation calculations based on flux history) and subsequent estimation of isotopic composition and burnup of spent fuel as a function of height in the fuel pin. These data are extremely important because measured releases of radionuclides during corrosion tests are related to the initial inventory of the radionuclide in the fuel sample, which may vary along the rod length. The primary means of estimating the initial inventory is use of the ORIGEN computer code.

b. Radionuclide Release Testing

Long-term (multi-year) unsaturated corrosion tests and shorter-term saturated batch tests are in progress with spent MOX fuel samples. The unsaturated tests subject spent fuel fragments to injections of simulated groundwater twice weekly at 90°C. Injected water reacts

with the fuel, percolates through a container holding the fragments, and is retained in the vessel until opened for analysis. The unsaturated tests were interrupted at 3, 7, and 12 months to determine the composition of leachate solution, vessel adsorbates, and incipient secondary (solid) phases on the fuel. Results indicated a decrease in solution pH from 8.4 to approximately 5 and incongruent release of elements from the fuel, with approximately 30% of I, 15% of Cs and Mo, and 10^{-3} to 10^{-4}% of Pu, Sr, and Tc released by 7 months. Of the plutonium released, over 40% was in the form of colloids. No secondary phases were observed on the sample surface, but microscopic analysis is pending.

In the saturated batch tests, powdered MOX fuel is wetted by simulated groundwater and maintained at 90°C. The objective of these tests is to determine the evolution of solution composition in parallel with formation and alteration of secondary phases. Four fuel samples are currently in test; no secondary phases were observed after 4 months.

Unsaturated corrosion tests are also underway with unirradiated metallic uranium (Hanford N-Reactor) fuel and simulated groundwater at 90°C. The release data indicated a very high degradation rate, with complete oxidation of 1-g uranium in approximately 2.5 months. Oxidation products were primarily UO_2, U_4O_9, and uranyl oxyhydroxides (schoepites). On the basis of X-ray diffraction and scanning electron microscopy, a significant fraction of the products appears to be colloidal in size. Since colloids may accelerate radionuclide movement in a repository environment, this is a significant finding, which will be quantified in the next year by means of colloidal-size and charge-distribution analysis. In addition, gas samples taken periodically indicate generation of H_2, CH_4, and CO_2 (H_2 from reaction of uranium with H_2O; CH_4 and CO_2 presumably from reaction of trace carbon in the fuel and from HCO_3^- present in the simulated groundwater). These gases can react with the fuel and produce pyrophoric material or create a combustible atmosphere in the waste container.

2. *Spent Fuel for Yucca Mountain*

During the past year, we continued to support the development of a technical basis for the "source term" (i.e., the rate of release of radionuclides from the disposed waste) for the candidate high-level nuclear waste repository in a hydrologically unsaturated zone of the volcanic tuff beds at Yucca Mountain. This effort includes characterizing high-burnup spent fuel, continuing unsaturated tests on UO_2 and spent fuel samples from commercial light water reactors, and preparing analysis and modeling reports (AMRs) that summarize the technical basis for modeling the source term in support of the upcoming decision to recommend the candidate Yucca Mountain site for development of a repository.

a. Characterization of High-Burnup Spent Nuclear Fuel

A model is being used to calculate concentrations of fissionable and neutron-absorbing nuclides in high-burnup spent nuclear fuel for criticality evaluation of the post-closure Yucca Mountain repository. The validation of the isotopic model will be performed to support the license application to the Nuclear Regulatory Commission for the proposed repository. Radiochemical assay is used, in part, to validate the model. The burnups of fuels used in model validation to date range from 7 to 46.5 gigawatt-days per metric ton uranium (GWd/MTU).

Additional radiochemical assays of higher burnup spent nuclear fuels from both pressurized water and boiling water reactors are required to validate the model.

To provide the information required for model validation, we analyzed 12 samples from fuel rods with burnups ranging from 45.8 to 77.6 GWd/MTU. These fuel rods originated from Three-Mile Island reactor 1 and from Quad Cities reactor 1. The complete analysis included the determination of 31 nuclides in each sample. Nuclides were selected so that atom percent fission burnup of each fuel segment could be calculated (^{148}Nd, Pu isotopes, and U isotopes). Additionally, nuclides possessing significant neutron-capture cross sections were determined because of their potential significance for assessing repository criticality.

A relatively new technique of coupling high-performance liquid chromatography (HPLC) with inductively coupled plasma-mass spectrometry (ICP-MS) was developed for these analyses. Inductively coupled plasma-mass spectrometry allows for rapid and accurate analysis of isobar-free nuclides with concentrations greater than 10 pg/mL in dissolved samples. The high sensitivity of ICP-MS allows the analyst to dilute the dissolved fuel sample prior to analysis and thereby minimize exposure to radiation. Several of the lanthanide nuclides (e.g., ^{147}Sm, ^{151}Eu, and ^{155}Gd) could not be determined directly with conventional ICP-MS due to significant isobaric interferences. As a result, analysis of these nuclides required chemical separation of interfering species. Chemical separations of Nd, Sm, Eu, and Gd were performed by use of HPLC with subsequent detection and analysis by ICP-MS. This technique allowed the determination of the isotopic distribution of each of these elements without resorting to classical wet chemical separation techniques, which are time consuming. The HPLC-ICP-MS technique provided a high-throughput method for a complete isotopic analysis of stable nuclides and radionuclides in spent nuclear fuel.

b. Unsaturated Testing of Unirradiated UO_2

Experiments in which low volumes of groundwater are periodically dripped onto unirradiated UO_2 and spent UO_2 fuels are effective ways to investigate the corrosion of spent UO_2 fuel in a hydrologically unsaturated, oxidizing environment, such as that expected in the proposed high-level waste repository at Yucca Mountain. In such "drip experiments," simulated groundwater is injected onto solid samples in stainless-steel reaction vessels maintained at 90°C and ~100% relative humidity. The UO_2 dissolves, and solid corrosion products precipitate on the surfaces of corroded UO_2 or fuel. We are conducting two series of drip tests on unirradiated UO_2. One test series was started in 1984 and the second in 1989; thus, these tests have been running continuously for 15 and 10 years, respectively. All tests involve right cylindrical UO_2 pellets, 13.9 mm in diameter. Some tests use 1.75-mm high pellets, one of which also contains crushed UO_2; other tests use 10-mm high pellets.[1] The pellets are stacked within Zircaloy tubes, and each pellet/Zircaloy assembly is placed into a stainless-steel reaction vessel with a water-injection port directly above the pellet assembly. Injected water contacts the top surface of each pellet, runs down the side, and drips from the bottom of the pellet into the base of the vessel; there is no direct contact between the pellets and the standing water (leachate) at the base of the vessel.

[1] D. J. Wronkiewicz, J. K. Bates, T. J. Gerding, E. Veleckis, and B. S. Tani, *J. Nucl. Mater.* **190**, 107-127 (1992).

Concentrations of uranium and elements derived from the injected groundwater are periodically determined by analysis of leachates after interaction with the UO_2. Solid corrosion products are also periodically sampled and analyzed.

This year, solids were analyzed from two 15-yr tests, PMP8U-3 and PMP8U-7, which had not been analyzed since those tests were started in 1984. We found the UO_2 pellet surfaces to be covered by uranyl corrosion products. Central regions on top of the pellet surfaces are covered by a relatively thick mat of uranophane, $Ca(UO_2)_2(SiO_3OH)_2(H_2O)_5$, and Na-boltwoodite, $Na(UO_2)(SiO_3OH)(H_2O)_{1.5}$. The silicates diminish toward the outer 2-3 mm of the pellet surfaces, with uranyl oxyhydroxides, such as schoepite (or metaschoepite), $(UO_2)_4O(OH)_6(H_2O)_{5\text{-}6}$, and becquerelite, $Ca(UO_2)_6O_4(OH)_6(H_2O)_8$, increasing in abundance. The bottom surface of UO_2 pellets is covered by abundant crystals of uranyl oxyhydroxides, but no uranyl silicates are evident there. These results are consistent with those reported for tests terminated after 1.5, 2.5, and 8 years. Wronkiewicz et al.[1,2] interpreted these observations as follows. At the initial point of contact of groundwater with the top of the UO_2 pellet, uranium dissolved from the UO_2 combines with elements in the groundwater (such as Na, Ca, and Si) to form complex uranyl silicates. Groundwater constituents become depleted as the water moves across and down the pellet surface, so that uranyl silicates do not precipitate far from the center of each pellet due to silicon depletion; this is followed by depletion of Na and Ca, resulting in only uranium being available by the time the water reaches the bottom of the pellet, where only uranyl oxyhydroxides precipitate.

Examinations conducted this year on solids from the 10-yr tests revealed substantially different results from those exhibited by the 15-yr tests. The 10-yr test samples did not react to the same degree as the 15-yr test samples even at much shorter reaction times (< 3 yr). Visible examinations of the 10-yr test samples have long indicated that the UO_2-pellet surfaces remain free of macroscopically visible precipitates, with the exception of PMP8U-10, the top surface of which is covered by a sparse layer of uranophane crystals. No uranyl oxyhydroxides are evident. Uranium releases to solution in PMP8U-10 are approximately ten times greater than those in PMP8U-9, -11, and -12 (Fig. II-1). The difference is due to the sorbed uranium plus particulate and suspended-particulate fractions. Scanning electron microscopy of PMP8U-9, -11, and -12 revealed that the top surfaces of the UO_2 pellets are remarkably unreacted. Grain boundaries are visible but display little evidence of preferential dissolution; only minor etching is apparent (Fig. II-2). Also, no solid precipitates are apparent on the top surfaces of pellets in these three tests, even after more than 10 years of continuous exposure to dripping groundwater. A potentially important consequence of this observation is that uranium release in these tests may be a reasonably accurate measure of UO_2 matrix dissolution under the test conditions. The uranium release rates in PMP8U-9, -11, and -12 have remained relatively constant over the ten years, corresponding to a dissolution rate for UO_2 of approximately $3\text{-}6 \times 10^{-3}$ mg/(m^2·day). We cannot explain at this time the reason for the observed differences between the two test series.

[2] D. J. Wronkiewicz, J. K. Bates, S. F. Wolf, and E. C. Buck, *J. Nucl. Mater.* **238**, 78-95 (1996).

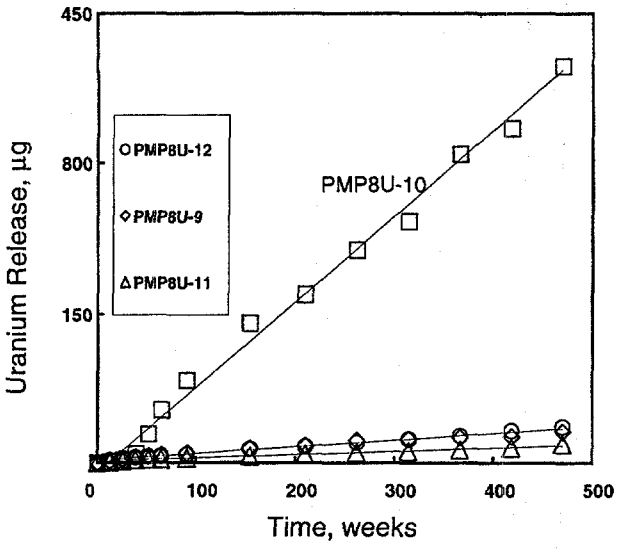

Fig. II-1.

Cumulative Uranium Releases for Ten-Year Drip Tests with Unirradiated UO_2. Mass-release rates for PMP8U-9, -10, -11, and -12 are 10, 120, 5, and 10 ng day^{-1}, respectively.

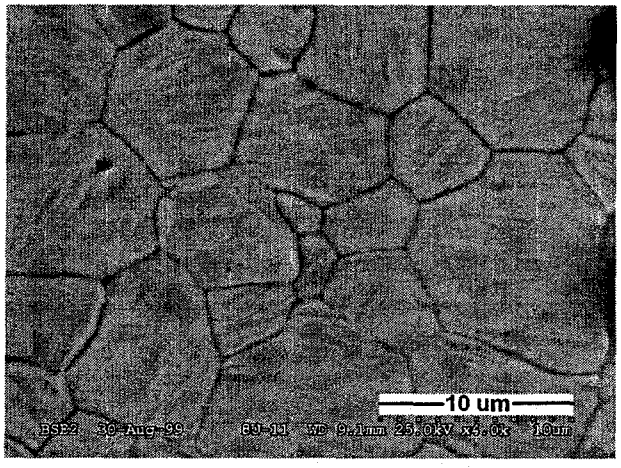

Fig. II-2.

Scanning Electron Image of Surface of UO_2 Pellet Showing Etching of Grain Boundaries in Test PMP8U-12

c. Tests with Spent Fuel Samples from Commercial Reactors

When the waste package containers and the fuel cladding are eventually breached in the repository, the fuel inside the cladding is expected to be exposed to humid air and/or dripping groundwater. Because most of the containers and fuel cladding are expected to remain intact for many thousands of years after emplacement, the conditions of interest for testing purposes involve fuel temperatures less than 100°C, relative humidity of ~100%, and contact with dripping groundwater. This section summarizes the results from corrosion tests conducted with commercial oxide spent fuels under conditions that are intended to simulate those expected in the repository (referred to as "service conditions"). These service condition tests are intended to provide information on the processes that control the corrosion of spent fuel and the associated radionuclide release.

The results discussed here are from three sets of ongoing service conditions tests conducted at 90°C using spent fuel pellet fragments from two commercial pressurized water

reactors. The fuel samples have a nominal burnup of 30 and 45 MWd/kg U and are designated ATM-103 and ATM-106, respectively. The tests, which were initiated in 1992, are configured to study the fuel corrosion and the associated radionuclide release when the fuel samples are exposed to saturated water vapor and to simulated groundwater (designated EJ-13) that is dripped onto the fuel at nominal rates of 0.21 and 0.021 mL/day. Samples of the leachate and the reacted fuel are collected and semiannually analyzed to measure the progress of the fuel corrosion and the associated radionuclide release. Unsaturated drip tests were also started this year with a high-burnup fuel sample (ATM-109, >65 MWd/kg U) from a boiling water reactor.

Analysis of the leachate solutions showed that most elements are released incongruently. These data show that technetium is released more rapidly than U and Sr. With the exception of iodine, technetium is released more rapidly than other radionuclides as the fuel corrodes under unsaturated conditions.

The complex, incongruent release behavior can be qualitatively explained by the formation of insoluble residue phases as the fuel matrix corrodes and by the precipitation of a suite of uranyl and other alteration phases that adsorb or incorporate radionuclides. Some fission elements (e.g., Pu, Zr, and Ru) are incorporated into an insoluble residue formed at the reaction interface, and some (e.g., Sr, Cs, and Mo) are incorporated into precipitated phases. The composition of the precipitated uranyl alteration phases that are formed depends strongly on water flux and its composition, with uranyl oxyhydroxides predominating in vapor tests, and alkali and alkaline earth uranyl silicates predominating in high-drip-rate tests. Samples from vapor tests display a relatively simple alteration-phase assemblage dominated by dehydrated schoepite and metaschoepite. This assemblage is readily explained by the lack of cations in the vapor and condensate that contact the fuel surface. Samples of ATM-103 from the high-drip-rate test at the 3.7-yr-test interval display a relatively simple alteration-phase assemblage dominated by the two structurally related uranyl silicates, Na-boltwoodite and β-uranophane. The Na-boltwoodite constitutes approximately 80 vol% of the corrosion layer, and β-uranophane accounts for about 20 vol%. This assemblage may reflect relatively late-stage alteration of the uranyl oxyhydroxides formed earlier. This hypothesis agrees with results of long-term drip experiments on unirradiated UO_2 and with observations from naturally weathered uraninite deposits.

The samples from low-drip-rate tests (0.021 mL/day) possess a much more complex assemblage of U^{6+} phases than observed in samples from either vapor or high-drip-rate tests. This complexity may reflect the limited influx of EJ-13 groundwater, which contributes Si, Na, Ca, and other cations. Common corrosion products from low-drip-rate tests include metaschoepite, an unidentified Na-uranyl oxyhydroxide tentatively identified as "Na-compreignacite," and soddyite. A minor constituent is the Cs-Ba-Mo-uranate phase that commonly occurs adjacent to dissolving fuel grains. A few isolated crystals of Na-boltwoodite were first detected in the low-drip-rate test with ATM-103 at the 4.1-yr test interval. They were abundant at the 5.2-yr test interval, but less abundant than soddyite. In one sample from the low-drip-rate test at the 5.2-yr test interval, soddyite appears to have replaced Na-compreignacite. These observations provide limited direct evidence for the replacement of uranyl oxyhydroxides by uranyl silicates. On the basis of studies on UO_2 corrosion under similar conditions, the

replacement of uranyl oxyhydroxides by uranyl silicates may become increasingly important at longer reaction times.

Because of its potential importance to the performance of the Yucca Mountain site, we have investigated the role that the uranyl and other alteration phases play in limiting the release of radionuclides. We have found that the incongruent release of cesium may be due to its precipitation in a Cs-Ba-Mo-uranate phase, which has been identified as $(Cs_{0.8}Ba_{0.6})[(UO_2)_5MoO_2O_4(OH)_6]$. However, the explanation for the observed incongruent release of neptunium, which is an important radionuclide, remains elusive. There is transmission electron microscopy evidence for neptunium being associated with dehydrated schoepite, which is the major phase in the vapor tests. A full explanation of the neptunium behavior and the role of the uranyl alteration phases in controlling its behavior is not yet available.

Because of the incongruent release behavior of the radionuclides and the precipitation of the dissolved uranium as uranyl alteration phases, the data for these tests do not provide a direct measure of the corrosion rate of the fuel. However, the normalized release rates (amount released divided by sample surface area times test duration) of selected radionuclides, like technetium, and the thickness of the precipitated corrosion layers can be used as indicators of the rate of fuel corrosion. The normalized technetium release rates for the high-drip-rate tests agree with the normalized release rates measured for fuel fragments under dynamic flow conditions.[3] However, for both the unsaturated tests and dynamic flow tests, because the effective surface area is unknown, the surface-area normalization complicates the comparison. If the normalized release rates for technetium provide an upper bound for the release rates of the other radionuclides in the unsaturated tests, they represent a conservative limit for the amount of radionuclides that can be released. These normalized rates are 54 mg/(m^2·day) for ATM-103 and 116 mg/(m^2·day) for ATM-106 in tests at 90°C. (The initial specific geometric surface area was used in the normalization. The rates would be reduced if surface roughness factors or if the surface area exposed as a result of grain boundary corrosion were included.) Despite these caveats, the consistency of our unsaturated drip tests with the dynamic flow tests indicates that the rate of matrix corrosion in dynamic flow tests is a conservative bound on the rate of radionuclide release in the more prototypical conditions in the unsaturated tests.

Future work will pursue a more complete understanding of the role that the alteration phases play in the observed incongruent release of important radionuclides (e.g., Np and Pu). In addition, we will focus on how grain boundary corrosion may influence the corroding surface area and the preferential release of important radionuclides such as Tc and I.

d. Tests on Clad Segments of Spent Nuclear Fuel

Once the waste package containers eventually breach and admit moist air and water, processes, such as crevice corrosion, are expected to result in localized breaching of the fuel cladding. The fuel inside the cladding will then be exposed to the unsaturated repository conditions and, as described above, is expected to corrode to form a variety of uranyl alteration

[3] W. J. Gray and C. M. Wilson, *Spent Fuel Dissolution Studies FY 1991-1994*, Pacific Northwest National Laboratory Report PNL-10450 (1995).

phases. The effects of the uranyl alteration phases on the cladding and on radionuclide release from breached fuel rods are uncertain. The possibilities range from splitting of the cladding along the length of the fuel rod as a result of the formation of expansive alteration phases as the fuel pellets corrode to a more benign scenario in which the alteration phases limit the rate of corrosion and radionuclide release from the breached fuel rods.

The uranyl alteration phases that are formed in experimental tests conducted under relevant conditions have been identified. The predominant uranyl alteration products formed upon contact with humid air are dehydrated schoepite ($UO_3 \cdot 0.8H_2O$) and metaschoepite ($UO_3 \cdot 2H_2O$), whereas sodium boltwoodite [$Na(UO_2)(SiO_3OH)(H_2O)_{1.5}$] is the predominant phase formed upon contact with dripping groundwater.[4] These reaction products have greater molar volumes than the molar volume of the UO_2 from which they are formed (45.5 to 94.5 cm^3/mol vs. 24.6 cm^3/mol). This increase in molar volume of the reaction products formed through oxidative dissolution of the fuel and precipitation of alteration phases has led to consideration of hypothetical splitting of the cladding in breached fuel rods. The mechanism that could cause splitting of the cladding is the crystallization pressure associated with precipitation of uranyl alteration phases as the fuel corrodes within the cladding. Analysis of the crystallization pressures suggests that the driving reactions are likely to be self-sealing, and as a result, the precipitation reactions involved are likely to proceed very slowly and are unlikely to generate crystallization pressures that will cause splitting of the cladding. This conclusion, however, needs to be verified.

Two complementary tests have been initiated to evaluate the effects of the fuel alteration phases on the cladding and on radionuclide release. The reaction of clad samples of light water reactor fuel with water vapor is being examined to determine if the formation of secondary reaction products will produce expansive forces sufficient to cause cladding failure. These vapor tests are performed at 175°C in 100% relative humidity to accelerate the rate of fuel reaction. In a second suite of tests, the reaction of the light water reactor fuels with periodic injection of silicon-rich groundwater at 90°C is being examined to investigate the effects of uranyl silicate alteration phase formation on the cladding and on radionuclide release. These drip tests are configured to allow the injected water to percolate through a fuel segment, determine changes in the hydraulic conductivity of the fuel sample segments as the fuel corrodes, and collect the water after it percolates through the sample to measure the radionuclide release.

Table II-1 gives the initial fractional release for five drip tests. The calculated values represent the amount of each radionuclide that was released into the approximately 20 mL of EJ-13 that was injected during the first 3 months of testing. In calculating the fractional releases, we used the ORIGEN code for estimation of the composition of ATM-103 and ATM-106. For the fractional releases of ATM-109C, we used the composition of an analyzed sample adjacent to the tested segment. As shown in Table II-1, the highest initial releases measured were for the soluble radionuclides ^{129}I and ^{137}Cs for all three fuel types. The initial

[4] R. J. Finch, E. C. Buck, P. A. Finn, and J. K. Bates, "Oxidative Corrosion of Spent UO_2 Fuel in Vapor and Dripping Groundwater at 90°C," Proc. of Materials Research Soc., Fall Meeting, Boston, MA, November 30-December 4, 1998 (1998).

Table II-1. Fractional Releases for Drip Tests with Clad Samples of ATM-103, -106, and -109C[a] after 3 Months

Radionuclide	ATM-103 (1.5 in.)[b]	ATM-103 (2.6 in.)[b]	ATM-103 (3.7 in.)[b]	ATM-106 (1.4 in.)[b]	ATM-109C (3.2 in.)[b]
^{90}Sr	$2.3x10^{-4}$	$4.6x10^{-4}$	$1.4x10^{-4}$	$1.5x10^{-4}$	-
^{99}Tc	$2.4x10^{-4}$	$1.7x10^{-4}$	$1.8x10^{-4}$	$3.6x10^{-4}$	$1.5x10^{-5}$
^{129}I	$1.4x10^{-2}$	$2.7x10^{-3}$	$1.5x10^{-2}$	$2.1x10^{-2}$	$3.7x10^{-2}$
^{137}Cs	$5.4x10^{-3}$	$5.0x10^{-3}$	$3.1x10^{-3}$	$8.5x10^{-2}$	$5.3x10^{-2}$
^{237}Np	$4.3x10^{-5}$	$9.6x10^{-5}$	$4.2x10^{-5}$	$2.4x10^{-6}$	$2.8x10^{-7}$
^{238}U	$9.0x10^{-6}$	$3.2x10^{-5}$	$6.6x10^{-6}$	$2.2x10^{-5}$	$1.4x10^{-6}$
^{239}Pu	$1.2x10^{-6}$	$1.8x10^{-6}$	$5.3x10^{-6}$	$5.4x10^{-7}$	$2.4x10^{-7}$

[a] Fuel burnups are 30, 45, and >65 MWd/kg for ATM-103, -106, and 109C, respectively.

[b] Different fuel sample lengths were used to investigate the effects of this parameter.

releases of ^{137}Cs correlate with, and are approximately equal to, the fission gas releases for each fuel type. The release values reported for ATM-106 and ATM-109C exceed the 2% estimate currently assumed in performance assessment calculations. Releases of actinides were generally inversely correlated with fuel burnup. Both the vapor and drip tests with clad fuel segments will continue.

3. Synthesis and Characterization of Waste Alteration Phases

Our earlier experimental studies on the corrosion of unirradiated UO_2 and spent UO_2 fuels demonstrated that UO_2 in spent fuel is unstable in oxidizing, humid-air, or aqueous environments, such as exist at the proposed high-level nuclear waste repository at Yucca Mountain. Fuel corrosion involves matrix dissolution of UO_2 and releases of radionuclides from the spent fuel. The most abundant corrosion products of spent UO_2 fuel are U^{6+} phases, including uranyl oxide hydrates and uranyl silicates. Studies of natural occurrences show that these phases may persist for hundreds of thousands of years, making them potentially important long-term radionuclide hosts. Most hazardous radionuclides (fission products and transuranic elements) in spent fuel exist in very low concentrations and are, therefore, unlikely to form pure phases; rather, trace levels of radionuclides may be incorporated into U^{6+} corrosion products. If so, this may significantly affect the long-term mobility of radionuclides released from corroded fuel.

A DOE-funded collaboration with the University of Notre Dame and the University of Missouri-Rolla is examining the potential for the incorporation of various radionuclides into the crystal structures of U^{6+} compounds. This effort includes synthesis of radionuclide-bearing U^{6+} solids (including those with surrogate radionuclide analogues), structural and chemical characterization of synthetic and natural U^{6+} minerals that are potentially important corrosion products of spent fuel, and ion-exchange experiments with natural and synthetic U^{6+} compounds.

The mixed-valence oxyhydroxide ianthinite, $U_2^{4+}(UO_2)_4O_4(OH)_6(H_2O)_9$, and the Ca-uranyl oxyhydroxide becquerelite, $Ca(UO_2)_6O_4(OH)_6(H_2O)_8$, were synthesized with small amounts of Ce^{4+} and Nd^{3+} (as actinide surrogates). The synthetic samples were then analyzed by analytical transmission electron microscopy (TEM). The results indicated that some neodymium may be present in the becquerelite, but at very low levels. The ianthinite contained a significant

amount of neodymium, although quantification was difficult. The Nd/O ratio was nearly constant for all material analyzed by TEM. Cerium-doped ianthinite was thought to contain a small amount of cerium (approximately 200 ppm); however, electron energy loss spectroscopy (EELS) showed no evidence for this element. A small amount of copper was identified in the sample and was attributed to the synthesis technique. Determining the mechanisms that control the incorporation of trace levels of actinides into U^{6+} phases provides a basis for extrapolating short-term experimental results to potential long-term behavior in the repository. These preliminary results suggest that ianthinite and becquerelite may be more accommodating to the incorporation of trivalent actinides [e.g., Am(III), Cm(III)] than they are to quadrivalent actinides [e.g., Pu(IV)].

Results reported this year also include the discovery of a naturally occurring U(V)-mineral, a mixed-valance uranium carbonate (wyartite).[5] The crystal structure was solved to a high degree of precision, and this finding demonstrates for the first time the existence of a naturally occurring mineral with U(V). The U(V) valence state is considered unstable in most natural waters; however, the reduction of dissolved UO_2^{2+} to U^{4+} may be kinetically inhibited, as this requires exchange of two electrons and a change in coordination. Reduction of UO_2^{2+} to UO_2^{+} may be kinetically favorable, and the persistence of UO_2^{+} may permit precipitation of a U^{5+}-bearing mineral, such as wyartite. This discovery has potentially profound implications for uranium geochemistry, as well as for the potential behavior of actinides such as Np(V) and Pu(V) in U(VI)-bearing solutions, such as might occur in a waste repository.

B. Immobilization of Plutonium

The DOE Fissile Materials Disposition (FMD) Program is considering several alternatives for the disposal of surplus plutonium resulting from the dismantlement of nuclear weapons. One such alternative is immobilization, where the plutonium would be fixed into a waste form that meets safety and security objectives. A titanate-based ceramic has been selected by DOE as the preferred waste form. This ceramic contains several phases, including pyrochlore ($A_2Ti_2O_7$), zirconolite ($ABTi_2O_7$), Hf-bearing rutile (TiO_2), and brannerite (BTi_2O_6), where A = calcium, actinides (ACT), and rare earth elements (REE), and B = ACT, REE, Zr, and Hf. A backscatter SEM image of this ceramic is shown in Fig. II-3. Argonne's participation in the FMD includes (1) ceramic fabrication, (2) ceramic characterization, and (3) corrosion testing.

1. *Ceramic Fabrication*

Carbon has been identified as a potential contaminant in the plutonium feedstream of the titanate-based ceramic waste form chosen for immobilization of surplus plutonium. Carbon, in either crystalline or amorphous form, may impede densification and/or alter the phase assemblage of the titanate-based ceramic. Experiments (with ceramic samples prepared by sintering of calcined powders at 1350°C) were designed and conducted to test for these effects. Prior to heating, carbon was added to the powders as either amorphous carbon or graphite. The

[5] P. C. Burns and R. J. Finch, *Amer. Mineral.* **84**, 1456 (1999).

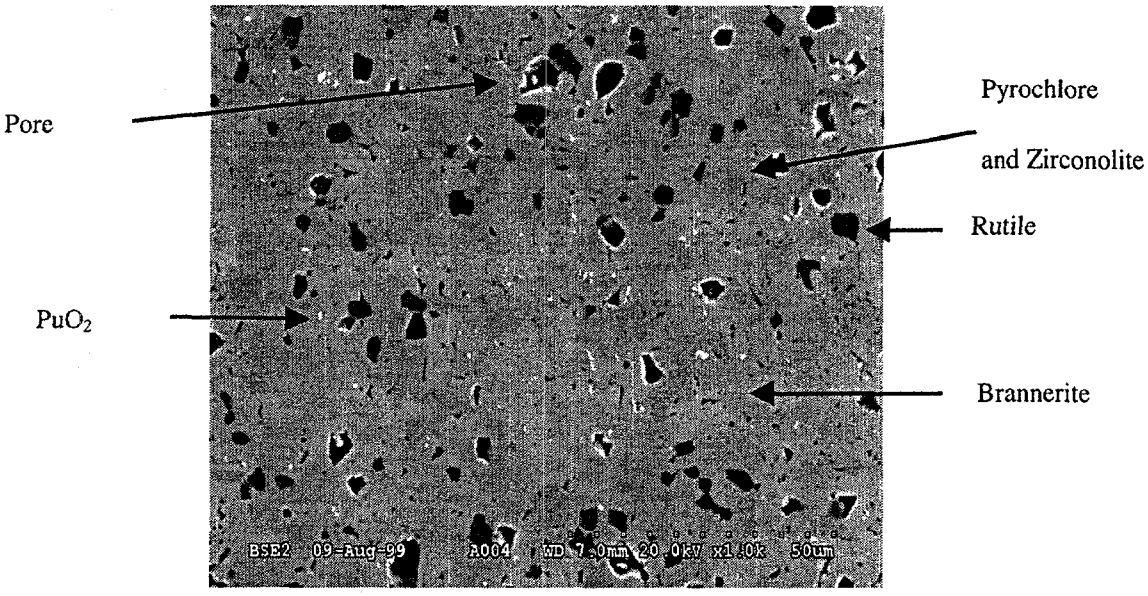

Fig. II-3. Scanning Electron Micrograph Backscatter Image of Hf-Ce-Pu Baseline Ceramic

specimens were produced under identical processing conditions, except for the initial level of carbon contamination (0-5 wt%). The amount of residual carbon not removed during heating is determined by heating rate and processing atmosphere.

No significant change in phase assemblage was apparent in these specimen, but bulk density trends did show a discernable effect. Since the densification rate is affected but the phase assemblage is not, we believe that the carbon merely interferes physically with reactive sintering mechanisms.

The residual porosities reported in Fig. II-4 were estimated from the theoretical density and the measured geometric density. As shown in Fig. II-4, residual porosity increases (or conversely, bulk density decreases) as the carbon level of the powder is increased. Ceramic waste forms with porosity levels nearing or beyond 8 vol% are likely to contain interconnected or open porosity.[6] Open porosity effectively increases the surface area exposed to corrosive environments and is therefore unwanted. The data in Fig. II-4 suggest that carbon levels should be kept below 3 wt% of the total batch. Since the carbon may be amorphous, crystalline (graphite), or a mixture of both, the worst case must be assumed. Carbon contamination is most likely present as part of the plutonium feedstream. Since the plutonium level in the Hf-Pu-U baseline titanate ceramic is on the order of 10 wt%, the carbon level of this precursor can be as high as 30 wt%.

[6] H. Shaw, Lawrence Livermore National Laboratory, personal communication (1999).

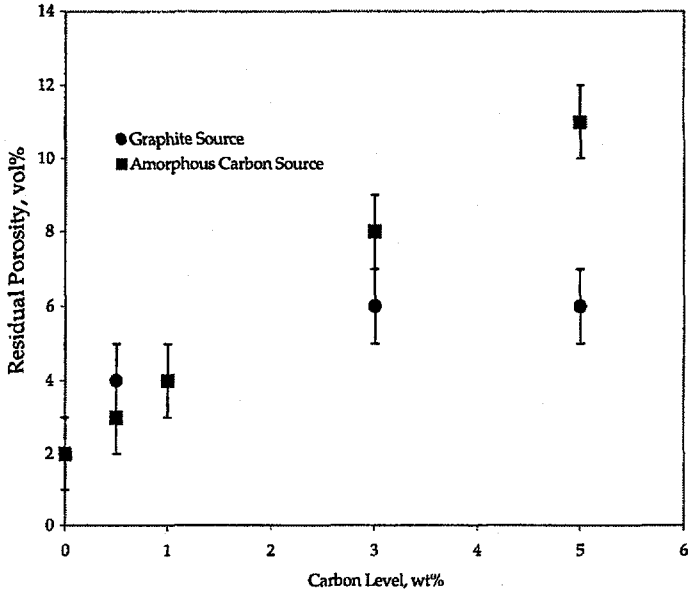

Fig. II-4. Residual Porosity of Ceramic Samples Made with Various Amounts of Carbon

2. Ceramic Characterization

Microstructural investigations are being used to help obtain thermodynamic data for the ceramic formulation and to assist in the interpretation of corrosion test data. This year, work was completed on the determination of cerium oxidation states in various ceramics. Determining the oxidation states of key elements in the ceramic helps to better understand the effect of processing variables and yields useful thermodynamic data. As processing conditions influence the distribution of element oxidation states and site occupancy in the different titanate phases, they may also lead to changes in the corrosion behavior.

Cerium is being used as a surrogate for plutonium in a number of waste form studies. Cerium(IV) is very nearly the same size (1.11 Å vs. 1.10 Å in eight-fold coordination) and chemically similar to Pu^{4+}. One difference is that Ce^{4+} is much easier to reduce to the trivalent species.[7] Two pyrochlore ceramics that were fabricated at the University of California-Davis were examined with electron energy loss spectroscopy (EELS) to determine the cerium oxidation state (Fig. II-5). The cerium oxidation state in the pyrochlore was determined by using the Ce-M_4/M_5 absorption edge ratio in the EELS spectra.[8] The pyrochlore that exhibits a greater proportion of Ce(IV) was synthesized from $CaCO_3$, TiO_2 (anatase), and CeO_2 at 1225°C in 100% O_2. The pyrochlore containing mainly Ce(III) was produced at 1300°C in air. The EELS data show that as long as the conditions of synthesis are sufficiently oxidizing, cerium is a good nonradioactive surrogate for plutonium in waste-form development studies.

[7] E. C. Buck and J. K. Bates, *Appl. Geochem.* **14,** 635-653 (1999).

[8] J. A. Fortner and E. C. Buck, *Appl. Phys. Lett.* **68,** 3817-3819 (1996).

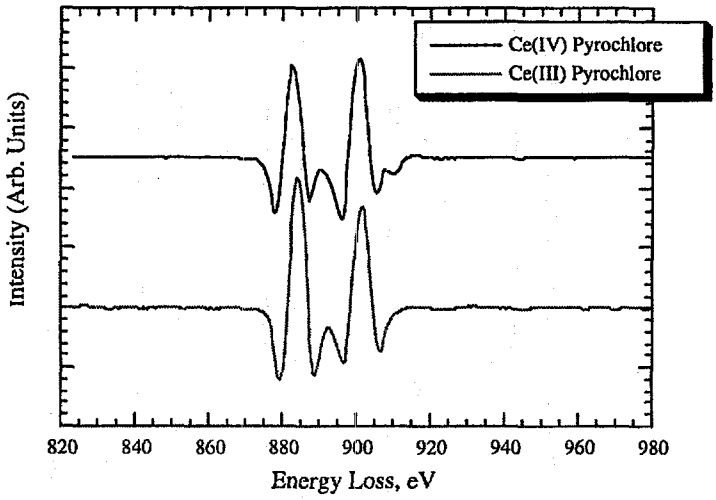

Fig. II-5. Electron Energy-Loss Spectroscopy of Cerium-Bearing Pyrochlores from the University of California-Davis. The spectra indicate a change in the cerium oxidation state between the two pyrochlores.

Our TEM sample preparation capabilities have been improved to characterize the microstructure of materials more completely. A technique called "tripod polishing" was investigated to produce larger samples of ceramic for TEM examination (Fig. II-6). This technique was used to prepare a sample of Hf-Ce-U ceramic for investigation. Previously, we had determined that the pyrochlore ceramics in a Hf-Ce-U formulation contained numerous intergrowths or lamallae.[9] In this case, the lamallae were thought to be zirconolite-4M within the pyrochlore. However, based upon samples prepared by tripod polishing, these features appear to be common to other pyrochlores, as Lumpkin has noted.[10] In the Hf-Ce-U series of ceramics, intergrowths of zirconolite within the pyrochlore were extremely common. The role that these might have in the corrosion behavior of the ceramics is under investigation.

3. Ceramic Corrosion Testing

The goal of the ceramic corrosion testing is to provide data for a mechanistically based corrosion model. Such a model will be used to quantitatively predict the corrosion rate of the ceramic under various repository conditions. Two important questions are:

- What is the bounding corrosion rate of the ceramic?
- Are there any conditions under which the corrosion rate of the ceramic will change?

[9] E. C. Buck, R. Gieré, and D. B. Chamberlain, Mater. Res. Soc. Symp. Proc. (in press).

[10] G. R. Lumpkin, Australian Nuclear Science and Technology Organization, personal communication (1999).

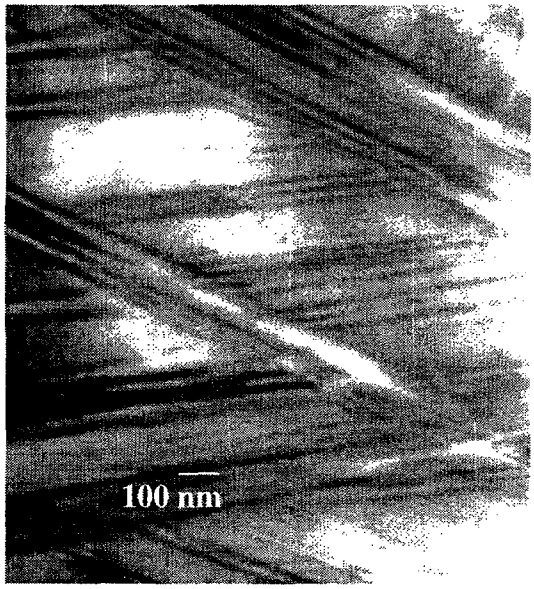

Fig. II-6.

Micrograph of Tripod Polished Sample of Hf-Ce-U Ceramic Showing a Large Number of Intergrowths within the Pyrochlore

Both short- and long-term corrosion tests are being used to help answer these questions. The short-term tests follow the MCC-1 protocol and involve several different ceramics. The goal is to measure the bounding corrosion rate for the material. The long-term tests are conducted for up to two years and follow the PCT-B protocol. Important results from these tests are the long-term corrosion rate of the ceramics and release data for Pu and Gd from the ceramic.

Figure II-7 shows the normalized calcium release for the MCC-1 tests. (The release of calcium is greater than the release of other elements and is, therefore, reported here.) The NL(Ca) values increase between 1 and 3 days at the rate of about 0.6 g/(m^2·day), and the NL(Ca) values also increase between 7 and 35 days but at a lower rate [about 0.02 g/(m^2·day)]. This change in the release rate of calcium probably reflects a change in the rate-controlling process. Several explanations have been proposed. The presence of particularly soluble phases, fined-grained material, or high-energy sites on the surface of the ceramic might lead to the observed behavior. In addition, the approach to saturation with respect to some solid phase or the

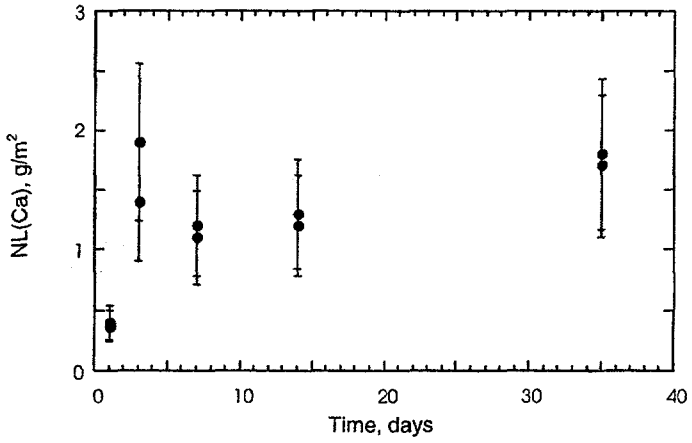

Fig. II-7. Normalized Mass Loss of Calcium from Titanate Ceramic in MCC-1 Tests

formation of some protective layer of alteration phases might decrease the corrosion rate. Experiments are planned or are underway to provide data that will help explain the observed change in corrosion rate.

Figure II-8 shows the results for release of Ca, Gd, and Pu in PCT-B tests that range from 98 to 728 days. Two important observations can be made from these data. First, the calcium release rate is constant from 98 to 728 days [~7 x 10^{-5} g/(m^2·day)]. This suggests that the corrosion continues for relatively long durations. The calcium release rate measured in these tests is consistent with corrosion rates measured for similar ceramics using single-pass flow through tests.[11] Second, the release rates of Gd and Pu increase by an order of magnitude between the test intervals of 98-128 days and 364-728 days (Table II-2). This is a particularly interesting result that cannot be explained at this time. Similar long-term PCT-B studies are underway with other ceramics.

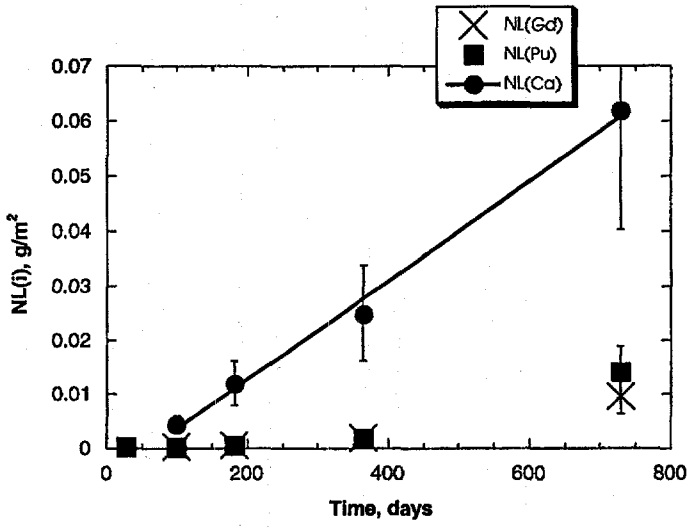

Fig. II-8. Normalized Mass Loss of Ca, Gd, and Pu from Titanate Ceramic in PCT-B Tests

Table II-2. Normalized Release Rates Calculated from PCT-B Tests for Several Time Intervals

Element	98-182 days	182-364 days	364-728 days
Ca	7 x 10^{-5}	9 x 10^{-5}	6 x 10^{-5}
Gd	3 x 10^{-6}	8 x 10^{-6}	2 x 10^{-5}
Pu	7 x 10^{-6}	1 x 10^{-5}	7 x 10^{-5}

[11] W. L. Bourcier, *Interim Report on Development of a Model to Predict Dissolution Behavior of Titanate Waste Form in a Repository*, Lawrence Livermore National Laboratory Report PIP-00-003 (1999).

C. Testing and Modeling of Waste Glasses

Waste glass testing under unsaturated conditions is being conducted to support development of models for the release rates of radionuclides as solutes and colloids from waste glass when it is eventually contacted by dripping groundwater or humid air in the repository. The release of radionuclides from waste glass will depend on the rate of hydrolysis and dissolution (also referred to as "corrosion") of the glass network under these conditions. Because the glass corrosion forms a layer of smectite clays and other alteration phases on the glass surface, colloids are formed as these alteration layers crack and spall from the corroding glass surface. This section summarizes our testing of waste glass corrosion in humid air (referred to as "hydration testing"), estimation of parameter values that can be used to calculate the waste-glass corrosion rates for different modes of water contact (i.e., immersion, dripping water, and humid air), and development of a model for the formation of colloids.

1. Hydration Testing

Vapor hydration refers to the alteration of waste glass upon exposure to humid air. The process is believed to occur in a film of water that condenses on the surface of the glass and can be interpreted as a special case of aqueous corrosion. To provide a basis for a model of the rate of hydration alteration under the conditions to which the glass may be exposed in the repository, we have conducted tests designed to characterize the hydration processes and to measure the temperature dependence of the hydration rate.

In the standard vapor hydration test, two monolithic samples of glass are fabricated, polished to a 600 grit finish, and suspended within a stainless steel reaction vessel (22 mL), as shown in Fig. II-9. The wafers are staggered from the suspension hanger to prevent them from coming into contact with each other or the vessel during the test. A volume of deionized water equal to 0.10 mL above that required to saturate the volume of the vessel is then added. The volume of 0.10 mL is chosen because (1) it is large enough to ensure that a saturated vapor phase exists at the desired test temperature after water has condensed on the samples, and (2) it is small enough such that condensed water will not drip from the samples.

After tests at elevated temperature (typically, 200°C), the rate of alteration is measured by first splitting the reacted glass specimen and embedding one-half of the specimen in epoxy such that its cross section is parallel with the polishing surface. The cross section is then polished and examined with scanning electron microscopy (SEM) to measure the thickness of the alteration layers.

During the past years, tests were conducted to investigate the influence of the amount of water in the test vessel on the hydration rate. The influence of this parameter was found to be considerable, as demonstrated in Fig. II-10. The alteration rate of the glass (131-TDS) increases rapidly to a maximum as the amount of water is decreased from the standard amount. The location of the peak is near the amount of water that is needed to just saturate the vessel, which is about 0.18 mL. The left side of the peak decreases continuously with the amount of water in the test vessel. This finding indicates that the hydration rate drops rapidly as the relative humidity in the test vessel decreases below 100%.

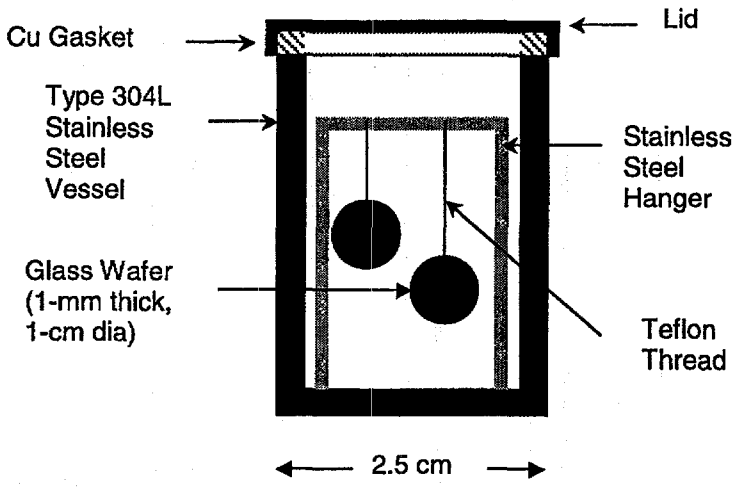

Fig. II-9. Schematic Diagram of Vapor Hydration Test Setup

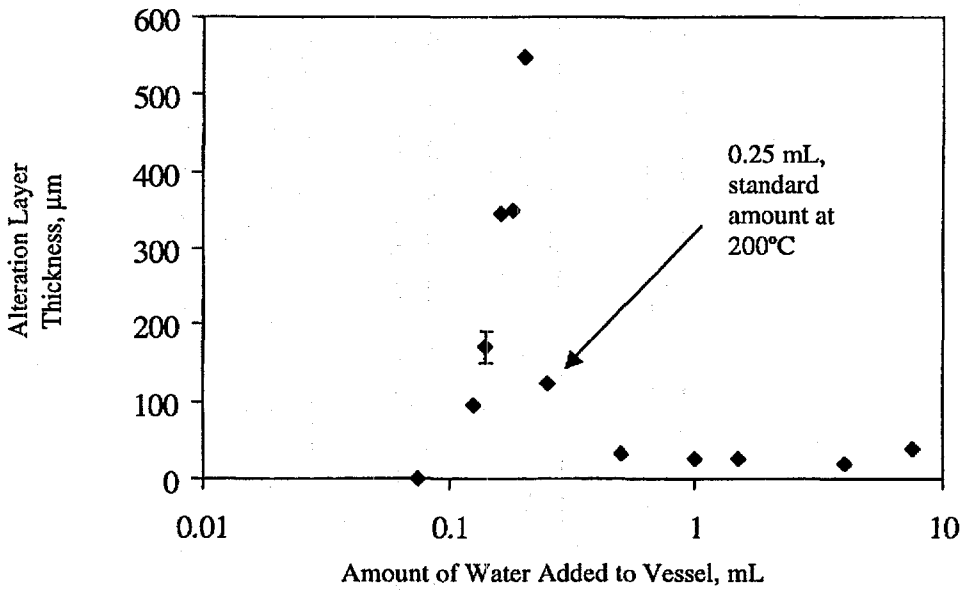

Fig. II-10. Average Alteration Layer Thickness versus Amount of Water in Vessel for Vapor Hydration Tests Conducted for 21 Days at 200°C with 131-TDS Glass. The error bars on the data point at 0.14 mL represent one standard deviation from three tests (12.5%).

When the amount of water is increased from the standard amount, the alteration rate also decreases to a constant rate. We believe that the excess water conditions are less corrosive because they result in continuous condensation onto, and dripping of water from, the glass samples. This limits the pH increase due to leaching of alkali metals from the glass. To check this hypothesis, we conducted several excess-water VHTs at 200°C for 21 days with 131-TDS glass and various amounts of excess water between 0.50 and 7.50 mL. The residual solutions

were analyzed by ICP-MS. The fraction of boron (known to be a highly soluble glass component) released to the bottom of the vessel was compared to the extent of alteration based on measurements of the original thickness of the glass sample and the alteration layer thickness. With high volumes of water (4 and 7.5 mL), the percent boron released from the glass correlated well with the extent of alteration. This finding indicates that the boron was washed to the bottom of the vessel upon alteration. With smaller volumes of water (0.5, 1, and 1.5 mL), the amount of boron released to the bottom was significantly less than the extent of alteration of the samples. These results are consistent with the hypothesis that excess water results in a continuous reflux (i.e., condensation onto, and dripping of water from, the test samples). They also suggest that such conditions are likely to be pertinent to glass hydration in the repository.

These data significantly changed our outlook on this research, as one of the main goals was to provide an upper bound for the vapor hydration rate. The data in Fig. II-10 indicate that the rates measured with the standard VHT, for the most part, do not represent the upper bound for the vapor hydration rate. Since the "high" rates appear to occur only within a very narrow range of conditions, they are probably irrelevant to repository conditions, so obtaining the upper bound vapor hydration rate is now probably irrelevant.

Figure II-11 shows semi-log plots of the alteration layer thickness versus time for two glasses (designated as 131-TDS and 51S) subjected to the standard VHT. Two distinct stages of corrosion are evident, an initial rapid one followed by the slower one indicated by straight lines in Fig. II-11. These stages are observed in the aqueous corrosion of waste glass under conditions of high surface area to solution volume (S/V).

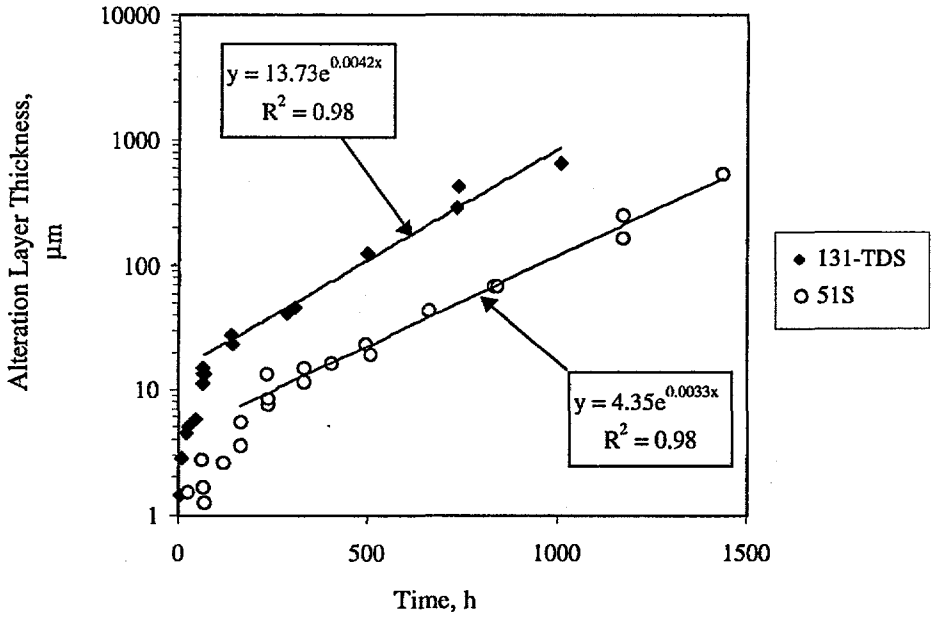

Fig. II-11. Alteration Layer Thickness versus Time for 131-TDS Glass and 51S Glass Vapor Hydrated at 200°C Using the Standard VHT

The effective activation energy for both stages of the reaction is ~80 kJ/mol. This result suggests that a similar mechanism is responsible for the rate-limiting step in both stages of the reaction. It is also consistent with the contention that the standard VHT is very similar to aqueous corrosion of waste glass under high S/V conditions. The continuing work in this area is intended to obtain a sufficient data base to show that vapor hydration is indeed a special case of glass aqueous corrosion.

2. Estimation of Dissolution Parametric Values

Calculations involved in a total system performance assessment will play an important role in the design and licensing of the federal repository for high-level radioactive waste disposal. These calculations will be used to evaluate the long-term containment of radionuclides by the waste forms and the engineered barrier systems and to ensure that regulatory requirements will be met throughout the service life of the disposal system. A mechanistic rate expression has been developed for borosilicate waste glasses. That expression contains terms for the forward dissolution rate (k_f), which depends on the glass composition, pH, and temperature, and for the reaction affinity term, which quantifies the feedback effect of solute species on the glass dissolution. The rate expression is

$$\text{rate} = S \cdot k_0 \cdot 10^{h \cdot pH} \cdot e^{(-E_a/RT)} \ (1 - Q/K) \qquad (1)$$

where S is the surface area, k_o is the intrinsic dissolution rate, h is a constant, and E_a is the activation energy; k_o, h, and E_a reflect the effects of the glass composition, pH, and temperature on the rate. The affinity term (1 – Q/K) accounts for the effect of dissolved species on the dissolution rate. Under dilute solutions, the value of the affinity term will remain near one, and glass will dissolve at its forward rate:

$$k_f = S \cdot k_0 \cdot 10^{h \cdot pH} \cdot e^{(-E_a/RT)} \qquad (2)$$

The parameter values needed to use Eq. 1 can be measured in tests in which the glass dissolves at its forward rate. Previous tests have shown the values of h and E_a can be assumed to be independent of the glass composition.[12,13,14,15] We have conducted short-term MCC-1 tests to determine the values of the intrinsic dissolution rate (k_0) for a range of possible waste glass compositions. The glasses used in these tests include reference compositions for the Defense Waste Processing Facility (DWPF), the West Valley Demonstration Project (WVDP), and the high- and low-level waste forms for Hanford tank wastes. Tests were conducted with two other

[12]P. K. Abraitis, D. J. Vaughan, F. R. Livens, L. Monteith, D. P. Trivedi, and J. S. Small, *Mater. Res. Soc. Symp. Proc.* **509**, 47-54 (1998).

[13]T. Advocat, J. L. Crovisier, E. Vernaz, G. Ehret, and H. Charpentier. *Mater. Res. Soc. Symp. Proc.* **212**, 57-64 (1991).

[14]K. G. Knauss, W. L. Bourcier, K. D. McKeegan, C. I. Merzbacher, S. N. Nguyen, F. J. Ryerson, D. K. Smith, and H. C. Weed, *Mater. Res. Soc. Symp. Proc.* **176**, 371-381 (1990).

[15]B. P. McGrail, W. L. Ebert, A. J. Bakel, and D. K. Peeler, *J. Nucl. Mater.* **249**, 175-189 (1997).

glasses (LD6-5412 and PNL 7668) to expand the composition range of the study and provide added insight regarding the effect of composition on the intrinsic dissolution rate.

Although the pH and temperature dependencies have only been measured for a few glasses, the values of h and E_a are similar for these glasses. For the present analysis, we used h = 0.4 and E_a = 80 kJ/mol. The pH at the test temperature of 90°C was assumed to be 1.6 units lower than the pH measured at room temperature, resulting from the difference in the equilibrium constants of water at 25 and 90°C. This adjustment to the pH has the effect of increasing the value of log k_0 by 0.64 (and the value of k_0 by a factor of 4.4) for all glasses. The temperature-adjusted pH values were used to calculate the value of the pH term (i.e., $10^{h \cdot pH}$) at 90°C. Since all tests were conducted at 90°C, the value of the temperature term is the same for all tests.

Table II-3 summarizes the intrinsic dissolution rates calculated by using Eq. 2 and the normalized dissolution rates based on B and Si. The average intrinsic dissolution rate of the reference high-level waste glasses is almost the same as the average for all nine glasses. Most of the difference in the dissolution rates of these glasses in short-term MCC-1 tests is due to the small differences in the solution pH values. The similarity in the intrinsic dissolution rates of glasses having significantly different compositions is probably an indication that the same rate-limiting reaction controls the dissolution rate for each glass.

Table II-3. Normalized Dissolution Rates (NR) and Intrinsic Rate Constants (k_0) for Various Waste Glasses

		NR, g/(m²·day)		log {k_0/[g/(m²·day)]}	
Glass	Average pH[a]	B	Si	B	Si
SRL 51S[b]	9.9	0.66	0.66	8.01	8.01
SRL 202U[b]	9.8	0.69	0.75	8.07	8.11
SRL 165U[b]	9.6	1.0	1.1	8.31	8.35
SRL 131U[b]	9.8	1.2	1.1	8.31	8.27
WV6[c]	9.5	0.69	0.70	8.19	8.20
Hanford-D[d]	10.5	1.3	0.90	8.57	8.27
Hanford-L[e]	9.5	0.97	1.0	8.34	8.35
LD6-5412[f]	9.3	0.47	0.71	8.10	8.28
PNL 7668[g]	9.2	1.1	1.0	8.51	8.47
High-level waste glasses (mean±s)		1.41 ± 1.26	1.07 ± 0.49	8.24 ± 0.19	8.20 ±0.11
All glasses (mean ±s)		1.22 ±1.08	1.01 ± 0.42	8.27 ± 0.18	8.26 ±0.13

[a] Average pH value measured at room temperature in tests included in regression analysis.

[b] Reference high-level waste glass for DWPF.

[c] Reference high-level waste glass for WVDP.

[d] Reference high-level waste glass for Hanford.

[e] Reference low-level waste glass for Hanford.

[f] Glass with high Al_2O_3 content.

[g] Glass with low Al_2O_3 content.

The intrinsic dissolution rates of the nine borosilicate glasses, which have a wide range of compositions, were estimated from the short-term MCC-1 tests by deconvoluting the effects of temperature and solution pH. The intrinsic dissolution rates extracted from the test results are similar: log $\{k_0/[g/(m^2 \cdot d)]\} = 8.3 \pm 0.2$. The very small variation in the rates indicates that the same intrinsic dissolution rate can be used for high-level waste glasses in performance assessment calculations with little added uncertainty. The intrinsic dissolution rate cannot be used to discriminate between glasses that have different chemical durabilities under anticipated disposal conditions. Instead, the response in a test that is sensitive to solution feedback effects must be used. We are currently evaluating the use of the PCT for this purpose.

3. Colloid Formation Modeling

We know from past corrosion tests that, during early reaction of waste glass under unsaturated drip and static test conditions, the glass dissolves and releases glass components at a rate proportional to the corrosion of the waste form. As the glass dissolves, dissolution of the waste form results in solution conditions that promote nucleation of clay colloids and the formation of clay alteration layers on the surface of the glass. These clay phases sorb ionic actinide species or colloidal actinide-bearing phases.

In a solution of low ionic strength, the colloids are stable, and the rate of formation of plutonium-bearing colloids ($dm_{Pu\text{-}coll}/dt$) is proportional to the amount of altered glass (M_{alt}). Boron is used as a marker of the extent of glass corrosion since it is a highly soluble glass component and does not get incorporated into alteration phases. Experimental data from the static PCT corrosion of two DWPF glasses (at two S/V ratios) show that the rate of plutonium-bearing colloid formation decreases as the glass alters (Fig. II-12). This behavior is also observed initially in drip tests with waste glass (Fig. II-13). The response is a power-law decrease in plutonium-bearing colloid formation rate as the glass corrodes:

$$\frac{dm_{Pu-coll}}{dt} = a(M_{alt})^{-b} \tag{3}$$

Variations in the constants, a and b, obtained for the various glasses may be a function of the S/V ratio, leachate composition (e.g., ionic strength), colloid composition, or other experimental parameters.

Another mechanism of colloid formation is evident in the drip tests at long test durations, where the spallation of plutonium-bearing colloids dominates the long-term release of plutonium from the waste form. Once the cumulative boron release is greater than ~1-3 g/m^2 (Fig. II-13), the release of plutonium is controlled by spallation of this layer and, thereby, related to the total amount of glass reacted. The release of spallation colloids is represented by

$$\frac{dm_{Pu-coll}}{dt} = \kappa M_{alt} \tag{4}$$

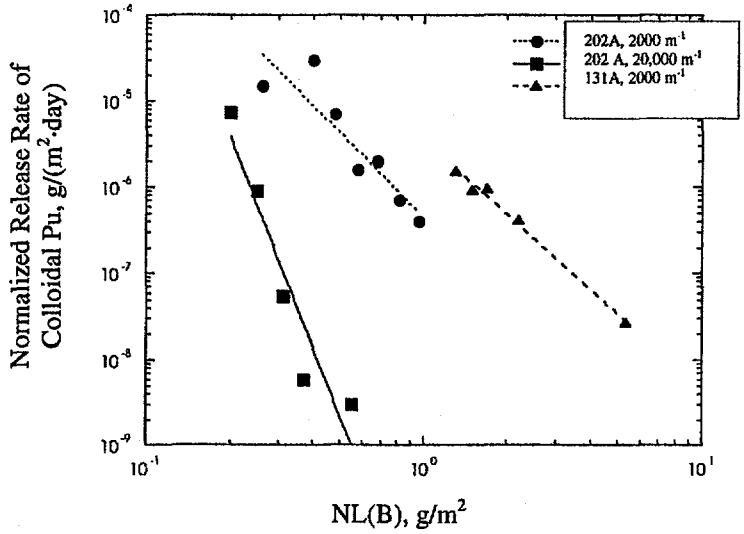

Fig. II-12. Normalized Release Rate of Colloidal Plutonium as Function of Normalized Mass Loss of Boron for Static Corrosion Tests of SRL 202A and SRL 131A glasses at S/V = 2000 and 20,000 m^{-1}.[16]

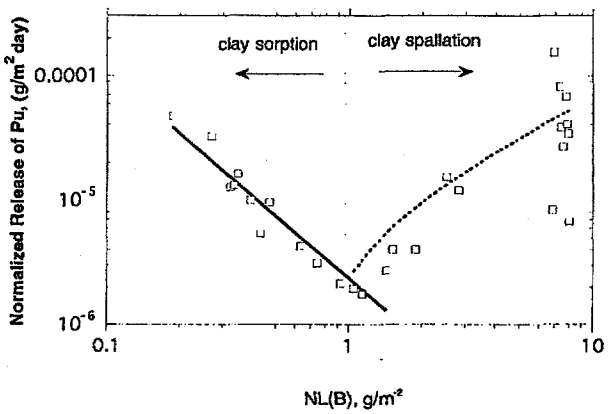

Fig. II-13. Plutonium Release Rate versus Cumulative Boron Release for Glass Drip Test with SRL-165 Glass. The total plutonium release (calculated for each sampling interval) is used, including vessel acid strip.[17]

[16]W. L. Ebert, *The Effects of the Glass Surface Area/Solution Volume Ratio on Glass Corrosion: A Critical Review*, Argonne National Laboratory Report ANL-94/34, pp. 196-283 (1995).

[17]J. A. Fortner and J. C. Cunnane, *Solution and Alteration Phase Data for Unsaturated Corrosion Testing of Glass Waste Forms*, Yucca Mountain Data Package, Argonne National Laboratory Report (1999).

where $m_{Pu-coll}$ is the mass release of plutonium suspended as colloidal particulates, and κ is a parameter that will depend on the mechanical condition of the altered waste form and other factors, including the flow rate of water over the waste form and the water chemistry. Note that the above mechanism considers only waste form colloids spalled from the glass; this mechanism does not apply to radiocolloids (colloids formed from hydrolysis of dissolved radionuclides in solutions), whereby the radionuclide release from the glass is governed by the radionuclide solubility. Future studies will attempt to verify the long-term release of colloids via the spallation mechanism for both waste glass and spent fuel.

D. Qualification Testing of Ceramic Waste Forms

Argonne has developed an electrometallurgical process to convert spent sodium-bonded nuclear reactor fuel into repository-acceptable forms (see Sec. III). This process is carried out in a molten salt (LiCl-KCl) electrolyte, in which easily oxidized fission products and transuranic elements accumulate. These radioactive materials must be removed periodically from the electrolyte, and the radioactive salt must ultimately be disposed of as high-level waste. To accomplish this goal, the waste salt is first blended with zeolite 4A at ~500°C to occlude most salt components within cages of the zeolite. The zeolite is mixed with a glass binder and heated under hot isostatic press (HIP) conditions to make a ceramic waste form (CWF) that consists of ~75 mass % sodalite (incorporating most of the salt), ~25 mass % glass, and small amounts of halite, clay, and oxides.

A "reference" CWF made without radionuclides is used in the majority of tests conducted to characterize the corrosion behavior of the different phases that make up the waste form. Tests are also conducted with glass binder and sodalite phases that are made separately. Characterization of the dissolution behavior of the separate phases facilitated analysis of the results of corrosion tests conducted with the composite material. Additional tests are being conducted with reference CWF containing U and Pu to study the effects of these radionuclides on the corrosion behavior.

1. *Characterization of Ceramic Waste Form*

The structure and composition of nonradioactive and radioactive ceramic waste forms have been determined by electron microscopy. The major phases are sodalite and glass. The minor phases (less than 5 vol%) that have been identified are aluminosilicates, silicates, oxides, and halite. Yttrium and the rare earths were found in separate silicate phases that aggregate in the glassy regions of the CWF; cesium and strontium are present in concentrations too low to be identified in any phase. Uranium and plutonium primarily formed crystalline $(U,Pu)O_2$ with crystallite sizes ~10 nm. These crystals occurred predominately within the glass phase at or near glass/sodalite interfaces but were also observed along sodalite grain boundaries. A U/Pu-bearing rare earth silicate (~50-1000 nm) was identified in the glass phase.

The most important CWF materials that have been characterized this year were glass-bonded sodalite made from zeolite that was blended in CMT with 0.15-0.44 wt% of uranium and plutonium as well as surrogate fission products. Two batches were made with zeolite containing minimal water content of 0.12 wt%, and two batches with water content of 3.5 wt%, which is

outside the specification of <1.0 wt%. They underwent hot isostatic pressing at Argonne-West, and half of each batch was returned to CMT for structural studies and corrosion testing. Transmission electron microscopy showed that the U and Pu in these CWF materials are present as aggregates of $(U,Pu)O_2$ crystallites within glass and near sodalite phase boundaries. Scanning electron microscopy (Fig. II-14) showed that $(U,Pu)O_2$ aggregates in CWF made from zeolite·0.12 wt% H_2O are more diffuse (spread out) than those in CWF made from zeolite·3.5 wt% H_2O. Corrosion tests are in progress on the U- and Pu-loaded CWF to establish whether the presence of actinides modifies the CWF behavior, and whether PuO_2 is released in a colloidal form. Scanning and transmission micrographic analyses will aid the interpretation of the release behavior of U and Pu.

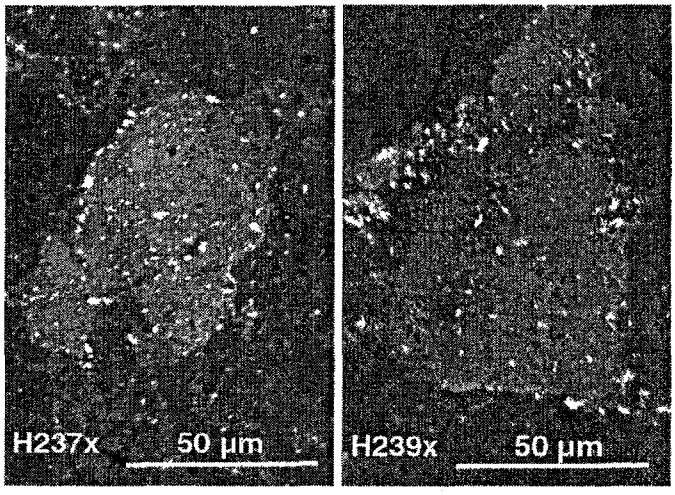

Fig. II-14. Scanning Electron Micrographs of Sodalite Grains in (U,Pu)-Loaded CWF Made from Zeolite·0.12 wt% H_2O (left) and Zeolite·3.5 wt% H_2O (right). White regions are aggregates of $(U,Pu)O_2$ crystallites surrounded by glass. The clusters on the left are spread more than those on the right.

2. *Corrosion Behavior of Ceramic Waste Form*

Several test methods have been used to study the corrosion behavior of the CWF and to develop a data base that can be used to support qualification of the waste form for disposal in a high-level radioactive waste repository. The test matrix was designed to accomplish three objectives: (1) support development of, and provide data for, a mechanistic corrosion model that can be used to calculate the long-term behavior of the CWF in a disposal site, (2) develop methodology to monitor the consistency of waste products, and (3) provide a data base to support process control.

Some tests were conducted following procedures that are used to study other waste forms, such as the MCC-1 test, PCT, and VHT, while other tests were designed to study unique aspects of corrosion behavior of the CWF, such as the accessible free salt measurement and the

solution exchange test. Information from all of the tests was used to support the development of a mechanistic model for waste form corrosion and to provide experimental data for that model. Summarized below are results from MCC-1 tests and PCTs.

a. MCC-1 Tests in Buffered pH Solutions

The MCC-1 test uses a monolithic (wafer) sample at a low S/V ratio to determine corrosion behavior under dilute conditions (forward dissolution rate). The MCC-1 tests were performed with polished wafers of sodalite, glass, and reference CWF in pure (ASTM Type I) water at 40 and 90°C, as well as dilute pH-buffered aqueous solutions in the pH range of 5-10 at 70 and 90°C. Unbuffered tests have been conducted for 1 to 364 days; the buffered MCC-1 tests have been conducted for 1-10 days. Forward dissolution rates and pH dependencies of the forward dissolution rates of the CWF and its components have been determined. The pH dependencies of the dissolution rates of sodalite, binder glass, and glass-bonded sodalite are similar to that of borosilicate nuclear waste glasses, with a negative pH dependence in the acidic region and a positive pH dependence in the basic region.

The concentration of silicon in solution after test termination provides the best measure of matrix dissolution of glass-bonded sodalite, since both glass binder and sodalite have high silicon concentrations. The measured silicon concentrations in solutions from buffered MCC-1 tests with each material (glass binder, sodalite, and CWF) were used to calculate the normalized mass losses, $NL(Si) = (m - m_b)/(f_{Si} \cdot S)$, where m is the mass of silicon in the test solution, m_b is the mass of silicon in an experimental blank, f_{Si} is the mass fraction of silicon in the material, and S is the specimen surface area. At each temperature, the NL(Si) from tests at each buffer pH increased rapidly during the first three days, then increased more slowly up to 10 days.

Normalized release rates were calculated by linear regression of the 3- to 10-day NL(Si) for glass, sodalite, and CWF at 70°C and the 1- to 5-day NL(Si) at 90°C. The rate increased with increasing temperature at each pH value. The changes in log [NR(Si)] as a function of pH from tests at each temperature represent values of h, a parameter that reflects the pH dependence of the dissolution rate equation (Eq. 1). Tentative dissolution rates have been calculated in the acidic and basic regions at 70 and 90°C. At both 70 and 90°C, the rates exhibit V-shaped behavior, with negative slope in the acidic region and positive slope in the basic region. In the basic region, h = 0.2, that is, the logarithm of the corrosion rate increases by 0.2 for each unit increase in pH. The corresponding value for most nuclear waste glasses is 0.4. The pH dependencies of the dissolution rates of glass binder and salt-loaded sodalite also display V-shaped behavior. These dissolution rates are consistent with those for natural sodalite[18] and other aluminosilicate minerals.[19]

Additional MCC-1 tests with buffered solution are being carried out to define the slopes for h more precisely. Tests are also in progress at 40°C. Values of h at three temperatures will

[18] K. Montgomery, "The Synthesis and Dissolution of Sodalite: Implications for Nuclear Waste Disposal," M.Sc. Thesis, Dept. of Geology, University of Alberta, Canada (1986).

[19] K. G. Knauss and T. J. Wolery, *Geochim. Cosmochim. Acta* **53**, 1493-1501 (1989).

permit the calculation of the activation energy (E_a), which reflects the temperature dependence in Eq. 1.

b. Product Consistency Tests

The PCTs use crushed material at high S/V ratios to study corrosion behavior as the test solutions become concentrated in matrix-element species. With the reference CWF, PCTs have been completed at two temperatures (40 and 90°C), at two S/V ratios (2,000 and 20,000 m^{-1}), and with two leachants (ASTM Type I water and EJ-13 water).

Silicon concentrations after test terminations, shown in terms of H_4SiO_4 concentration in Fig. II-15, appear to approach saturation within 7 or 28 days. The extrapolated saturation concentrations for reference CWF, glass binder, and sodalite (31-120 mg/L) are much less than the value (528 mg/L) cited for defense high-level waste (DHLW) glass in the Total System Performance Assessment for the Viability Assessment (TSPA-VA). This finding indicates that the CWF performance will be bounded by the performance of high-level waste glasses in a repository. A mechanistic corrosion model has been developed to calculate the long-term behavior of the CWF in a disposal site.[20] The experimental results from the PCTs have been incorporated in preliminary calculations using this model; these calculations also show that high-level waste glass dissolution will represent an upper bound on CWF dissolution. Product

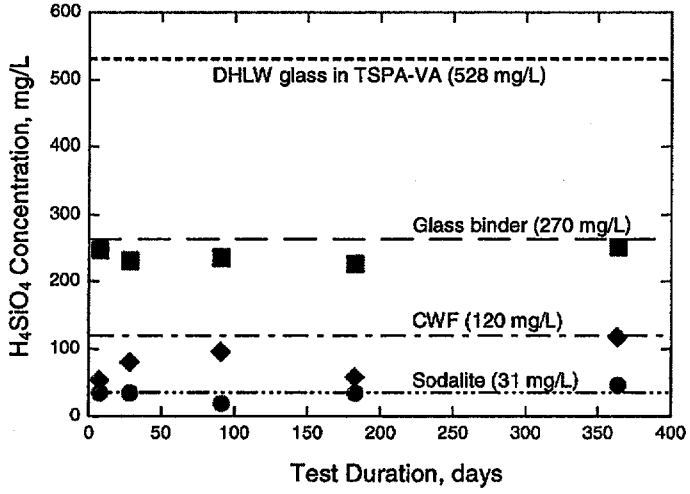

Fig II-15. Concentration of Orthosilicic Acid, H_4SiO_4, in PCT Solutions after Termination of Tests through 1 Year. Horizontal lines show estimated extrapolated saturation concentrations.

[20]R. A. Wigeland, L. L. Briggs, T. H. Fanning, E. E. Feldman, E. E. Morris, and M. C. Petri, Argonne National Laboratory, personal communication (1999).

Consistency Tests are now being conducted with CWF samples that have been loaded with U and Pu, as well as surrogate fission products, at concentrations similar to those in electrorefiner salt that has processed up to 300 driver fuel assemblies.

E. Fundamental Studies of Actinide Behavior

The behavior of radionuclides is being investigated under conditions relevant to subsurface groundwaters on DOE sites. Emphasis is on factors that affect mobilization and immobilization of actinides. Results of this work will establish key factors concerning the chemistry of actinide/organic mixtures in the presence of microbes, inorganic substrates, and metal cations.

1. *Microbiological-Actinide Interactions in Subsurface Environments*

The interactions between actinides and microorganisms in subsurface environments play an important role in determining the fate of actinide species dissolved in subsurface groundwaters. The fate of actinides in microbiologically active systems is being investigated in collaboration with investigators at Northwestern University. Emphasis has been on radiotoxicity effects and the fate/speciation of neptunium in the presence of sulfate-reducing bacteria.

Two studies were completed on the radiotoxicity of actinides toward soil bacteria. In the first, the toxicity of plutonium toward *Chelatobacter heintzii* was investigated in Pu(IV)-nitriloacetic acid (NTA) systems. Experiments were conducted with both Pu-239 and Pu-242 as a function of plutonium concentration (10^{-5} to 10^{-7} M) to vary the activity of the sample. Here, both chemical and radiolytic contributions toward toxicity were evident. Plutonium-239, which is the higher activity isotope, was primarily toxic due to radiolytic processes. This was only observed after the bioassociation of plutonium onto the microbe and was suppressed by complexation with the NTA. For Pu-242, the toxicity was primarily chemical, rather than radiolytic.

In the second study, the toxicity of uranyl (0-0.5 mM) toward *Pseudomonas fluorescens* was investigated. Uranyl was only toxic when it was present as an aqueous complex of citrate. Acetate, nitrate, and phosphate complexes were not toxic. The aquo form, which is strongly hydrolyzed at near-neutral pH, was not toxic. The high toxicity of the uranyl-citrate complex stabilized it toward degradation (see Fig. II-16). The special properties of uranyl-citrate complexes have been observed in other metal systems. Citrate facilitates metal transport across the cell wall and leads to, based on our results, enhanced metal toxicity. X-ray absorption near edge spectroscopy (XANES) of the uranyl associated with the biomass showed that the uranium oxidation state remained +6; thus, there was no evidence that bioreduction was an important and contributing factor to the toxicity noted.

Neptunium speciation studies in microbiological systems were extended to investigate the fate of neptunium in sulfate-reducing bacteria under anaerobic systems. These bacteria are

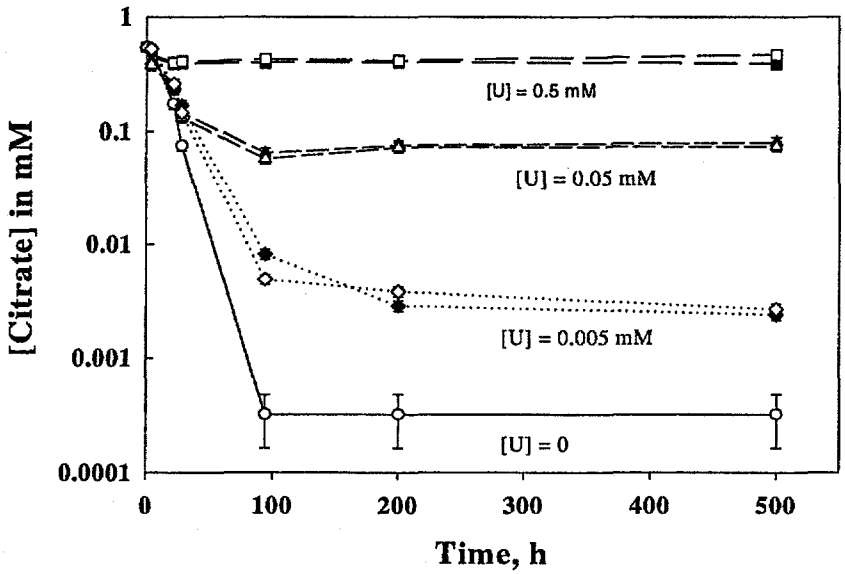

Fig. II-16. Concentration of Citrate as a Function of Time in Aqueous Solution Containing *Pseudomonas fluorescens* and Various Uranium Concentrations. Residual concentrations of citrate that appear to be non-biodegradable are evident because of the high toxicity of the uranyl-citrate complex.

among the most ubiquitous metal reducers in natural systems. Experiments were performed with an isolate (*Desulfovibrio vulgaris*) and an anaerobic consortium that predominantly included sulfate-reducing bacteria. In all cases investigated, Np(V) was reduced to Np(IV) as a result of biological activity, and this led to its eventual precipitation from solution. The percent neptunium in various solutions as a function of time in experiments with *Desulfovibrio vulgaris* is shown in Fig. II-17. The solutions tested used different electron donor substrates: pyruvate, H_2, and a combination of the two. Although neptunium precipitation occurred in all cases except the blank, it was most rapid when H_2 alone was supplied as the electron donor substrate. Analysis by XANES of the neptunium solids precipitated confirmed that bioreduction to Np(IV) had occurred. The exact mechanism for the reduction and precipitation noted is the subject of ongoing investigations. That neptunium is reduced in anaerobic systems by biological activity has important and beneficial implications for the migration of neptunium on DOE lands, since most migration pathways proceed through anaerobic zones.

2. Synchrotron-Based Studies of Actinide Species

Studies are underway to extend and develop X-ray synchrotron radiation (XSR) techniques with which to determine the chemical structure of aqueous, adsorbed, and solid actinide species of importance to environmental and nuclear waste issues. These data are needed to help resolve a number of fundamental structural issues related to the speciation (e.g.,

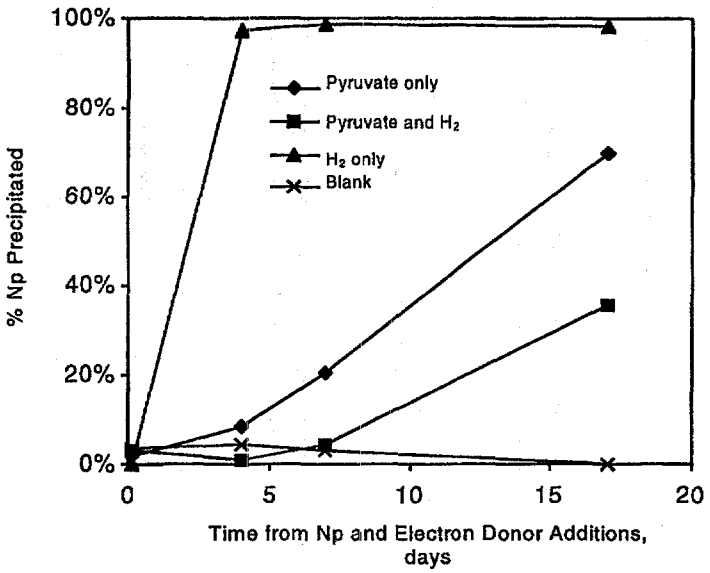

Fig. II-17. Fate of Neptunium during Growth of Mixed Anaerobic Consortium in Aqueous Solution. Neptunium added as Np(V).

complexation, oxidation state, and aggregation) of actinides. Emphasis in our research is on the collection of synchrotron data on actinide systems and the modeling of these data by use of improved calculation methods and theory.

In the past year, experiments were focused on neptunium systems under conditions relevant to the subsurface. Analyses by XANES were used to identify neptunium oxidation states by comparison of the spectra of unknowns to those in standards synthesized in the laboratory. These data were collected at the beam line of the Materials Research Collaborative Access Team (MRCAT) at the ANL Advanced Photon Source.

The references used in this study were neptunium(IV) fluoride, $Np(V)O_2NaCO_3$, and Np(VI) phosphate. The XANES spectra for these references were utilized to identify the oxidation state in two applications where unknowns were precipitated. First, the precipitates in Np(VI) stability studies, performed in support of the Waste Isolation Pilot Plant (WIPP) project (Sec. V.B.4), were collected and analyzed. The neptunium in WIPP brine precipitated, leading to a steady-state concentration. Our XANES analysis showed that the neptunium precipitated as Np(V), rather than Np(VI), and this result confirmed that reduction in solution was a necessary precursor to precipitation. That neptunium was being reduced was also corroborated by XANES spectra, indicating that Np(V) was the predominant oxidation state in solution.

The neptunium phase present when Np(V) was added to a biologically active sulfate-reducing bacteria (SRB) was also collected and analyzed by means of XANES. These data are shown in Fig. II-18. Here, the unknown precipitate was shown to be Np(IV) rather than Np(V), confirming that reduction had taken place.

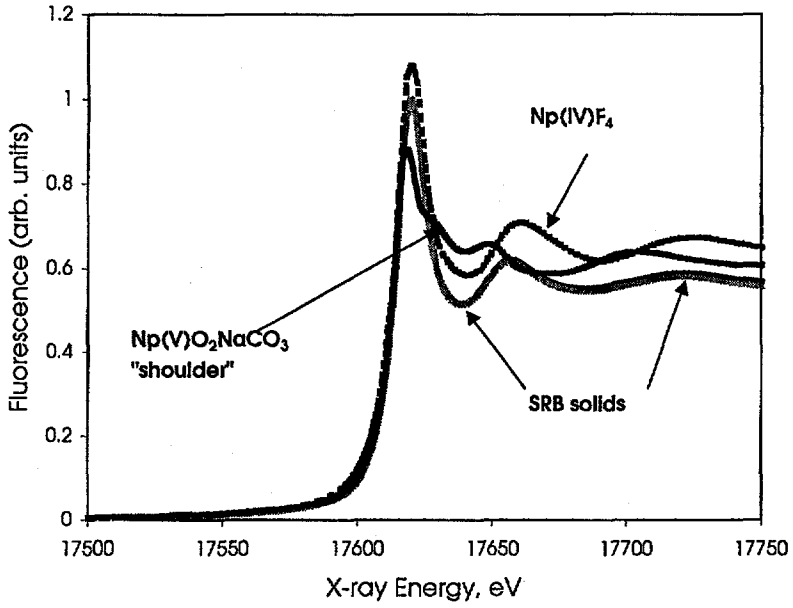

Fig. II-18. Comparison of XANES Spectra from Neptunium Precipitated during Lactate Fermentation to Np(IV) and Np(V) Solid Standards. The spectra for SRB-precipitated neptunium lack the near-edge shoulder associated with Np(V), indicating that Np(V) was reduced to Np(IV) during lactate fermentation.

The results for the WIPP and SRB analyses are excellent examples of the utility of XANES to identify oxidation states. This information is key to understanding the fate/transport of actinides in the subsurface of environmentally relevant systems.

In theoretical studies of plutonium systems, XANES calculations using the FEFF 8 computational code (latest version of a program for *ab initio* multiple scattering calculations of XSR spectra for clusters of atoms) have confirmed experimental results that the oxidation state, not geometry, is the most important factor in defining XANES edge position in the plutonium system. This theoretical finding indicates that the XANES edge position can be used to identify the oxidation state when the plutonium is primarily present as a single oxidation state in solution. Further refinements of these theoretical studies are ongoing.

F. Development, Characterization, and Testing of Various Waste Forms

1. *Development of Test Methods for Low-Activity Product Acceptance*

A round-robin test program was conducted with a glass that was developed for use as a standard test material for acceptance testing of low-activity waste glasses made with Hanford tank

wastes.[21] The glass is referred to as "low-activity test reference material" (LRM). The performance of that glass in several tests that were specified in the DOE contract for immobilizing Hanford tank waste was evaluated previously.[22] A round-robin testing program was conducted to measure the interlaboratory reproducibility of composition analysis and durability test results. This information is needed to establish the precision and bias for use of that glass in product acceptance. Participants were allowed to select the methods used to analyze the glass composition. The durability tests closely followed the PCT-A Method, except that tests were conducted at both 40 and 90°C, and that parallel tests with a reference glass were not required. Samples of LRM glass that had been crushed, sieved, and washed to remove fines were provided to participants for tests and analyses.

Table II-4 provides the mean concentration of LRM glass in terms of oxide mass percent for the interlaboratory analyses. The consensus average and estimated interlaboratory variability provide a measure of the range with which DOE can evaluate the accuracy of waste glass analyses performed by contractor laboratories. The reproducibility of the composition results compares favorably with the results of interlaboratory studies conducted with other glasses.[23,24] From the perspective of reproducibility of analysis results, LRM glass is acceptable for use as a composition standard for nonradioactive components of low-activity waste forms present at >0.1 elemental mass %.

Table II-4. Results for Interlaboratory Composition Analysis of LRM Glass

Oxide	Comp.,[a] mass%	Variability[b]	Oxide	Comp.,[a] mass%	Variability[b]	Oxide	Comp.,[a] mass%	Variability[b]
Al_2O_3	9.51	0.336	I	ND	ND	NiO	0.19	0.020
B_2O_3	7.85	0.311	K_2O	1.48	0.489	P_2O_5	0.54	0.065
BaO	0.00	ND[c]	La_2O_3	0.02	ND	PbO	0.10	0.026
CaO	0.54	0.086	Li_2O	0.11	0.026	SO_3	0.30	0.068
CdO	0.16	0.015	MgO	0.10	0.009	SiO_2	54.20	1.318
Cr_2O_3	0.19	0.021	MnO	0.08	0.013	TiO_2	0.10	0.013
F	0.86	0.106	MoO_3	0.10	0.009	ZrO_2	0.93	0.064
Fe_2O_3	1.38	0.181	Na_2O	20.03	1.202			

[a] The consensus average of the composition, in oxide mass percent.

[b] The estimated interlaboratory variability, expressed as the square root of the component of variance.

[c] ND = not determined.

[21] W. L. Ebert, D. M. Strachan, and S. F. Wolf, *Formulation of a Candidate Glass for Use as an Acceptance Test Standard Material*, Argonne National Laboratory Report ANL-98/10 (1998).

[22] S. F. Wolf, W. L. Ebert, J. S. Luo, and D. M. Strachan, *A Data Base and a Standard Material for Use in Acceptance Testing of Low-Activity Waste Products*, Argonne National Laboratory Report ANL-98/9 (1998).

[23] G. L. Smith and Steven Marschman, *Mater. Res. Soc. Symp. Proc.* **333,** 461-472 (1994).

[24] G. L. Smith, D. L. Eggert, and H. D. Smith, *Mater. Res. Soc. Symp. Proc.* **465**, 173-180 (1997).

The use of LRM glass as a test standard for PCTs at 40 and 90°C was also evaluated. On the basis of the measured interlaboratory precision, the expected test results at the 95% confidence level are given in Table II-5. These results can be used to evaluate the accuracy of PCTs conducted at other laboratories.

A supply of about 1000 pounds of LRM glass is being maintained at CMT. Aliquots of the glass have been supplied to other laboratories for use in tests to develop other acceptance test methodologies. The LRM glass is a well-characterized glass that is available for use by DOE as a standard material for acceptance testing of vitrified low-activity waste forms.

2. *Transmutation Effects in Crystalline Waste Forms*

The goal of this research is to determine the effect of transmutation of ^{137}Cs to ^{137}Ba in crystalline pollucite ($CsAlSi_2O_6$). Small, sealed, stainless steel capsules containing pollucite have been in storage for over 20 years. The decay of ^{137}Cs to ^{137}Ba has placed the pollucite structure under significant strain because of the limited solubility of barium in pollucite. These studies of transmutation effects will help evaluate the long-term stability and performance of the many crystalline waste forms being considered for the disposal and stabilization of radioactive waste.

The effects of transmutation on the pollucite are being established by three complementary methods: transmission electron microscopy (TEM), XANES/extended X-ray fine structure (EXAFS), and solid-state nuclear magnetic resonance (NMR).

The TEM analysis of the samples is in progress. Several specimens from one of the capsules were prepared for TEM by ultramicrotome thin sectioning. Preliminary TEM examination revealed a homogeneous, crystalline matrix, with no evidence of distinct barium phases or exsolution phenomena resulting from the ^{137}Cs transmutation.

Synchrotron methods (XANES/EXAFS) provide the best chance of meaningful *in situ* analysis of unopened capsules with the radioactive pollucite. This is because of the highly penetrating nature of X-rays. Plans are in place to perform K-edge (high-energy) EXAFS/XANES analysis of these samples. We are also pursuing L-edge (lower energy) EXAFS/XANES on radioactive pollucite samples from opened capsules. These require surface mounting and, therefore, higher safety controls. Cold testing of this approach has already been successfully demonstrated.

The NMR work in progress is by far the most developmental of the three techniques. Yet, success in this approach will likely lead to applications beyond the pollucite samples being studied. Our preliminary experiments have demonstrated the ability of solid-state NMR to reveal

Table II-5. Expected Results for Elemental Release and Solution pH in PCT with LRM Glass

Temp., °C	pH	Conc., mg/L		
		B	Na	Si
40	9.86 ± 0.96	2.30 ± 1.25	19.7 ± 7.3	13.7 ± 4.2
90	10.92 ± 0.43	26.7 ± 7.2	160 ± 13	82.0 ± 12.7

information about the structure and dynamics of small cesium-bearing samples. Recent results on rotating samples of pollucite have shown that ^{29}Si NMR can differentiate between cesium-pollucite and barium-bearing pollucite. This capability is important because the environment of silicon is directly affected by the transmutation of the cesium. Therefore, ^{29}Si and ^{27}Al NMR may provide the most information about defect sites in radioactive pollucite.

3. Self-Radiation Damage in YPO_4 Single Crystals

Amorphization has been commonly believed to be the most important effect of radiation damage in crystalline and ceramic materials. Our study, however, suggests that this may not be the case for Cm-doped phosphate crystals. By use of TEM, we have characterized the nature and degree of damage induced by ^{244}Cm self-irradiation in orthophosphate crystals of YPO_4. A radiation dose as high as 5×10^{16} α-decay events/per milligram has been accumulated in crystals doped with 1 wt% ^{244}Cm over a period of 18 years. In a bright-field TEM micrograph (Fig. II-19), an array of individual defect clusters was observed to form in the crystalline matrix. The clusters typically have diameters of 5-20 nm and may be related to the highly disordered fission tracks which are produced by the ^{244}Pu recoil nucleus emitted during the alpha decay of ^{244}Cm. The structure of these defects is not known, but this irradiated material may be assumed to be amorphous if these are fission tracks, since fission fragments are known to induce amorphization in crystalline materials. Analysis of the clusters with energy dispersive spectroscopy (EDS) and a focused electron beam showed no difference in composition from the surrounding areas.

Despite the high accumulated dose, the samples exhibited sharp diffraction patterns and periodic lattice spacings. This result suggests that the sample remained largely crystalline. Our studies on Cm-doped YPO_4 single crystals show that amorphization is not a significant effect of radiation damage, and that the radiation damage is recovered at a rate comparable to that of damage production. This high recovery rate is ascribed to effects such as ionization annealing, as well as thermally activated and diffusion-driven annealing.

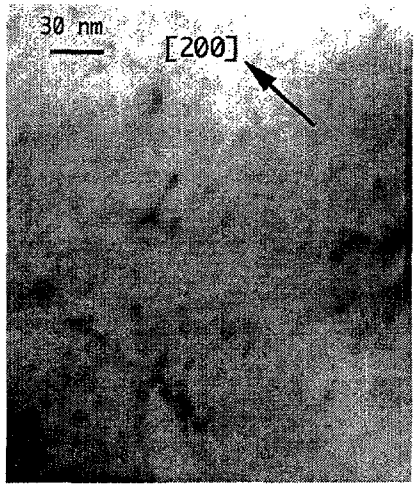

Fig. II-19.

Bright-field TEM Micrograph of ^{244}Cm-Doped YPO_4 Crystal Showing Arrays of Nanometer-Sized Clusters. Micrograph taken with g close to [200].

4. Testing of Glass Waste Form for Low-Level Hanford Waste

We are providing glass corrosion testing in support of the performance assessment calculations for the low-activity waste storage system at Hanford and for product acceptance testing. We are collaborating with scientists at Pacific Northwest National Laboratory, the Savannah River Technology Center, and BNFL, Inc., to evaluate the chemical durability of low-activity waste forms under conditions anticipated in the Hanford storage system. The corrosion behavior of several glass compositions is being evaluated in laboratory tests to characterize corrosion mechanisms, identify alteration phases, and measure parameters needed for modeling long-term behavior. Tests are in progress with six glass compositions selected to represent the range of concentrations of key glass components anticipated for waste glasses. The effects of the concentrations of Al, B, Fe, Na, Si, and Zr are being studied. At CMT, tests are being conducted at several temperatures following the PCT and VHT protocols. The results of these tests will provide insight regarding the effects of dissolved glass components on the continued glass dissolution and will identify alteration phases, the effects of which must be taken into account when modeling the long-term corrosion behavior of the waste glasses.

G. Related Work

1. Procedure Writing

Several CMT scientists are active in committees of the American Society for Testing and Materials, developing and standardizing testing and analytical protocols for waste forms. Currently, they are involved in writing standard methods addressing the measurement of model parameters for glass dissolution, expanding test methods used for waste-form product acceptance, and evaluating the stability of spent nuclear fuel during storage. These standards are important to most of the current programs in CMT waste materials research.

2. Development of Rheology Control Aids

Water-based (aqueous) products, such as paints and cosmetics, are increasing in popularity at the expense of their oil-based counterparts because aqueous formulations are typically easier to use and are more environmentally friendly. This creates tremendous demand for water-based additives to modify a product's viscosity and flow properties. These additives include "organoclays," which are chemically treated, highly dispersed clay particles that are very small (nanometers). Organoclays are used to improve many commercial products, including water-based paints, inks, food additives, lubricants, and adhesives. Ultra-pure organoclays also can be incorporated into raw materials to improve properties in end-use applications, such as plastic coatings and packaging.

Conventional organoclays repel water and are not compatible with water-based systems, so more expensive polymer-based thickeners have been used. A unique method is being developed for preparing ultra-pure organoclays for use in water-based systems, as well as in solvent-based systems. This method employs aqueous biphasic extraction (ABE), a process

originally developed for nuclear waste treatment and soil remediation.[25] It simultaneously converts low-grade clay ores into a sodium form, separates the organoclay particles from the mineral impurities present in the ore, and generates a highly exfoliated (dispersed) organoclay without mechanical grinding or high-speed centrifugation. The ABE process provides a level of purity in organoclays that cannot normally be attained with any conventional processing technology and has been used to prepare clay suspensions and thin-film composites that are colorless and transparent.

3. *Development of Synchrotron X-ray Techniques for Protein Analysis*

The purpose of this project is to collect preliminary data showing that coherent, monolayer films of protein can be spread at the water/water interface of an aqueous biphase system. These two-dimensional crystals could be used in mechanistic studies and would provide a means of determining the three-dimensional structure of fully hydrated proteins, thereby giving a more realistic view of biologically active structures.

Aqueous biphase systems consist of two immiscible aqueous phases and form spontaneously from mixtures of aqueous solutions of unlike polymers, typically a straight-chain polymer such as polyethylene glycol and a highly branched polymer such as dextran. The tendency for proteins to adsorb at the water/water interface has been noted in the literature,[26] but this phenomenon has been considered little more than a nuisance. We are utilizing this adsorption tendency of proteins to form spread monolayers, which can be manipulated by simple mechanical compression to produce coherent, two-dimensional solids.

Initial results from X-ray reflectivity measurements performed at beam line X19C of the National Synchrotron Light Source, Brookhaven National Laboratory, have confirmed that it is possible to spread ultrathin (50-500 Å) aqueous films onto of an aqueous subphase. Thin liquid films of these dimensions are critical in producing a measurable diffraction signal from the water/water interface. Initial results from X-ray reflectivity measurements of ferritin indicated that this protein forms a two-dimensional array at the water/water interface. We are now attempting to optimize this and other protein systems for two-dimensional crystal growth.

H. Separation Science and Technology

Waste materials research in separation science and technology covers several diverse projects, summarized below.

---

[25] J. J. Laidler et al., *Chemical Technology Division Annual Technical Report, 1997,* Argonne National Laboratory Report ANL-98/13, 43-46 (1998).

[26] J. Milton Harris, *Poly(Ethylene Glycol) Chemistry Biotechnical and Biomedical Applications*, Plenum Press, New York (1992).

1. Conversion of Targets for ^{99}Mo Production

The Reduced Enrichment for Research and Test Reactors (RERTR) program has been active for 22 years at ANL and many countries throughout the world. Researchers in CMT are part of the ANL team. The RERTR program's major objective is to modify reactor and fuel designs so that reactors can switch from high-enriched uranium (HEU) to low-enriched uranium (LEU) with no or little loss in flux or cycle time. Many reactors have converted to LEU, and many more are in the process. While conversions of reactor fuel have proceeded, the amount of HEU being exported from the United States for use in ^{99}Mo production has become an ever more visible proliferation concern.

Technetium-99m ($t_{1/2}$ = 6.02 h), the daughter of ^{99}Mo ($t_{1/2}$ = 66.02 h), is the most commonly used medical radioisotope in the world. It is relied upon for over nine million medical procedures each year in the U.S. alone, comprising 70% of all nuclear-medicine procedures. Most ^{99}Mo is produced in research and test reactors by the irradiation of HEU targets. Because the worldwide effort to fuel research and test reactors with LEU instead of with HEU has been so successful, HEU is now used only for ^{99}Mo production in some countries. In addition, while there are only a few major producers of ^{99}Mo, many nations with developing nuclear programs are seeking to become producers of ^{99}Mo, both for domestic and foreign consumption. Therefore, one of the U.S. RERTR program's goals is the development of means to produce ^{99}Mo by using LEU. The two principal aspects of the work are (1) target development and (2) testing and modification of the chemical process. A third, equally important aspect, is cooperation with international producers of ^{99}Mo. The RERTR program has working relationships with three producers—the Indonesian National Nuclear Energy Agency (BATAN), the Argentine National Atomic Energy Commission (CNEA), and the Australian Nuclear Science and Technology Organization (ANSTO)—and growing relationships with many others.

Low-enriched uranium contains <20% ^{235}U. Currently, most of the world's supply of ^{99}Mo is produced by fissioning the ^{235}U in HEU targets—in most cases, enriched to 93% ^{235}U. Because of the lower isotopic fraction of ^{235}U in LEU, five times more uranium is required to produce the same yield of fission-product ^{99}Mo. Therefore, substituting LEU for HEU will require changes to both target design and chemical processing. Three major challenges have been identified with substituting LEU for HEU: (1) modifying the targets and purification processes as little as possible, (2) assuring continued high yield and purity of the ^{99}Mo product, and (3) limiting additional costs. Keeping the target geometry the same, thereby minimizing the effects of LEU substitution on target irradiation, necessitates modifying the form of uranium used. Also changing the amount and form of the uranium in the target necessitates modifying at least one or, possibly, two target processing steps—dissolution and initial molybdenum recovery.

a. Progress in Target Development

Targets containing LEU in the form of a metal foil are being developed. During irradiation, a large quantity of heat is generated in the uranium foil, up to 200 W/cm^2 in some reactors. For the heat to be dissipated to the coolant, the uranium foil must be in good thermal contact with the target structural materials (i.e., the target tubes). Poor thermal contact between the uranium foil and the target walls can lead to high temperature in the uranium foil during

irradiation. In the worse scenario, its temperature would increase to the point that the uranium would melt and/or react with the target structural materials, conditions that must be avoided.

The original target for irradiating the uranium foils encased the foil between tapered inner and outer tubes.[27] During fabrication, the inner tube was pushed into the outer tube, and the taper would push the uranium foil against the outer wall of the target tube. This design ensured good thermal contact of the foil with the target walls. Unfortunately, this target was expensive to make (due to the fabrication of the tapered tubes). Also, this design allows coolant to flow only over the outside of the target. Nonetheless, we were able to complete several irradiations using this style of target and to prove that LEU metal foil can be used to produce ^{99}Mo. A new annular-style target was developed in CMT during 1999. The design of the new target significantly reduces the cost of target fabrication by using target tubes that are not tapered. In addition, its annular design will allow coolant to flow over the outside and through the inside of the target, effectively doubling the heat transfer surface. In general, the annular target is fabricated by expanding an inner tube into an outer tube, with uranium foil located between the tubes. The target can be inserted into a reactor via an insertion rig that balances the flow of coolant between the inside and outside of the target.

To verify that the new annular target tubes are in good contact with the uranium foil, several prototype targets were fabricated. These prototypes underwent thermal cycling to simulate the mechanical and thermal performance of the targets during irradiation. Thermal cycling simulates irradiation conditions by "stress relieving" the target tubes. The contact of the tubes with the uranium foil relies on the fact that the outer tube squeezes down on the inner tube, owing to the residual hoop stress remaining from its elastic deformation during drawing. Irradiation in a reactor can relieve stress; if all of the hoop stress in the outer tube is relieved during irradiation, then good contact between the target tubes and uranium may not be maintained. After completion of the thermal cycling, the targets were cut into several small sections. The sections were examined microscopically, or the residual hoop stress was measured in the section. Microscopic examination of the critical interface between the foil and the target tubes (Fig. II-20) showed excellent contact between the two materials. Thus, the targets should perform well during irradiation. Measurements of the residual hoop stress after thermal cycling indicated very little stress relief in the prototype targets during the thermal cycle tests.

Seven targets of the new annular design containing LEU foils were fabricated. These targets were then irradiated in the Indonesian RSG-GAS reactor at a reactor power of 15 MW for approximately 120 h. The overall irradiation performance of the targets was good (Sec. II.H.1.b). There was no evidence of heat-transfer problems during irradiation. All targets were easily removed from the rigs after irradiation; this indicates that no significant mechanical distortions occurred during irradiation. Overall, the target was successful and will provide an inexpensive, efficient way to irradiate LEU metal foil for the production of ^{99}Mo. Further

[27] G. L. Hofman, T. C. Wiencek, E. L. Wood, J. L. Snelgrove, A. Suripto, H. Nasution, D. L. Amin, and A. Gogo, "Irradiation Tests of ^{99}Mo Isotope Production Employing Uranium Metal Foils," Proc. of the 19th Int. Meeting on Reduced Enrichment for Research and Test Reactors, Seoul, Korea, October 7-10, 1996, pp. 161-171 (1997).

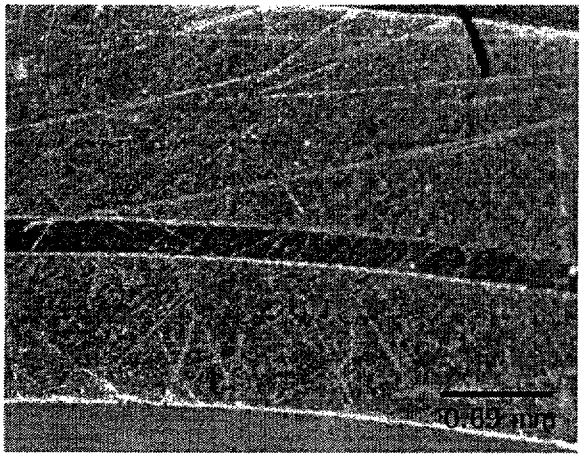

Fig. II-20.

Micrograph of Interface between Inner and Outer Tubes with Uranium Foil in Middle

demonstration of these targets is planned in Indonesia during March and September 2000 and in Argentina during April 2000. A similar target will be tested in Australia in about a year.

b. Progress in Processing Development

Research and development activities are underway in CMT under cooperative agreements with BATAN and CNEA. The cooperation with BATAN has been underway since November 1994. In that time, we have developed means to convert the Cintichem process that BATAN is using to LEU targets, and this modified process is now in the demonstration stage. The agreement with CNEA began in January 1999. According to the agreed schedule, our R&D activities will lead to giving them the ability to convert to LEU targets at the end of three years. Summaries of 1999 progress for these two activities follow.

Indonesian National Nuclear Energy Agency. At present, BATAN is producing ^{99}Mo from neutron-irradiated HEU-UO_2 targets in the Radioisotope and Radiopharmaceutical Production Centre at PUSPIPTEK, Serpong, Indonesia. The chemical procedure that is used to recover and purify the ^{99}Mo is the Cintichem process. The proprietary rights for the process rest with DOE; BATAN uses the process under a licensing agreement.

Targets were fabricated at ANL for irradiation in the RSG-GAS reactor for ~120 h at 15 MW. Foils were extracted from the targets by cutting off both ends of the concentric tubes and separating the inner and outer tubes. The geometry of the uranium foil and the presence of the fission barrier hold fission gases inside the uranium foil until it is dissolved. Except for the dissolver, all equipment was identical for HEU and LEU processing. Except for the dissolution step and elimination of sulfuric acid from all process solutions, all processing steps and reagents were identical. Solution samples were collected during processing and analyzed by gamma spectrometry to measure ^{99}Mo yield and purity from step to step.

Once the foil was placed inside the dissolver, the dissolver was evacuated to test for leaks, and then nitric acid was added through a septum. Dissolution was complete in $\leq$10 min, as observed by the pressure inside the dissolver first rising then falling as the exothermic reaction concluded. Because of three modifications to the dissolution step of the Cintichem process, the processing time was shortened: (1) fission gases from the target are

trapped before dissolution is complete, (2) dissolution of a uranium-metal foil is much faster than dissolution of the UO_2 coating from a target tube, and (3) dissolution volumes are considerably less.

After dissolution, the gas in the dissolver (mostly NO and fission gases) was evacuated. Then, the uranium solution was transferred from the dissolver, and a rinse solution was added to the dissolver and combined with the uranium solution. Molybdenum was recovered from the uranium solution by precipitation with alpha-benzoin oxime (ABO). Earlier work[28,29] had shown that, by washing adequately and moving quickly to avoid radiation damage to the ABO, high yield and decontamination are possible for this step. It is likely that the lower feed volume and, therefore, higher concentrations of constituents (due to a lower dissolver-solution volume) facilitate the molybdenum separation. Earlier studies[27] have shown that increased uranium concentrations do not compromise this separation. Following the precipitation, the steps are the same for HEU and LEU targets. Gamma measurements of yield and decontamination for each step showed the steps to be equivalent for HEU and LEU target processing. The overall ^{99}Mo yield for LEU-foil processing has consistently been ~79% overall (calculated from total ^{99}Mo in dissolver solution). The yield for the HEU runs that we have monitored has been ~65%. The difference, as stated above, appears to be in the initial Mo-ABO precipitation step. Other factors may also be important. For example, the LEU process allows better control of the acid concentration following dissolution.

Figure II-21 shows the decontamination of the ^{99}Mo from three isotopes of iodine, and Fig. II-22 shows the decontamination from a variety of other isotopes. These results demonstrate the excellent separation of the ^{99}Mo from other isotopes. Note that the impurity levels in the product sample (that following column 2) are known. An extraction process quantitatively separates radioiodine from the bulk of the ^{99}Mo and thereby makes accurate analysis possible. Likewise, another extraction process removes the bulk of the molybdenum from the other isotopes to measure their contamination levels. On the other hand, in the intermediate samples (samples taken between purification steps), the orders-of-magnitude higher ^{99}Mo and ^{99m}Tc activities (and the many possible interference peaks they possess) make determination of impurity levels tenuous and inaccurate. The gamma spectrum contains 42 peaks for ^{99}Mo and 5 for ^{99m}Tc, as well as four potential summation peaks from these isotopes.[30] These difficulties aside, based on these results, the ^{99}Mo from this demonstration would have been an acceptable feed for a technetium generator.

---

[28]D. Wu, S. Landsberger, and G. F. Vandegrift, "Progress in Chemical Treatment of LEU Targets by the Modified Cintichem Process," 19th Int. Meeting on Reduced Enrichment for Research and Test Reactors, Seoul, Korea, October 6-10, 1996, pp. 172-179 (1996).

[29]A. Mutalib, B. Purwadi, H. G. Adang, L. Hotan, K. Moeridoen, A. Kadarisman, S. Sukmana, A. Suripto, H. Nasution, D. L. Amin, A. Basiran, A. Gogo, D. Sunaryadi, T. Taryo, G. F. Vandegrift, G. Hofman, C. Conner, J. Sedlet, D. Walker, R. A. Leonard, T. C. Wiencek, E. L. Wood, and J. L. Snelgrove, "Full-Scale Demonstration of the Cintichem Process for the Production of Mo-99 Using a Low-Enriched Target," Proc. of the XXIst International Meeting on Reduced Enrichment for Research and Test Reactors, Sâu Paulo, Brazil, October 18-23, 1993, in press.

[30]Richard B. Firestone, Virginia S. Shirley, Coral M. Baglin, S. Y. Frank Chu, and Jean Zipkin, *Table of Isotopes*, 8th Ed., John Wiley & Sons, New York (1996).

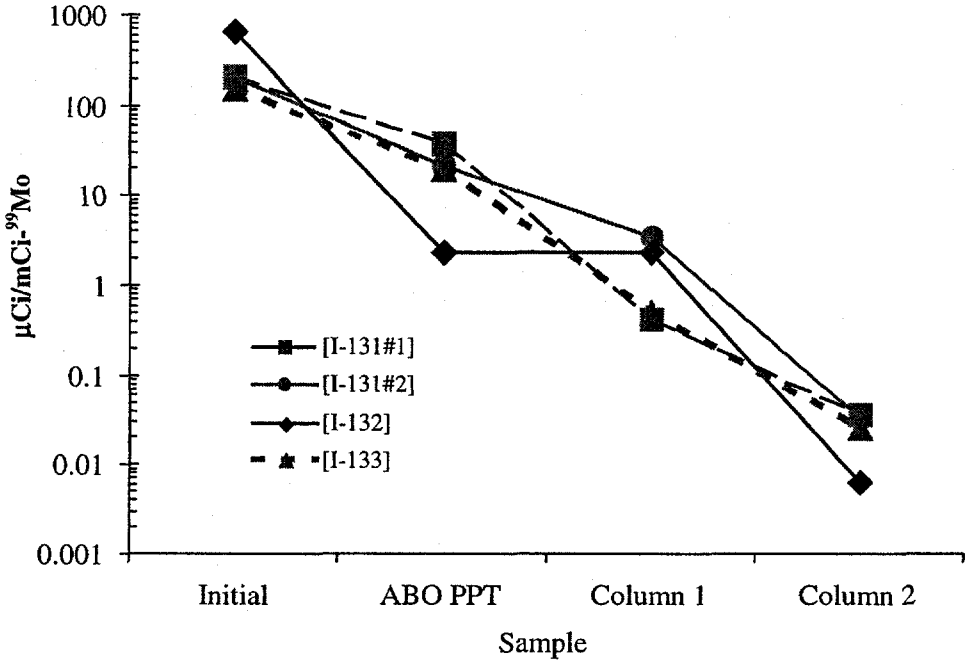

Fig. II-21. Decontamination of ^{99}Mo from Radioiodine in the LEU-Modified Cintichem Process

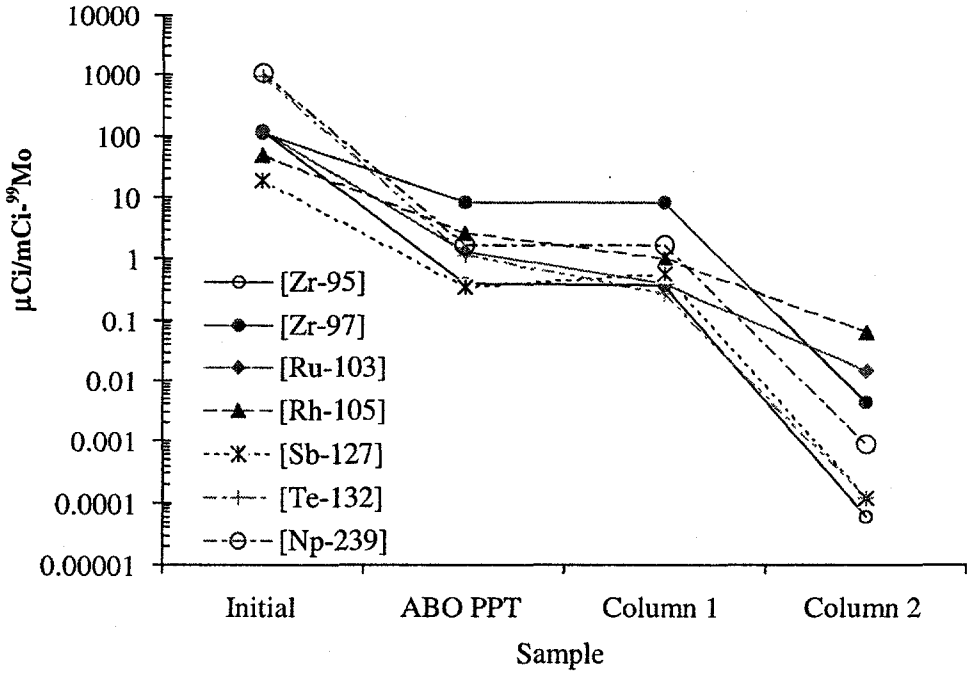

Fig. II-22. Decontamination of ^{99}Mo from ^{239}Np and Various Fission Products by the LEU-Modified Cintichem Process

In sum, the substitution of LEU for HEU is viable. Our method for LEU substitution

- Provides the specified purity of the ^{99}Mo from gamma-emitting impurities.
- Provides a higher yield of ^{99}Mo due to a decrease of 1.5 to 2.0 h in the processing time and potentially higher processing efficiency.
- Cuts waste-treatment and disposal costs by less liquid waste per target and elimination of sulfuric acid.

Future demonstrations will provide additional proof of these conclusions and provide alpha-decontamination data. We will assess other process modifications to improve yield. Thus far, target disassembly has been performed in a hot cell located in the BATAN Radio-metallurgical Installation; future targets will be disassembled in a hot cell in the Radioisotope and Radiopharmaceutical Production Centre, where the ^{99}Mo is processed. Demonstrations will continue during 2000. At that point, a decision will be reached on the need for further work.

Argentine National Atomic Energy Commission. A number of current producers dissolve uranium-aluminide/aluminum dispersion plates in alkaline solution as an initial step to recovering fission-product ^{99}Mo from irradiated HEU. We have begun a cooperative effort with one of them, CNEA, to convert their process to LEU. The CNEA process has been described in the literature.[31] In this process, the irradiated targets are heated in sodium hydroxide solution. The aluminum cladding and meat in the targets are dissolved to form sodium aluminate, and the uranium is precipitated, primarily as UO_2. Molybdenum is soluble in alkaline solutions as the molybdate ion, but the actinides and many of the metallic fission-products precipitate as hydroxide salts. Following filtration of the dissolver solution, the filtrate is fed into an anion-exchange column, which retains molybdenum and some other anionic species. A series of separation processes purifies the molybdenum to meet pharmaceutical standards. As is common to all HEU processes we have studied, only the dissolution and primary molybdenum-recovery steps should be affected by conversion to LEU.

Early in 1999, ANL and CNEA began active cooperation with a goal to allow CNEA to convert to LEU at the end of three years. It is a multifaceted program with many steps. Progress during 1999 was substantial, and we are on target to complete this effort on schedule. Thus far, we have shown that:

- Metal-foil targets of LEU can replace the current HEU targets in the reactor and allow the same or more ^{235}U to be irradiated.
- Zinc-plated uranium foil can be digested in sodium hydroxide at a sufficient rate if done in a closed dissolver at elevated temperature. Another option is

[31] R. O. Marques, P. R. Cristini, H. Fernandez, and D. Marziale, "Operation and Installation for Fission ^{99}Mo Production in Argentina," Fission Molybdenum for Medical Use, Proc. of Technical Committee Mtg., International Atomic Energy Agency, Karlsruhe, October 13-16, 1987, IAEA-TECDOC-515, pp. 23-33 (1989).

dissolving in nitric acid followed by precipitation of $Na_2U_2O_7$, but it would be more complex and time-consuming.

- Initial experiments suggest that the zinc fission-recoil barrier required on the LEU foil should not present a problem to the current processing scheme.

Future activities will move the process chemistry to CNEA hot cells and eventually to full LEU-process demonstrations. However, our current plan and schedule must be modified based on a recent CNEA decision to take full benefit of our conversion activities by modifying their current process to increase molybdenum yield and shorten processing time. At present, CNEA is investigating acidic dissolution of targets and use of alumina as a primary molybdenum-recovery step.

2. Solvent Extraction for Removal of ^{137}Cs from Savannah River Tank Waste

During 1999, we completed our multi-year collaboration with Oak Ridge National Laboratory in the development of new solvent-extraction processes for separating Sr, Tc, and Cs from alkaline supernatant in radioactive waste storage tanks. The focus in the final year of the project was to improve the solvent designed to remove ^{137}Cs from Savannah River Site (SRS) tank waste, correct a solvent deficiency uncovered during earlier ANL tests in a multistage 2-cm centrifugal contactor, and find a more stable solvent modifier. After the solvent was improved and characterized at Oak Ridge, we developed a new flowsheet that will perform at or above the process goals over the normal range of flow rate variations, other-phase carryover, and stage efficiencies. The flowsheet design was extended to take advantage of the improved ability of the solvent to extract cesium at increased temperature. The original solvent required 30 process stages at room temperature, while the new solvent requires only 22 stages and has much improved thermal stability. At higher temperature (50°C), the number of process stages can be reduced further, to 18 stages. Based on the promising results from the new solvent and the resulting flowsheets, SRS personnel are re-evaluating solvent extraction as a possible replacement for the in-tank precipitation process initially chosen for treatment of the tank waste.

3. Open-Gradient Magnetic Separation

The CMT Division, jointly with the Energy Systems, Energy Technology, and Materials Science Divisions, is developing a physical separation method for high-level waste. Vitrification has been selected as a final-waste-form technology in the U.S. for long-term storage of high-level waste. However, a foreseeable problem during vitrification of some waste feed streams lies in the presence of transition metals that may cause instabilities in the final glass product. The formation of spinel compounds, such as Fe_3O_4, $MgFe_2O_4$, $NiFe_2O_4$, and $FeCrO_4$, results in glass phase separation and reduces vitrifier lifetime and the durability of the final waste form. Use of superconducting open-gradient magnetic separation (OGMS) could reduce the volume of vitrified high-level waste and ensure a stable product by removing the deleterious transition metals (e.g., Fe, Cr, Co, and Ni) and other elements (lanthanides) from the vitrification feed streams, which are either ferromagnetic or paramagnetic. The OGMS systems are designed to deflect and collect paramagnetic minerals as they interact with a magnetic field gradient. In order

to design efficient OGMS and high-gradient magnetic separation (HGMS) processes, various simulant waste streams (solid-solid and solid-liquid) from the Savannah River, Hanford, and Rocky Flats sites were physically and chemically characterized. These waste streams were evaluated by using breakthrough curves to describe processing characteristics in an HGMS separator. On the basis of these curves, the OGMS unit at ANL (Fig. II-23) has been modified to handle hazardous and radioactive liquids and slurries. In addition, single-particle models have been developed to predict the separation capability for a superconducting OGMS system We are pursuing the possibility for continued funding for a one-year demonstration effort at Rocky Flats.

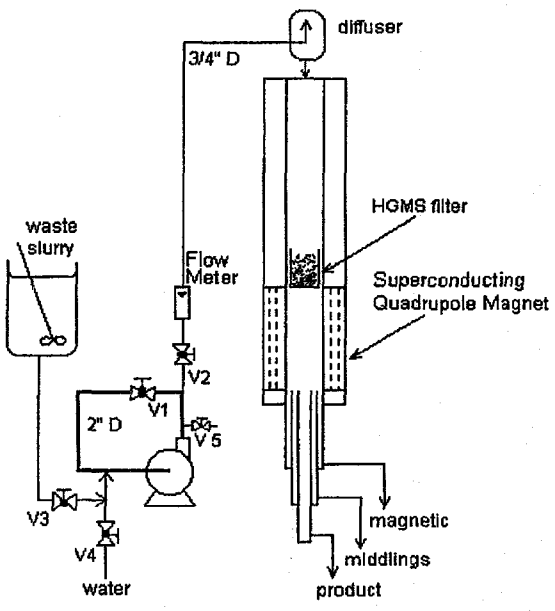

Fig. II-23.

Schematic of Superconducting Open-Gradient Magnetic Separator

4. *Magnetically Assisted Chemical Separation*

The magnetically assisted chemical separation (MACS) process, developed in CMT, may provide an efficient and cost-effective way of removing radionuclides and hazardous components from the environment and nuclear and industrial waste streams. The MACS process has the potential for significant improvement over traditional separation methods such as membrane filtration, ion exchange, and solvent extraction for the recovery of chemical species from dilute waste streams. Tiny, inexpensive superparamagnetic particles (30 nm to 25 μm), with selective chemical extractants, provide a simple way to remove these contaminants from solutions under a wide range of chemical conditions. The magnetic particles are coated with an extractant or ion exchange material. After sufficient mixing with the waste solution, magnetic fields are used to separate the particles from solution. The contaminant-laden coating is stripped by using a small volume of stripping agent, and the magnetic carriers are then regenerated. The strip solution can be treated further to prepare for disposal or to recover the contaminants.

The MACS technology may be applicable to treatment of contaminated milk. The Chernobyl nuclear reactor disaster in 1986 contaminated vast regions of prime grazing land. Subsequently, milk produced in the region was contaminated with small amounts of the long-

lived fission product ^{137}Cs. The Ukraine is seeking to deploy a simple separation process that will remove the cesium and preserve the nutritional value of the milk. Magnetic particles containing a cationic exchanger of crystalline silicotitanates have been manufactured and tested to this end. The results show that partitioning efficiency is optimized with low ratios of particle mass to volume. Less than 3 g/L is required to achieve 90% ^{137}Cs decontamination in a single-stage process. A two-stage process would utilize <0.4 g/L per stage. The MACS technology, with its inherent simplicity and efficiency, may be useful in other areas of the food and beverage industry, and we are pursuing these avenues with companies such as Kraft Foods, Inc.

5. *Decontamination of Stainless Steel*

Argonne National Laboratory has developed a novel decontamination solvent for removing oxide scales formed on ferrous metals typical of nuclear reactor piping. The decontamination process is based on the solvating properties of 1-hydroxyethane-1,1-diphosphonic acid (HEDPA) coupled with strong reducing agents such as sodium formaldehyde sulfoxylate (SFS) and hydroxylamine nitrate (HAN). The solvent has been tested on actual stainless steel piping that had been recently removed from the Palisades Nuclear Plant (Covert, MI). The piping has radioactive contamination from both neutron activation and surface-scale deposits. Wetted surfaces of the pieces were covered with a smooth, adherent, black/brown scale that could not be scratched or removed except by aggressive mechanical means such as filing or cutting. The composition of the scales was perceived to be spinel structure nickel and chromium iron oxides, which are difficult to remove. Therefore, an aggressive mixture of HEDPA, SFS, and HAN was employed in the decontamination of the piping. The solution was heated to 85±3°C and monitored over a couple of days. The metal pieces were removed after 12-48 h of cleaning and analyzed by visual examination and gamma spectroscopy.

Post-decontamination gamma-ray analysis of a pipe section quantified the decontamination factor, which was computed by dividing the total activity before decontamination by the total activity following decontamination. These measurements showed the piece to be completely decontaminated. The decontamination factors for suspected surface radionuclides were >7.8 for Eu-152, >70 for Sn-113, >79 for Sb-125, >36 for Ag-110m, >111 for Co-58, and >16 for Mn-54, respectively. The activities of Cr-51, Fe-59, and Co-60 were reduced by only a factor of 1.5. However, their activities are obviously due to internal activation of the steel piece, which cannot be removed under any means short of complete dissolution. To show the contrast between a cleaned and original surface, only half of a piece was submerged in the HEDPA/SFS/HAN solution. In Fig. II-24, one can easily discern the interface line between the submerged and non-submerged half. Some oxide material can still be seen on the cleaned fraction.

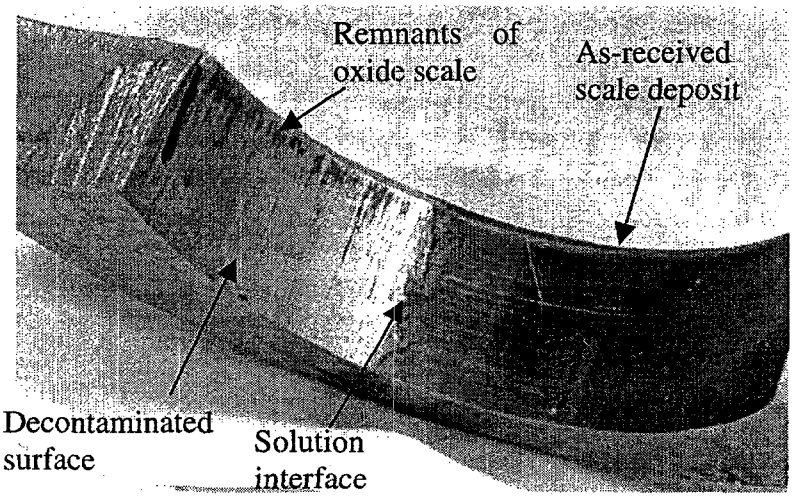

Fig. II-24. Photograph of Pipe Section after Decontamination

6. Waste Management Activities at ANL

We have continued to work with Argonne Waste Management Operations to get waste-treatment equipment operational and to consult on ongoing processes. In particular, a system for treatment of aqueous mixed waste is targeted for full operational capacity in early 2000. Components of this system have been modified and upgraded from the system's original design to streamline operations. When the system becomes operational, ANL will be able to process the aqueous mixed waste currently stored on-site. Future activities for CMT include (1) troubleshooting and organizing repair of mixer equipment used in preparing radioactive liquids for immobilization and shipment to disposal sites, (2) operations and process development for treatment of transuranic waste, and (3) development of a photo-oxidation system for mixed waste.

III

Electrometallurgical Treatment Technology

The CMT Division is developing an electrometallurgical process for treatment of spent nuclear fuels for disposal in a geological repository. It is capable of handling most types of spent fuel and is especially intended for fuels at risk of chemical reaction with the groundwater in the repository. These "at risk" spent fuels include metal fuels with various cladding and matrix materials, reactive compounds, and highly enriched fuels. The central feature of the electrometallurgical treatment is electrorefining of the spent fuel in a molten salt electrolyte at 500°C (773 K). The LiCl-KCl eutectic electrolyte is formulated to contain about 2 mol% UCl_3. A potential is applied between a solid cathode and anodic dissolution baskets containing chopped segments of spent fuel in the molten salt. Uranium, active fission products, and transuranic (TRU) elements dissolve at the anode, while pure uranium product is deposited on the solid cathode. The fission products and TRU elements are left behind to accumulate, either in the anodic dissolution baskets (more noble fission products) or in the molten salt electrolyte (active fission products and TRU elements). The TRU elements and more active fission products may be extracted by passing the molten salt through anhydrous zeolite. The loaded zeolite may then be combined with a suitable glass frit and hot pressed to make a stable waste form for repository disposal. Fuel cladding, assembly hardware, and the noble metal fission products left in the anodic dissolution basket are melted together to form a Zr-Fe-based metal waste form for repository disposal.

All the electrorefining process steps were developed in laboratory-scale experiments, and most have been demonstrated at the engineering scale (10- to 150-kg batch size). Past work also demonstrated the feasibility of using this process for treatment of N-Reactor fuel (Zircaloy-clad uranium), single-pass reactor fuel (aluminum-clad uranium), Experimental Breeder Reactor-II (EBR-II) fuel (steel-clad uranium alloy), aluminum-based fuel (an aluminum-alloy fuel), and fluoride salt fuel containing actinides and fission products. Select topics from the electrometallurgical treatment programs in CMT are discussed below.

A. Electrorefining Development

Work continues on development of uranium electrorefining, the key step in electrometallurgical treatment of metallic spent nuclear fuel. The major focus during this reporting period was to determine the operating procedure and conditions that provide sustained operation of the high throughput electrorefiner (HTER), referred to as the Mark-V anode-cathode module (Mk-V ACM), that will be used to treat the EBR-II blanket fuel in the Fuel Conditioning Facility (FCF) at ANL-West. Key design improvements for the ACM were based on testing of the 25-in. (0.6-m) dia HTER in CMT.[1] Testing of this HTER, as well as a 10-in. (25-cm) dia model, was continued as needed to support the development of the ACM.

1. Operating Procedure

The operating procedure for the Mk-V ACM was developed based on glovebox tests discussed in Sec. III.A.2 and 3. The objective of the procedure is to provide sustained operation of the ACM at a high uranium throughput rate. The main steps of the operating procedure are as follows:

- Limited (200 Ah) electrotransport of uranium from the anode baskets to the cathode tubes (deposition step)
- Molten-salt washing to remove uranium holdup from the electrotransport region of the ACM
- Stripping to electrotransport uranium from the cathode tubes back to the anode baskets
- Repeat of the molten-salt washing

The purpose of the deposition step is to electrotransport uranium from the fuel in the anode baskets to the cathode surface. The electrodeposited uranium is scraped off the cathode surface and falls down into the product collector. This scraping, however, leaves a dense layer of uranium on the cathode surface. If this uranium is not electrotransported from the cathode back to the anode baskets during the stripping step, the thickness of the dense layer increases as the amount of uranium electrotransported from the anode baskets is increased. Formation of a thick, dense uranium deposit may cause the anode drive to stall and may cause damage to the cathode scrapers.

A typical deposition is initially dominated by electrotransport of uranium, which had been deposited on the anode basket surface during an earlier stripping step, back onto the cathode. Subsequent electrotransport is from the fuel inside the baskets for the remainder of the deposition step.

---

[1] J. P. Ackerman et al., *Chemical Technology Division Annual Technical Report, 1998*, Argonne National Laboratory Report ANL-99/10, pp. 90-91 (1999).

The purpose of the molten-salt washing is to dislodge uranium that may be held up in the electrotransport region (i.e., between the faces of the anode baskets and the cathode tubes or on the support ring connected to the bottom of the anode baskets) so that this material can fall down into the product collector. Higher rotation speeds for the anode and multiple changes in direction of rotation will improve the efficiency of this step. Implementation of this step decreased the frequency of anode drive stalls.

2. Conditions of Parametric Tests

Electrorefiner development work at CMT is directed to improving the uranium throughput rate of the Mk-V ACM at ANL-West. This involves glovebox tests with the 10-in. (25-cm) dia ACM at CMT to study key parameters that may affect the throughput of an essentially identical unit at ANL-West. Results from the glovebox parametric tests are summarized in Sec. III.A.3. An investigator at CMT and one at ANL-West were assigned the task of coordinating tests at the two sites. Most of the parameters tested were common to the two sites.

The objective of these tests was to develop a procedure that provides sustained high-throughput operation of the ACM at ANL-West during electrorefining of EBR-II blanket fuel. In the CMT tests, the rotation speed of the anode baskets was increased from 40 to 60 rpm, the electrodeposition current was reduced from 600 to 25 A, the cutoff voltage was increased from 0.45 to 0.75 V, the stripping current was varied over a range of 50 to 600 A, the molten-salt washing times were increased from 2 to 6 min with forward and reverse rotation of the anode drive, zero to three empty anode baskets were used in the cathode channels, and the space between the faces of the anode baskets and cathode tubes was doubled. Two types of chopped fuel segments have been tested: Zircaloy-clad, unirradiated, N-Reactor fuel and steel-clad depleted uranium. Results from ANL-West tests with irradiated, sodium-bonded fuel showed that the glovebox tests with unirradiated fuel were relevant to the hot cell tests. The dimensions of the steel-clad fuel segments tested at CMT were approximately the same as those of the EBR-II blanket fuel segments used at ANL-West.

3. Results of Parametric Tests

Parametric testing of the 10-in. (25-cm) dia ACM in a glovebox at CMT was started during June 1998. Test results are summarized for several experiments.

a. Run Mk-V7

This was the first glovebox test with steel-clad uranium fuel segments in the 10-in. (25-cm) dia ACM. At the start of an earlier test with N-Reactor fuel, 200 Ah of uranium was electrotransported from the anode baskets to the cathode tubes. About two-thirds of the ampere-hours was passed at an electrodeposition current of 200 A, and the remainder at 100 A. In the present test with steel-clad fuel segments, the initial resistance between the anode and cathode was about 1.7 mΩ, much lower than the 2.5 mΩ in the earlier test with N-Reactor fuel. At this lower resistance, all of the 200-Ah electrodeposition was made at 200 A (i.e., none of the

ampere-hours was passed at 100 A). This slightly higher throughput, however, was not sustained. After several hours of operation, uranium holdup caused the ACM anode drive to stall.

b. Run Mk-V7b

In Run Mk-V7b, the uranium holdup was removed, and operation of the ACM was continued with an electrodeposition current of 100 A. The ACM operated for several hours under this condition. As the test was continued, anode stalls did occur. In Run Mk-V7b, the results indicated that the greater packing density of the steel-clad uranium fuel (compared to unirradiated N-Reactor fuel segments) may have restricted the molten salt flow through the anode baskets. As a result, the washing step in the above procedure (Sec. III.A.1) may not have been effective in preventing uranium holdup between the electrodes.

c. Run Mk-V7c

This test used a modified ACM having an anode assembly with thinner baskets. Also, the distance between the face of the anode baskets and cathode tubes was increased from 0.64 to 1.27 cm. This more open electrode structure was expected to provide more effective molten-salt washing and to reduce uranium holdup between the electrodes. For this run, the rotation speed of the anode baskets was increased from 40 to 60 rpm, the electrodeposition current was reduced from 200 to 100 A, and the space between the face of the anode baskets and cathode tubes was doubled. With a 0.6-V deposition cutoff voltage, however, reducing the electrodeposition current and increasing the anode basket rotation speed did not reduce the uranium holdup.

As part of Run Mk-V7c, an experiment was completed to determine how much of the uranium product could be dumped from the collection crucible after it had been separated from the ACM. In an earlier experiment, the crucible had been heated overnight in the hot gas (about 400°C) above the molten salt in the electrorefiner. About 11 kg of the initial 16 kg product in the crucible fell into the receiver crucible when the salt in the product melted. About 3.5 kg of product that remained in the crucible was scooped out at room temperature. About 1.5 kg of the product was left in the crucible, which was used in the next electrorefining run. In a second experiment associated with Run Mk-V7c, nearly all of the uranium product fell from the collection crucible after the salt in the product was melted. In this experiment, the crucible was heated over a weekend in the gas space above the molten salt in the electrorefiner. At the start of this experiment, the collection crucible contained 11.2 kg of uranium product. After melting of the salt in the product, the bulk of the product fell from the collection crucible, and only about 0.5 kg of product remained. This result indicates that nearly all of the product can be removed from the ACM collection crucible by melting the salt in the product. A means of rapidly heating the collection basket to remove the product is needed for operations in a hot cell, or a mechanical means is needed to remove the fuel.

d. Run Mk-V7f

The following operating conditions, used in Run Mk-V7f, demonstrated sustained operation in tests with steel-clad fuel segments: anode-drive rotation speed of 60 rpm, a cutoff voltage of 0.75 V, 7 wt% uranium in the molten salt in the electrorefiner, electrodeposition

currents of 50-600 A, a stripping current of 600 A, and no uranium loaded in the anode baskets in the inner cathode channel. About 6.8 kg of uranium was collected during this run in 36.4 h.

e. Run Mk-V8/8b

This run demonstrated the higher uranium throughput rate achieved by coupling the previously developed operating procedure for the ACM with a higher cutoff voltage (0.75 V compared with 0.45 V). Other changes in the operating conditions included: (1) all of the anode baskets in the outer cathode channel were filled with steel-clad uranium fuel segments, and (2) no fuel was added to the anode baskets in the inner channel formed by the concentric steel cathode tubes. The general operation of this test went very well. Several stalls of the anode drive were eliminated by reversing the direction of rotation momentarily and then restoring normal operation.

f. Run Mk-V9

Additional UCl_3-LiCl-KCl electrolyte was added to the electrorefiner prior to Run Mk-V9. This was necessary to raise the salt level in the electrorefiner above the holes in the upper region of the cathode tubes and to provide flow of molten salt between the channels formed by these tubes. Tests have shown that this flow reduces the occurrence of uranium holdup between the electrodes.

The objective of Run Mk-V9 was to determine an operating procedure that provides sustained operation of the ACM with fuel segments loaded in all the anode baskets. In previous tests (Runs V-7f and V-8/8b), sustained operation was achieved with no fuel loaded in the anode baskets of the inner cathode channel. Run Mk-V9 was terminated after 21.6 h because of an anode stall at the end of a stripping current of 600 A. The weight of cathode product collected during this period was 8.5 kg. The post-test examination of Run Mk-V9 showed two small dense regions of uranium (about 0.16-cm thick by 1.9-cm dia) on the inner steel tube of the inner cathode channel. After the ACM was reassembled, attempts to rotate the anode assembly were unsuccessful. The small region of dense uranium deposit on the cathode tube hindered the anode rotation. The anode baskets were then replaced with the stripper cathode, which consisted of several steel rods. The polarity across the ACM was reversed, the stripping current (electrotransport of uranium from the concentric tubes to the stripper rods) was reduced from 600 to 100 A, and testing resumed. The post-test examination showed that even lower stripping currents are necessary to remove all of the dense uranium deposit from the cathode tubes. As a result of this run, the recommended operating conditions were changed to decrease the stripping current from 600 to about 50 A. This result was a major finding because it indicated a change in the operating procedure that is necessary for sustained operation of the ACM.

g. Run Mk-V9a

In Run Mk-V9a, the initial loading in the anode baskets was about 36 kg of uranium. All of the baskets in the inner and outer cathode channels were loaded with steel-clad depleted uranium rods. Over about 28 h of operation, two stalls of the anode drive occurred. In both cases, rotation of the anode drive was resumed by reversing the direction of rotation for

about 6 min and continuing normal operation. No other intervention by the operator, such as separating the anode from the cathode, was necessary to remove the uranium holdup.

The voltage trace across the ACM during this test showed evidence of higher electrical short circuiting than the previous two tests (Mk-V7f and V8/8b), which achieved sustained operation with no uranium holdup necessitating the removal of the anode drive to eliminate a stall. This observation was consistent with the large amount of uranium holdup (0.85 kg) that was removed from the anode baskets during Run V-9a, and the approximately 600 net Ah (electrodeposition minus stripping) required per kilogram of uranium electrotransported. In Runs V-7f and V-8/8b, approximately 460 net Ah was required per kilogram of uranium electrotransported.

h. Run Mk V9c-d

During Run Mk V9c-d, the stripping current was dropped from an initial 600 to 50 A. As the ACM voltage approached the 0.45-V cutoff, the power supply was programmed to reduce the current to 50 A. This operating procedure was followed for each stripping step. By using this procedure, all of the uranium was removed from the cathode tubes. Near the end of the test, the 50-A stripping was limited to twice daily. This limited stripping at 50 A was also successful in removing all of the uranium from the cathode tubes.

4. Conclusion

On the basis of the parametric tests, the recommended operating procedure for the ACM is as follows: (1) electrotransport 200 Ah of uranium from the anode baskets to the cathode tubes, (2) turn off the ACM current and the anode drive for 2 min, reverse the direction of rotation for 2 min, and return to the normal direction of rotation for 2 min, (3) reverse the polarity of the power supply across the ACM to strip uranium off the concentric tubes, (4) reduce the stripping current to 50 A, at the beginning and end of each working day, as the ACM voltage increases toward the 0.45-V cutoff, and (5) repeat the washing step. This operating procedure should be continued for about 5500 net Ah. If the anode drive stalls during this operating period, reverse the direction of rotation for the anode drive until the stall is eliminated and resume the procedure.

In tests at ANL-West, this procedure achieved a throughput rate of 167 g of uranium per hour per ACM. This rate is sufficient to meet the goal of at least 150 kg uranium per month for the demonstration phase of the program. However, the peak throughput rate of ~300 g of uranium per hour in the CMT tests is not sufficient to reach the 450 kg/month goal for the treatment phase of the program. Several proposed design improvements will be evaluated.

B. Waste Form Development

The electrometallurgical treatment process generates two high-level waste streams. One is a metal waste stream composed of cladding remnants, noble alloying fuel constituents (such as zirconium), noble-metal fission products, and small amounts of actinides that may not have been electrotransported. These metals are alloyed to make a compact and durable waste form.

Development of the metal waste form is mostly complete, and our present major emphasis is on the qualification of the waste form for geologic disposition.

The process salt from the electrorefiner must be disposed of from time to time for any of several reasons, including buildup of radionuclides; this generates a second waste stream. This salt is incorporated into the lattice of zeolite A, and the resulting "salt-loaded zeolite" is blended with glass and consolidated to make a durable ceramic waste form. Overall, our efforts have been focused on the characterization of the waste form and two improvements to the process that have large potential payoffs—development of advanced fabrication methods for the ceramic waste and development of a molten salt ion-exchange column that will concentrate radionuclides in the zeolite and allow indefinite reuse of the process salt.

1. Ceramic Waste Form

a. Development of Pressureless Consolidation Process

The ceramic waste form is designed to immobilize the salt-borne wastes in the electrometallurgical treatment process; this includes fission products and actinides that are oxidized in the electrorefiner to form soluble chlorides. The waste salt is immobilized in the crystal structure of zeolite 4A, an aluminosilicate mineral, by ion exchange and salt occlusion. The salt-loaded zeolite is mixed with glass and consolidated into a dense ceramic waste form. The ceramic consolidation process initially developed for the program is hot isostatic pressing (HIP), but we have developed an alternative process that is being scaled up for demonstration and may replace HIP in the future. This "pressureless consolidation" process involves mixing glass and salt-loaded zeolite (1:1 ratio), heating the powder mixture to ~850°C (where the zeolite transforms to sodalite), and densifying the waste form through viscous consolidation of the glass phase and intrusion of the glass into the porosity in the sodalite phase. The HIP process is similar, except that the glass-sodalite mixture (1:3 ratio) is sealed in a welded stainless steel can and high pressure (~100 MPa) is applied to force the glass into the sodalite porosity and thereby attain a high density.

The motivation for developing this new process stems from several difficulties with HIP, the current consolidation technique being employed in engineering- and pilot-scale operations at ANL-West. The first and most notable is the need for the high-pressure gas to provide isostatic pressure. Safety concerns arise because the material being produced is a high-level (radioactivity) waste, and any catastrophic failure during HIP processing could lead to a major contamination event. Another undesirable feature of HIP is the numerous handling and preparation operations needed to ready the waste for final processing. These include canister loading, canister bake-out and evacuation, and welding, all of which must be done remotely.

Pressureless consolidation provides a robust, simple alternative to HIP because it appears amenable to remote processing and employs simple powder preparation and handling techniques. Monolithic ceramic bodies are shaped by pouring the glass and salt-loaded zeolite mixture into a graphite form and leveling the top surface by vibration. The particle size distributions of both the zeolite and glass raw materials are adjusted such that the two materials not only dry mix well but also flow and pack to unfired, tap densities of nearly 50 vol% solids.

The loose-packed powders are then heated to 850°C for several hours under an argon atmosphere. The argon, or a comparable low-oxygen containing atmosphere, is needed to prevent oxidation of the graphite form. During this heating cycle, the ceramic uniformly densifies into a cylindrical monolith, which can be efficiently packed into secondary waste containers.

Specimens produced are routinely characterized by bulk density and apparent porosity measurements, microscopy, and corrosion and leaching test methods. The largest sodalite-glass composite ceramic waste form produced thus far is 5 kg, with an initial diameter of 30 cm and height of 5 cm. These dimensions were reduced to 26 cm and 4.4 cm after consolidation. The density profile of this specimen appears to be uniform throughout the sample (~2.17 g/cm^3), and the low apparent porosity values (0.62-1.35%) indicate that the remaining porosity in the material is closed and isolated.

A full- or production-scale ceramic waste form is expected to have a mass of ~250 kg. For comparison, current processing facilities at the laboratory scale have a maximum capacity of ~30 kg; the largest ceramic sample made to date is ~26 kg. A number of empirical and theoretical predictive tools are being used to facilitate the scaleup of this process. These include *in situ* tracking to measure temperatures at various locations within the ceramic parts during thermal processing. We are also developing a computer-based thermal simulator, which uses data derived from the *in situ* experiments to predict thermal gradients and temperature distributions within full-scale ceramic parts.

Another part of our scaleup activity is the conceptual design of full-scale processing equipment and facilities. One of the first issues considered was how to lift the products out of the graphite forms and load them into secondary waste containers. The use of graphite forms affords much flexibility in terms of specimen configuration. Graphite forms can easily be machined to provide pressureless consolidation products with lifting devices in place. An example is shown in Fig. III-1. A well-defined hole is formed within the ceramic waste form by using a two-piece graphite form. This hole can facilitate lifting. It also allows internal heating of the ceramic part, which may be necessary for efficient heating of large parts. Similarly, parts can be made with multiple holes or with lifting devices located by the graphite form of choice

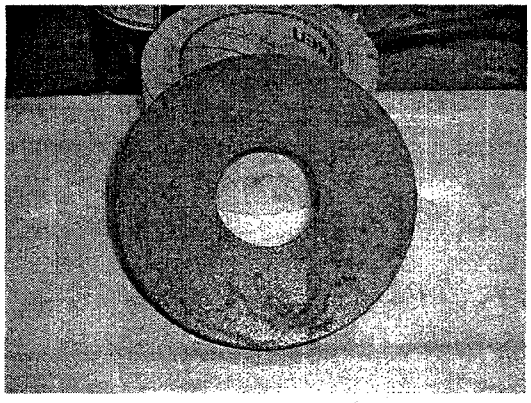

Fig. III-1.

Ceramic Waste Form "Donut" Made by Pressureless Consolidation

In summary, pressureless consolidation has been demonstrated as a viable alternative to HIP on the laboratory scale for ceramics up to 26 kg. The full-scale process may require a 50-250 kg ceramic part, so scaleup activities are underway.

b. Studies of Fundamental Ion Exchange

Fundamental studies are in progress on the ion exchange behavior that governs the incorporation of salt-borne wastes from the electrometallurgical process into the zeolite structure. Since the most immediate application of this process is for EBR-II spent fuel, the ion exchange experiments have focused on salt components expected from the processing of this fuel. The primary component (70 wt%) of this spent salt is 58 mol% LiCl-42 mol% KCl eutectic. In addition, the salt will contain NaCl, formed from the oxidation of sodium metal, and numerous fission product chloride and iodide salts dissolved in the host eutectic salt. There will also be ~2 mol% actinide chlorides, such as UCl_3, $NpCl_3$, and $PuCl_3$. The melting temperature of this salt is ~325°C.

The ion exchange behavior is important for understanding and modeling the immobilization process for the salt waste treatment. Two options are being considered: batch processing and salt treatment via a zeolite column. The batch method involves incorporating the entire spent salt volume from the electrorefiner into a batch of zeolite; this option is attractive when relatively small total volumes of salt are involved. The zeolite column method entails treating the spent salt to concentrate fission products in the zeolite while the LiCl-KCl salt is recycled; the development of the zeolite column is the primary motivation for this fundamental ion exchange study. Both options are carried out at ~550°C, producing a salt-loaded zeolite that may be processed and consolidated to form the sodalite-glass waste form.

The first portion of this study examined the simple occlusion of the LiCl-KCl eutectic salt by zeolite. This was studied first to establish a baseline for our understanding of the basic interaction between the host salt (without fission products and actinides) and the zeolite. The partial molar enthalpies of occlusion of LiCl-KCl in zeolite 4A were measured by differential scanning calorimetry (DSC) at the salt melting temperature of 355°C for different mole fractions of the salt in the salt-zeolite mixture. In addition, *in situ* DSC and temperature-resolved X-ray diffraction (TR-XRD) measurements were performed at the ANL Advanced Photon Source (APS). This custom-designed analytical method provided new insights into the mechanism of the LiCl-KCl occlusion between 25 and 525°C. For example, the XRD peaks for the zeolite crystal structure shift and split during salt occlusion. The shift can only partially be accounted for by thermal expansion. Hence, the occlusion causes an expansion of the zeolite lattice. The peak split seems to indicate two distinct zeolite phases with different degrees of salt occlusion.

The advanced portion of this study is focused on the partitioning behavior of sodium and the prominent fission products (e.g., Cs, Sr, Rb, and Ba) between the zeolite and molten salt phases. For the successful development, design, and implementation of a zeolite column, it is essential that this partitioning be well understood and modeled. This is being accomplished through a series of "equilibrium" ion exchange experiments in which zeolite 4A is contacted with LiCl-KCl containing various concentrations of NaCl and fission product

chlorides. One of the important fundamental parameters that we measure in this experiment is the equilibrium ion-exchange separation factors. The separation factor is determined from the following equation:

$$SF_i = (x_i^Z/x_i^S) / (x_{Li}^Z/x_{Li}^S)^n \quad (1)$$

where x_i^Z and x_i^S are the mole fractions of the i'th cation in the zeolite and molten salt, respectively; x_{Li}^Z and x_{Li}^S are the mole fractions of the lithium in the zeolite and salt, respectively; and n is the charge of the i'th cation.

The equilibrium exchange tests have been completed for a number of pseudo-ternary systems, including NaCl-LiCl-KCl, CsCl-LiCl-KCl, and RbCl-LiCl-KCl, where the ternary salt composition is varied to examine concentration effects on the exchange behavior. In all cases, the zeolite samples were equilibrated with the molten salt bath at 525°C, and both the zeolite and the molten salt samples were submitted for chemical analysis. Figure III-2 shows the exchange isotherms for Na^+, Rb^+, and Cs^+, in which a strong concentration dependence is evident. The relative affinity of the cations for the zeolite phase at high concentrations increases in the order Na^+, Rb^+, Cs^+. Separation factors calculated from isotherm slopes extrapolated to zero concentrations are 1.1 for Na^+, 0.8 for Rb^+, and 2.0 for Cs^+. We are still in the early stages of these experiments and our analysis is incomplete. Nevertheless, it is apparent that cation size plays a significant role in the occlusion behavior. In addition to continued analysis, future work will include equilibrium exchange experiments with salts containing $MgCl_2$, $SrCl_2$, and $BaCl_2$.

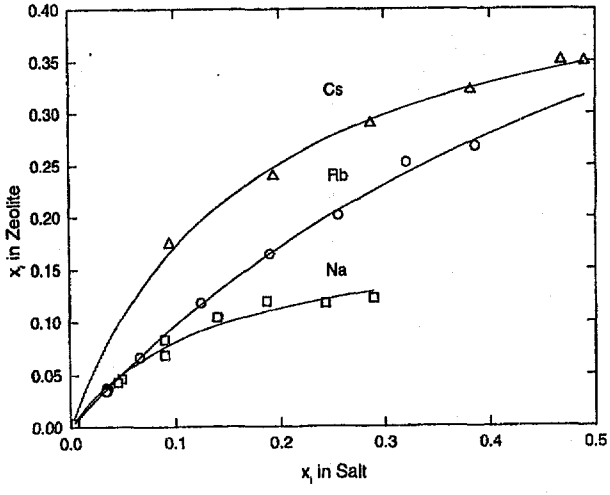

Fig. III-2.

Ion Exchange Isotherms at 550°C Showing the Partitioning of Na^+, Rb^+, and Cs^+ between Zeolite 4A and the Molten Salt

c. Actinide Behavior in the Ceramic Waste Process

Also under investigation is the interaction of uranium and plutonium chlorides with the zeolite and sodalite aluminosilicates during the processing operation and in the final waste form. This mission is comparable to the evaluation of the fission product and sodium exchange behavior described in Sec. III.C.2, but understanding the interaction of these compounds is essential to the development of an acceptable ceramic waste form.

The LiCl-KCl electrorefiner salt contains ~2 mol% UCl_3 at the beginning of electrometallurgical treatment of the spent fuel. Over time, some of the UCl_3 is replaced by $PuCl_3$ from the spent fuel such that the final waste salt at the end of operation will contain both chemical species. Because of the strong thermodynamic stability of uranium and plutonium oxides, there is a reasonable expectation that the UCl_3 and $PuCl_3$ will react with zeolitic water and could react with the aluminosilicate matrix to form UO_2 and PuO_2. Because of this, we applied a variety of analytical methods to study the actinide behavior during simulated processing conditions and in the final waste form material. The analytical paths for uranium and plutonium were slightly different because of the complexity and safeguards involved in any work with plutonium.

Let us first consider uranium by itself. There is a strong thermodynamic driving force for reaction between UCl_3 and both the zeolite 4A framework and the water contained therein to form UO_2. (Although the zeolite is aggressively dried in our process prior to its use, it still contains 0.1-1.0 wt% water; this is enough water to completely consume the 2 mol% UCl_3 content from the salt.) The possible reactions are

$$4\ UCl_3 + 8\ H_2O(g) = 4\ UO_2 + 12\ HCl(g) + 2\ H_2(g) \qquad (2)$$

$$4\ UCl_3 + Na_{12}(AlSiO_4)_{12} = 4\ UO_2 + Si + 11\ SiO_2 + 6\ Al_2O_3 + 12\ NaCl \qquad (3)$$

Our free energy estimates indicate that both reactions may be possible (note that this statement is also true for plutonium, but the uranium reactions are even more favored). However, the free energy calculation for Eq. 3 is an approximation because there are no relevant thermodynamic data for zeolite or sodalite; nepheline, a similar aluminosilicate mineral, was used as a surrogate. The reaction with water is not a serious problem for the ceramic waste form, unless UO_2 introduces a waste-form performance problem, but the reaction with the zeolite 4A framework could compromise its capability to retain the fission products.

To examine these reactions, we contacted a highly concentrated UCl_3-bearing salt (the UCl_3-LiCl-KCl eutectic with 52.3 wt% U) with zeolite. The salt-to-zeolite weight ratio was 3:7, which is higher than the nominal ratio for the batch process of ~1:9. This high salt-to-zeolite ratio was combined with the excessive UCl_3 content to saturate the zeolite with enough UCl_3 to complete the reactions in Eqs. 2 and 3.

The reactions of this salt-zeolite system were studied by several methods. *In situ* TR-XRD provided conclusive evidence that UO_2 is formed upon heating the zeolite-salt mixture.

Figure III-3 shows a three-dimensional representation of a portion of the temperature-dependent diffraction patterns. The major peak for UO_2 is seen growing at a temperature slightly below the salt melting temperature of ~325°C. This behavior indicates a possible reaction with water vapor. With increasing temperature, the zeolite peak undergoes a modest shift to a higher 2θ, and the peak intensity also diminishes. These results indicate lattice expansion from salt occlusion. The principal findings are that UO_2 is a definite reaction product, but the other solid-state reaction products from Eq. 3 (Si, SiO_2, Al_2O_3, and NaCl) are not.

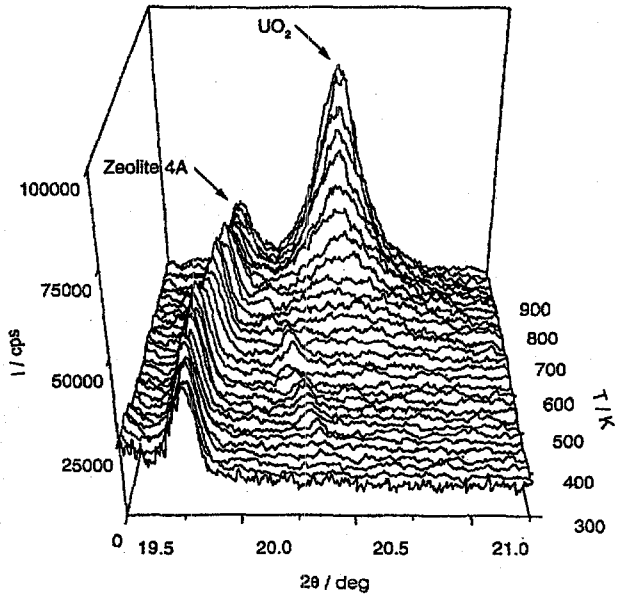

Fig. III-3. Three-Dimensional Representation of Portion of TR-XRD Patterns Showing the Formation of UO_2 and a Distortion of Zeolite Structure near the Salt Melting Point

In addition, DSC of the same salt-zeolite mixture was performed between 25 and 725°C. At ~175°C, the onset of an exothermic process, accelerating with increasing temperature, was observed. At ~325°C, the exothermic character of the signal started to diminish abruptly. While this may have been caused by the completion of the exothermic process, it was more likely the result of the onset of a different endothermic process, one peaking at ~525°C and completed at ~725°C. Also, interrupting the smooth character of this broad endothermic region is a sharp feature at ~410°C. This feature was previously found to represent the salt melting (endothermic) and the molten salt occlusion (exothermic). These data were used to pinpoint the nature and onset temperature of the reactions that occur during processing of the waste form.

Finally, an evolved gas experiment was performed between 25°C and 525°C, in which the salt-zeolite mixture was heated in a vacuum and analyzed by a mass-spectroscopic (MS) detection system. The same salt-zeolite mixtures were used as in the TR-XRD and DSC experiments. The MS detected peaks in the ion intensities for H_2, ^{35}HCl, and ^{37}HCl occurred at temperatures between 325 and 525°C. These species, H_2 and HCl, are the expected products from the reaction between UCl_3 and water (Eq. 2).

Combining the information obtained by the above analyses, we propose the following sequence of events as taking place as the salt (UCl_3-LiCl-KCl eutectic) and zeolite 4A mixture is heated. First, between 25 and 175°C, no chemical changes occur. Second, at ~175°C, the LiCl and/or the KCl start diffusing into the zeolite 4A lattice, forming an occlusion compound. This process is exothermic and results in a significant zeolite 4A lattice contraction. Third, at ~325°C, continuing LiCl and/or KCl occlusion leads to the expulsion of the zeolitic H_2O (<0.2 wt%) from the zeolite 4A lattice, which reacts with $K_3U_5Cl_{18}$, a solid phase in the UCl_3-LiCl-KCl eutectic salt, according to the reaction:

$$8/7\ K_3U_5Cl_{18} + 8\ H_2O = 12/7\ K_2UCl_5 + 4\ UO_2 + 12\ HCl\ (g) + 2\ H_2\ (g) \qquad (4)$$

This reaction is endothermic. Fourth, the UO_2 crystallites being formed increase in size from ~2 nm at ~325°C to ~20 nm at ~625°C. Fifth, at ~410°C, the UCl_3-LiCl-KCl eutectic salt melts and is occluded by the zeolite 4A.

No solid-state decomposition products were observed that would result from a reaction between UCl_3 and zeolite 4A. Hence, we concluded that the UCl_3 in the UCl_3-LiCl-KCl eutectic salt does not react with the zeolite 4A to any appreciable extent. However, thermodynamically spontaneous reactions between UCl_3 and zeolite 4A have been identified. This discrepancy, explainable by sluggish kinetics or inaccurate thermodynamic data, will require further study. Since the UCl_3-to-zeolite 4A ratio in the production of the glass-zeolite waste form is significantly lower than the one used in this work, the H_2O present in the dehydrated zeolite 4A is expected to react with all the UCl_3 from the process salt to form UO_2. Hence, the presence of UCl_3 in the process salt should not have any adverse effects on the performance of the glass-zeolite waste form.

While the above study of uranium interactions with zeolite is now complete, another, more extensive investigation was initiated to evaluate the behavior of Pu and U in representative processing conditions for the ceramic waste form. The test that was devised required the fabrication of four batches of material to evaluate the effects from high and low plutonium concentrations and high and low water concentrations. The uranium + plutonium content was fixed at 2 mol%, and two salt batches were prepared containing U:Pu ratios of 1:3 (high Pu) and 3:1 (low Pu). A representative selection of simulated fission product chlorides (e.g., CsCl, $SrCl_2$, and $NdCl_3$) was incorporated into both salt batches to simulate the electrorefiner salt after processing 300 driver fuel elements from EBR-II. Dried zeolite was also prepared in two batches to produce water levels of 0.1 and 3.5 wt% H_2O in the zeolite matrix. These four materials were blended to create ceramic waste forms with high Pu-low H_2O, high Pu-high H_2O, low Pu-low H_2O, and low Pu-high H_2O. The blended zeolites were mixed with glass and sealed into stainless steel cans (2.5-cm diameter by 7.5-cm tall); four HIP cans were prepared for each type of Pu/H_2O mixture. The sealed cans were shipped to ANL-West for HIP processing, and the resulting ceramic waste form materials have been distributed throughout ANL for testing and analysis.

For our part in this post-production analysis, simple X-ray diffraction (XRD), X-ray absorption fine structure (XAFS) spectroscopy, and X-ray absorption near edge (XANES)

spectroscopy are being used to examine the salt-loaded zeolites and the ceramic waste form materials.

This analytical work will build on a data base that was established in previous years from a set of simulated ceramic waste forms made by hot uniaxial pressing (HUP). In these previous tests, XRD data indicated that the formation of plutonium oxide was preferred over plutonium oxychloride, and there was no indication of decomposition products of the zeolite. Using previously analyzed and verified standards for plutonium in various chemical forms (i.e., PuO, Pu_2O_3, PuOCl, $PuCl_3$, K_2PuCl_5, and K_2PuCl_6), we found that the plutonium was present in a Pu(IV) oxidation state as PuO_2. The XANES patterns from a PuO_2 standard and from the plutonium in the HUP samples are identical except for their respective amplitudes, indicating that the plutonium in the waste form must be at least 95% PuO_2 (detectability limit <5 wt%).

Initial XRD data of HIP samples indicate that the actinides are present as oxides, as seen in the HUP samples. Also, representative fragments from the HIP samples and the salt-loaded zeolites from the four types of samples were subjected to XAFS analysis to characterize the U and Pu disposition. Initial indications are that both U and Pu are present mostly as the dioxide in the HIP samples. This is generally consistent with our previous data and with related data being generated by other groups within ANL. It is apparent that the uranium and plutonium chlorides form very fine oxide particles during the blending step, and that they remain in that phase throughout the HIP process. Planned for the next year are TR-XRD and DSC experiments with HIP samples.

2. *Metal Waste Form*

a. Alloy Characterization

The metal waste stream from the electrometallurgical process includes cladding hulls, assembly hardware, fission products that are noble to the electrorefining process (such as Nb, Pd, Rh, Ru, and Tc), and actinide elements left behind in the anodic dissolution baskets of the electrorefiner. The waste is consolidated by melting at 1600°C under an argon atmosphere and cast into ingots. The baseline metal waste form for spent EBR-II fuel is a stainless steel-15 wt% Zr (SS-15Zr) alloy. In practice, the zirconium content may vary from 5 to 20 wt%, depending on the fuel being treated. The fission product and actinide contents of the waste form depend on the fuel type (driver or blanket), fuel burnup, and the operating conditions in the electrorefiner. The nominal content of the noble metal fission products (NMFP) in the waste form is expected to be <1 wt%, whereas the nominal actinide content is expected to be ~2 wt%, mostly in the form of uranium.

The SS-15Zr alloy has been characterized by various analyses. As shown in Fig. III-4, this alloy displays a eutectic microstructure comprising dark areas that contain the iron solid-solution phases, ferrite and austenite, and light areas containing $ZrFe_2$-type Laves polytypes C36 (dihexagonal, $MgNi_2$-type) and C15 (cubic, $MgCu_2$-type). Small amounts of an $Fe_{23}Zr_6$-type intermetallic are also observed in an as-cast alloy. The compositions of individual phases were determined by energy-dispersive spectroscopy. The Laves intermetallics contain

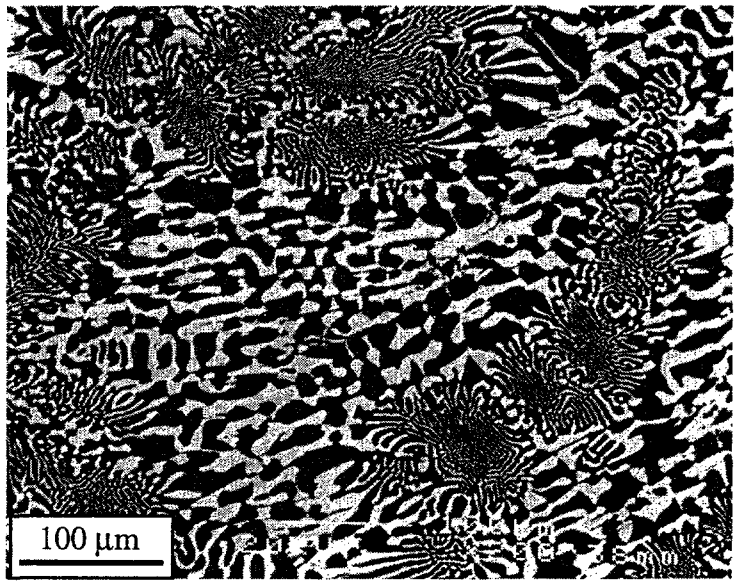

Fig. III-4. Typical Scanning Electron Microscopy Image from an SS-15Zr Alloy. The dark areas are mainly ferrite, while austenite can be seen under appropriate contrast conditions. The bright areas are the $ZrFe_2$-type intermetallics.

~24 at.% Zr, a difference of more than 25% from the expected 33.3 at.% Zr. The Ni/Cr ratio is the main compositional difference between the C36 and C15 polytypes observed in an SS-15Zr alloy: Ni/Cr ~1.5-2 for the C36 polytype and >2.5 for the C15 polytype. The $Fe_{23}Zr_6$ intermetallic has a Ni/Cr ratio of ~1 and a zirconium content very close to the stoichiometric value.

One very important feature of the SS-15Zr alloy is that its component phases exhibit solubility for noble metal fission products and actinides. Representative noble metals were tested and found to be soluble to some degree in the $ZrFe_2$-type Laves intermetallics. Some of them (Co, Mn, Mo, Sn, and Tc) are also soluble in the iron solid-solution phases. Detailed studies conducted on SS-15Zr-2Tc samples showed that the noble metal was incorporated into all phases of the alloy; discrete technetium-rich phases were never observed by electron microscopy, X-ray diffraction, or neutron diffraction. The noble metals were always incorporated in the phases of alloys containing 15 and 20 wt% Zr alloy, but noble metal-rich phases were observed in low-Zr alloys (<5 wt% Zr) when the total noble metal content was above ~1 wt%. Noble metal-rich phases appeared only when the $ZrFe_2$-type intermetallics were saturated with these elements. In stainless steel alloys with no zirconium, noble metals such as Nb, Pd, Ag, and Sn always precipitated to form noble metal-rich phases.

All the actinide elements studied (U, Pu, and Np) were present exclusively in the $ZrFe_2$-type intermetallics. Neutron diffraction experiments were carried out at the ANL Intense Pulsed Neutron Source, and the results showed that the addition of uranium to SS-15Zr does not result in the formation of discrete uranium-rich phases. The lattice parameters of the $ZrFe_2$-type intermetallics are larger in uranium-containing SS-15Zr alloys. This result is consistent with the

substitution of uranium at zirconium sites of the $ZrFe_2$ lattice. Scanning electron microscopy studies revealed the presence of actinide-rich and actinide-deficient areas within the Laves compound. Transmission electron microscopy data imply that the simultaneous presence of multiple Laves polytypes, each with a different preference for the uranium atom, is related to the uranium concentration gradients observed within the Laves intermetallics.

The principal conclusions from these results are the following:

1. The SS-15Zr waste form has a high capacity to accommodate noble metal fission products and actinide elements.

2. The incorporation of these elements distorts the lattice crystal structures of the component phases, most notably, the Laves intermetallic phase.

3. The alloy component phases and the various effects that arise from fission product and actinide additions have been well characterized.

4. At low zirconium concentrations (i.e., <5 wt% Zr), discrete fission product-rich phases have been identified.

b. Qualification Testing

To be acceptable in a geologic repository, high-level nuclear waste forms must have acceptable physical characteristics and demonstrate acceptable corrosion and leaching behavior. An extensive testing program has been completed to evaluate the corrosion behavior, mechanical properties, thermophysical properties, and phase stability of the SS-15Zr metal waste form. The testing approach is based on a methodology outlined by the American Society for Testing and Materials (ASTM C 1174-91). The tests were intended to support the goals of the EBR-II Spent Fuel Treatment Demonstration (Sec. III.A), address DOE repository-related requirements, and support development of radionuclide release models.

A significant number of immersion corrosion, electrochemical corrosion, and vapor hydration tests were conducted on SS-Zr waste form alloys. The immersion tests involved exposing a monolithic alloy sample to a static solution (deionized water or simulated groundwater) at a fixed test temperature (90°C) for up to a year. The test results showed that the corrosion behavior of the SS-Zr waste form is similar over a wide range of zirconium (5-20 wt%) and noble metal (0-4 wt%) compositions and comparable to that of 316 stainless steel. The measured leaching rates for tests in simulated groundwater and deionized water were comparable. Furthermore, the data for normalized mass loss as a function of time were within the same scatter band for 90- and 365-day samples tested at 90°C. Minimal surface corrosion was observed on the specimens tested in the 90°C solution; most samples retained their as-polished surfaces even after the 365-day test. Excellent retention of fission product elements was also observed in immersion tests designed to accelerate alloy corrosion (200°C in deionized water for 28 days).

Electrochemical corrosion rates were measured by the linear polarization method in test solutions that ranged in pH from 2 to 10; selected results are shown in Fig. III-5. It is evident from the data that the corrosion rates for U- and Tc-bearing alloy samples are similar to those measured for nonradioactive samples. Measurements on nonradioactive samples were also conducted in 1000 ppm chloride, 10,000 ppm chloride, and concentrated groundwater solutions (727 ppm chloride), which represent stringent conditions that may be postulated as potential repository environments for the waste forms. Table III-1 shows that the corrosion rates under these stringent conditions are roughly 5-10 times higher than the rates measured in simulated groundwater solution (4.3 ppm chloride). In addition, the results show that the corrosion rates of waste form alloys are (1) comparable in magnitude to those for Alloy C-22 (57Ni-21Cr-13Mo), which is the current choice for the "corrosion resistant" lining of the nuclear waste canisters, and (2) 100-1000 times lower than the rate for mild steel, which is the "corrosion allowance" material in the canister.

In electrochemical galvanic corrosion tests with both simulated groundwater and acidic (pH=2) solutions, experimental conditions simulated the interaction between the metal waste forms and the inner lining of the nuclear waste container (assumed to be Alloy C-22). The results showed that enhanced corrosion due to galvanic coupling with the inner lining of the waste form is not likely for the SS-15Zr waste forms. The SS-15Zr alloys are electrochemically noble to C22, and the steady-state galvanic currents are very small (levels of 10^{-9} amperes), even in the acidic solution.

In another set of tests, the corrosion behavior of waste form alloys was studied by a vapor hydration test. Monolithic alloy specimens were suspended in a sealed stainless steel

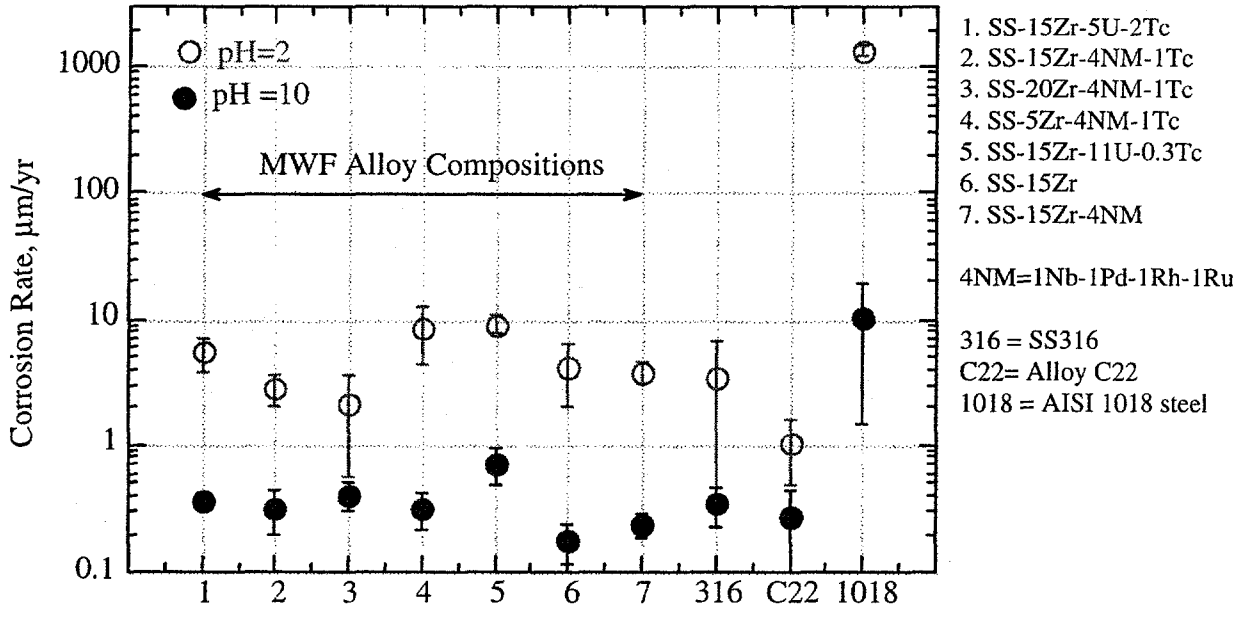

Fig. III-5. Corrosion Rates Measured by Polarization Resistance of Various Alloys in pH=2 and pH=10 Solutions at Room Temperature. The data for U-bearing and Tc-bearing samples were generated at ANL-West.

Table III-1. Average Corrosion (μm/yr) Rates and Standard Deviations (1σ) Measured in Various Test Solutions

	Simulated Groundwater (pH~9)		Concentrated Groundwater (pH~8)		1000 ppm Cl (pH~5.8)		10,000 ppm Cl (pH~6.4)	
	Avg.	Std. Dev.	Avg.	Std. Dev.	Avg.	Std. Dev.	Avg.	Std. Dev.
SS316	0.42	0.15	2.18	1.40	1.70	0.65	2.31	1.41
SS-15Zr	0.12	0.05	0.70	0.25	0.91	0.18	0.94	0.51
SS-5Zr-2Nb-1Pd-1Ru	0.12	0.05	1.25	1.00	0.70	0.56	0.75	0.86
SS-20Zr-2Nb-1Pd-1Ru	0.19	0.02	1.80	0.91	0.99	0.59	2.12	1.62
SS-15Zr-1Nb-1Pd-1Rh-1Ru	0.19	0.07	2.18	2.02	0.52	0.17	1.53	1.89
Alloy C-22	0.17	0.08	0.88	0.38	0.56	0.04	0.81	0.56
AISI 1018	16.9	6.64	2.20	0.19	105	23.9	176	14

vessel containing a small quantity of deionized water. During this type of test, the water vaporizes and creates a saturated steam environment when the vessel is heated to 200°C. Oxide layers formed on the waste form alloys were less than 1 μm thick, even after 182 days. In contrast, pure iron specimens showed a 10-60 μm oxide layer after only 7 days. The relatively thin corrosion layers that form on the SS-Zr alloys demonstrate the excellent durability of these waste forms.

A preliminary study of corrosion layers that form on the SS-Zr alloy samples has been conducted by auger electron spectroscopy (AES) at the Center for Microanalysis of Materials, University of Illinois at Urbana-Champaign. The samples were sputtered with argon (Ar^+) ions to measure elemental composition as a function of depth. The typical depth profiles obtained from a SS-15Zr alloy sample that was tested by vapor hydration for 182 days at 200°C are shown in Fig. III-6. The oxide layer thicknesses estimated by depth-profiling AES are comparable to measurements made by SEM. The AES data show that the oxide layers formed on the ferrite and intermetallic phases have distinct layered structures. The information obtained by AES will be complemented with data obtained by transmission electron microscopy (TEM) to determine the nature of the oxide layers that form on the alloys.

The surface-layer corrosion products formed on SS-15Zr were also examined after alloy particles had been immersed in deionized water at 90°C for two years. The surfaces layers were analyzed with TEM. Two corrosion products were identified on an austenite particle: trevorite ($NiFe_2O_4$) in the layer close to the metal and maghemite (Fe_2O_3) in the outer layer. The corrosion layers on intermetallic particles were small and ranged in thickness from 10 nm to 0.1 μm. A bright-field TEM image showed the typical corrosion layer to be uniform and well adherent to the metallic surface. Electron diffraction patterns obtained from the corrosion layer exhibited broad diffuse rings and indicated that the layer was largely amorphous. Identifying the corrosion layers that form on SS-15Zr alloy phases is critical to delineating the corrosion mechanisms for the metal waste form.

In summary, the corrosion behavior of the SS-15Zr waste form is being characterized to support its disposal in a geologic repository. A wide variety of methods point to the corrosion

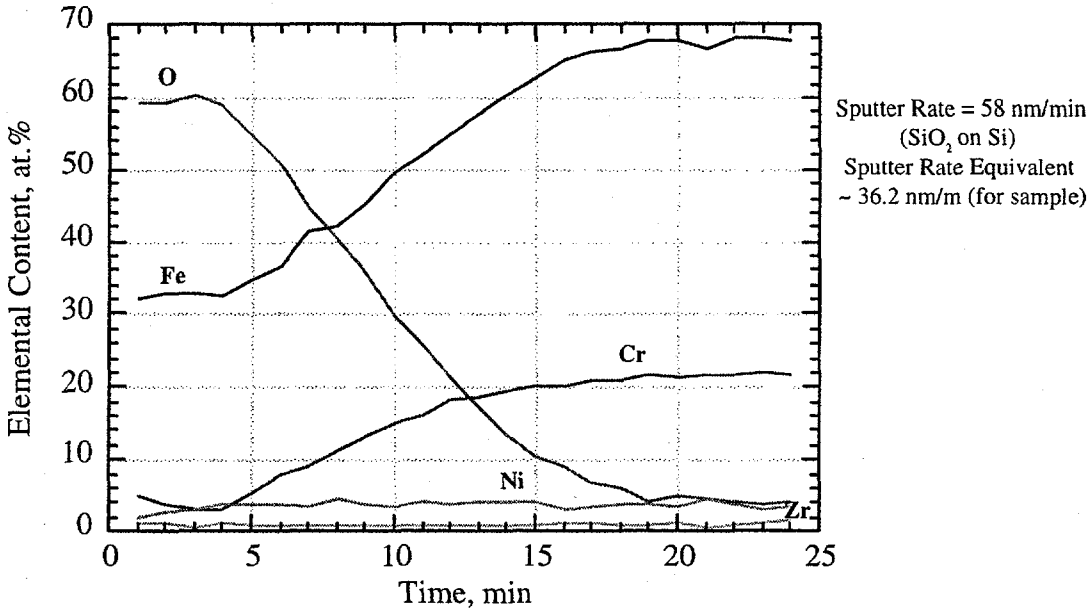

Fig. III-6. Sputter-Depth Profile from SS-15Zr Alloy Sample Tested by Vapor Hydration for 182 Days at 200°C. The oxide layer is ~0.34 μm thick and is probably on the ferrite phase.

mechanism being oxidation and passivation through the formation of a thin adherent surface layer. Our future work will be focused on quantifying this corrosion behavior for use in developing a corrosion model required for repository acceptance.

C. Pyrochemical Process Development

The objective of this effort is to develop process chemistry and engineering concepts that enable the electrometallurgical technology to be applied to treatment of oxide fuels, as well as support studies for the electrometallurgical treatment of metal fuels. Section III.A discusses work on the electrorefining of metal fuels.

1. Lithium Reduction of Oxide Fuel

The electrometallurgical treatment of oxide fuels requires a head-end step to reduce the actinide oxides to the metallic form prior to further separation by electrorefining. To accomplish this reduction, the CMT Division has been developing a pyrochemical process that uses lithium at 650°C in the presence of molten lithium chloride. This process has two components: (1) a reduction step in which the actinide oxides are reduced, yielding the corresponding metals and lithium oxide, and (2) a salt-recovery step in which the lithium oxide is electrolytically decomposed to form lithium and oxygen. The salt-recovery step allows recovery and reuse of the lithium and lithium chloride in subsequent reductions.

During the past year, studies were performed to determine the effect of fuel morphology on reduction kinetics. Concepts for containing very small fuel particles were tested, and a

promising technique was demonstrated at the engineering scale. Improved anode designs, based on tin oxide, were tested at the laboratory scale.

a. Reduction Step

The first step in the lithium reduction process is a head-end step to cut up the fuel assemblies and expose the fuel to the molten salt. The reference process is to shear the fuel assemblies into 1-cm-long sections. The sheared fuel mixture is expected to consist of a wide range of particle sizes: from relatively large, intact UO_2 fragments inside cladding hulls to fragments of UO_2 dislodged from the cladding, including very small particles. The size of these fuel particles is an important design parameter—the largest particles determine the duration of the reduction step, while the smallest particles present handling and containment problems. This past year, the focus of the work on the reduction step was to demonstrate that it would be feasible to design a large-scale system that could handle the wide range of fuel morphologies.

Laboratory-scale experiments were performed with simulated fuel prepared by shearing stainless steel-clad UO_2 rods into 1-cm-long segments. The shearing was accomplished with a hydraulic press and a clamping device for positioning the UO_2 rods during the shearing operation. About 50% of the UO_2 was dislodged from the cladding during this operation. This material was sieved to remove that portion with particle sizes <45 μm (325 mesh) because the pouches holding the fuel in the fuel basket were lined with 325-mesh stainless steel. The remaining fuel and cladding, weighing 300 g, were reduced by using lithium in lithium chloride at 650°C with a stirring rate of 200 rpm.

As shown in Fig. III-7, the reduction was complete in about 40 h. This is comparable to the 35-40 h measured for the reduction of fuel containing only large intact UO_2 fragments (nominally 1-cm long) inside cladding hulls. Reduction times on the order of 10-20 h had been recorded earlier for reduction of crushed UO_2 (particle-size range of 45-4000 μm) when accompanied by stirring.[2] Thus, for the reduction of a sheared fuel mixture, the overall reduction time appears to be controlled by the reduction rate of the large, intact UO_2 fragments inside the cladding hulls.

For fuel particles smaller than 45 μm, a new basket material was required. For this fuel, cylindrical crucibles (1.27-cm ID) were fabricated from a porous stainless steel material (316 SS) obtained from Mott Corp. This 10 μm-grade porous material was rated at 100% for retention of 17 μm particles, 95% for 9 μm particles, and 49% for 5 μm particles. In this experiment, 135 g of U_3O_7 fines (<45 μm) was loaded into five porous crucibles. The U_3O_7 material was selected because of its consistency (like talcum powder) and availability in large quantity. The crucibles were placed in a rectangular outer basket and then immersed in lithium-saturated LiCl salt containing 1.2 wt% Li_2O. The reduction was carried out at 650°C with a stirring rate of 200 rpm.

---

[2] J. J. Laidler et al., *Chemical Technology Division Annual Technical Report, 1997*, Argonne National Laboratory Report ANL-98/13, p. 124 (1998).

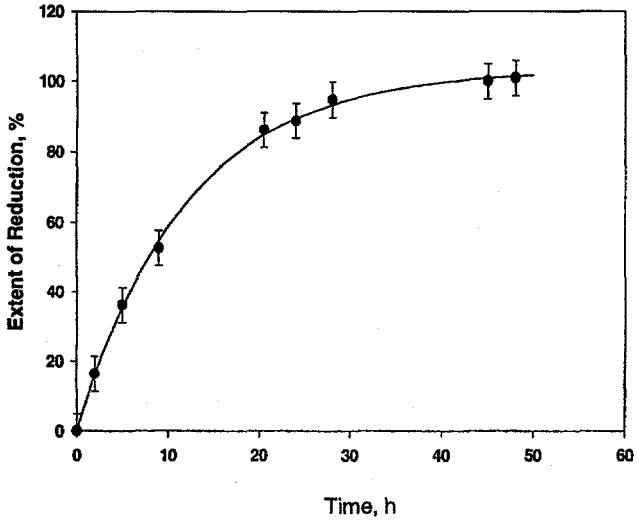

Fig. III-7.

Reduction of Sheared Fuel (UO_2) Mixture in Laboratory-Scale Experiment UR-206

As shown in Fig. III-8, the reduction was complete in about 20 h. The reduced material was consolidated in a packed bed, presumably containing a mixture of uranium metal fines and salt. The reduction product in the crucibles was estimated to contain 50 wt% uranium and 50 wt% LiCl salt. The reduction time of 20 h is satisfactory, and it shows that the porous crucibles do not adversely affect the reduction rate. Following the success of this experiment, an engineering-scale demonstration of the fines reduction in porous crucibles was performed. This experiment is described in Sec. III.C.1.c.

b. Salt-Recovery Step

In a series of laboratory-scale experiments, tin oxide anodes were investigated as a replacement for the platinum anode material in the electrowinning cell used for salt recovery. This substitution would be beneficial, as SnO_2 electrodes are relatively inexpensive and readily available commercially. Our experiments showed that under practical conditions of

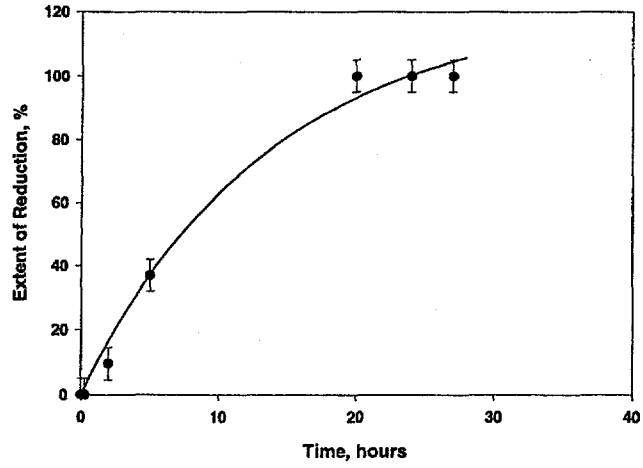

Fig. III-8.

Reduction of UO_2 Fines in Crucibles Fabricated from Porous Stainless Steel in Laboratory-Scale Experiment UR-207

electrowinning, the SnO_2 electrode is stable. In several experiments, lithium electrowinning electrolysis lowered the Li_2O concentration from 2 to 0.5 wt%, at about 50-60% current efficiency.

Several technical issues that are important to consider for effective, safe electrowinning by the SnO_2 anode have been identified. First, the SnO_2 anode—like the platinum anode—is subject to attack by metallic lithium. Thus, the same precautions must be taken that were used in the experiments with the platinum anode. Second, the SnO_2 electrode has a high resistivity compared with the metal electrode; therefore, the resistance drop in the cell is high. To overcome the problem of the resulting high internal cell resistance, a new SnO_2 anode design, termed "low-resistance anode," has been introduced and successfully tested in small-scale laboratory cells. This new anode reduces the resistance to about a tenth of the standard SnO_2 anode. The maximum useful current density on the SnO_2 anode, however, is less than with a platinum anode, 0.3 A/cm^2 compared to 2.0 A/cm^2. Future work with SnO_2 will focus on methods to increase its current density.

c. Engineering-Scale Experiments

The purpose of the engineering-scale experiments is to obtain design information and operating experience needed for scaling up the reduction and electrowinning processes to equipment sizes required for processing DOE spent oxide fuels. The facility used for the engineering-scale experiments was designed to support the reduction of kilogram quantities of fuel. During the past year, an engineering-scale experiment (designated ES-10) was performed to demonstrate that the porous crucible fuel baskets designed to hold fuel fines could be scaled up to practical sizes.

A new fuel basket design using porous stainless steel material, developed for handling fuel fines (particle size <45 μm), was successfully tested in laboratory-scale reduction experiments (Sec. III.C.1.b). A scaled-up version of the same design was tested in ES-10. The fuel fines were contained in two identical fuel baskets, each consisting of 10 porous stainless steel crucibles (ID = 1.27 cm). The total fuel loading included 1.4 kg of mock spent fuel (98.5% UO_2 plus simulated fission products), 1.2 kg of U_3O_7, and 0.7 kg of UO_2. Each tube was loaded to a height of 36 cm, resulting in packing densities of 6.9 g/cm^3 for the mock fuel, 2.4 g/cm^3 for the U_3O_7, and 6.1 g/cm^3 for the UO_2. The lower packing density for the U_3O_7 is thought to result from its finer particle size. The reduction was carried out at 650°C in 77 kg of LiCl with a stirring rate of 500 rpm. Lithium was supplied to the melt through lithium-saturated porous stainless steel disks.

During the course of ES-10, the Li_2O concentration of the reduction salt was periodically measured with 0.1 N HCl by titration of salt samples. The extent of reduction was calculated from the measured Li_2O of the reduction salt. As shown in Fig. III-9, the final extent of reduction appears to be close to 90%. Although the reduction was carried out for 48 h, no significant reduction occurred after 20 to 25 h, which compares fairly well with the 20 h measured in the laboratory-scale experiment. Inspection of the fuel baskets after the reduction indicated that one of the tubes had cracked, but it is not known whether this took place during the

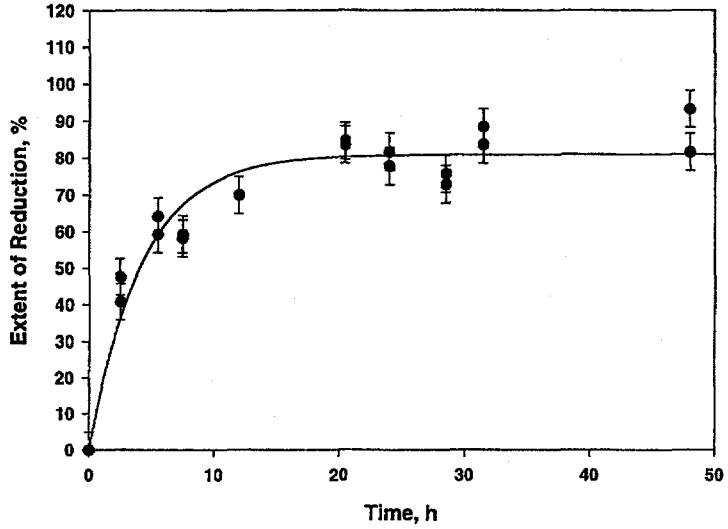

Fig. III-9. Reduction of UO_2 Fines in Porous Crucible Fuel Basket in Engineering-Scale Experiment ES-10

reduction or upon removal from the melt. Visual inspection indicated that little if any fuel material had been lost from the tube.

In summary, the successful reduction of fuel fines in ES-10 proves that porous crucibles will provide the fines containment needed for the lithium reduction process.

2. *Lithium-Aluminum Reduction of Electrolyte Salt*

Periodic removal and subsequent treatment of salt from the electrorefiner currently being operated at ANL-West are expected (Sec. III.A). During this process, active fission product chlorides accumulate in this salt due to the reaction of fission product elements with UCl_3. This buildup of fission product chlorides with continued operating time at some point results in (1) too high a heat load in the salt, (2) phase relationship changes that increase the liquidus temperature of the salt, and (3) possible precipitation of some chlorides due to exceeding the solubility in the matrix salt, which consists of the LiCl-KCl eutectic (58.2 mol% LiCl) and ~2 mol% UCl_3. Obviously, the inventory of fission product chlorides must not reach the point where any of the above happen; thus, the salt must be periodically treated if the electrochemical operations are to be continued.

The steps involved for disposal of the waste salt are described in the literature.[3,4] Briefly, they include removing the salt from the electrorefiner, passing the salt through zeolite to remove TRU elements and more active fission products, combining the loaded zeolite with borosilicate glass, and heating the mixture to 900°C in order to convert the mixture to a glass-

[3] J. P. Ackerman, S. M. McDeavitt, C. Pereira, and L. J. Simpson, "Waste Form Development and Characterization in Pyrometallurgical Treatment of Spent Nuclear Fuel," Proc. of Third Topical Meeting on DOE Spent Nuclear Fuel and Fissile Material Management, American Nuclear Society, Charleston, SC, September 8-11, 1998 (1998).

[4] C. Pereira, M. Hash, M. Lewis, and M. Richmann, *J. Mater.* **49**(7), 34 (1997).

sodalite composite. The resulting product is highly leach resistant and appears suitable for disposal.

Before the salt is contacted with zeolite, the uranium concentration in the salt could be reduced by (1) a chemical method using a suitable reductant such as lithium or sodium or (2) an electrochemical method using a suitable anode material and collecting the uranium on a solid cathode. For the chemical method, the bond sodium present in the fuel can be used as the reductant. For the electrochemical method, the choice of anode material is limited to those elements whose chlorides are more stable than UCl_3, and whose chemical activity is sufficiently reduced so that chemical reduction of UCl_3 is not possible. Our brief examination of the possible candidate materials indicated that alloys of Li and either Bi, Zn, Cd, Sb, or Al were good choices for initial examination. Out of these choices, we narrowed the field to alloys of either Sb or Al. As the work began, we encountered difficulties in preparing the Li_3Sb material. Because of this and subsequent environmental concerns related to Li_3Sb, we excluded antimony. To begin, a Li-Al alloy was tested as the chemical reductant.

We conducted seven tests with Li-Al alloy (6.5 to 30 g) as the reductant in LiCl-KCl eutectic (200-600 g). In the first four tests, UCl_3 was added to the LiCl-KCl salt; in the next test, UCl_3 and representative rare earth chlorides were added; and in the last two tests, UCl_3, $PuCl_3$, and representative rare earth chlorides were added. Our objective in these tests was to demonstrate UCl_3 reduction, and to determine whether the reduction of $PuCl_3$ and rare earth chlorides is also possible, if needed. The advantage of removing these chlorides in the electrorefiner is twofold: (1) the salt does not have to be treated as often, and (2) it is possible that the treated salt would be non-TRU. These advantages would reduce subsequent process operations.

The general test procedure consisted of placing the salt constituents into a stainless steel beaker (~600 mL), heating the contents to 500°C, then mixing the molten mixture for at least several hours. Afterwards, a salt sample was taken by dipping a metal rod into the melt and rapidly withdrawing it. The adhering salt was then removed for analysis. After this initial sampling, a metal cylinder, which contained the Li-Al, was lowered in the melt. This cylinder had holes drilled on its circumference; these holes were then covered with a stainless steel screen, as was the bottom of this cylinder. We tried a number of designs for the Li-Al container because the initial ones plugged up during operation. For the last tests, we used a design that allowed us to add Li-Al powder at test temperature to the metal housing. In this design, the cylinder housing was made out of a stainless steel beaker. The bottom and top of this housing were covered with a stainless steel screen, and a fill tube was attached to allow addition of Li-Al, which was added in increments of ~1.5 to 3.0 g during operation. We took samples with this type of housing within 100 min after each Li-Al addition. Near the end of the last three tests, samples were taken after waiting as long as 66 h.

The first four tests provided information on the reduction of UCl_3 by Li-Al. As shown in Table III-2, the results from all tests except Test 3 indicated a substantial reduction in uranium content. In Test 3, the housing had become plugged, and no salt could enter to react with the

Table III-2. Reduction of UCl_3 by Li-Al in Molten LiCl-KCl Eutectic

Test No.	U Conc., wt%	
	Initial	Final
1	3.58	0.09
2	2.01	<0.02
3	2.90	2.66
4	1.18	0.061
5[a]	0.14	<0.02
6[b]	2.85	0.018
7[b]	0.37	0.011

[a] Rare earths added to salt.

[b] Plutonium and rare earths added to salt.

Li-Al; hence, there was little change in uranium content. The results in Table III-3 indicate that the concentrations for plutonium and rare earth elements were also reduced to low values. Further, the analytical results from each reduction indicated no aluminum in the salt, as did analysis of the Li-Al housing at the end of the tests.

Better recoveries of uranium (more than three times higher), as well as plutonium and the rare earth elements, were achieved in Tests 6 and 7. The following recoveries were obtained: U, 70%; Pu, 79%; Nd, 84%; La, 91%; Ce, 76%; Y, 65%; Pr, 91%; Eu, 80%; and Sm, 75%. These results indicate that it is advantageous to add the Li-Al powder to the housing in small increments. Surprisingly, both the europium and samarium chlorides were reduced to the metals. This result was not expected, as thermodynamic calculations and prior chemical tests indicated that both $EuCl_3$ and $SmCl_2$ can be reduced only to the divalent state by lithium. Thus, the reduction of these chlorides to the metals suggests that intermetallic compounds with aluminum must have formed.

Table III-3. Reduction of $PuCl_3$ and Rare Earth Chlorides by Li-Al in Molten LiCl-KCl Eutectic. Concentrations in wt%.

	Test 5		Test 6		Test 7	
	Initial	Final	Initial	Final	Initial	Final
La	0.87	0.22	1.12	0.072	0.22	0.0026
Ce	0.41	0.061	0.45	0.03	0.081	0.0017
Pr	0.096	0.011	0.11	0.005	0.016	0.0006
Nd	0.90	0.098	0.98	0.048	0.17	0.0015
Sm	0.099	0.071	0.10	0.0098	0.026	0.0002
Eu	0.10	0.10	0.10	0.0067	0.029	0.0005
Y	0.35	0.16	0.36	0.09	0.081	0.0025
Pu	NA	NA	0.29	0.018	0.041	0.004

The results from these tests indicate that Li-Al is a good candidate for reducing the concentration of UCl_3, $PuCl_3$, and rare earth chloride to low values in the electrorefiner salt. Moreover, since a high fraction of the metals formed are captured in the Li-Al housing, it is possible to convert these metals to a suitable waste form in a subsequent step. The advantage of this treatment is that it reduces the amount of zeolite needed to treat the salt and, thus, the amount of sodalite formed. If the metal chlorides tested here are not present in the salt that is to be processed, the zeolite treatment has to only remove Ba, Sr, and Cs (the primary heat generators left in the salt). Since the salt to be treated would be considered non-TRU waste, the subsequent waste form would also be non-TRU, which should reduce storage and handling problems.

IV

Basic Chemistry Research

Basic chemistry research is being pursued on fundamental issues related to homogeneous and heterogeneous catalysis, ion transport mechanisms in electrochemical devices, the preparation of high-critical-temperature superconducting materials, and the decontamination of radioisotope-impregnated materials.

A. Physical Organometallic Chemistry

This program uses an array of *in situ* spectroscopic techniques to explore organometallic reaction chemistry that is aimed at achieving chemical and electrochemical processes that are more energy efficient and environmentally benign. Research is conducted in three areas: (1) homogeneous catalysis in supercritical fluids, (2) the Shell process, and (3) ion transport mechanisms. Highlights of recent prior research include the first use of transition metal complex catalysts in supercritical media, the invention of a nuclear magnetic resonance (NMR) device called the "toroid cavity imager," and the development of extremely robust polyfluorophthalocyanine catalysts for hydrocarbon activation. Current research focuses on investigation of the chemistry associated with potential ethylene glycol synthesis processes, the first *in situ* high-pressure NMR studies of the commercial Shell process for the hydroformylation of olefins, and the development of an NMR pulse technique that allows faster imaging with the toroid cavity imager and its counterpart in electrochemistry, the near-electrode imager.

1. Homogeneous Catalysis in Supercritical Fluids

Dow and Mitsubishi Corporations were early developers of a process that uses $HCo(CO)_4$ as a catalyst to convert formaldehyde (and its precursors, paraformaldehyde and formalin) to ethylene glycol (and the byproducts methanol and methyl formate) via the following hydroformylation chemistry:

$$CH_2O + 2H_2 + CO = C_2H_4(OH)_2 \quad (1)$$

$$CH_2O + H_2 = CH_3OH \quad (2)$$

$$CH_2O + H_2 + CO = CH_3OC(O)H \quad (3)$$

The process would change the source of ethylene glycol from petroleum base to natural gas. Our interest in the hydroformylation of formaldehyde and its precursors stems from our earlier work on CO hydrogenation, wherein we proposed that formaldehyde is an early intermediate in CO hydrogenation, and hence, the products from CO hydrogenation are identical to those produced from formaldehyde.[1]

We recently decided to test some new liquid-phase and the first supercritical-phase versions of the formaldehyde hydroformylation process and have obtained encouraging results that warrant further work. We have found that supercritical CO_2 solutions containing high concentrations of relatively pure monomeric formaldehyde (determined by integration of the aldehydic proton NMR resonance at $\delta = 9.57$ ppm) are easily made by heating solid paraformaldehyde in CO_2 near its critical density. The results of our NMR measurements in supercritical CO_2, along with comparable literature data[2] for measurements in the absence of CO_2 (i.e., in a vacuum), are plotted in Fig. IV-1. As shown in Fig. IV-1, for measurements at 125°C, the solubility of monomeric formaldehyde in supercritical CO_2 is 0.134 M, while the concentration in the absence of CO_2 at this temperature is only 0.034 M. The monomeric solutions are of interest because monomeric formaldehyde might react differently from the oligomerized forms of formaldehyde present in paraformaldehyde or in formalin, which had been investigated in the early industrial research. In addition, use of a supercritical fluid is expected to inhibit the undesired $HCo(CO)_4$-catalyzed homologation of the methanol produced in Eq. 2. Homologation leads to the production of higher alcohols

$$CH_3OH + 2nH_2 + nCO = CH_3(CH_2)_nOH + nH_2O \quad (4)$$

where n is a measure of the degree of higher alcohol formation. Extensively homologated solutions contain high-boiling alcohols that are difficult to separate from ethylene glycol. Use of supercritical CO_2 as the reaction medium, because of its low dielectric constant, would tend to inhibit the formation of higher alcohols via disfavoring the protonation of methanol by $HCo(CO)_4$,

$$CH_3OH + HCo(CO)_4 = CH_3OH_2^+ + Co(CO)_4^- \quad (5)$$

This is a key step in the catalytic homologation reaction.

We recently tested the first supercritical hydroformylation of formaldehyde. For this testing, supercritical CO_2 solutions of monomeric formaldehyde were prepared by taking into account the data of Fig. IV-1. At 100°C and at relatively low pressures of CO and H_2, reaction in the presence of the catalyst precursor, $Co_2(CO)_8$, was comparable in rate to the hydroformylation of propylene under the same conditions. The expected inhibition of methanol homologation was thus achieved. However, even with this improvement a severe problem remains with the formaldehyde hydroformylation. The conventional liquid-phase process and this new supercritical one both produce large amounts of undesired methanol as the major reaction product.

---

[1] R. J. Klingler and J. W. Rathke, *Prog. Inorg. Chem.* **39**, 113-180 (1991).

[2] H. H. Nielsen and E. S. Ebers, *J. Chem. Phys.* **5**, 384 (1937).

In future work, we will attempt to determine what factors influence the product selectivity. Our preliminary experiments in supercritical CO_2 have uncovered at least two new ^{59}Co NMR resonances, whose rates of formation and decay might yield information on the factors determining product selectivity. Our future work will measure and compare reaction parameters for the new supercritical fluid process with the conventional liquid-phase system, and will determine the identity and the role of the new cobalt species in the catalytic reaction.

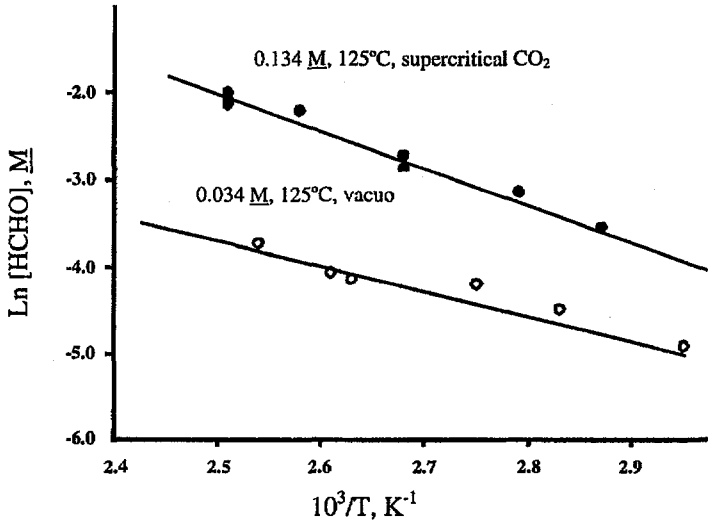

Fig. IV-1. Equilibrium Concentration of Monomeric Formaldehyde Produced by the Dissociation of Paraformaldehyde in Supercritical Carbon Dioxide (filled circles) and in a Vacuum (open circles)

2. The Shell Process

The Shell process,[3] which employs phosphine-modified cobalt carbonyl complexes as the catalyst, is used commercially for the hydroformylation of olefins to produce alcohols:

$$RHC{=}CH_2 + 2H_2 + CO = RCH_2CH_2CH_2OH \qquad (6)$$

Olefin hydroformylation processes are usually conducted in organic media, the exception being the Ruhrchemie/Rhône-Poulenc process,[4] which uses a rhodium catalyst in an environmentally benign aqueous solution. We have initiated a study of the hydroformylation of olefins using water-soluble Shell-type catalysts, with the hope of developing less expensive water-soluble phosphine-based cobalt catalysts. Since phosphine-modified cobalt catalysts have proven to be effective in organic media in the Shell process, the challenge is to come up with a phosphine-modified hydrido cobalt complex $(CO)_{4-x}L_xCoH$ (where L = phosphine) that is not so acidic as to be inactive in aqueous solutions. The high acidity of $(CO)_4CoH$ makes it non-catalytic for hydroformylation in aqueous

[3] L. H. Slaugh and R. D. Mullineaux, U.S. Patents 3,239,569 and 3,239,570 (1966).

[4] B. Cornils and E. G. Kuntz, *J. Organomet. Chem.* **502**, 177 (1995).

solutions, but the substitution for a carbonyl ligand with the phosphine should make the hydride ligand less acidic. Our initial investigation with the water-soluble catalyst $[(CO)_3(TPPTS)Co]_2$ [where TPPTS = $P(m\text{-}C_6H_4SO_3Na)_3$] revealed that the sulfonated triphenylphosphine is replaced by CO under oxo reaction conditions, and a more basic phosphine is needed. We have subsequently synthesized $[(CO)_3(THPP)_2Co][Co(CO)_4]$ [where THPP = $P(CH_2CH_2CH_2OH)_3$]. A single-crystal X-ray diffraction study of this compound shows that the cation assumes a trigonal bipyramidal structure, while the anion is tetrahedral (Fig. IV-2). As is known for its tributylphosphine analogue, this complex is converted to the dimeric $[(CO)_3(THPP)Co]_2$ reversibly:

$$[(CO)_3(THPP)_2Co][Co(CO)_4] = [(CO)_3(THPP)Co]_2 + CO \quad (7)$$

Work is in progress to study the reaction of $[(CO)_3(THPP)Co]_2$ with hydrogen to generate $(CO)_3(THPP)CoH$ and its catalytic activity for the *oxo* reaction. Also to be included in the study is the use of water-soluble diphosphines $R_2P(CH_2)_2PR_2$ (where R = hydroxyalkyl). It is reasonable to expect that the diphosphine-modified $(CO)_2(R_2PCH_2CH_2PR_2)CoH$ is less acidic and that its diphosphine ligand is more strongly bonded to cobalt.

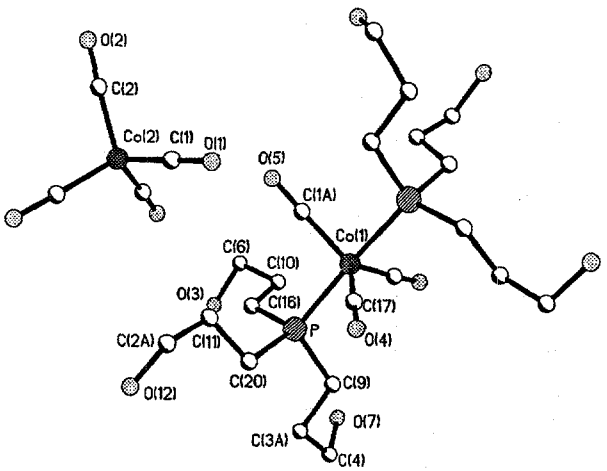

Fig. IV-2.

Molecular Structure of the Water-Soluble Catalyst $[Co(CO)_3(THPP)_2][Co(CO)_4]$. The hydrogen atoms are omitted for clarity.

3. Ion Transport Mechanisms

This program uses *in situ* magnetic resonance imaging (MRI) to investigate the electrode-electrolyte interface in batteries, fuel cells, and components of advanced electrochemical systems. Analysis is conducted with a toroid cavity imager developed at Argonne.[5] This specialized MRI device is capable of providing high-resolution NMR spectra as a function of distance from a working electrode with 2-μm resolution. In contrast to most conventional approaches to MRI, the toroid-cavity imaging method maintains all of the NMR chemical shift, coupling constant, and spin relaxation information. The toroid-cavity imaging method is used to probe the micro-environment immediately adjacent to the electrode for comparison to the properties of the bulk materials. In addition, a related NMR method has been developed to map the chemical concentration profiles

[5] J. W. Rathke, R. J. Klingler, R. E. Gerald, K. W. Kramarz, and K. Woelk, *Prog. Nucl. Magn. Reson. Spectrosc.* **30**, 209 (1997).

within the electrical conduction layer of a metal electrode.[6] Together, these *in situ* spectroscopic methods are capable of resolving structure, phase composition, mobility, redox chemistry, and spatial distribution of electroactive species located on, within, and adjacent to the electrodes in a variety of electrochemical devices. The toroid cavity imager has been used to follow the electrolyte depletion zones that form adjacent to the electrodes in lithium-polymer battery materials.[7] In addition, the method has been used to follow lithium intercalation into carbon electrode materials that are under development for use in lithium-ion batteries.[8]

Recently, we have demonstrated a new method of collecting images that provides a substantial improvement in the data acquisition time. For example, a typical ^{19}F profile using the original rotating-frame-imaging (RFI) technique requires several hours. It is a repetitive process that involves recording the NMR response under conditions of varying transmitter irradiation times. Our new data collection method is able to follow fast (millisecond) kinetic processes that occur on or near the working electrode by rapidly collecting repetitive images. Significantly, this method achieves the same distance resolution, 2 μm, as the original RFI method.

Figure IV-3 depicts an ^{19}F spin-labeled sample of polymer electrolyte (CF_3SO_3Li/polyethylene oxide) that was collected by the standard procedure and the new technique. This comparison illustrates the time advantage of the new technique without loss of resolution. Spin-labeled grids of the type in Fig. IV-3 are used to measure diffusion coefficients and to follow the motion of ions under the influence of an applied electric field. In Fig. IV-3, the regions of space where the ^{19}F nuclei have been labeled to contain an excess of the α spin state exhibit positive values of magnetization, while regions of space with an excess of β spin have negative values of the observed magnetization. Diffusion of the $CF_3SO_3^-$ anion intermixes these spin-labeled ^{19}F nuclei, causing the net magnetization to approach zero. Quantitative analysis of the oscillations in Fig. IV-3 as a function of the evolution time between when the spin-labeled grid is produced and the time when the image is taken yields the self-diffusion coefficients for the mobile species involved.

Future effort will focus on exploring the application of the new method in probing the dynamics of polymer-electrolyte battery materials. We have found that the ^{19}F longitudinal spin-relaxation time for CF_3SO_3Li varies in response to the salt concentration within the electrolyte depletion zones that form next to the cathode.[7] These measurements of NMR spin relaxation time will be extended by use of the new method. This new method makes it possible to probe for changes in the ion solvation sphere on the millisecond time scale following the passage of current. In addition, we will extend the range of electrolytes under study. We have started working with the imide salt $LiN(SO_2CF_3)_2$ and have some promising composite electrolyte materials that are available to us from various sources. Other work involves investigation of lithium insertion electrodes. The ^7Li NMR Knight shift is a useful probe of the lithium binding sites within these

---

[6] R. E. Gerald, R. J. Klingler, J. W. Rathke, and L. H. Nuñez, *The Chemist* **76**, 45-50 (1999).

[7] R. E. Gerald, R. J. Klingler, J. W. Rathke, G. Sandí, and K. Woelk, "In Situ Imaging of Charge Carriers in an Electrochemical Cell," in *Spatially Resolved Magnetic Resonance*, Eds., P. Blümler et al., Wiley-VCH, Weinheim, pp. 103-110 (1998).

[8] G. Sandí, R. E. Gerald, L. G. Scanlon, K. A. Carrado, and R. E. Winnans, *Mater. Res. Soc. Symp. Proc.* **496**, 95-101 (1998).

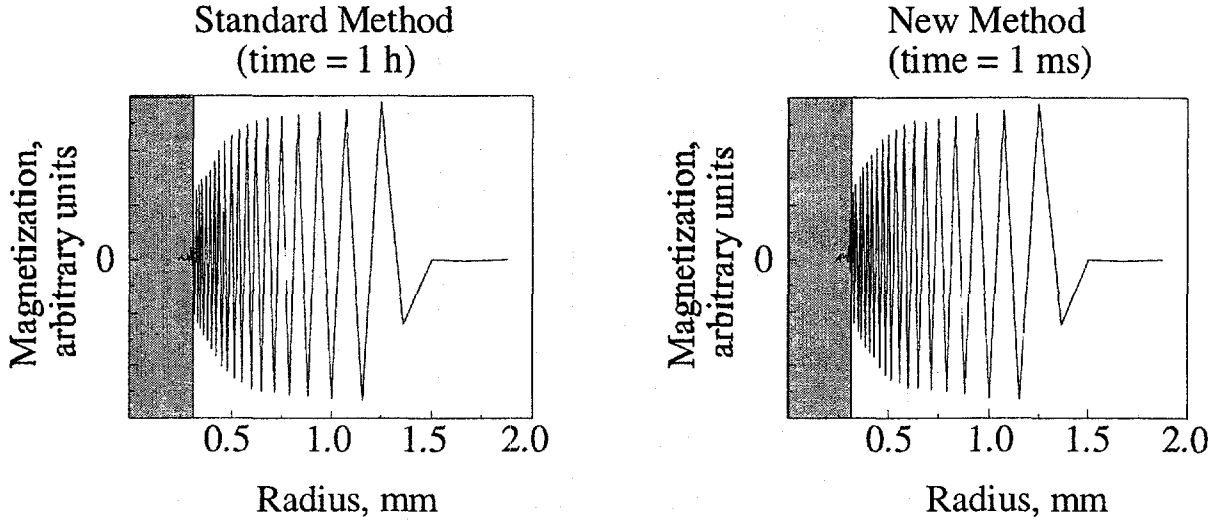

Fig. IV-3. Profiles for ^{19}F z-Magnetization Grid in CF_3SO_3Li/Polyethylene Oxide Obtained by Different NMR Imaging Methods

materials. In addition, we will extend earlier studies[9] to better define the factors that influence lithium dendrite formation. We are also interested in defining the location and chemical composition of any irreversibly bound lithium in the carbonaceous materials.

B. Heterogeneous Catalysis

The heterogeneous catalysis research is aimed at understanding the fundamental chemistry of solid catalyst systems. Systems being investigated are of fundamental interest to the petroleum, chemical, and transportation industries. Special emphasis is being placed on developing new tools (such as synchrotron X-ray techniques) for analyzing catalysts *in situ* under realistic conditions (temperature, pressure, and feed composition).

1. Selective Desulfurization of Diesel Fuel

Because the sulfur content of crude oil is rising as oil quality declines, refiners need more robust, higher-activity catalysts for hydrodesulfurization (HDS). Past work (at Argonne and elsewhere) in HDS catalysis has concentrated on single aspects, such as activity or selectivity. Current CMT projects seek to optimize all aspects of the catalyst, including active-phase type and synthesis, support porosity, and so on, while also gaining a fundamental understanding of the oil to be processed. This work is being done under a cooperative R&D agreement with UOP (Des Plaines, Illinois).

The pore size of the catalyst is being investigated in experiments using unique materials to support the active phase. Mesoporous clays and molecular sieves are custom-synthesized with pores that more closely match the molecular diameters of the feed molecules as determined by neutron

[9] R. E. Gerald II, R. J. Klingler, G. Sandí, C. Johnson, Lawrence Scanlon, and J. W. Rathke, to be published in *J. Power Sources*.

scattering.[10] Catalysts containing pores approximately 50% larger than the feed molecules (Fig. IV-4) have been shown to have improved catalyst performance when compared to catalysts with pores that are either significantly larger or smaller. The focus of our current work is on optimization of these mesoporous materials.

Two types of synthetic mesoporous materials were investigated as size-selective supports for HDS catalysts. In the first, mesoporous synthetic clays (MSCs) were synthesized in the presence of a neutral polymer, polyvinyl-pyrrolidone (PVP), to systematically vary the pore size (in the mesoporous range of 40-100 Å). The second material, MCM-41 (Mobil crystalline material), is a new family of mesoporous molecular sieves patented in the early 1990s.[11,12] This material has a uniform, one-dimensional hexagonal pore structure in the range of 20-100 Å. Both materials have very uniform pore size distributions and show great promise as a catalyst support for HDS purposes.

To simulate the heavy oil feed, dibenzothiophene (DBT) in hexadecane (0.75 wt% S) was used as liquid feed for HDS tests. The reaction was carried out at 300-400°C and 400 psi (27 atm) with 0.5-g catalyst diluted with a low-surface-area alumina. The liquid feed was preheated at 350°C and combined with a gas mixture of H_2/N_2.

Figure IV-5 shows that metal loading affects the DBT conversion of MCM-41 supported catalysts at 400°C. When normalized to the total metal content, the HDS activities decrease

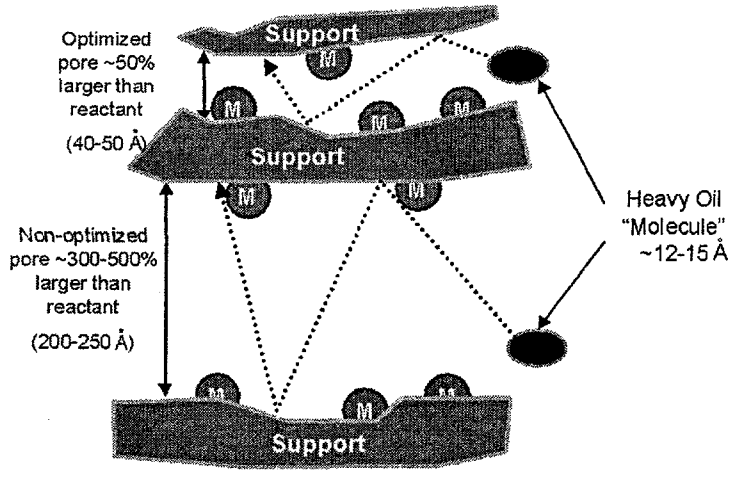

Fig. IV-4. Schematic of Optimized Pore (top) versus Oversized Pore (bottom) for Processing Heavy Oil. The "M" species represent the active metals located on the surface of the catalyst.

[10]P. Thiyagarajan, J. E. Hunt, R. E. Winans, K. B. Anderson, and J. T. Miller, *Energy & Fuels* **9**, 829-833 (1995).

[11]C. T. Krege, M. E. Leonowicz, W. J. Roth, J. C. Vartuli, and J. S. Beck, *Nature* **359**, 710 (1992).

[12]J. S. Beck, J. C. Vartuli, W. J. Roth, M. E. Leonowicz, C. T. Kresge, K. D. Schmitt, C. T-W. Chu, D. H. Olson, E. W. Sheppard, S. B. McCullen, J. B. Higgins, and J. L. Schlenker, *J. Am. Chem. Soc.* **114**, 10834 (1992).

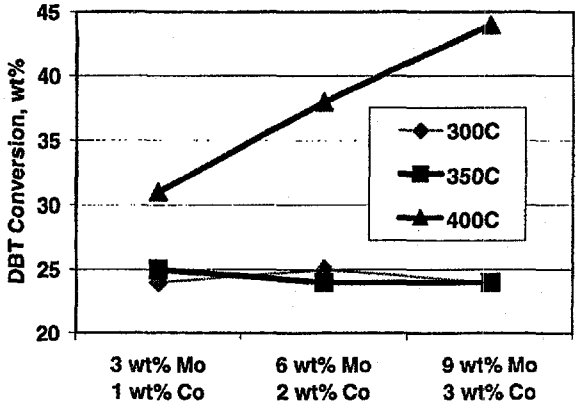

Fig. IV-5.

Effect of Metal Loading and Temperature on HDS Activity of the MCM-41 Supported Catalyst

monotonically with increasing metal loading. This finding suggests that higher metal loadings resulted in a lower metal dispersion. However, a higher dispersion may lead to a higher hydrogenation rate because of a higher percentage of so-called "rim sites."[13] This may explain why the catalyst with a medium metal loading (6 wt% Mo and 2 wt% Co) showed the highest selectivity. The constant activity with metal loading at 300°C and 350°C (Fig. IV-5) indicates that activity at these temperatures is controlled by internal sites; large molecules such as DBT apparently have difficulty diffusing into and reaching the active sites within the MCM-41 channels. Therefore, catalysts having varied Al/Si ratios were prepared with the medium metal loading.

While increasing the Al/Si ratio of the MCM-41 catalysts improved metal dispersion, it was found to have another effect on HDS performance. The HDS activity at 400°C increased with increasing aluminum content (to a maximum at Al/Si ≈ 0.02) and then decreased. This suggests that increasing amounts of aluminum may create more sites for anchoring the Co-Mo-S within the MCM-41 framework. Increasing the Al/Si ratio, however, decreases the HDS selectivity. The selectivity loss is probably due to an increase in acidity, which shifts the reaction network from HDS to hydrocracking. Titration of the acid sites on the surface has been shown to minimize this problem.

Mesoporous synthetic clays were obtained when polymer-containing silicate gels were hydrothermally crystallized to form layered magnesium silicate hectorite clays containing polymers that were incorporated *in situ.*[14] With this *in situ* technique, we achieved interlayer intercalation of polyvinyl-pyrrolidone (PVP) of several average molecular weights. The molecular weight of the PVP was varied from 10,000 to 1.3×10^6, with polymer loadings varying from 10 to 20 wt%. The PVP was removed from synthetic polymer-clay complexes via calcination. The active components (Mo, Co) were separately loaded by incipient wetness impregnation using $(NH_4)_6Mo_7O_{24}$ (6 wt% Mo) and $Co(NO_3)_2$ (2 wt% Co), followed by recalcination at 500°C in air. Pore diameter, surface areas, and pore volumes of the resulting catalysts were then measured (Table IV-1). The physisorption data indicated a very narrow pore-size distribution, which is correlated to both the PVP molecular weight and polymer loading.

[13] M. Daage and R. R. Chianelli, *J. Catal.* **149**, 414 (1994).

[14] K. A. Carrado, C. L. Marshall, J. R. Brenner, and K. Song, *Micropor. Mesopor. Mater.* **20**, 17 (1998).

Table IV-1. Physical Properties of Mesoporous Synthetic Clay Catalysts

Catalyst	PVP Molec. Wt.	PVP Loading, %	Surface Area, m^2/g	Pore Volume, cm^3/g	Pore Diameter, Å
MSC1	10^4	10	250	0.37	42
MSC2	5.5×10^4	20	217	0.40	58
MSC3	3.6×10^5	10	233	0.46	74
MSC4	1.3×10^6	10	227	0.54	91

The pore diameter of the tailored clay catalysts was found to have a strong effect on both the HDS activity and selectivity (Fig. IV-6). An increasing pore diameter led to a nearly linear increase of activity and a boost of biphenyl selectivity. This finding may indicate that the internal diffusion of large molecules, such as DBT, still plays a critical role in the HDS reaction. The higher selectivity was achieved in large pores because such pores make it easier for biphenyl to diffuse out of the pores and prevent it from further hydrogenation and hydrocracking.

Temperature programmed reduction (TPR) can provide information on the reducibility of surface species. It often correlates with the performance of the catalysts. In the current case, TPR was done with the catalysts from HDS reaction by measuring the hydrogen consumption. The TPR spectrum mainly consisted of two major peaks centered in the range of 250-375°C and 300-650°C. The nonstoichiometric sulfur species on the surface may have led to the TPR peaks, since the removal of the stoichiometric sulfur species in the bulk material usually occurs at temperatures above 600°C. The TPR peak temperature correlated well with the yield of biphenyl. We found that surface sulfur species, which are easier to react, or equivalently, the metal sites, which are easier to be reduced, result in higher biphenyl yield.

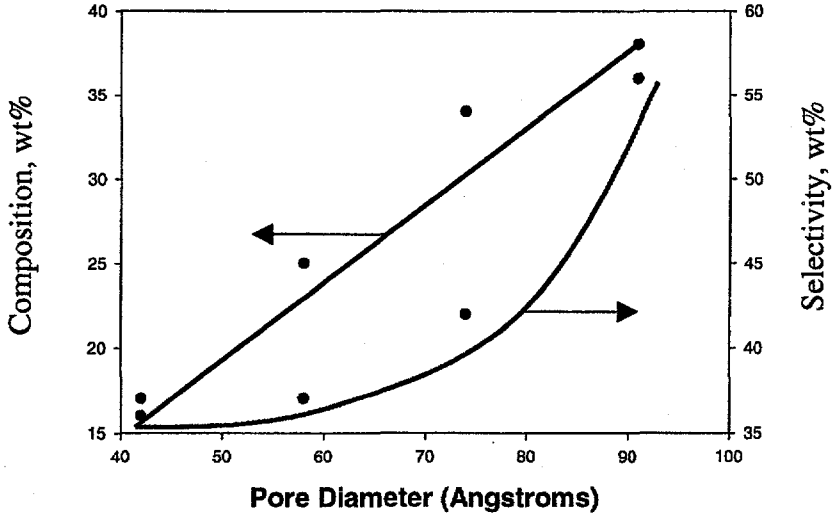

Fig. IV-6. Activity and Selectivity of HDS Catalysts Based on Mesoporous Clays

Future work will examine these new mesoporous materials for catalysts using "real" heavy oil feeds. In a short-term project in collaboration with Conoco Oil, we will investigate whether the encouraging findings for the test probe molecule (DBT) translate into improved HDS activity for real heavy oil feed.

2. Etherification of Synfuel-Derived Phenolics

We have prepared and evaluated heterogeneous catalysts with the goal of promoting the etherification of synfuel-derived phenolics to form aryl alkyl ethers that can serve as oxygenates for blending with diesel fuels. At the same time, it is necessary to avoid promoting alkylation reactions that result in the attachment of methyl or ethyl groups to the phenolics that yet retain their functionality. This work was undertaken considering that (1) distillate fractions derived from synfuel sources contain high levels of phenolics (up to 20 wt%), (2) the removal of phenolics by existing routes such as hydrotreating consumes large quantities of hydrogen, and (3) phenolics are unstable when present in fuels.

Experiments have been completed by etherification of model reactants (phenol with either methanol or ethanol) with a number of active catalysts. The most active catalyst consists of sulfated $KMnO_4$ on γ-Al_2O_3. We have found it to be effective for etherification at reaction temperatures in the range of about 230 to 315°C. Along with increased conversion with increasing reaction temperatures, there is an accompanying decreased selectivity that leads to products with higher phenolic content. At higher temperatures, there is also a reaction of the light alcohols to form byproduct dimethyl and diethyl ethers. Sulfated γ-Al_2O_3 catalyst is also active for the primary reactions, but the generation of light ethers is excessive.

Methanol is preferred over ethanol as the light reactant alcohol. Reaction selectivity in forming aryl alkyl ethers vs. higher molecular weight phenolics is much higher. However, there is a balance in that the formation of light ethers is also greater. In a commercial facility, the light ethers would be recycled, thereby solving the yield problem.

A final report is being prepared, and the program likely will be closed out upon its completion. A series of runs with coal-derived liquids is planned as an extension of the above experiments. However, this work depends upon the results of a short evaluation of an analytical system using ^{17}O NMR. The liquids for the experiments have been obtained from the sub-bituminous coal pyrolysis demonstration plant of the TEK-KOL Partnership (Gillette, WY).

3. Selective Oxidation of Benzene to Phenol

Catalytic chemical synthesis accounts for 60% of today's chemical products and 90% of the current chemical processes. Given this dominance, catalytic oxidation has been targeted by the strategic plan for the U.S. chemical industry, "Technology Vision 2020," as one of the most significant areas for continued development. The goal of this project is to investigate a new one-step

process for the selective oxidation of benzene or toluene to phenol by using a heterogeneous catalyst and molecular oxygen:

$$C_6H_6 + ½\ O_2 \rightarrow C_6H_5OH \quad (8)$$

If successful, this one-step process would require much less energy and produce fewer wastes than the conventional process. The work has been done as part of a cooperative research and development agreement (CRADA) with Akzo Nobel Chemical, Inc., and Northwestern University. As of June 1999, Akzo Nobel Chemical has withdrawn from the CRADA, and we are negotiating with several companies as replacement partners.

This project is still in an early stage of development, and while concurrent effort in the two areas is an important focus, most of the emphasis to date has been on catalyst synthesis and testing. The starting points for catalyst testing have come from a review of the literature. Northwestern has started with a binary catalytic system to oxidize toluene to benzoic acid and then to phenol, and Argonne is testing a catalytic system that uses HNO_3 for the direct oxidation of benzene to phenol.

Experiments at Northwestern began with the second, more difficult step of transforming benzoic acid to phenol. The performance of the catalysts reported in the literature (NiO-Fe_2O_3, NiO-Fe_2O_3, 1% Na_2O/NiO-Fe_2O_3, 3% $V_2O_5/Na_2O/NiO$-Fe_2O_3, and V_2O_5-K_2SO_4/TiO_2-Na_2O/NiO-Fe_2O_3) has been verified, although the reported phenol yield of 93% was not attained. Next, V_2O_5 was added to the nickel catalyst in order to aid the oxidation of the nickel oxide species. It was found that conversion increased with temperature up to 400°C. When MoO_3 was added to $NiVO_4$, selectivity increased, while conversion decreased. This catalyst was active up to 500°C.

The primary focus of work at Argonne has been the catalytic oxidation of benzene by using nitric acid as the oxygen source. The catalysts were MoO_3, V_2O_5, and MoO_3/V_2O_5 supported on silica. While these catalysts do show activity for benzene oxidation, we are getting a lower yield and more byproducts than indicated in the literature.[15,16]

Along with the MoO_3 and V_2O_5 systems, other classes of catalysts are being evaluated for catalytic activity. These include layered double hydroxides, polyoxmetalates, zeolites, and zeolitic materials. In addition to the catalytic tests, these catalysts are being characterized by appropriate methods such as TPR/desorption, X-ray diffraction, surface area measurement, infrared spectroscopy (IR), and ultraviolet/visible spectroscopy to elucidate structure/reactivity relationships.

When promising catalysts are identified, they will be optimized in conjunction with information gathered from the characterization tasks, which will correlate the chemical characteristics of the catalyst with catalyst activity and selectivity. The characterization will include X-ray absorption spectroscopy, *in situ* diffuse reflectance IR Fourier transform spectroscopy, and ^{13}C NMR. We will also use TPR conditions to study the ease of oxidation and reduction of the catalytic systems. A cell for *in situ* extended X-ray absorption fine structure analysis has been designed to study the metal atom valence and local structure of the catalyst at Argonne's Advanced Photon

[15]J. S. Yoo, A. R. Sohail, S. S. Grimmer, and J. Z. Shyu, *Applied Catal. A* **117**, 1 (1994).

[16]F. Matsuda and T. Kato, Japanese Patents 61-236738 and 62-67038 (1985).

Source. Computational chemistry using state-of-the-art quantum chemical techniques will be used for modeling the mechanisms of the catalytic reactions. Optimization steps will likely include varying the ion-exchange method and degree, and varying the catalyst pretreatment. Finally, scaleup and pilot-plant testing of the most promising catalysts will be undertaken.

C. Energy and Environmental Research

This aspect of the CMT basic chemistry studies involves fundamental studies that are relevant to new electric power technologies and new decommissioning/decontamination strategies for nuclear facilities—two subjects of forefront interest to DOE. The specific research topics relate to improvements in the performance of high-temperature ceramic superconductors and the detailed characterization of surfaces contaminated with radionuclides.

1. *High Temperature Superconductivity*

The research program on high-critical-temperature superconductivity (HTS) is directed primarily at the study of phase evolution and microstructure development in silver-sheathed $(Bi,Pb)_2Sr_2Ca_2Cu_3O_x$ (Ag/Bi-2223) composite conductors. This research is carried out in close collaboration with American Superconductor (ASC)—a leading manufacturer of HTS products. The conventional technology that has evolved for producing Ag/Bi-2223 composite conductor involves heat treatment of an oxide powder precursor (composed of Bi-2212 and second phases) that reacts to form Bi-2223 in a pre-drawn and rolled silver sheath. During the past year, we investigated a new approach to the formation of Ag/Bi-2223 based on the decomposition and subsequent reformation of a fine-grained, fully reacted Bi-2223 precursor in silver-sheathed form. The purpose of this study was to explore the prospects for growing textured, large-grain-size Bi-2223 from the pre-converted precursor.

The monofilamentary composite tape employed in this research was formed by standard oxide-powder-in-tube (OPIT) methods for drawing and rolling. The precursor powder had the nominal composition $Bi_{1.7}Pb_{0.3}Sr_{1.9}Ca_{2.0}Cu_{3.0}O_y$ and was composed primarily (>95%) of fine-grained Bi-2223 mixed with small amounts of residual Bi-2212 and alkaline earth cuprates. Samples (about 2.5 cm long) were heated at either 10 or 100°C/min to an initial processing temperature of 825°C under an oxygen partial pressure of 0.075 atm. Following an initial 3000-min hold at 825°C in 0.075 atm O_2 to equilibrate the pre-existing Bi-2223 phase with respect to other residual phases, temperature excursions (downward and upward) were programmed into the anneal cycle. Oxygen pressure transients to lower partial pressures during annealing at 825°C were also studied. Samples were either quenched or furnace cooled at selected times during each heat treatment and at the end of the heat treatment, then characterized with scanning electron microscopy (SEM), energy dispersive X-ray analysis, and X-ray diffraction.

Figure IV-7 shows an SEM micrograph of the transverse cross section of a sample annealed for 6000 min in 0.075 atm O_2 at 825°C and furnace cooled. The micrograph shows that layered phase grain growth is essentially nonexistent under these conditions, which are standard for processing conventional Bi-2223 precursors by the OPIT method and which yield Bi-2223 with the extended grain colony microstructure that is required for achieving high critical current. This result, we

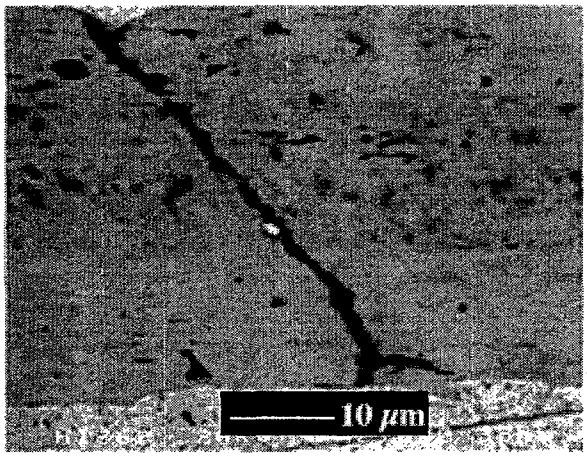

Fig. IV-7.

Micrograph in SEM Backscatter Mode of Transverse Section of Monofilament Sample. Annealed for 6000 min at 825°C in 0.075 atm O_2.

believe, is due to the fact that during normal OPIT processing of a tape with Bi-2223 as the major phase to begin with, no liquid phase is formed during heat treatment to facilitate grain growth. Also, transverse cracks (like the one shown in Fig. IV-7) tend to form during the deformation processing prior to heat treatment and cannot be healed due to the persistent absence of a liquid phase.

Figure IV-8 shows an SEM micrograph of a sample annealed using a cycle that featured a 20-min excursion to 855°C followed by a 3000-min recovery treatment at 825°C. It is evident from the micrograph that layered phase grain growth does occur under these conditions. Also, no cracks are visible in the sample. Apparently, all cracks formed during the deformation processing had been healed, most probably due to the presence of a liquid phase. X-ray diffraction showed that the sample is 80% Bi-2223, 16% Bi-2212, and approximately 4% Bi-2201. These results demonstrate the ability to produce Bi-2223 having an extended grain colony microstructure in a silver sheath by a processing route that involves Bi-2223 decomposition/reformation. This new approach offers the possibility of improving the critical current and flux pinning in Ag/Bi-2223 composite conductors.

Efforts during this study to investigate reduced temperature dips in the heat treatment cycle produced no discernable evidence of a change in the Bi-2223 microstructure. Also, attempts to use longer excursion periods to 855°C resulted in substantial decomposition of the Bi-2223 phase (>80%) with concomitant formation of large second phases that could not be reformed by post-annealing at 825°C in 0.075 atm O_2. Some efforts were also made to manipulate the microstructure

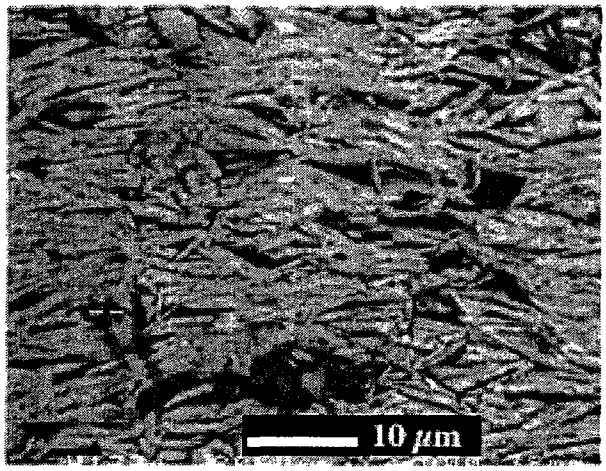

Fig. IV-8.

Micrograph in SEM Backscatter Mode of a Transverse Section of a Heat-Treated Sample. Heat treatment consisted of 3000 min at 825°C in 0.075 atm O_2 followed by a 20-min temperature ramp to 855°C, a 20-min hold at 855°C, a 20-min ramp back to 825°C, and another 3000 min at 825°C in 0.075 atm O_2.

via an anneal using oxygen partial pressures as low as 0.002 atm; however, these manipulations led to results similar to the extended high temperature excursions, namely, substantial decomposition of the Bi-2223 phase (over 80%), which could not be recovered to any significant extent by post-annealing.

Current work on HTS systems is directed at developing new heat-treatment strategies for dissipating the nonsuperconducting second phases that tend to block supercurrent pathways and cause damage to the Bi-2223 grains during the intermediate deformation steps of the OPIT process. The goal is to reduce second-phase particles to the submicron range, where they will actually augment flux pinning but be too small to cause other deleterious effects.

2. *Environmental Management Science*

The objective of this research program is to elucidate the structure of radioactive and heavy metal ion contaminants incorporated into surface films of metals and alloys. Fundamental knowledge obtained from the study will be used for the development of processes and techniques for decontaminating storage tanks, piping systems, equipment, etc., in DOE nuclear facilities, as well as in other environmental remediation programs. We employ electrochemical techniques to simulate the formation of oxide films on metals and *in situ* spectroscopic techniques for their structural characterization. The latter consisted mainly of X-ray absorption spectroscopy (XAS) coupled with X-ray absorption near edge structure (XANES) and extended X-ray absorption fine structure (EXAFS) analysis methods.

During the past year, we studied the incorporation of U and Fe into nickel hydroxide films electrodeposited on graphite substrates, as well as the structure of $Fe(OH)_2$ and Fe(VI). Uranium was found to co-deposit with $Ni(OH)_2$ from nitrate solution as U(VI), without incorporation into lattice sites. This result is not unreasonable because of the large size of the U(VI) ion. In contrast, iron was found to substitute for nickel in lattice vacancies as Fe(III) and to be further oxidized to Fe(IV) upon anodic oxidation of the nickel hydroxide film to γ-NiOOH. Structural parameters for the $Ni(OH)_2$ have been obtained from fitting the EXAFS data. The XAS of $Fe(OH)_2$ has also been obtained, and structural parameters have been derived for the first time. This finding is of importance since $Fe(OH)_2$ is believed to be the precursor to the passive film on iron and is therefore of great interest in the field of aqueous corrosion.

Also investigated was the electrochemical formation of Fe(VI) in highly alkaline solutions. Anodic oxidation of an iron wire in 14 M NaOH resulted in a purple solution due to dissolved Fe(VI) species. The XANES spectrum of the frozen solution at liquid nitrogen temperature is shown in Fig. IV-9 (curve a). The spectrum of the solution after about 24 hours also appears in Fig. IV-9 (curve b). It is essentially that of Fe(III), and indicates the chemical reduction of Fe(VI) by impurities in the solution. These results are of significance not only in environmental remediation but also in more recent attempts to develop electric-vehicle batteries based on a cheap electrode material like iron.

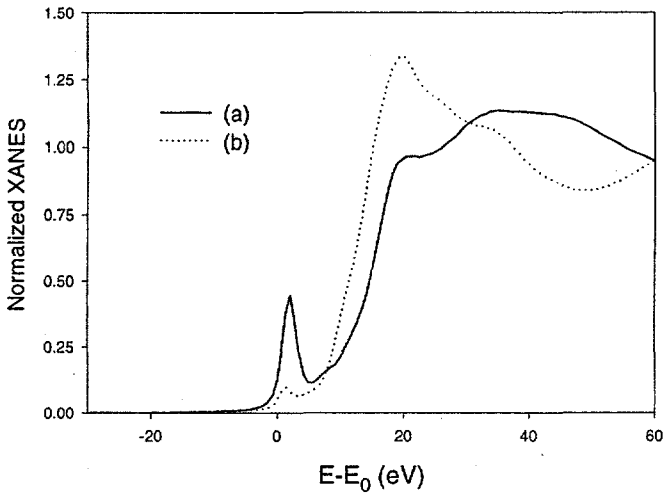

Fig. IV-9. Plots Obtained from XANES at the K-Edge of Fe(VI) in NaOH Solution. Curve a is for frozen solution at liquid nitrogen temperatures, and curve b is for the same solution after 24 hours at 25°C.

This project has now been completed, and a final report has been submitted to DOE, along with recommendations for applications and for further research. Based on knowledge gained from the present studies, principles and methods for decontamination have become apparent. Radionuclides and heavy metal ion contaminants sorbed on oxide surfaces or coprecipitated may be removed by acid wash or by selective dissolution and/or complexation. Ions incorporated into lattice sites and interlamellar layers will require more drastic cleaning procedures. Electropolishing and the use of an "electrochemical brush" are among the procedures that should be considered seriously for the latter cases. The incorporation of radionuclides into the structure of highly defective, insoluble oxides and clays should be considered for long-term storage and disposal.

V

Analytical Chemistry Laboratory

A. Introduction

The Analytical Chemistry Laboratory (ACL) operates in the Argonne system as a full-cost-recovery service center, but it has a mission that includes a complementary research and development component in analytical chemistry and its applications. Because of the diversity of research and development work at ANL, the ACL handles a wide range of analytical problems in its technical support role. Some routine or standard analyses are done, but the ACL usually works with commercial laboratories if high-volume, production analyses are required by its clients. It is common for the Argonne R&D programs to generate unique problems that require significant development of methods and adaptation of techniques to obtain useful analytical data. Thus, much of the support work done by the ACL is very similar to applied research in analytical chemistry.

The ACL is administratively within CMT, its principal ANL client, but it provides technical support for many of the other technical divisions and programs at ANL. The ACL has three groups—Chemical Analysis, Instrumental Analysis, and Organic Analysis, which together include about 20 staff members. Talents and interests of staff members cross group lines, as do many projects within the ACL. The ACL receives about 1000 jobs annually—many of which involve several samples.

The Chemical Analysis Group uses wet-chemical and instrumental methods for elemental, compositional, and isotopic determinations in solid, liquid, and gaseous samples and provides specialized analytical services. The Instrumental Analysis Group uses nuclear counting techniques to determine the radiochemical constituents in a wide range of sample types, from environmental samples with low radioactivity to samples with high radioactivity that require containment. The Organic Analysis Group uses a number of complementary techniques to separate organic compounds and measure them at trace levels and has performed development work in sensors, chemometrics, and detectors.

B. Technical Highlights

The ACL provides analytical chemistry support to CMT, other ANL divisions and programs, other DOE sites, DOE's Chicago Operations Office, and DOE Headquarters. In addition, ACL conducts research and development programs funded by DOE and other sponsors. Selected accomplishments for 1999 are summarized here. In addition, the ACL did analytical work on other projects, many of which are described in more detail elsewhere.[1]

1. Support for Pyrochemical Process Development

The CMT efforts in developing a pyrochemical process for separating actinides from spent nuclear fuel included experiments using Li-Al alloys as reductants for UCl_3, $PuCl_3$, and select rare earth chlorides in molten LiCl-KCl electrolyte. In these tests, lithium, either pure or as an alloy of aluminum, was added to the electrolyte containing dissolved UCl_3, $PuCl_3$, and rare earth chlorides (Ce, La, Pr, Nd, Sm, Eu, and Y). The ACL prepared and analyzed samples taken periodically during these experiments. After the samples had been dissolved, we determined their U, Pu, and rare earth element concentrations using inductively coupled plasma-atomic emission spectroscopy (ICP-AES) and inductively coupled plasma-mass spectrometry (ICP-MS). Data from these analyses confirmed thermodynamic expectations that the concentration of these chlorides can be decreased by the pyrochemical process to very low levels. Of particular interest was the finding that both $EuCl_3$ and $SmCl_3$ were reduced to the metal, and that the $PuCl_3$ and UCl_3 were reduced to low concentrations; thus, a salt waste that is "non-transuranic" can be obtained by the pyrochemical process. Analytical results appear in Sec. III.C.2.

2. Measurement of Lithium Metal Dissolved in Molten Salt

A process being developed by CMT staff (Sec. III.C.1) uses lithium at 650°C in the presence of LiCl to reduce actinide oxides to the corresponding metals, producing Li_2O. In support of this project, the ACL contributed to the measurement of the solubility of lithium metal in LiCl/Li_2O molten salts. Salt samples withdrawn from a molten salt bath as its composition was varied were reacted with water in a special apparatus designed to permit the collection and precise measurement of hydrogen gas evolved when the lithium metal reacts with water. Sensitivity was easily sufficient to measure the lithium metal concentrations at levels below 0.1 wt% in the salt. Precision of the measurements is estimated to be about 3%, relative. The results of these measurements are expected to provide fundamental properties data that are not only applicable to the CMT reduction process, but also of general interest to pyrometallurgical process engineers, thermodynamicists, and other scientists.

3. Determination of Stibine Evolution from Lithium Antimonide

Researchers in CMT synthesized a batch of lithium antimonide, Li_3Sb, for use in experiments related to development of a high-throughput electrorefiner for treatment of spent

[1] D. W. Green, D. G. Graczyk, D. L. Bowers, and A. S. Boparai, *Analytical Chemistry Laboratory Progress Report for FY 1999*, Argonne National Laboratory Report ANL/ACL-99/2 (December 1999).

fuel (Sec. III.A). They were concerned about its potential to evolve stibine gas (SbH_3) during operations outside of the inert-atmosphere glovebox where it was made. Stibine is a poisonous gas that has a threshold limit value of 0.1 ppm (0.58 mg SbH_3 per m^3). Exposure to a concentration of 10 ppm can be fatal. The ACL was asked to determine whether stibine is produced when the Li_3Sb compound is exposed to moist air, water, or acid solution.

A gas analysis train in a fume hood was used to react the lithium such that any stibine released would be carried into a set of gas-washing bottles filled with an absorber solution composed of I_2 and KI in 3 N sulfuric acid (Holland's solution). Stibine was converted to a colored anion, SbI_4^-, that could be measured photometrically after the iodine in the solution was reduced with hypophosphite. No stibine (< 3 µg) was detected in these tests after exposing 1 g of Li_3Sb to moist air for over two hours, but when the 1 g Li_3Sb was contacted with liquid water, we recovered 1.76 mg of stibine. With 6 M hydrochloric acid, 1.23 mg SbH_3 was evolved. Results from these tests contributed to the operational safety review for work with the lithium antimonide material and helped to ensure that the material was handled with appropriate precautions.

4. Performance Demonstration Programs for the WIPP

The Waste Isolation Pilot Plant (WIPP) is a DOE installation designed to dispose of transuranic (TRU) waste left from the research and production of nuclear weapons. The WIPP site consists of large interconnecting cavities hollowed out of deep geologic salt beds approximately 600 m underground and is located in the vicinity of Carlsbad, New Mexico. The first shipment of waste for disposal was received at the WIPP site in March 1999.

Wastes to be shipped to WIPP must first be characterized to identify the presence of any hazardous materials in the waste besides the radioactive ones. As part of the WIPP TRU Waste Characterization Program, a Performance Demonstration Program (PDP) was established in 1995. The purpose of this PDP is to test laboratory performance for the analysis of solidified TRU waste samples for specified metal, semivolatile and volatile organic compounds, and polychlorinated biphenyls. During 1999 the ACL prepared approximately 2 kg each of uncemented and cemented samples of simulated solidified waste. The waste matrix was then supplied to a WIPP contractor to be spiked with metal analytes.

In addition, headspace gas from wastes destined for WIPP must be characterized to identify nonradioactive hazardous materials. The National TRU Program Office of the Carlsbad Area Office of DOE has established a PDP for laboratories that will participate in the analysis of headspace gas to be shipped to the WIPP site. The ACL prepares, analyzes, and distributes samples for the headspace-gas PDP.

During 1999, the ACL prepared 11 sets of headspace-gas PDP samples for Cycle 13 of this program. Nine sets were sent to participating laboratories, one set was used for verification analysis, and one set was archived. Each set of PDP samples consisted of 6-L SUMMA canisters containing low, high, special, and duplicate mixtures of analytes.

5. National Analytical Management Program

The ACL has been developing and implementing the Integrated Performance Evaluation Program (IPEP) for DOE's National Analytical Management Program (NAMP). The IPEP database provides information on the quality of data being produced by all analytical chemistry laboratories that provide DOE and its contractors with data on environmental restoration and waste management samples. We have been collecting performance data from the Water Supply (WS) and Water Pollution (WP) studies of the Environmental Protection Agency (EPA), the Quality Assessment Program of the DOE Environmental Measurements Laboratory, and the Mixed Analyte Performance Evaluation Program of the DOE Radiological and Environmental Sciences Laboratory. In 1999 we accumulated new data from the performance-evaluation programs and produced reports on laboratory performance. As the EPA continues its privatization of the WS and WP studies, the IPEP staff has maintained contact with the EPA (National Exposure Research Laboratory in Cincinnati) to ensure a smooth transition and continued access to the performance-evaluation information needed by the IPEP.

In 1999, three databases were transferred from other DOE sites to ANL: the DOE Procedures Database, which was used to produce a World Wide Web document called "DOE Methods for Evaluating Environmental and Waste Management Samples (DOE Methods Compendium)"; the National Sample Tracking System (NSTS); and the Directory of EM Sampling and Analysis Resources (DEMSAR). The transfer of these databases was done to consolidate and streamline the gathering of information required for IPEP reports and other projects within NAMP. During 1999, we merged and restructured the DEMSAR and NSTS databases and linked them to the existing IPEP database.

6. Preparation of Osmium Targets for Photon Excitation Studies

In collaboration with a researcher from the ANL Physics Division, the ACL prepared an osmium target for photon excitation studies by electroplating osmium metal onto a copper backing. The resulting metal planchet was then used as a target for photon excitation studies in which the high flux of protons from the ANL Advanced Photon Source (APS) would excite osmium nuclei by a process entailing nuclear excitation by electronic transition.

In previous work, osmium targets were produced by dissolving osmium tetraoxide (OsO_4) in a plating solution containing sodium hydroxide, sodium monohydrogen phosphate, sulfamic acid, and potassium hydroxide. In 1999, we were requested to produce ^{189}Os isotope targets from 100 mg of metallic ^{189}Os powder rather than osmium oxide. To ensure the successful conversion of this limited amount of ^{189}Os metal into osmium tetraoxide, a separate experiment was carried out successfully with "natural" metallic osmium in which the metal was heated in the presence of oxygen. The resultant ^{189}Os electroplated targets were used in APS to generate useful data.

Additional experiments were designed where ^{189}Os was electroplated on both sides of a much thinner copper. This new experiment is expected to improve experimental sensitivity by a factor of 10 to 15.

7. Radiological Analysis Support for U.S. EPA Region V

Since 1994, the EPA and ACL have participated in an interagency agreement intended to provide EPA Region V with special analytical services for samples collected from that region. For the past two years, analytical effort has been principally focused on the mixed waste samples, which have been submitted as a part of EPA remediation focused on site cleanup. Numerous samples were received in 1999 for the determination of ^{226}Ra and ^{228}Ra. The samples were submitted as a continuation of remediation programs initiated earlier at three sites: Ottawa, Illinois; Benton Harbor, Michigan; and Lindsay Light in Chicago, Illinois.

Ottawa was the site of a company that applied luminescent paint containing ^{226}Ra to clock dials. Samples were taken from landfills used to hold waste removed from this site after its demolition, the area around the company building foundation, and the surrounding grounds. Ten water and 15 soil samples were submitted to the ACL for the determination of ^{226}Ra and ^{228}Ra by gamma spectroscopy and $^{235/238}$U and ^{232}Th by alpha spectroscopy. Benton Harbor Warehouse was the site of a privately owned facility used to store hundreds of World War II artifacts, which included airplane instrument panel gauges, switches, and compasses coated with luminescent paint containing ^{226}Ra. In previous work, material stored there was found to be contaminated with radium dust from deteriorating gauges. This year, a subsequent investigation of the grounds surrounding the demolished buildings resulted in 26 water and 67 soil samples being analyzed by the ACL for $^{226/228}$Ra and ^{226}Ra, respectively. The Lindsay Light site was used to manufacture thorium lantern mantles in the Chicago downtown area. As part of its remediation plan, the ACL analyzed 25 soil samples by gamma spectroscopy, looking for ^{226}Ra "hot spots."

8. High-Precision Assay of Lithium and Aluminum

The ACL has implemented a novel methodology developed at the National Institute of Standards and Technology (NIST) for the chemical analysis of lithium aluminate. It allows exceptionally precise measurements using ICP-AES by applying a drift-correction algorithm to compensate for long-term noise in a series of internal-standard-corrected measurements. This approach has been used by NIST to measure the lithium and aluminum content of lithium aluminate ceramics and offers considerable advantages compared to the classical methods currently used (isotope dilution for determining lithium and gravimetric analysis for aluminum). The ACL is seeking to demonstrate that the NIST approach can be established in other laboratories where reasonably good analytical skills exist and to transform the NIST approach into a standard operating procedure that can be qualified and transferred to private sector laboratories for lithium and aluminum assay of production-lot ceramics.

Earlier work in the ACL showed that the method provided excellent precision (relative standard deviation, 0.1%) with our grating-polychromator instrument when standard solutions were analyzed. Later work with standards that contained lithium and aluminum in differing proportions and measurements with lithium aluminate materials of known composition showed bias in the measurements. This bias appears to have been overcome for aluminum by selecting appropriate ICP-AES operating conditions. With lithium, a more daunting problem arose from isotopic differences between samples and standards. This problem occurs because the grating polychromator achieves partial resolution of the isotopic emission wavelengths from ^{6}Li and ^{7}Li.

This effect may ultimately obviate the use of a grating system for lithium assay with the NIST approach. Using solutions prepared by microwave-accelerated acid dissolution, we achieved aluminum assays with a precision of a few tenths of a percent relative standard deviation and a relative bias smaller than 0.3%. These results indicate that the sample preparation and handling methodology established in the ACL is capable of meeting the goals of high precision and small bias for assay of the lithium aluminate major constituents, and that the currently available procedures and equipment will provide satisfactory aluminum assays. To apply the method to the lithium assay, instrumentation with array detection, comparable to that used by NIST in their measurements, appears to be required. Because the ICP-AES methodology shows such decided advantages over classical methods, we plan to continue work on the lithium assay in the coming year.

9. Assembled Chemical Weapons Assessment Program

The U.S. Army's Chemical Agent Munitions Disposal System, which is part of the Assembled Chemical Weapon Assessment Program, is evaluating alternative technologies to incineration for decommissioning and disposal of munitions containing chemical warfare agents. For agent GB (Sarin, or isopropyl methylphosphonofluoridate), the technologies under consideration all begin with chemical neutralization in which a strong caustic solution rapidly hydrolyses GB into various degradation products. The resulting solution of caustic and degraded GB is called "hydrolysate."

The Army is producing a large amount of hydrolysate at the Desert Chemical Depot (DCD) near Tooele, Utah, which is a major storage site for several chemical warfare agents. For the Army to provide hydrolysate samples to contractors, the GB concentration in the hydrolysate must be no higher than the Army's drinking water standard for GB of 20 μg/L. In collaboration with personnel of the ANL Energy Systems Division, the ACL provided on-site technical assistance in the analysis of hydrolysate. The work has involved both the adaptation of the Army's gas chromatography/mass spectrometry (GC/MS) method for determining GB in hydrosylate at the 20-ppb level and the preparation of an analytical laboratory. The sample preparation method has been streamlined to minimize exposure of the analysts to hydrosylates and to maximize recovery of unreacted GB. We have determined the method detection limits using GB hydrosylate provided by the Army for the liquid and solid components of the hydrosylate. After the method was validated, many field samples were analyzed for the presence of GB.

10. Multi-agency Radiochemistry Laboratory Analytical Procedures (MARLAP)

A manual is being prepared by the MARLAP Working Group to provide guidance in all relevant areas of radioanalytical laboratory work for laboratory personnel and project managers. In addition to DOE, the EPA, Department of Defense, and Nuclear Regulatory Commission are contributing to the MARLAP Working Group.

Because of our radiological expertise, the ACL was asked to provide technical support to the preparation of the MARLAP Manual. This support included writing significant sections of

the manual as well as reviewing the work of other authors. In 1998, members of the ACL authored two chapters: "Sample Dissolution, Separation Techniques" and "Evaluation of Radiological Laboratories." This past year, the ACL was asked to write the "Sample Preparation" chapter. Following interagency review, this manual should be published in FY 2001.

11. Quality Assurance Laboratory Support to the U.S. Army Corps of Engineers

In October 1997, the U.S. Army Corps of Engineers (USACE) assumed responsibility for the Formerly Utilized Sites Remedial Action Program (FUSRAP), which had been the responsibility of the DOE since 1974. The objectives of this program are to study and remediate sites having radioactive materials from DOE and its predecessors' operations, dating back in some cases to the Manhattan Project.

The Buffalo District of the USACE is responsible for several FUSRAP sites within their jurisdiction. The ACL serves the Buffalo District as a quality assurance laboratory for the analysis of ambient matrix samples (e.g., soil, sediment, ground, or surface water) from various remediation sites.

The ACL received 43 samples in 1999 from the Luckey, Ohio, site and an additional 18 samples from the Ashland 2 site in Tonawanda, New York. Both the sites are the object of remediation efforts requiring analytical data for making decisions. All organic and inorganic analytes were determined by existing procedures and methods described in the U.S. EPA laboratory manual "Test Methods for Evaluating Solid Waste, Physical/Chemical Methods" (SW-846) in accordance with instructions from the USACE. Radiological measurements were carried out according to U.S. EPA methods and established ANL methods and procedures.

In 1998, the ACL received samples through the Baltimore District of the USACE from the Colonie, New York, site; those analyses were completed in early 1999. Our data for this site helped the Baltimore District ensure the quality of the data received from the production analytical laboratories.

12. Characterization of Unidentified Waste Materials

Many ANL facilities have unidentified waste materials that have unknown origins or inadequate documentation or that remain from programs that are no longer active. These wastes must be characterized and documented so that they can be disposed of properly. In support of this effort, the ACL performs chemical and radiological analyses to provide the composition and hazards-classification data needed by the treatment/storage/disposal facilities that ultimately process the wastes.

Many different types of wastes were characterized by the ACL in 1999. Beakers, flasks, and bottles containing unlabeled radioactive solids and liquids from two ANL radioactive material handling facilities were characterized, as were unidentified solids, sludges, aqueous and organic liquids, and oils from several ANL divisions. Also characterized were commercial

solvents, cleaners, and other compounds with no list of ingredients and no Material Safety Data Sheet (MSDS) information.

When the materials appeared to be pure chemical compounds or simple mixtures, the ACL identified the material and then supplied the submitter with an MSDS listing the pertinent hazard information. Direct identification of solids was provided by X-ray diffraction and/or scanning electron microscopy. Direct identification of liquids was provided by GC/MS or Fourier transform infrared spectroscopy. Those wastes that could not be identified or that proved to be complex mixtures were evaluated for the Resource Conservation and Recovery Act (RCRA) characteristics of ignitability, corrosivity, toxicity, and reactivity. These evaluations included the following: pH, water miscibility, and flash point determinations; mercury analysis by cold vapor atomic absorption; and As, Ba, Cd, Cr, Pb, Se, and Ag determinations by ICP-AES. The ACL used GC/MS to identify RCRA target organic components and ion chromatography to identify any acids present. In some cases the amount of water in a waste had to be determined by a Karl-Fischer titration. Wastes from radiologically controlled areas or wastes suspected of containing radioactivity were analyzed by gamma spectrometry, gas proportional counting, liquid scintillation counting, and/or alpha pulse height analysis.

13. Method for Determining Halide Impurities in Refractory Materials

Measuring small amounts of halides contained in refractory materials is difficult because methods generally used for decomposing the refractory can volatilize the sought-for elements or introduce reagents (e.g., hydrochloric or hydrofluoric acid) that interfere with their determination. One approach that has been considered in the ACL for some time is to decompose siliceous or aluminosilicate refractories by fusion with potassium hydroxide, treat the fusate with water, and measure the halides in the resulting basic solution with ion chromatography. Although sometimes successful, this approach often failed when the aluminum content of the refractory was so high that fluoride was complexed, or when the halide content was low. Recently, we tried a modification of the method that appears to overcome these problems for analyzing lithium aluminate. In this method, a 0.5-g sample is fused with 4 g of KOH in a zirconium crucible. The fusate is carefully neutralized and then dissolved with dilute sulfuric acid, which completely decomposes the sample. Then, more sulfuric acid is added, and the halides are steam distilled from the mixture. The distillate is analyzed by ion chromatography. Preliminary tests of the method have shown that when the distillation is carried to the formation of incipient sulfuric acid fumes, near-quantitative recovery of fluoride and chloride is achieved at levels equivalent to 0.03 wt% in the solid sample. Bromide recoveries are on the order of 80% at the same concentration levels. Iodide is lost during the distillation when aluminum is present, presumably through oxidation to iodine that is not retained in the distillate. If additional testing upholds these initial observations, this new approach will be applied to lithium aluminate ceramics. It promises to be useful for analyzing glasses, zeolites, waste-form samples, and other materials as well.

14. Top of Rail Lubricant

The ANL Energy Technology Division, in cooperation with Tranergy Inc. and Texaco Inc., is testing several proprietary lubricants developed by Texaco to reduce friction between rail

tracks and locomotive wheels. The reduction in friction should lead to lower energy consumption by locomotive engines and less wear on the rail hardware. When the engines are in front of the train, the lubricant is applied on the rail tracks behind the engines to allow normal traction between the tracks and the wheels of the engine while friction between the tracks and the rail cars is minimized. The automated system that applies the lubricant calculates the amount of lubricant needed based on the weight of the rail cars and the length of the train. The lubricant is expected to significantly lose its lubrication power as a train passes over the treated tracks and before the next train uses the tracks.

A laboratory-scale device has been constructed by Tranergy that allows accurate measurement of friction between a simulated track and wheel system. This device was used to apply lubricant and collect residue from the tracks after defined periods of use. One of the tasks of the project is to identify volatile and semivolatile by-products produced during use of the lubricants. The ACL analyzed samples of lubricants before and after use. The ACL utilized GC/MS to identify major components of the proprietary lubricant. In preliminary work, we detected only minor semivolatile by-products in the lubricant after its use in the test apparatus. Identification of these compounds is in progress. The Tranergy device was modified to collect volatile organic compounds on Tenax traps produced from the use of the lubricant on the simulated track; analyses are underway.

VI

Publications and Presentations—1999

The Division's publications and oral presentations for 1999 were entered into a bibliographic data base. The pages that follow are a printout of this information sorted into five categories: (1) patents, (2) journal articles, books, and book chapters, (3) ANL progress and topical reports, as well as contributions to reports published by organizations other than ANL, (4) abstracts and papers published in proceedings of conferences, symposia, workshops, etc., and (5) oral presentations at scientific meetings and seminars not referenced in the fourth category.

Chemical Technology Division
Publications and Presentations—1999

A. Patents and Inventions

Methanol Partial Oxidation Reformer
S. Ahmed, R. Kumar, and M. Krumpelt
Patent No. 5,939,025, issued August 17, 1999

Methanol Partial Oxidation Reformer
S. Ahmed, R. Kumar, and M. Krumpelt
Patent No. 5,942,346, issued August 24, 1999

High Performance Electrolytes for MCFC
T. D. Kaun and M. F. Roche
Patent No. 5,942,345, issued August 24, 1999

Method for Making Hydrogen Rich Gas from Hydrocarbon Fuel
M. Krumpelt, S. Ahmed, R. Kumar, and R. Doshi
Patent No. 5,929,286, issued July 27, 1999

Electrochemical Fabrication of Capacitors
A. N. Mansour and C. A. Melendres
Patent No. 6,001,237, issued December 14, 1999

Solid Oxide Fuel Cell with Multi-Unit Construction and Prismatic Design
C. C. McPheeters, D. W. Dees, and K. M. Myles
Patent No. 5,882,809, issued March 16, 1999

Near Real Time Vapor Detection and Enhancement Using Aerosol Adsorption
V. J. Novick and S. A. Johnson
Patent No. 5,932,818, issued August 3, 1999

Method for Synthesizing Pollucite from Chabazite and Cesium Chloride
C. Pereira
Patent No. 5,875,407, issued February 23, 1999

Pseudo-Capacitor Device for Aqueous Electrolytes
J. Prakash, M. M. Thackeray, D. W. Dees, D. R. Vissers, and K. M. Myles
Patent No. 5,841,627, issued November 24, 1998

B. Journal Articles, Books, and Book Chapters

Fuel Processing for Fuel Cell Power Systems
A. Ahmed, R. Kumar, and M. Krumpelt
Fuel Cells Bull., No. 12, pp. 4–7 (1999)

β-FeOOH, A New Positive Electrode Material for Lithium Secondary Batteries
K. Amine, H. Yasuda, and M. Yamachi
J. Power Sources **81–82**, 221–223 (1999)

Synthesis and Properties of Ceramics-Polymer Composite Membranes as High Temperature Proton Conducting Electrolytes
J.-M. Bae, I. Honma, and S. Hirakawa
J. Korean Phys. Soc. **35**, S315–S319 (1999)

Properties of Pyrochlore Ruthenate Cathodes for Intermediate Temperature Solid Oxide Fuel Cells
J.-M. Bae and B. C. H. Steele
J. Electroceram. **3**(1), 37–46 (1999)

Selective Site Occupancy Exhibited by Cr^{3+} and Cr^{6+} Incorporated into Electrochemically Deposited Nickel Hydroxide Films
M. Balasubramanian and C. A. Melendres
Electrochem. Solid State Lett. **2**(4), 167–169 (1999)

An X-ray Absorption Near-Edge Spectroscopy Study of the Oxidation State of Chromium in Electrodeposited Oxide Films
M. Balasubramanian and C. A. Melendres
Electrochim. Acta **44**, 2941–2945 (1999)

X-ray Absorption Specroscopy Study of the Local Structure of Heavy Metal Ions Incorporated into Electrodeposited Nickel Oxide Films
M. Balasubramanian, C. A. Melendres, and A. N. Mansour
J. Electrochem. Soc. **146**(2), 607 (1999)

An X-ray Absorption Study of the Local Structure of Cerium in Electrochemically Deposited Thin Films
M. Balasubramanian, C. A. Melendres, and A. N. Mansour
Thin Solid Films **347**, 178–183 (1999)

Mathematical Modelling of the Effects of Aerobic and Anaerobic Chelate Biodegradation on Actinide Speciation
J. E. Banaszak, J. M. Van Briesen, B. E. Rittmann, and D. T. Reed
Radiochim. Acta **82**, 445–451 (1998)

Effect of Spectral Resolution on Pattern Recognition Analysis Using Passive Fourier Transform Infrared Sensor Data
A. S. Bangalore, J. C. Demirgian, A. S. Boparai, and G. W. Small
Appl. Spectrosc. **53**(11), 1382–1391 (1999)

Atomic Structure and Electrochemical Potential of $Li_{1+x}V_3O_8$
R. Benedek, M. M. Thackeray, and L. H. Yang
Phys. Rev. B **60**(9), 6335–6342 (1999)

First-Principles Calculation of Atomic Structure and Electrochemical Potential of $Li_{1+x}V_3O_8$
R. Benedek, M. M. Thackeray, and L. H. Yang
J. Power Sources **81–82**, 487–490 (1999)

The Development of $LiFeO_2$-$LiCoO_2$-NiO Cathodes for Molten Carbonate Fuel Cells
I. Bloom, M. T. Lanagan, M. Krumpelt, and J. L. Smith
J. Electrochem. Soc. **146**(4), 1336–1340 (1999)

Microanalysis of Colloids and Suspended Particles from Nuclear Waste Glass Alteration
E. C. Buck and J. K. Bates
Appl. Geochem. **14**, 635–653 (1999)

Uranium: Minerals, Chemistry and the Environment
P. C. Burns and R. J. Finch, Eds.
Reviews in Mineralogy, Mineralogical Soc. of America, Washington, DC, Vol. 38 (1999)

Wyartite: Crystallographic Evidence for the First Pentavalent-Uranium Mineral
P. C. Burns and R. J. Finch
Am. Mineral. **84**, 1456–1460 (1999)

Aqueous Biphasic Systems for Metal Separations: A Microcalorimetric Analysis of Polymer/Salt Interactions
D. J. Chaiko, T. A. Hatton, and B. Y. Zaslavsky
Metal Separation Technologies Beyond 2000: Integrating Novel Chemistry with Processing, Eds., K. C. Liddell and D. J. Chaiko, The Minerals, Metals, and Materials Soc., Warrendale, PA, pp. 167–179 (1999)

Structural Changes of $LiMn_2O_4$ Spinel Electrodes During Electrochemical Cycling
J. Cho and M. M. Thackeray
J. Electrochem. Soc. **146**(10), 3577–3587 (1999)

Yrast Spectroscopy of N = 82,83 Isotopes ^{136}Xe and ^{137}Xe from ^{248}Cm Fission
P. J. Daly, P. Bhattacharyya, C. T. Zhang, Z. W. Grabowski, R. Broda, B. Fornal, I. Ahmad, T. Lauritsen, L. R. Morss, W. Urban, W. R. Phillips, J. L. Durell, M. J. Leddy, A. G. Smith, B. J. Varley, N. Schulz, E. Lubkiewicz, M. Bentaleb, and J. Blomqvist
Phys. Rev. C **59**(6), 3066–3070 (1999)

Diminution of Supercooling of Electrolyte by Carbon Particles
S. P. Ding, K. Xu, S. S. Zhang, T. R. Jow, K. Amine, and G. L. Henriksen
J. Electrochem. Soc. **146**(11), 3974–4980 (1999)

Structure Investigations of the SOFC Anode CERMETS. Part I: Porosity Investigations
J. Divisek, J. Volfkovich, and R. Wilkenhoener
J. Appl. Electrochem. **29**, 153–163 (1999)

Development of Solid-Oxide Fuel Cells That Operate at 500°C
R. Doshi, V. L. Richards, J. D. Carter, X. Wang, and M. Krumpelt
J. Electrochem. Soc. **146**(4), 1273–1278 (1999)

High Gradient Magnetic Separation for the Treatment of High Level Radioactive Waste
A. D. Ebner, J. A. Ritter, and L. Nuñez
Sep. Sci. Technol. **34**(6–7), 1333–1350 (1999)

$LiNi_xCu_{0.5-x}Mn_{1.5}O_4$ Spinel Electrodes—Superior High Potential Cathode Materials for Li Batteries. I. Electrochemical and Structural Studies
Y. Ein-Eli, S. Mukerjee, X. Q. Wang, J. McBreen, J. T. Vaughey, and M. M. Thackeray
J. Electrochem. Soc. **146**, 908–913 (1999)

Refinement of the Crystal Structure of Rutherfordine
R. J. Finch, M. A. Cooper, F. C. Hawthorne, and R. C. Ewing
Can. Miner. **37**, 935–944 (1999)

Systematic Mineralogy and Paragenesis of Uranium Minerals
R. J. Finch and T. Murakami
Chapter 3 of *Uranium: Minerals, Chemistry and the Environment*, Vol. 38, *Reviews in Mineralogy*, Eds., P. C. Burns and R. J. Finch, Mineralogical Soc. of America, Washington, DC, pp. 91–179 (1999)

^{7}Li NMR Imaging at the Surface of an Aerospace Alloy
R. E. Gerald, L. Nuñez, R. J. Klingler, and J. W. Rathke
The Chemist **76**(2), 45–50 (1999)

Application of Lithium in Molten-Salt Reduction Processes
K. V. Gourishankar and E. J. Karell
Light Metals, 1999, Ed., C. Edward Eckert, The Minerals, Metals, and Materials Soc., Warrendale, PA, pp. 1123–1128 (1999)

What is Important?
D. W. Green
Managing the Modern Laboratory **3**(4), 59A–60A (1999)

Forum on When is Quality Assurance Cost Effective?
D. W. Green
Managing the Modern Laboratory **3**(4), 68A–75A (1999)

Fads, Truth, Wisdom, and Experiments
D. W. Green
Managing the Modern Laboratory **4**(1), 2A–3A (1999)

Team Celebration
D. W. Green
Managing the Modern Laboratory **4**(2), 19A–20A (1999)

The Evaluation of Sintered Sodalite-Glass Composites
M. C. Hash, J. P. Thalacker, D. R. Simon, G. L. Burns, and R. H. Woodman
Environmental Issues and Waste Management Technologies in the Ceramic and Nuclear Industries IV, Eds., J. C. Marra and G. T. Chandler, pp. 229–237 (1999)

Synthesis of Organic/Inorganic Nanocomposites Protonic Conducting Membrane through Sol-Gel Processes
I. Honma, S. Hirakawa, K. Yamada, and J.-M. Bae
Solid State Ionics **118**, 29–36 (1999)

Corrosion Performance of Ferrous and Refractory Metals in Molten Salts under Reducing Conditions
J. E. Indacochea, J. L. Smith, K. R. Litko, and E. J. Karell
J. Mater. Res. **14**(5), 1990–1995 (1999)

Development of a High-Power Lithium-Ion Battery
A. N. Jansen, A. J. Kahaian, K. D. Kepler, P. A. Nelson, K. Amine, D. W. Dees, D. R. Vissers, and M. M. Thackeray
J. Power Sources **81–82**, 902–905 (1999)

Tritium Behavior in Lithium Ceramics
C. E. Johnson
J. Nucl. Mater. **270**, 212–220 (1999)

Structural and Electrochemical Analysis of Layered Compounds from Li_2MnO_3
C. S. Johnson, S. D. Korte, J. T. Vaughey, M. M. Thackeray, T. E. Bofinger, Y. Shao-Horn, and S. A. Hackney
J. Power Sources **81–82**, 491–495 (1999)

Extractant-Coated Magnetic Particles for Cobalt and Nickel Recovery from Acidic Solutions
M. D. Kaminski and L. Nuñez
J. Magn. Magn. Mater. **194**, 31–36 (1999)

Evaluation of Extractant-Coated Ferromagnetic Microparticles for the Recovery of Hazardous Metals from Waste Solution
M. D. Kaminski, L. Nuñez, and A. V. Visser
Sep. Sci. Technol. **34**(6–7), 1103–1120 (1999)

$Li_xCu_6Sn_5(0<x<13)$: An Intermetallic Insertion Electrode for Rechargeable Lithium Batteries
K. D. Kepler, J. T. Vaughey, and M. M. Thackeray
Electrochem. Sol. State Lett. **2**, 307–309 (1999)

Copper-Tin Anodes for Rechargeable Lithium Batteries: An Example of the Matrix Effect in an Intermetallic System
K. D. Kepler, J. T. Vaughey, and M. M. Thackeray
J. Power Sources **81/82**, 383–387 (1999)

Amorphous Manganese Oxyiodides Exhibiting High Lithium Intercalation Capacity at Higher Current Density
J. Kim and A. Manthiram
Electrochem. Solid State Lett. **2**, 55–57 (1999)

Amorphous Manganese Oxides for Rechargable Lithium Batteries
J. Kim and A. Manthiram
Selected Battery Topics, Vol. 98-15, Eds., G. Halpert, M. L. Gopikanth, K. M. Abraham, W. R. Cieslak and W. A. Adams, The Electrochemical Society, Pennington, NJ, pp.281–289, (1999)

Low Temperature Synthesis and Electrode Properties of $Li_{14}Mn_5O_{12}$ Spinel Oxides
J. Kim and A. Manthiram
Lithium Batteries, Vol. 98-16, Eds., S. Surampudi and R. A. Marsh, Electrochemical Society, Pennington, NJ, pp. 271–278 (1999)

Synthesis and Lithium Intercalation Properties of Nanocrystalline Lithium Iron Oxides
J. Kim and A. Manthiram
J. Electrochem. Soc. **146**, 4371–4374 (1999)

Synthesis of $LiCoO_2$ Cathodes by an Oxidation Reaction in Solution and Its Electrochemical Properties
J. Kim, P. Fulmer, and A. Manthiram
Electrochem. Solid State Lett. **34**, 571–57 (1999)

Toroid NMR Probes for the *In Situ* Examination of Homogeneous Cobalt Hydroformylation Catalysts at High Pressures and Temperatures
K. W. Kramarz, R. J. Klingler, D. E. Fremgen, and J. W. Rathke
Catal. Today **49**(4), 339–352 (1999)

XAFS Studies of Interfaces in MnSe/ZnTe Superlattices
A. J. Kropf, B. A. Bunker, and J. K. Furdyna
J. Synch. Rad. **6**(3), 370–372 (1999)

Design Rules for Solvent Extraction
R. A. Leonard
Solvent Extr. Ion Exch. **17**(3), 597–612 (1999)

Developing and Testing an Alkaline-Side Solvent Extraction Process for Technetium Separation from Tank Waste

R. A. Leonard, C. Conner, M. W. Liberatore, P. V. Bonnesen, D. J. Presley, B. A. Moyer, and G. J. Lumetta

Sep. Sci. Technol. **34**(6–7), 1043–1068 (1999)

Preparation and Physical Characteristics of a Lithium-Beryllium-Substituted Fluorapatite

D. Lexa

Metall. Mater. Trans. A **30A**(1), 147–153 (1999)

Hermetic Sample Enclosure for Simultaneous Differential Scanning Calorimetry/Synchrotron Powder X-ray Diffraction

D. Lexa

Rev. Sci. Instrum. **70**(5), 2242–2245 (1999)

The Enthalpy of Occlusion of the LiCl-KCl Eutectic Salt in Zeolite 4A

D. Lexa

J. Chem. Thermodyn. **31**, 811–817 (1999)

Metal Separation Technologies Beyond 2000: Integrating Novel Chemistry with Processing

K. C. Liddell and D. J. Chaiko, Eds.

The Minerals, Metals, and Materials Soc., Warrendale, PA (1999)

Manganese Oxides for Rechargable Lithium Batteries

A. Manthiram and J. Kim

Trans. SAEST **34**, 1–5 (1999)

Oxide Electrodes for Rechargable Lithium Batteries

A. Manthiram and J. Kim

Recent Research Developments in Electrochemistry, Vol. 2, Ed., S. G. Pandalai, Transworld Research Network, Trivandrum, India, pp. 31–69 (1999)

Synthesis of Spinel $Li_4Mn_5O_{12}$ Cathodes by Oxidation Reactions in Solutions

A. Manthiram and J. Kim

Ceramic Transactions **92**, 291–302 (1999)

Using Imaging Raman Microscopy to Explore Phase Evolution in Composite Ceramic Superconductors

V. A. Maroni, A. K. Fischer, and K. T. Wu

Chapter 11 in *Spectroscopy of Superconducting Materials*, Ed., E. Faulques, ACS Symp. Ser. 730, Am. Chem. Soc., Washington, DC, pp. 156–167 (1999)

An Environmental Scanning Electron Microscope Study of the Ag/Bi-2223 Composite Conductor from 25 to 840°C

V. A. Maroni, M. Teplitsky, and M. W. Rupich

Physica C **313**, 169–174 (1999)

Phase Formation and Microstructure Development in Silver-Clad Bi-2223 Multifilament Composite Conductors

N. N. Merchant, J. S. Luo, A. K. Fischer, V. A. Maroni, E. R. Podtburg, W. L. Carter, Q. Li, A. Otto, M. W. Rupich, and G. N. Riley

Supercond. Sci. Technol. **12**, 327–336 (1999)

Phase Stability and Grain Growth in an Ag/Bi-2223 Composite Conductor Prepared Using Fine-Grained Bi-2223 as a Precursor

N. N. Merchant, D. J. Miller, V. A. Maroni, R. D. Parrella, Q. Li, M. W. Rupich, W. L. Carter, and G. N. Riley

IEEE Trans. on Applied Superconductivity **9**(2), 2545–2548 (1999)

Lithium Insertion into Hollandite-Type TiO_2

L. D. Noailles, C. S. Johnson, J. T. Vaughey, and M. M. Thackeray

J. Power Sources **81–82**, 259–263 (1999)

Real Time Chemical Vapor Detection and Enhancement Utilizing Aerosol Adsorption

V. J. Novick, S. A. Johnson, H. A. Hisgen, and V. J. Reyes

Rev. Sci. Instrum. **70**(3), 1829–1834 (1999)

Waste from the Medical Industries

L. Nuñez

Chapter 26 in *Industrial Processes and Waste Stream Management*, Ed., H. Guyer, John Wiley, New York, pp. 469–481 (1998)

Transuranic Separation Using Organophosphorus Extractants Adsorbed onto Superparamagnetic Carriers

L. Nuñez and M. D. Kaminski

J. Magn. Magn. Mater. **194**, 102–107 (1999)

NMR Spectroscopy

J. W. Rathke, R. J. Klingler, R. E. Gerald, D. E. Fremgen, K. Woelk, S. Gaemers, and C. J. Elsevier

Chemical Synthesis Using Supercritical Fluids, Eds., P. G. Jessop and W. Leitner, Wiley-VCH, Weinheim, pp. 165–194 (1999)

Radiotoxicity of Plutonium in NTA-Degrading *Chelatobacter heintzii*, Cell Suspensions

D. T. Reed, Y. Vojta, J. W. Quinn, and M. K. Richmann

Biodegradation **10**, 251–260 (1999)

Carbons for Lithium Battery Applications Prepared Using Sepiolite as Inorganic Template

G. Sandí, K. A. Carrado, R. E. Winans, C. S. Johnson, and R. Csencsits

J. Electrochem. Soc. **146**, 3644–3648 (1999)

Structural Characterization of Layered $LiMnO_2$ Electrodes by Electron Diffraction and Lattice Imaging

Y. Shao-Horn, S. A. Hackney, A. R. Armstrong, P. G. Bruce, R. L. Gitzendanner, C. S. Johnson, and M. M. Thackeray

J. Electrochem. Soc. **146,** 2404–2412 (1999)

Structural Fatigue in Spinel Electrodes in $Li/Li_x[Mn_2]O_4$ Cells

Y. Shao-Horn, S. A. Hackney, A. J. Kahaian, K. D. Kepler, E. Skinner, J. T. Vaughey, and M. M. Thackeray

J. Power Sources **81–82,** 496–499 (1999)

Coprocessing Coal with Hydrogenated Vacuum Pyrolyzed Tire Oil

Y. Shi, L. Shao, W. F. Olson, and E. M. Eyring

Fuel Process. Technol. **58,** 135 (1999)

Electrochemical Separation of Aluminum from Uranium for Research Reactor Spent Nuclear Fuel Applications

S. A. Slater, A. G. Raraz, J. L. Willit, and E. C. Gay

Sep. Purif. Technol. **15,** 197–205 (1999)

The Li-Mn-O Phase Diagram and Its Importance for Rechargeable Lithium/Spinel Cells

M. M. Thackeray

ITE Battery Letters **1**(1), 21–25 (1999)

The Structural Stability of Transition Metal Oxide Insertion Electrodes for Lithium Batteries

M. M. Thackeray

Handbook of Battery Materials, Ed., J. O. Besenhard, Wiley-VCH, Weinheim, pp. 293–317 (1999)

Spinel Electrodes for Lithium Batteries

M. M. Thackeray

J. Am. Ceram. Soc. **82**(12), 3347–3354 (1999)

Composite Electrodes for Lithium Batteries

M. M. Thackeray, C. S. Johnson, A. J. Kahaian, K. D. Kepler, and J. T. Vaughey

ITE Battery Letters **1,** 26–32 (1999)

Stabilization of Insertion Electrodes for Lithium Batteries

M. M. Thackeray, C. S. Johnson, A. J. Kahaian, K. D. Kepler, J. T. Vaughey, Y. Shao-Horn, and S. A. Hackney

J. Power Sources **81–82,** 60–66 (1999)

Intermetallic Insertion Electrodes Derived from NiAs-, Ni_2In-, and Li_2CuSn-Type Structures for Lithium-Ion Batteries

M. M. Thackeray, J. T. Vaughey, A. J. Kahaian, K. D. Kepler, and R. Benedek

Electrochem. Commun. **1,** 111–115 (1999)

NiAs- vs. Zinc-Blende-Type Intermetallic Insertion Electrodes for Lithium Batteries: Lithium Extraction from Li_2CuSu

J. T. Vaughey, K. D. Kepler, R. Benedek, and M. M. Thackeray
Electrochem. Comm. **1**, 517–521 (1999)

Stabilization of Rocky Flats Pu-Contaminated Ash within Chemically-Bonded Phosphate Ceramics

A. S. Wagh, R. V. Strain, S.-Y. Jeong, D. T. Reed, T. R. Krause, and D. Singh
J. Nucl. Mater. **265**, 295–307 (1999)

Mechanically Alloyed Ni/8YSZ Powder Mixtures: Preparation, Powder Characterization, and Sintering Behavior

R. Wilkenhoener, R. Vassen, H. P. Buchkremer, and D. Stoever
J. Mater. Sci. **34**, 257–265 (1999)

Uranium Mineralogy and the Disposal of Spent Nuclear Fuel

D. J. Wronkiewicz and E. C. Buck
Uranium: Mineralogy, Geochemistry, and the Environment, Reviews in Mineralogy, Vol. 38, *Reviews in Mineralogy,* Eds., P. C. Burns and R. J. Finch, Mineralogical Soc. of America, Washington, DC, pp. 475–498 (1999)

Structure and Morphology of Electrodeposited $CaCO_3$: X-ray Diffraction and Microscopy Studies

S. Xu, C. A. Melendres, J. H. Park, and M. A. Kamrath
J. Electrochem. Soc. **146**(9), 3315–3323 (1999)

C. Reports

Chemical Technology Division Annual Technical Report, 1998
J. P. Ackerman et al.
ANL-99/10 (July 1999)

PEM Systems Modeling and Analysis
R. K. Ahluwalia, E. D. Doss, H. K. Geyer, R. Kumar, and M. Krumpelt
In *FY 1999 Progress Report for Fuel Cells for Transportation*, Department of Energy Report, pp. 19–22 (October 1999)

Integrated Fuel Processor Development
S. Ahmed, S. H. D. Lee, C. Pereira, and M. Krumpelt
In *FY 1999 Progress Report for Fuel Cells for Transportation*, Department of Energy Report, pp. 34–37 (October 1999)

Practical Superconductor Development for Electrical Power Applications, Annual Report for FY 1999
T. R. Askew, Y. S. Cha, S. E. Dorris, J. T. Dusek, J. E. Emerson, B. L. Fisher, K. C. Goretta, K. E. Gray, J. R. Hull, M. T. Lanagan, M. Lelovic, V. A. Maroni, R. L. McDaniel, N. N. Merchant, D. J. Miller, J.-H. Park, J. J. Picciolo, and J. P. Singh
ANL-99/20 (October 1999)

Long Term Testing of Titanate Ceramics for Plutonium Immobilization
A. J. Bakel, E. C. Buck, C. J. Mertz, and D. B. Chamberlain
Plutonium Immobilization Project Report PIP-99-073 (June 1999)

Characterization and Corrosion Behavior of Hafnium-Cerium-Uranium Ceramics Containing Impurities
A. J. Bakel, E. C. Buck, V. N. Zyryanov, C. J. Mertz, and D. B. Chamberlain
Plutonium Immobilization Project Report PIP-99-077 (June 1999)

Corrosion Behavior of Titanate Ceramics in Short-Term MCC-1 Tests: Results from Tests with Zirconolite-rich, Baseline and Impurity Ceramics
A. J. Bakel, C. J. Mertz, M. K. Nole, and D. B. Chamberlain
Plutonium Immobilization Project Report PIP-99-102 (August 1999)

Chemical Analyses for GB (SARIN) in Media Generated by Munitions Disposal
K. L. Brubaker, J. F. Schneider, H. J. O'Neill, L. L. Reed, A. S. Boparai, C. T. Snyder, N. A. Tomczyk, and L. L. Jensen
ANL/ACL-99/1 (November 1999)

Characterization of Celotex and Thermodynamic Calculations of the Formation of Corrosion Precursors on Beryllium

A. Diaz-Ortiz, J. Stolk, J. Kim, J. M. Sanchez, and A. Manthiram

Amarillo National Resource Center- DOE, Vol. ANRCP-1999-16, Ed., A. L. Woods, Amarillo National Resource Center for Plutonium, Amarillo, TX, pp. 1–15 (1999)

Round-Robin Testing of a Reference Glass for Low-Activity Waste Forms

W. L. Ebert and S. F. Wolf

ANL-99/22 (October 1999)

Chemical Synthesis of Magnetic Fe-B and Fe-Co-B Particles and Chains

P. Fulmer, J. Kim, A. Manthiram, and J. M. Sanchez

Amarillo National Resource Center-DOE, Vol. ANRCP-1999-15, Ed., A. L. Woods, Amarillo National Resource Center for Plutonium, Amarillo, TX, pp. 1–19 (1999)

Analytical Chemistry Laboratory Progress Report for FY 1999

D. W. Green, A. S. Boparai, D. L. Bowers, and D. G. Graczyk (with contributions from ACL Staff)

ANL/ACL-99/2 (December 1999)

Catalytic Partial Oxidation Reforming Materials and Processes

M. Krumpelt, S. Ahmed, R. Wilkenhoener, J. D. Carter, and Y. Shi

In *FY 1999 Progress Report for Fuel Cells for Transportation*, Department of Energy Report, pp. 60–62 (October 1999)

Alternative Water-Gas Shift Catalyst Development

R. Kumar, D. J. Myers, C. R. Kinsinger, J. D. Carter, T. R. Krause, and M. Krumpelt

In *FY 1999 Progress Report for Fuel Cells for Transportation*, Department of Energy Report, pp. 63–66 (October 1999)

Preparation of a Technology Development Roadmap for the Accelerator Transmutation of Waste (ATW) System: Report of the ATW Separations Technologies and Waste Forms Technical Working Group

J. J. Laidler, E. Collins, J. Duguid, R. Henry, E. J. Karell, S. M. McDeavitt, M. Thompson, M. Toth, M. Williamson, and J. L. Willit

ANL-99/15 (August 1999)

Evaluation of an Alkaline-Side Solvent Extraction Process for Cesium Removal from SRS Tank Waste Using Laboratory-Scale Centrifugal Contactors

R. A. Leonard, C. Conner, M. W. Liberatore, J. Sedlet, S. B. Aase, and G. F. Vandegrift

ANL-99/14 (August 1999)

Limits of Thermodynamic Stability of Pyrochlore Waste Forms for Excess Weapons Plutonium: Inferences from Calorimetry of $CaCeTi_2O_7$

R. L. Putnam, K. B. Helean, A. Navrotsky, B. Ebinghaus, H. F. Shaw, O. Krikorian, and E. C. Buck

Lawrence Livermore National Laboratory Report PIP-99-073 (June 1999)

D. Abstracts and Proceedings Papers

Phase Stability of Laves Intermetallics in a Stainless Steel-Zirconium Alloy
D. P. Abraham and J. W. Richardson
Proc. of the Long Term Stability of High Temperature Materials Conf., Eds., G. E. Fuchs, K. A. Dannemann, and T. C. Deragon, TMS, Warrendale, PA, pp. 169–179 (1999)

Corrosion Behavior of Stainless Steel-Zirconium Alloy Waste Forms
D. P. Abraham, L. J. Simpson, M. J. DeVries, and D. E. Callahan
Proc. of the Corrosion '99 Conf., San Antonio, TX, April 25–30, 1999, Paper No. 466 (1999)

Fuel Processing for Fuel Cell Powered Vehicles
S. Ahmed, R. Wilkenhoener, S. H. D. Lee, J. D. Carter, R. Kumar, and M. Krumpelt
Abstracts, 195th Electrochem. Soc. Meeting, Seattle, WA, May 2–7, 1999, Vol. 99-1, Abstract No. 547 (1999)

Entropy Changes Due to Structure Transformation of the Graphite Anode and Phase Changes of $LiNi_{0.8}Co_{0.2}O_2$ Cathode
S. Al Hallaj, R. Venkatachalapathy, J. R. Selman, J. Prakash, K. Amine, and G. L. Henriksen
Abstracts, 196th Electrochem. Soc. Meeting, Honolulu, HI, October 17–22, 1999, p. 249 (1999)

Development of High Power Lithium Ion Battery for Hybrid Vehicle Application
K. Amine, J. Liu, A. N. Jansen, A. E. Newman, D. R. Simon, and G. L. Henriksen
Abstracts, 196th Electrochem. Soc. Meeting, Honolulu, HI, October 17–22, 1999, p. 117 (1999)

Iron Oxide Positive Active Material for Lithium Ion Batteries
K. Amine, H. Yasuda, and M. Yamachi
Abstracts, Fall Meeting of the Materials Research Soc., Boston, MA, November 30–December 4, 1998, Vol. 1, p. 571 (1999)

Olivine $LiMePO_4$ (Me:Co,Cu) as New 4.8 and 2V Positive Active Materials for Lithium Batteries
K. Amine, H. Yasuda, and M. Yamachi
Abstracts, 196th Electrochem. Soc. Meeting, Honolulu, HI, October 17–22, 1999, p. 277 (1999)

New Iron Oxide Positive Active Material for Lithium Secondary Batteries
K. Amine, H. Yasuda, and M. Yamachi
Mater. Res. Soc. Symp. Proc. **548**, 271–282 (1999)

Corrosion Behavior of Pyrochlore-Rich Titanate Ceramics for Plutonium Disposition: Impurity Effects

A. J. Bakel, V. N. Zyryanov, C. J. Mertz, E. C. Buck, and D. B. Chamberlain
Mater. Res. Soc. Symp. Proc. **556**, 181–188 (1999)

Fate of Neptunium in an Anaerobic, Methanogenic Microcosm

J. E. Banaszak, S. M. Webb, B. E. Rittmann, J.-F. Gaillard, and D. T. Reed
Mater. Res. Soc. Symp. Proc. **556**, 1141–1149 (1999)

Second Difference Electron Energy-Loss Spectroscopy with the Gatan Imaging Filter

E. C. Buck
Proc. of the Microscopy and Microanalysis '99 Annual Meeting, Portland, OR, August 1–5, 1999, pp. 808–809 (1999)

Supercooling of Electrolytes for Lithium Batteries and Its Diminution by Carbon Particles

S. P. Ding, K. Xu, S. S. Zhang, T. R. Jow, K. Amine, and G. L. Henriksen
Abstracts, 196th Electrochem. Soc. Meeting, Honolulu, HI, October 17–22, 1999, p. 343 (1999)

Pressurized and Atmospheric Pressure Gasoline-Fueled Polymer Electrolyte Fuel Cell System Performance

E. D. Doss, R. K. Ahluwalia, and R. Kumar
Proc. of the 34th Intersoc. Energy Conversion Eng. Conf., Vancouver, Canada, August 2–5, 1999 (1999)

Corrosion of Spent Fuel in Vapor and Dripping Groundwater at 90°C

R. J. Finch, E. C. Buck, P. A. Finn, and J. K. Bates
Mater. Res. Soc. Symp. Proc. **556**, 121-126 (1999)

Structural Analysis of a Completely Amorphous ^{238}Pu-Doped Zircon by Neutron Diffraction

J. Fortner, Y. Badyal, D. C. L. Price, J. M. Hanchar, and W. J. Weber
Mater. Res. Soc. Symp. Proc. **540**, 349–353 (1999)

EELS and XANES Analysis of Plutonium and Cerium Edges from Titanate Ceramics for Fissile Materials Disposal

J. Fortner, E. C. Buck, A. J. Kropf, A. J. Bakel, M. C. Hash, S. B. Aase, and D. B. Chamberlain
Proc. of the Microscopy and Microanalysis '99 Annual Meeting, Portland, OR, August 1–5, 1999, pp. 768–769 (1999)

Design Considerations for Heated Wells in Gloveboxes

A. A. Frigo and D. E. Preuss
Proc. of the 1999 Annual Conf. and Exposition of the Am. Glovebox Soc., San Francisco, CA, July 19–21, 1999, CD-ROM, Am. Glovebox Soc., Santa Rosa, CA (1999)

Evaluation and Design of Toroid Cavity Probes Based on Calculated Distortions
E. S. Growney, G. Friedman, R. E. Gerald, R. J. Klingler, J. W. Rathke, and L. Nuñez
Program Binder for the 40th Experimental Nuclear Magnetic Resonance Conf., Orlando, FL, February 28–March 5, 1999, p. 129 (1999)

Correlation between Electrochemical-Calorimetry Characteristics and Kinetic Property Changes Due to Phase Transition Upon Lithiation/Delithiation in a Li_xCoO_2 Lithium Ion Cell
J.-S. Hong, K. Amine, and J. R. Selman
Abstracts, 196th Electrochem. Soc. Meeting, Honolulu, HI, October 17–22, 1999, p. 278 (1999)

Intermetallic Insertion Electrodes for Li-Ion Batteries
C. S. Johnson, M. M. Thackeray, J. T. Vaughey, K. D. Kepler, A. J. Kahaian, and K. Amine
Proc. of the 40th Battery Symp., Kyoto, Japan, November 14–16, 1999, pp. 55–56 (1999)

Electrometallurgical Treatment of Oxide Spent Fuels
E. J. Karell, K. V. Gourishankar, L. S. H. Chow, and R. E. Everhart
Proc. of the Int. Conf. on Future Nuclear Systems, Global '99 Conf. on Nuclear Technology—Bridging the Millennia, Jackson Hole, WY, August 29–September 3, 1999, CD-ROM, Am. Nucl. Soc., La Grange Park, IL (1999)

In Situ XAFS Characterization of Intermetallic and Metal Oxide Insertion Electrodes for Lithium Ion Batteries
A. J. Kropf and C. S. Johnson
Abstracts, Fall Meeting of the Materials Research Soc., Boston, MA, November 29–December 3, 1999, Abstract R14.7, p. 96 (1999)

Comparison of Different Fuels and Fuel Processing Options for Automotive Fuel Cells
R. Kumar, H. K. Geyer, R. K. Ahluwalia, and M. Krumpelt
Abstracts, 195th Electrochem. Soc. Meeting, Seattle, WA, May 2–7, 1999, Vol. 99-1, Abstract No. 551 (1999)

Corrosion Behaviors of a Glass-Bonded Sodalite Ceramic Waste Form and Its Constituents
M. A. Lewis, W. L. Ebert, and M. L. Stanley
Proc. of the Int. Conf. on Future Nuclear Systems, Global '99 Conf. on Nuclear Technology—Bridging the Millennia, Jackson Hole, WY, August 29–September 3, 1999, CD-ROM, Am. Nucl. Soc., La Grange Park, IL (1999)

High Power Lithium Ion Batteries
J. Liu, A. N. Jansen, D. Simon, A. E. Newman, G. L. Henriksen, and K. Amine
Abstracts, 195th Electrochem. Soc. Meeting, Seattle, WA, May 2–7, 1999, p. 52 (1999)

Selecting the Right Glovebox
R. F. Malecha, E. F. Bielick, and B. A. Size
Proc. of the 1999 Annual Conf. and Exposition of the Am. Glovebox Soc., San Francisco, CA, July 19–21, 1999, CD-ROM, Am. Glovebox Soc., Santa Rosa, CA (1999)

Synthesis and Casting of a Lithium-Bismuth Compound for an Ion-Replacement Electrorefiner
S. M. McDeavitt
Light Metals, 1999, Proc. of the Technical Sessions Presented at the 128th Annual Meeting of the Minerals, Metals, and Materials Soc., San Diego, CA, February 15–19, 1999, pp. 1139–1142 (1999)

Nondestructive Evaluation of Nuclear Packaging Materials by Toroid NMR
L. Nuñez, R. E. Gerald, and S. E. Aumeier
Proc. of the Third Topical Meeting on DOE Spent Nuclear Fuel and Fissile Materials Management, Am. Nucl. Soc., Charleston, SC, September 8–11, 1998 Vol. 1, pp. 327–334 (1999)

Incorporation of Radionuclides from the Electrometallurgical Treatment of Spent Fuel into a Ceramic Waste Form
C. Pereira, M. C. Hash, M. A. Lewis, M. K. Richmann, and J. K. Basco
Mater. Res. Soc. Symp. Proc. **556**, 115–120 (1999)

First Principles Calculations for Lithiated Manganese Oxides
R. Prasad, R. Benedek, M. M. Thackeray, J. M. Wills, and L. H. Yang
Proc. of the Fall Meeting of the Materials Research Soc., Boston, MA, November 30–December 4, 1998 (1999)

Improving Gd-Doped Ceria Electrolytes for Low Temperature Solid Oxide Fuel Cells
J. M. Ralph, J. G. Klinger, and B. C. H. Steele
Abstracts, Materials Research Soc. Meeting, San Francisco, CA, April 5–9, 1999 (1999)

XAF/XANES Studies of Plutonium-Loaded Sodalite/Glass Composite Waste Forms
M. K. Richmann, D. T. Reed, A. J. Kropf, S. B. Aase, and M. A. Lewis
Proc. of the Int. Nucl. Mater. Management Conf., Phoenix, AZ, July 26–29, 1999, CD-ROM, Inst. Nucl. Mater. Management Soc., Northbrook, IL (1999)

XAFS/XANES Studies of Plutonium-Loaded Sodalite/Glass Waste Forms
M. K. Richmann, D. T. Reed, A. J. Kropf, S. B. Aase, and M. A. Lewis
Proc. of the 40th Annual Meeting of the Institute of Nuclear Materials Management, Phoenix, AZ, July 26–29, 1999 (1999)

Carbons for Lithium Ion Cells Prepared Using Sepiolite as Inorganic Template
G. Sandí, K. A. Carrado, R. E. Winans, C. S. Johnson, and K. D. Kepler
Proc. of the Symp. on Lithium Batteries, Electrochemical Society, Pennington, NJ, Vol. 98-16, pp. 11–18 (1999)

Studies of Electrolyte Penetration in Carbon Anodes by NMR Techniques

G. Sandí, R. E. Gerald, R. J. Klingler, J. W. Rathke, K. A. Carrado, and R. E. Winans

Proc. of the Lithium Battery Symp., 194th Electrochem. Soc. Meeting, Boston, MA, November 1–6, 1998, Vol. 98-16, pp. 11–18 (1999)

Radiochemical Analysis Using Empore™ Rad Disks

L. L. Smith and K. A. Orlandini

Proc. of the Int. Conf. on Future Nuclear Systems, Global '99 Conf. on Nuclear Technology—Bridging the Millennia, Jackson Hole, WY, August 29–September 3, 1999, CD-ROM, Am. Nucl. Soc., La Grange Park, IL (1999)

Altering the Equilibrium Condition in Sr-Doped Lanthanum Manganite

J. T. Vaughey, X. Wang, J. D. Carter, and M. Krumpelt

Proc. of the 196th Electrochem. Soc. Meeting, Solid Oxide Fuel Cells VI, Honolulu, HI, October 17–22, 1999, Vol. 99-19, pp. 361–366 (1999)

E. Papers Presented at Scientific Meetings

Phase Stability of Laves Intermetallics in a Stainless Steel-Zirconium Alloy
D. P. Abraham and J. W. Richardson
Presented at the Metallurgical Soc. Annual Meeting, San Diego, CA, February 28–March 4, 1999

Microstructure of the Zirconium-8 wt% Stainless Steel Alloy
D. P. Abraham, J. W. Richardson, and S. M. McDeavitt
Presented at the Metallurgical Soc. Annual Meeting, San Diego, CA, February 28–March 4, 1999

Automotive Fuel Cell Systems Modeling
R. K. Ahluwalia, E. D. Doss, H. K. Geyer, R. Kumar, and M. Krumpelt
Presented at the Annual Meeting, DOE Fuel Cells for Transportation National Laboratory R&D Program, Argonne, IL, June 23–25, 1999

Fischer-Tropsch Light Synthetic Paraffin Fuels for Fuel Cell Power Generation
S. Ahmed, J. P. Kopasz, B. J. Russell, and H. L. Tomlinson
Presented at the Sixth Grove Fuel Cell Symp., London, United Kingdom, September 13–16, 1999

Gas-to-Liquid Synthetic Fuels for Use in Fuel Cells: Reformability, Energy Density, and Infrastructure Compatibility
S. Ahmed, J. P. Kopasz, B. J. Russell, and H. L. Tomlinson
Presented at the Third Int. Fuel Cell Conf., Nagoya, Japan, November 30–December 3, 1999

The Argonne Catalytic Fuel Processor for Automotive and Small Fuel Cell Power Systems
S. Ahmed, S. H. D. Lee, R. Kumar, J. D. Carter, R. Wilkenhoener, and M. Krumpelt
Presented at the Sixth Grove Fuel Cell Symp., London, United Kingdom, September 13–16, 1999

Integrated Fuel Processor Development
S. Ahmed, S. H. D. Lee, C. Pereira, and M. Krumpelt
Presented at the Annual National Laboratory R&D Meeting of the DOE Fuel Cells for Transportation Program, Argonne, IL, June 23–25, 1999

Advanced High Power Battery for Hybrid Vehicle Application
K. Amine
Presented at the 13th Int. Battery Association Materials Symp., Marakech, Morocco, November 7–12, 1999

The Corrosion Behavior of Titanate Ceramics for Pu Disposition: Rate-Controlling Processes
A. J. Bakel, C. J. Mertz, and D. C. Chamberlain
Presented at the Fall Meeting of the Materials Research Soc., Boston, MA, November 29–December 3, 1999

The Long-Term Corrosion Behavior of Titanate Ceramics for Pu Disposition: Rate-Controlling Processes

A. J. Bakel, C. J. Mertz, M. C. Hash, and D. C. Chamberlain

Presented at the Fall Meeting of the Materials Research Soc., Boston, MA, November 29–December 3, 1999

In Situ Spectro-electrochemical Studies on Simulated Corrosion Films

M. Balasubramanian, C. A. Melendres, S. Mini, and A. N. Mansour

Presented at the Am. Phys. Soc. Centennial Meeting, Atlanta, GA, March 20–26, 1999

Thermodynamics as a Tool to Predict Microbiological-Actinide Interactions

J. E. Banaszak, B. E. Rittmann, and D. T. Reed

Presented at the 22nd Rare Earth Research Conf. on Environmental Lanthanide and Actinide Processes, Argonne National Laboratory, Argonne, IL, July 10–15, 1999

Reduction and Precipitation of Neptunium(V) by Sulfate-Reducing Bacteria

J. E. Banaszak, B. E. Rittmann, and D. T. Reed

Presented at the Migration '99 Conf., Lake Tahoe, NV, September 26–October 1, 1999

Synthesis of Li-M-O Spinel Oxides from M_3O_4 (M=Co, Mn) Templates

T. E. Bofinger, Y. Shao-Horn, S. A. Hackney, C. S. Johnson, J. T. Vaughey, and M. M. Thackeray

Presented at the 196th Joint Meeting of Electrochem. Soc., Honolulu, HI, October 17–22, 1999

Evidence for the Corrosion of Noble Metal Particles: TEM Investigation

E. C. Buck

Presented at the 1999 Spent Fuel Workshop, Hart House, University of Toronto, Toronto, Canada, September 21–23, 1999

Modeling the Formation of Colloids during Nuclear Waste Form Corrosion

E. C. Buck

Presented at the Seventh Int. Conf. on the Chemistry and Migration of Actinides and Fission Products in the Geosphere, Lake Tahoe, NV, September 26–October 1, 1999

The Behavior of Silicon and Boron in the Surface of Corroded Nuclear Waste Glasses: An EFTEM Study

E. C. Buck, K. L. Smith, and M. G. Blackford

Presented at the Fall Meeting of the Materials Research Soc., Boston, MA, November 29–December 3, 1999

Characterization of Actinide Phosphates in Silo Wastes
E. C. Buck, S. F. Wolf, and C. J. Mertz
Presented at the Seventh Int. Conf. on the Chemistry and Migration of Actinides and Fission Products in the Geosphere, Lake Tahoe, NV, September 26–October 1, 1999

Wyartite: Crystallographic Evidence for the First Pentavalent-Uranium Mineral
P. C. Burns and R. J. Finch
Presented at the Joint Annual Meeting of the Geologic Assoc. of Canada and the Mineralogical Assoc. of Canada, Sudbury, Ontario, May 26–28, 1999

Aqueous Biphasic Systems for Metal Separations: A Microcalorimetric Analysis of Polymer/Salt Interactions
D. J. Chaiko, T. A. Hatton, and B. Y. Zaslavsky
Presented at the Engineering Foundation Conf. on Metal Separation Technologies Beyond 2000, Oahu, HI, June 13–18, 1999

Clay Based Thickeners for Aqueous Systems
D. J. Chaiko and W. F. Moll
Presented at the Euroclay '99 Conf., Institute of Geological Science, Krakow, Poland, September 6–10, 1999

Fuel Cell Technology: Status of the Partnership for a New Generation of Vehicles Initiative
S. G. Chalk, W. F. Podolski, and J. F. Miller
Presented at the Fuel Cell Technology Conf., Chicago, IL, March 24–25, 1999

Corrosion Behavior of Titanate Ceramics Developed for the Immobilization of Plutonium
D. B. Chamberlain, A. J. Bakel, E. C. Buck, J. Fortner, M. C. Hash, C. J. Mertz, and S. F. Wolf
Presented at the Global '99 Int. Conf. on Future Nuclear Systems, Jackson Hole, WY, August 30–September 2, 1999

Electrochemical Studies of Mg-Doped $Li_4Ti_5O_{12}$ Anodes
C. H. Chen, J. T. Vaughey, A. N. Jansen, A. J. Kahaian, and M. M. Thackeray
Presented at the 196th Joint Int. Electrochem. Soc. Meeting, Honolulu, HI, October 17–22, 1999

Development of a Multistage Pyrocontactor
L. S. H. Chow, J. K. Basco, and J. P. Ackerman
Presented at the Global '99 Int. Conf. on Future Nuclear Systems, Jackson Hole, WY, August 30–September 2, 1999

Development of Annular Targets for ^{99}Mo Production
C. Conner, E. F. Lewandowski, J. L. Snelgrove, M. W. Liberatore, D. E. Walker, T. C. Wiencek, D. J. McGann, G. L. Hofman, and G. F. Vandegrift
Presented at the Int. Meeting on Reduced Enrichment for Research and Test Reactors, Budapest, Hungary, October 3–8, 1999

Overview of Electrochemical Power Sources for Electric and Hybrid-Electric Vehicles

D. W. Dees

Presented at the Special Session on Electric Vehicle Technology, IEEE-IEMDC '99, Seattle, WA, May 9–12, 1999

Towards Standardizing the Measurement of Electrochemical Properties of Solid State Electrolytes in Lithium Batteries

D. W. Dees and G. L. Henriksen

Presented at the Advanced Lithium Solid State Batteries Workshop, Towson, MD, July 13–15, 1999

Round-Robin Testing of a Standard Material for Acceptance Testing of Low-Activity Radioactive Waste Products

W. L. Ebert

Presented at the 101st Am. Ceram. Soc. Meeting, Indianapolis, IN, April 25–28, 1999

Estimating Model Parameter Values for High-Level Waste Glasses for Total System Performance Assessment

W. L. Ebert, S.-W. Tam, and J. C. Cunnane

Presented at the Fall Meeting of the Materials Research Soc., Boston, MA, November 29–December 3, 1999

Application of an Acceptance Test for Low-Activity Radioactive Waste Glasses

W. L. Ebert, S. F. Wolf, and V. N. Zyryanov

Presented at the 101st Am. Ceram. Soc. Meeting, Indianapolis, IN, April 25–28, 1999

Estimating Model Parameter Values for Total System Performance Assessment

W. L. Ebert, V. N. Zyryanov, and J. C. Cunnane

Presented at the Fall Meeting of the Materials Research Soc., Boston, MA, November 29–December 4, 1999

Evidence for the Release of Tc from Fuel-Grain Boundaries During the Oxidative Corrosion of Spent UO_2 Fuel

R. J. Finch

Presented at the Spent Fuel Workshop, Toronto, Canada, September 21–23, 1999

The Role of Radiogenic Rb in the Alteration and Paragenesis of Uranium Minerals

R. J. Finch

Presented at the Annual Meeting of the Geological Society of America, Denver, CO, October 25–29, 1999

Interactions between U(VI) Solids and Np-Bearing Groundwater at 90°C
R. J. Finch, E. C. Buck, P. A. Finn, and J. C. Cunnane
Presented at the Spent Fuel Workshop, Toronto, Canada, September 21–23, 1999

The Roles of Solid Alteration Products in Limiting Releases of U, Np, Pu, and Lanthanides from Corroded Nuclear-Waste Forms
R. J. Finch, E. C. Buck, J. Fortner, C. J. Mertz, S. F. Wolf, P. A. Finn, W. L. Ebert, and J. C. Cunnane
Presented at the Seventh Int. Conf. on the Chemistry and Migration Behavior of Actinides and Fission Products in the Geosphere, Lake Tahoe, NV, September 26–October 1, 1999

Unsaturated Tests with Fast-Flux Fuels
P. A. Finn
Presented at the Spent Fuel Workshop, University of Toronto, Toronto, Canada, September 21–23, 1999

Radionuclide Release Rates and Concentrations in Unsaturated Test with Oxide Fuels–First 4.8 Years
P. A. Finn, S. F. Wolf, and R. A. Leonard
Presented at the Seventh Int. Conf. On the Chemistry and Migration Behavior of Actinides and Fission products in the Geosphere, Lake Tahoe, NV, September 26–October 1, 1999

Corrosion of Mixed Oxide Fuel under Unsaturated and Oxidizing Conditions
P. A. Finn, S. F. Wolf, Y. Tsai, and M. M. Goldberg
Presented at the Fall Meeting of the Materials Research Soc., Boston, MA, November 29–December 3, 1999

EXAFS and XANES Analysis of Plutonium and Cerium Edges from Titanate Ceramics for Fissile Materials Disposal
J. Fortner, E. C. Buck, A. J. Kropf, A. J. Bakel, M. C. Hash, S. B. Aase, and D. B. Chamberlain
Presented at the Fall Meeting of the Materials Research Soc., Boston, MA, November 29–December 3, 1999

The Origin of Colloids from High Level Waste Glass Corrosion
J. A. Fortner, E. C. Buck, S. F. Wolf, and J. K. Bates
Presented at the Seventh Int. Conf. on the Chemistry and Migration of Actinides and Fission Products in the Geosphere, Lake Tahoe, NV, September 26–October 1, 1999

Plutonium Silicate Alteration Phases Produced by Aqueous Corrosion of Borosilicate Glass
J. Fortner, C. J. Mertz, A. J. Bakel, R. J. Finch, and D. B. Chamberlain
Presented at the Fall Meeting of the Materials Research Soc., Boston, MA, November 29–December 3, 1999

NMR Detection and Imaging of Gas Phase Micelles

D. E. Fremgen, R. E. Gerald, R. J. Klingler, E. S. Smotkin, and J. W. Rathke

Presented at the 41st Rocky Mountain Conf. on Analytical Chemistry, Denver, CO, July 30–August 5, 1999

Hydroformylation in Gas Phase Microemulsions

D. E. Fremgen, R. J. Klingler, R. E. Gerald, M. J. Chen, J. W. Rathke, and E. S. Smotkin

Presented at the Spring Symp. of the Catalysis Club of Chicago, Chicago, IL, May 12, 1999

Gas Phase Micelles as Microreactors for Oxo Catalysis

D. E. Fremgen, E. S. Smotkin, R. J. Klingler, and J. W. Rathke

Presented at the DOE National Laboratory Research Symp., Albuquerque, NM, February 24–25, 1999

Application of the American Glovebox Society's Guideline for Gloveboxes

A. A. Frigo

Presented at the 12th Annual Conf. and Equipment Exhibit of the Am. Glovebox Soc., San Francisco, CA, July 19–21, 1999

New Catalyst Technology for the Selective Oxidation of Feedstock Aromatic Compounds to Commodity Chemicals

E. A. Gardner, C. L. Marshall, L. E. Iton, H. H. Kung, K. Popp, F. Sherif, R. Rao, Z. C. Zhang, and G. Whitwell

Presented at the 218th Am. Chem. Soc. National Meeting, New Orleans, LA, August 22–26, 1999

Imaging Diffusion of Small Molecules in a Toroid Cavity NMR Probe

R. E. Gerald, E. T. Chainani, E. S. Growney, D. E. Fremgen, L. Nuñez, R. J. Klingler, and J. W. Rathke

Presented at the Small Molecule NMR Conf., Argonne, IL, August 15, 1999

Distribution of Crystalline and Amorphous Polymer Electrolyte in an Electrochemical Cell

R. E. Gerald, E. T. Chainani, R. J. Klingler, and J. W. Rathke

Presented at the 41st Rocky Mountain Conf. on Analytical Chemistry, Denver, CO, July 30–August 5, 1999

Applications of Toroid Cavity NMR Detectors to Metals, Polymers, Radioactive Materials and Supercritical Fluids

R. E. Gerald, D. E. Fremgen, L. Nuñez, D. T. Reed, R. J. Klingler, J. W. Rathke, and K. Woelk

Presented at the 41st Rocky Mountain Conf. on Analytical Chemistry, Denver, CO, July 30–August 5, 1999

Toroid Cavity NMR Detector: Application to Battery Research

R. E. Gerald, R. J. Klingler, J. W. Rathke, and G. Sandí

Presented at the Eveready Battery Company, Westlake, OH, February 15, 1999

NMR Spectroscopy and Imaging of an Electrochemical Cell with a Carbon Working Electrode
R. E. Gerald, G. Sandí, R. J. Klingler, and J. W. Rathke
Presented at the 41st Rocky Mountain Conf. on Analytical Chemistry, Denver, CO, July 30–August 5, 1999

Growth and Alteration of Uranium-Rich Microlite
R. Giere, R. J. Swope, E. C. Buck, R. Guggenheim, D. Mathys, and E. Reusser
Presented at the Fall Meeting of the Materials Research Soc., Boston, MA, November 28–December 4, 1999

Growth and Alteration of Uranium-Rich Microlite from Mozambique
R. Giere, R. J. Swope, E. C. Buck, R. Guggenheim, D. Mathys, and E. Reusser
Presented at the Annual Meeting of the Geological Society of America, Denver, CO, October 25–28, 1999

Becoming a Better Analytical Lab Manager
D. W. Green
Presented at the Pittcon '99 Symp. on Managing the Modern Analytical Laboratory, Orlando, FL, March 7–12, 1999

Common Interests of the DOE Analytical Managers Group (DAM) and the DOE Metrology Committee
D. W. Green
Presented at the DOE Metrology Meeting, Las Vegas, NV, March 24, 1999

Are Analytical Chemists Metrologists?
D. W. Green
Presented at the 17th Meeting of the DOE Analytical Managers Group, Idaho Falls, ID, August 17–19, 1999

Better Radiological Measurements Through Better Sample Preparation
D. W. Green and L. L. Smith
Presented at the ACS Division of the Analytical Chemistry Awards Symposium, American Chemical Society National Meeting, New Orleans, LA, August 22–26, 1999

Passive-Shimming Designs of Toroid Cavity Probes Using Spectral Distortion Parameters
E. S. Growney, R. E. Gerald, R. J. Klingler, J. W. Rathke, and G. Friedman
Presented at the 41st Rocky Mountain Conf. on Analytical Chemistry, Denver, CO, July 30–August 5, 1999

Reactive Sintering of Plutonium-Bearing Titanates
M. C. Hash, J. K. Basco, V. N. Zyryanov, and D. B. Chamberlain
Presented at the 101st Am. Ceram. Soc. Meeting, Indianapolis, IN, April 25–28, 1999

Characterization of Titanate-Based Ceramics Developed for Immobilization of Plutonium
M. C. Hash, V. N. Zyryanov, A. J. Bakel, S. F. Wolf, J. K. Basco, and D. B. Chamberlain
Presented at the Global '99 Int. Conf., Jackson Hole, WY, August 30–September 1, 1999

Structural Reaction Mechanisms for Lithium Insertion in Lithium Manganese Oxides
C. R. Horne, U. Bergmann, M. M. Grush, J. Kim, A. Manthiram, S. P. Cramer, K. A. Streibel, and E. J. Cairns
Presented at the 196th Meeting of the Electrochem. Soc., Honolulu, HI, October 17–22, 1999

Surface Enhanced Infrared Spectroscopy: The Influence of Metal Film Architecture on Enhancement Mechanism(s) and Practical Utilization
T. R. Jensen, S. A. Johnson, R. P. Van Duyne, and V. A. Maroni
Presented at the Society for Applied Spectroscopy Meeting, Chicago Section, Arlington Heights, IL, November 9, 1999

Aqueous Complexation of Trivalent Lanthanide and Actinide Cations by N,N,N'$_2$,N'-tetrakis(2-pyridylmethyl)ethylenediamine
M. P. Jensen, L. R. Morss, J. V. Beitz, and D. D. Ensor
Presented at the 22nd Rare Earth Research Conf., Argonne, IL, July 10–15, 1999

Structure and Insertion Chemistry of New Composite Electrodes for Lithium Batteries
C. S. Johnson
Presented at The Society for Advanced Battery Technology Meeting, Osaka National Research Institute, Osaka, Japan, November 17, 1999

Measurement of Structure and Structural Change for Li-Insertion Electrodes at Argonne's Advanced Photon Source
C. S. Johnson, A. J. Kropf, J. T. Vaughey, and M. M. Thackeray
Presented at the Second Hawaii Battery Conf., HI, January 4–7, 1999

Synthesis and Characterization of Alternative Anode Materials for Li-Ion Batteries
A. J. Kahaian, J. T. Vaughey, K. D. Kepler, C. Chen, A. N. Jansen, and M. M. Thackeray
Presented at the Third Int. Symp. on New Materials for Fuel Cell and Modern Battery Systems, Montreal, Canada, July 6–10, 1999

Improved MCFC Performance with Li/Na/Ba/Ca Carbonate Electrolyte
T. D. Kaun, A. C. Schoeler, C.-J. Centeno, and M. Krumpelt
Presented at the Fifth Int. Symp. on Molten Carbonate Fuel Cell Technology, 196th Electrochem. Soc. Meeting, Honolulu, HI, October 17–22, 1999

Incorporation of Radionuclides in the Alteration Phases of Spent Nuclear Fuel
C.-W. Kim, D. J. Wronkiewicz, and E. C. Buck
Presented at the Migration '99 Conf., Lake Tahoe, NV, September 26–October 1, 1999

Potential Incorporation of Transuranics into Uranium Phases
C. W. Kim, D. J. Wronkiewicz, and E. C. Buck
Presented at the Fall Meeting of the Materials Research Soc., Boston, MA, November 29–December 3, 1999

Magnetic Resonance Imaging of Polymer Electrolytes and Insertion Electrodes
R. J. Klingler, R. E. Gerald, and J. W. Rathke
Presented at the Advanced Lithium Solid State Batteries Workshop, Towson, MD, July 13–15, 1999

Effects of Fuel Constituents on Catalytic Fuel Processor Performance
J. P. Kopasz, D. V. Applegate, L. Ruscic, and M. Krumpelt
Presented at the Annual National Laboratory R&D Meeting of the DOE Fuel Cells for Transportation Program, Argonne, IL, June 23–25, 1999

Fuel Flexible Partial Oxidation Reforming of Hydrocarbons for Automotive Applications
J. P. Kopasz, R. Wilkenhoener, S. Ahmed, J. D. Carter, and M. Krumpelt
Presented at the Symp. on Hydrogen Production, Storage, and Utilization, Am. Chem. Soc. National Meeting, New Orleans, LA, August 22–26, 1999

Sulfur Removal from Reformate
T. Krause
Presented at the Annual National Laboratory R&D Meeting of the DOE Fuel Cells for Transportation Program, Argonne, IL, June 23–25, 1999

In Situ XAFS of Metal Oxide and Intermetallic Insertion Electrodes for Lithium-Ion Batteries
A. J. Kropf
Presented at the Fall Meeting of the Materials Research Soc., November 29–December 3, 1999

In Situ XAFS of the $Li_xNi_{0.8}Co_{0.2}$ Cathode for Lithium-Ion Batteries
A. J. Kropf and C. S. Johnson
Presented at the Symp. on Applications of Synchrotron Meeting, Boston, MA, November 29–December 3, 1999

Partial Oxidation Fuel Reforming for Automotive Power Systems
M. Krumpelt, S. Ahmed, R. Kumar, S. G. Chalk, and J. Milliken
Presented at the Third Int. Fuel Cell Conf., Nagoya, Japan, November 30–December 3, 1999

Catalytic Partial Oxidation Reforming Materials and Processes
M. Krumpelt, S. Ahmed, R. Wilkenhoener, J. D. Carter, and C. L. Marshall
Presented at the Annual National Laboratory R&D Meeting of the DOE Fuel Cells for Transportation Program, Argonne, IL, July 23–25, 1999

Design Considerations for a Gasoline-Fueled Automotive Fuel Cell System
R. Kumar, R. K. Ahluwalia, E. D. Doss, H. K. Geyer, and M. Krumpelt
Presented at the Fuel Cell Gordon Research Conf., Plymouth State College, Plymouth, NH, June 27–July 2, 1999

Alternative Water-Gas Shift Catalysts
R. Kumar, D. Myers, C. R. Kinsinger, and M. Krumpelt
Presented at the 1999 Annual National Laboratory R&D Meeting of the DOE Fuel Cells for Transportation Program, Argonne, IL, June 23–25, 1999

Evaluation of an Alkaline-Side Solvent Extraction Process for Cesium Removal from SRS Tank Waste
R. A. Leonard, C. Conner, M. W. Liberatore, J. Sedlet, S. B. Aase, G. F. Vandegrift, L. H. Delmau, P. V. Bonnesen, and B. A. Moyer
Presented at the Eleventh Symp. on Separation Science and Technology for Energy Applications, Gatlinburg, TN, October 18–21, 1999

Comparison of the Corrosion Behaviors of the Glass-Bonded Sodalite Ceramic Waste Form and Reference HLW Glasses
M. A. Lewis and W. L. Ebert
Presented at the Annual Meeting and Exposition of the Am. Ceram. Soc., Indianapolis, IN, April 25–28, 1999

Corrosion Behaviors Sodalite, Glass and Composite Glass-Bonded Sodalite Ceramic Waste Form
M. A. Lewis, M. L. Stanley, and W. L. Ebert
Presented at the Fall Meeting of the Materials Research Soc., Boston, MA, November 29–December 3, 1999

Development of High-Power Lithium Ion Batteries
J. Liu, A. N. Jansen, K. D. Kepler, A. E. Newman, G. L. Henriksen, and K. Amine
Presented at the 195th Electrochem. Soc. Meeting, Seattle, WA, May 2–7, 1999

Transmission Electron Microscopy of Corrosion of Stainless Steel-Zirconium Metal Waste Forms
J. S. Luo and D. P. Abraham
Presented at the Microscopy and Microanalysis '99 Conf., Portland, OR, August 1–5, 1999

Alpha-Decay-Induced Defects in ^{244}Cm-Doped Xenotime Structures
J. S. Luo and G. K. Liu
Presented at the 101st Am. Ceram. Soc. Meeting, Indianapolis, IN, April 25–28, 1999

Characterization of Phase Chemistry and Distribution in Hf-Ce-U Ceramics with SEM and X-ray Mapping

J. S. Luo, V. N. Zyryanov, A. J. Bakel, E. C. Buck, and D. B. Chamberlain

Presented at the 101st Am. Ceram. Soc. Meeting, Indianapolis, IN, April 25–28, 1999

Characterization of Phase Assemblage and Distribution in Titanate Ceramics with SEM/EDS and X-ray Mapping

J. S. Luo, V. N. Zyryanov, A. J. Bakel, and D. B. Chamberlain

Presented at the 101st Am. Ceram. Soc. Meeting, Indianapolis, IN, April 25–28, 1999

Characterization of a Glass-Bonded Ceramic Waste Form Loaded with U and Pu: The Gross Microstructure

J. S. Luo, V. N. Zyryanov, W. L. Ebert, T. P. O'Holleran, and W. Sinkler

Presented at the Fall Meeting of the Materials Research Soc., Boston, MA, November 29–December 3, 1999

Computational Chemistry Integration into Hydrodesulfurization Catalysis Research

C. L. Marshall, J. L. Tilson, A. D. Dutoi, and J. R. Brenner

Presented at the Divisional Colloid Chemistry Meeting, Am. Chem. Soc. Annual Meeting, Anaheim, CA, March 21–25, 1999

Improved Catalysts for the Removal of Sulfur from Heavy Hydrocarbons

C. L. Marshall, D. Wei, and J. R. Brenner

Presented at the DOE National Laboratory Catalysis Research Symp., Albuquerque, NM, February 24–25, 1999

A Durable Waste Form for Disposal of Chloride Wastes

C. C. McPheeters and J. P. Ackerman

Presented at the Global '99 Int. Conf. on Future Nuclear Systems, Jackson Hole, WY, August 30–September 2, 1999

In-Situ Observations of Adsorption and Film Formation on Metal Electrodes by Synchrotron Far Infrared Reflectance Spectroscopy

C. A. Melendres, F. Hahn, J. M. Leger, and G. A. Bowmaker

Presented at the Eighth Int. Symp. on Passivity, Ontario, Canada, May 9–15, 1999

Application of the Aqueous Biphasic Separation (ABS) Process for the Separation of Ultrafine Industrial Minerals

R. Mensah-Biney, D. J. Chaiko, R. Neff, and P. Ward

Presented at the 1999 SME Annual Meeting, Denver, CO, March 1–3, 1999

Forecasting Tape Performance from Microstructural Studies on Ag-Clad Bi-2223 Composite Conductors

N. N. Merchant, V. A. Maroni, A. K. Fischer, G. N. Riley, and R. D. Parrella

Presented at the Annual Meeting and Exhibition of the Minerals, Metals, and Materials Soc., San Diego, CA, February 28–March 4, 1999

The Formation and Stability of Glass Waste Form Colloids

C. J. Mertz, E. C. Buck, J. A. Fortner, and S. F. Wolf

Presented at the Seventh Int. Conf. on the Chemistry and Migration of Actinides and Fission Products in the Geosphere, Lake Tahoe, NV, September 26–October 1, 1999

Dissolution Behavior of Glass-Bonded Sodalite Containing Rare Earth and Actinide Elements

L. R. Morss, M. A. Lewis, W. L. Ebert, M. K. Richmann, and D. Lexa

Presented at the 22nd Rare Earth Research Conf., Argonne, IL, July 10–15, 1999

Testing and Modeling a Ceramic Nuclear Waste Form: Glass-Bonded Sodalite

L. R. Morss, M. A. Lewis, T. H. Fanning, and W. L. Ebert

Presented at the Amer. Chem. Soc. National Meeting, Anaheim, CA, March 21–25, 1999

Glass-Bonded Sodalite: A Ceramic Nuclear Waste Form

L. R. Morss, M. K. Richmann, and D. Lexa

Presented at the 218th Am. Chem. Soc. National Meeting, New Orleans, LA, August 22–26, 1999

Corrosion of Glass-Bonded Sodalite as a Function of pH and Temperature

L. R. Morss, M. L. Stanley, C. D. Tatko, and W. L. Ebert

Presented at the Fall Meeting of the Materials Research Soc., Boston, MA, November 29–December 3, 1999

Radionuclide Separation Using Functionalized Ferromagnetic Composites

L. Nuñez and M. D. Kaminski

Presented at the 217th Am. Chem. Soc. National Meeting, Anaheim, CA, March 21–25, 1999

Liquid Fuel Reformer Development

C. Pereira, R. Wilkenhoener, S. Ahmed, and M. Krumpelt

Presented at the DOE Hydrogen Program Annual Review Meeting, Lakewood, CO, May 4–6, 1999

Toroid NMR Studies of Some Catalytic Carbonylations

J. W. Rathke, R. J. Klingler, M. J. Chen, and D. E. Fremgen

Presented at the General Electric Corporate R&D Seminar Series, Niskayuna, NY, August 5, 1999

Reduction of Pu(V) and Pu(VI) by Citric Acid
D. T. Reed and S. B. Aase
Presented at the Migration '99 Conf., Lake Tahoe, NV, October 10–14, 1999

In Situ Studies in Carbon Anodes by NMR Techniques
G. Sandí, R. E. Gerald, R. J. Klingler, J. W. Rathke, K. A. Carrado, and R. E. Winans
Presented at the Eveready Battery Company, Westlake, OH, February 15, 1999

Implementation Details for NAMP Information Systems
A. E. Scandora, W. E. Streets, J. S. Morton, L. Ekman, and S. Woolf
Presented at NAMP '99: Analytical Solutions for Successful Environmental Cleanup, Gaithersburg, MD, June 15–17, 1999

Special Analytical Services for U.S. EPA Region V Emergency Response Branch: Chemical Agent Analysis
J. F. Schneider
Presented at the U.S. EPA Region V ER-NBC Exercise, Cincinnati, OH, October 19–21, 1999

Influence of the Alloying Elements Mn and Co on the Electrical Resistance and Corrosion Behavior of Bipolar Plate Materials in MCFC
A. C. Schoeler, T. D. Kaun, and M. Krumpelt
Presented at the 196th Joint Int. Electrochem. Soc. Meeting, Honolulu, HI, October 17–22, 1999

The MRCAT Insertion Device Beamline at the Advance Photon Source
C. U. Serge, N. E. Leyarovska, W. M. Lavender, P. W. Plag, A. S. King, A. J. Kropf, B. A. Bunker, K. M. Kemner, P. Dutta, R. S. Duran and J. Kaduk
Presented at the 11th U.S. National Synchtron Radiation Instrumentation Conference, Stanford, CA, Oct. 13–15, 1999

Catalytic Conversion of Waste Materials and Coals to Transportation Fuels
Y. Shi, C. L. Marshall, and E. M. Eyring
Presented at the Gordon Research Conf., New London, NH, June 20–25, 1999

Empore™ Rad Disks: Waste Minimization through an Innovative Sample Preparation Technique
L. L. Smith, K. A. Orlandini, K. M. Hoffmann, and D. C. Seely
Presented at the 13th Int. Forum on Process Analytical Chemistry, IFPAC '99, San Antonio, TX, January 24–27, 1999

Status of Implementation of DOE-EM's NAMP Informational Databases
W. E. Streets
Presented at NAMP '99: Analytical Solutions for Successful Environmental Cleanup, Gaithersburg, MD, June 15–17, 1999

The Integrated Performance Evaluation Program (IPEP)—A Component of the DOE's National Analytical Management Program (NAMP)

W. E. Streets, P. C. Lindahl, J. R. Dahlgran, J. S. Morton, and L. Ekman

Presented at the Waste Management '99 Symp., Tucson, AZ, February 28–March 4, 1999

Development and Implementation of Information Systems for DOE's National Analytical Management Program (NAMP)

W. E. Streets, A. E. Scandora, J. S. Morton, L. Ekman, and S. Woolf

Presented at NAMP '99: Analytical Solutions for Successful Environmental Cleanup, Gaithersburg, MD, June 15–17, 1999

Status of Development of NAMP Informational Database Systems

W. E. Streets, A. E. Scandora, J. S. Morton, and S. Woolf

Presented at the National Analytical Management Program Workshop '99, Las Vegas, NV, October 28–29, 1999

A Fuel-Cell Primer: Fundamentals, Applications and Advancements in the Technology

W. M. Swift

Presented at Conf. on the Business Case for Fuel Cells, Boston, MA, July 15–16, 1999

ANL Fuel Cell Test Facility

W. M. Swift

Presented at the Annual National Laboratory R&D Meeting of the DOE Fuel Cells for Transportation Program, Argonne, IL, June 23–25, 1999

Thermodynamic and Nonstoichiometric Behavior of Promising High-T_c Cuprate Systems via EMF Measurements: A Short Review

M. Tetenbaum

Presented at the Milton Blander Int. Symp. on Thermodynamic Predictions and Applications, The Minerals, Metals, and Materials Soc., San Diego, CA, February 28–March 4, 1999

Phase Transitions in Insertion Electrodes for Lithium Batteries

M. M. Thackeray

Presented at the Amer. Cer. Soc. 101st Annual Meeting, Indianapolis, IN, April 25–28, 1999

From Gems to Battery Materials

M. M. Thackeray

Presented at the Int. Symp. on Solid Electrolytes: Advances in Science and Technology, Bethlehem, PA, April 10, 1999

Phase Transitions in Transition-Metal-Oxide Electrodes for Lithium Batteries
M. M. Thackeray, R. Benedek, A. J. Kahaian, V. S. Battaglia, A. N. Jansen, and C. S. Johnson
Presented at the 101st Am. Ceram. Soc. Meeting, Indianapolis, IN, April 25–28, 1999

$Li_xCu_6Sn_5(0<x<13)$: An Intermetallic Insertion Electrode for Rechargeable Lithium Batteries
M. M. Thackeray, K. D. Kepler, J. T. Vaughey, and A. J. Kahaian
Presented at the 16th Int. Seminar and Exhibit on Primary and Secondary Batteries, Fort Lauderdale, FL, March 1–4, 1999

Intermetallic Insertion Anodes for Lithium Batteries
M. M. Thackeray, J. T. Vaughey, C. S. Johnson, and K. D. Kepler
Presented at the 13th Int. Battery Association Materials Symp., Marrakesh, Morocco, November 7–11, 1999

Utility Connections—Maintaining the Barrier
R. L. Tollner
Presented at the Twelfth Annual Conf. and Equipment Exhibit of the Am. Glovebox Society, San Francisco, CA, July 19–21, 1999

Demonstration of ^{99}Mo Production Using LEU Metal-Foil Targets in the Cintichem Process
G. F. Vandegrift, C. Conner, G. L. Hofman, J. L. Snelgrove, A. Mutalib, B. Purwadi, H. G. Adang, L. Hotman, Kadarisman, A. Sukmana, T. J. Dicky, Sriyono, A. Suripto, D. Lutfi, D. L. Amin, A. Basiran, A. Gogo, Sarwani, and T. Taryo
Presented at the Int. Meeting on Reduced Enrichment for Research and Test Reactors, Budapest, Hungary, October 3–8, 1999

Progress in Converting Mo-99 Production from High- to Low-Enriched Uranium
G. F. Vandegrift, C. Conner, R. A. Leonard, M. W. Liberatore, J. Sedlet, D. E. Walker, and J. L. Snelgrove
Presented at the 23rd Annual Actinide Separations Conf., Kennewick, WA, June 7–10, 1999

Modification of Base-Side ^{99}Mo Production Processes for LEU Metal-Foil Targets
G. F. Vandegrift, R. A. Leonard, S. B. Aase, J. Sedlet, Y. Koma, C. Conner, C. R. Clark, and M. K. Meyer
Presented at the Int. Meeting on Reduced Enrichment for Research and Test Reactors, Budapest, Hungary, October 3–8, 1999

ANL Progress in Process Development for CNEA/ANL Cooperation
G. F. Vandegrift, R. A. Leonard, S. B. Aase, J. Sedlet, Y. Koma, C. Conner, and J. L. Snelgrove
Presented to the National Atomic Energy Commission, Buenos Aires, Argentina, July 14, 1999

Intermetallic Insertion Anodes for Lithium Batteries
J. T. Vaughey, K. D. Kepler, M. Scott, C. S. Johnson, A. J. Kahaian, and M. M. Thackeray
Presented at the 196th Joint Int. Electrochem. Soc. Meeting, Honolulu, HI, October 17–22, 1999

Demonstration of Packaging of Fernald Silo 1 Waste in Chemically Bonded Phosphate Ceramic
A. S. Wagh, D. Singh, S.-Y. Jeong, D. G. Graczyk, and L. B. TenKate
Presented at the Waste Management '99 Symp., Tucson, AZ, February 28–March 4, 1999

Cathode Materials for Solid Oxide Fuel Cells
X. Wang, J. M. Ralph, J. T. Vaughey, and M. Krumpelt
Presented at the Joint DOE/EPRI/GRI Fuel Cell Technology Review Conf., Chicago, IL, August 3–5, 1999

Effect of Aluminum Concentration on Hydrodesulfurization Activity and Selectivity of MCM-41 Supported Catalysts
D. Wei, C. L. Marshall, L. Xu, and K. A. Carrado
Presented at the 16th North American Catalysis Soc. Meeting, Boston, MA, May 30–June 4, 1999

Hydrodesulfurization of Heavy Oil Utilizing Polymer Tailored Mesoporous Clays as Catalyst Supports
D. Wei, Y. Shi, C. L. Marshall, L. Xu, and K. A. Carrado
Presented at the 16th North American Catalysis Soc. Meeting, Boston, MA, May 30–June 4, 1999

Heat-Resistant, Electrically Conducting Joint between Ceramic End Plates and Metallic Conductors in Solid Oxide Fuel Cell
R. Wilkenhoener, H. P. Buchkremer, D. Stoever, D. Stolten, and A. Koch
Presented at the Spring Meeting of the Materials Research Soc., San Francisco, CA, April 5–9, 1999

High-Throughput Electrorefining of Metals
J. L. Willit, E. C. Gay, and D. J. Chaiko
Presented at the Engineering Foundation Conf. on Metal Separation Technologies Beyond 2000, Oahu, HI, June 13–18, 1999

Recent Developments in Toroid Cavity NMR Spectroscopy, Rheology, and Imaging
K. Woelk, R. E. Gerald, R. J. Klingler, and J. W. Rathke
Presented at the 41st Rocky Mountain Conf. on Analytical Chemistry, Denver, CO, July 30–August 5, 1999

Analysis of High Burnup Nuclear Fuel by HPLC-ICPMS

S. F. Wolf and D. L. Bowers

Presented at the American Society for Testing and Materials Committee C-26 Meeting on Nuclear Fuel Cycles, Memphis, TN, January 24–28, 1999

Material Accountancy Measurement Techniques in Dry-Powdered Processing of Nuclear Spent Fuels

S. F. Wolf, D. L. Bowers, P. J. Persiani, J.-S. Hong, and H.-D. Kim

Presented at the ESARDA Conf., Sevilla, Spain, May 4–6, 1999

Measurement Techniques in Dry-Powdered Processing of Spent Nuclear Fuels

S. F. Wolf, D. L. Bowers, P. J. Persiani, J.-S. Hong, and H. D. Kim

Presented at the 40th Annual Meeting of the Institute of Nuclear Materials Management, Phoenix, AZ, July 25–29, 1999

Effects of Alteration Phase Formation under Unsaturated Conditions in LWR Fuels with Breached Cladding

S. F. Wolf, R. J. Finch, R. A. Olson, and J. C. Cunnane

Presented at the Fall Meeting of the Materials Research Soc., Boston, MA, November 29–December 3, 1999

Mineralogy of Spent Fuel

D. J. Wronkiewicz and E. C. Buck

Presented at the Annual Meeting of the Geological Society of America, Denver, CO, October 25–28, 1999

Distribution for ANL-00/15

Internal:

D. P. Abraham
J. P. Ackerman
S. Ahmed
K. Amine
J. M. Andrew
A. J. Bakel
J. E. Battles
R. W. Benedict
P. R. Betten (5)
S. K. Bhattacharyya
I. D. Bloom
A. S. Boparai
D. L. Bowers
L. M. Boxberger
E. C. Buck
J. D. Carter
D. J. Chaiko
D. B. Chamberlain
Y. I. Chang
L. S. H. Chow
J. C. Cunnane
D. W. Dees
L. W. Deitrich
H. Drucker
B. D. Dunlap
W. L. Ebert
R. E. Einziger
P. A. Finn
J. Fortner
S. C. Foster
F. Y. Fradin
E. C. Gay
M. M. Goldberg
K. V. Gourishankar
D. G. Graczyk
D. W. Green
D. M. Gruen
J. E. Harmon (3)
J. E. Helt
G. L. Henriksen
D. J. Hill
L. R. Johnson
E. J. Karell
T. D. Kaun
J. P. Kopasz
T. R. Krause
M. Krumpelt
R. Kumar
J. J. Laidler
L. Leibowitz
R. A. Leonard
D. Lewis (75)
M. A. Lewis
M. J. Lineberry
J. S. Luo
V. A. Maroni
S. M. McDeavitt
J. F. Miller
W. E. Miller
D. J. Myers
L. Nunez
W. H. Perry
W. F. Podolski
R. B. Poeppel
J. W. Rathke
D. T. Reed
M. K. Richmann
W. W. Schertz
D. K. Schmalzer
D. L. Smith
M. J. Steindler
W. M. Swift
S. Tam
M. Thackeray
M. C. Thurnauer
Z. Tomczuk
G. F. Vandegrift
D. C. Wade
L. C. Walters
C. L. Wilkinson
J. L. Willit
S. F. Wolf
A. M. Wolsky
R. D. Wolson
TIS Files

External:

DOE-OSTI (2)
ANL-E Library
ANL-W Library
A. Bindokas, DOE-CH
J. R. LaFevers, DOE-CH
P. M. Ferrigan, DOE-CH
J. C. Haugen, DOE-CH
S. Ludwig, DOE-CH
R. L. San Martin, DOE-CH
A. L. Taboas, DOE-CH

Chemical Technology Division Review Committee Members:
H. U. Anderson, University of Missouri-Rolla, Rolla, MO
A. L. Bement, Purdue University, West Lafayette, IN
C. Hussey, University of Mississippi, University, MS
M. V. Koch, University of Washington, Seattle, WA
V. P. Roan, University of Florida, Palm Beach Gardens, FL
J. R. Selman, Illinois Institute of Technology, Chicago, IL
J. S. Tulenko, University of Florida, Gainsville, FL
University of California Library, Berkeley, CA
R. C. Alkire, University of Illinois, Champaign, IL
R. A. Bajura, USDOE, Federal Energy Technology Center, Morgantown, WV
S. Barker, Lockheed Martin Corporation, Bethesda, MD
S. E. Berk, USDOE, Office of Fusion Energy, Germantown, MD
A. L. Boldt, Lockheed Martin Corporation, Bethesda, MD
G. G. Boyd, USDOE, Office of Science and Technology, Washington, DC
S. A. Butter, USDOE, Office of Basic Energy Sciences, Washington, DC
L. Camara, MC Power Corporation, Burr Ridge, IL
M. H. Campbell, MACTECH, Richland, WA
S. G. Chalk, USDOE, Office of Transportation Technologies, Washington, DC
H. Cost, Chrysler Corporation, Auburn Hills, MI
P. Davis, USDOE, Office of Transportation Technologies, Washington, DC
C. Donnelly, 3M Center, St. Paul, MN
J. Dunning, GM EV, Troy, MI
T. Dvong, USDOE, Office of Transportation Technologies, Washington, DC
J. J. Eberhardt, USDOE, Office of Transportation Technologies, Washington, DC
R. E. Erickson, USDOE, Office of Environmental Management, Germantown, MD
G. Escobar, LATO Office Rocky Flats Plant, Golden, CO
R. C. Ewing, University of Michigan, Ann Arbor, MI
R. J. Fiskum, USDOE, Office of Building Energy Research, Washington, DC
M. W. Frei, USDOE, Office of Waste Management, Germantown, MD
T. Fryberger, Pacific Northwest National Laboratory, Richland, WA
D. R. Funk, USDOE, Office of Nuclear Energy, Germantown, MD
D. Geiser, USDOE, Office of Technology Development, Germantown, MD
M. R. Ghate, USDOE, Federal Energy Technology Center, Morgantown, WV
R. Gilchrist, Pacific Northwest National Laboratory, Richland, WA
T. J. Gross, USDOE, Office of Transportation Technologies, Washington, DC
H. Haskins, Ford Motor Company, Dearborn, MI
K. L. Heitner, USDOE, Office of Transportation Technologies, Washington, DC
T. M. Hohl, COGEMA Engineering Corporation, Richland, WA
N. Iyer, Westinghouse Savannah River Company, Aiken, SC
G. Jansen, Lockheed Martin Corp., Richland, WA
L. J. Jardine, Lawrence Livermore National Laboratory, Livermore, CA
E. F. Johnson, Princeton University, Princeton, NJ
E. Jones, Pacific Northwest National Laboratory, Richland, WA
F. Kane, University of Idaho, Moscow, ID
R. D. Kelley, USDOE, Office of Basic Energy Sciences, Germantown, MD

C. Kincaid, USDOE, Office of Nonproliferation and National Security, Washington, DC
R. Kinney, 3M Industrial and Electronic Sector Research Lab., St. Paul, MN
R. S. Kirk, USDOE, Office of Transportation Technologies, Washington, DC
B. Knutson, Lockheed Martin Corporation, Bethesda, MD
L. J. Krause, 3M Industrial and Electronic Sector Research Lab., St. Paul, MN
K. Krist, Gas Research Institute, Chicago, IL
S. C. T. Lien, USDOE, Office of Technology Development, Germantown, MD
P. Loscoe, USDOE, Richland Operations Office, Richland, WA
W. D. Magwood, USDOE, Office of Nuclear Energy, Washington, DC
P. Marpin, USDOE, Office of Science, Germantown, MD
J. Milliken, USDOE, Office of Transportation Technologies, Washington, DC
A. C. Muscatello, Rocky Flats Plant, Golden, CO
R. J. Nowak, DARPA/DSO Defense Sciences Office, Arlington, VA
J. B. O'Sullivan, Electric Power Research Institute, Palo Alto, CA
J. Owendoff, USDOE, Office of Environmental Management, Washington, DC
P. G. Patil, USDOE, Office of Transportation Technologies, Washington, DC
R. Paur, Army Research Office, Research Triangle Park, NC
D. Pepson, USDOE, Office of Waste Management, Germantown, MD
R. Person, USDOE, Materials Disposition, Washington, DC
L. Petrakis, Brookhaven National Laboratory, Upton, NY
S. T. Picraux, Sandia National Laboratories, Albuquerque, NM
G. Reddick, Lockheed Martin Corporation, Bethesda, MD
S. Rogers, USDOE, Office of Transportation Technologies, Washington, DC
P. S. Schaus, Lockheed Martin Corporation, Bethesda, MD
L. H. Schwartz, National Institute of Standards and Technology, Gaithersburg, MD
A. W. Searcy, Lawrence Berkeley Laboratory, Berkeley, CA
W. A. Siegel, USDOE, Office of Transportation Technologies, Washington, DC
M. I. Singer, USDOE, Advanced Research/Special Technologies, Washington, DC
S. Singhal, Westinghouse Electric Corporation, Pittsburgh, PA
E. Slaathug, Lockheed Martin Corporation, Bethesda, MD
C. Sloane, GM Research and Development Center, Warren, MI
J. P. Strakey, USDOE, Federal Energy Technology Center, PGH, Pittsburgh, PA
R. A. Sutula, USDOE, Office of Transportation Technologies, Washington, DC
R. Swaroop, Electric Power Research Institute, Palo Alto, CA
T. A. Thornton, Framatome Cogema Fuels, Las Vegas, NV
J. A. Turi, USDOE, Office of Environmental Management, Germantown, MD
M. Williams, USDOE, Coal Projects Management Division, Morgantown, WV
R. E. York, General Motors Corporation, Warren, MI
C. Zeh, USDOE, Federal Energy Technology Center, MGN, Morgantown, WV
S. Zimmer, Chrysler Corporation, Auburn Hills, MI
R. J. Harrison, Atomic Energy of Canada, Ltd., Chalk River, Ontario, CANADA
M. Ozawa, PNC Tokai-Works, Ibaraki-ken, JAPAN